NATIONAL COOPERATIVE HIGHWAY RESEARCH PROGRAM
REPORT 188

FATIGUE OF WELDED STEEL BRIDGE MEMBERS UNDER VARIABLE-AMPLITUDE LOADINGS

TRANSPORTATION RESEARCH BOARD
NATIONAL RESEARCH COUNCIL

NATIONAL COOPERATIVE HIGHWAY RESEARCH PROGRAM
REPORT 188

FATIGUE OF WELDED STEEL BRIDGE MEMBERS UNDER VARIABLE-AMPLITUDE LOADINGS

C. G. SCHILLING, K. H. KLIPPSTEIN,
J. M. BARSOM, AND G. T. BLAKE
U. S. STEEL CORPORATION
MONROEVILLE, PA.

RESEARCH SPONSORED BY THE AMERICAN ASSOCIATION OF STATE HIGHWAY AND TRANSPORTATION OFFICIALS IN COOPERATION WITH THE FEDERAL HIGHWAY ADMINISTRATION

AREA OF INTEREST:
BRIDGE DESIGN

TRANSPORTATION RESEARCH BOARD
NATIONAL RESEARCH COUNCIL
WASHINGTON, D.C. 1978

NATIONAL COOPERATIVE HIGHWAY RESEARCH PROGRAM

Systematic, well-designed research provides the most effective approach to the solution of many problems facing highway administrators and engineers. Often, highway problems are of local interest and can best be studied by highway departments individually or in cooperation with their state universities and others. However, the accelerating growth of highway transportation develops increasingly complex problems of wide interest to highway authorities. These problems are best studied through a coordinated program of cooperative research.

In recognition of these needs, the highway administrators of the American Association of State Highway and Transportation Officials initiated in 1962 an objective national highway research program employing modern scientific techniques. This program is supported on a continuing basis by funds from participating member states of the Association and it receives the full cooperation and support of the Federal Highway Administration, United States Department of Transportation.

The Transportation Research Board of the National Research Council was requested by the Association to administer the research program because of the Board's recognized objectivity and understanding of modern research practices. The Board is uniquely suited for this purpose as: it maintains an extensive committee structure from which authorities on any highway transportation subject may be drawn; it possesses avenues of communications and cooperation with federal, state, and local governmental agencies, universities, and industry; its relationship to its parent organization, the National Academy of Sciences, a private, nonprofit institution, is an insurance of objectivity; it maintains a full-time research correlation staff of specialists in highway transportation matters to bring the findings of research directly to those who are in a position to use them.

The program is developed on the basis of research needs identified by chief administrators of the highway and transportation departments and by committees of AASHTO. Each year, specific areas of research needs to be included in the program are proposed to the Academy and the Board by the American Association of State Highway and Transportation Officials. Research projects to fulfill these needs are defined by the Board, and qualified research agencies are selected from those that have submitted proposals. Administration and surveillance of research contracts are responsibilities of the Academy and its Transportation Research Board.

The needs for highway research are many, and the National Cooperative Highway Research Program can make significant contributions to the solution of highway transportation problems of mutual concern to many responsible groups. The program, however, is intended to complement rather than to substitute for or duplicate other highway research programs.

NCHRP Report 188

Project 12-12 FY '71
ISBN 0-309-02776-4
L. C. Catalog Card No. 78-66461

Price: $6.40

Notice

The project that is the subject of this report was a part of the National Cooperative Highway Research Program conducted by the Transportation Research Board with the approval of the Governing Board of the National Research Council, acting in behalf of the National Academy of Sciences. Such approval reflects the Governing Board's judgment that the program concerned is of national importance and appropriate with respect to both the purposes and resources of the National Research Council.

The members of the technical committee selected to monitor this project and to review this report were chosen for recognized scholarly competence and with due consideration for the balance of disciplines appropriate to the project. The opinions and conclusions expressed or implied are those of the research agency that performed the research, and, while they have been accepted as appropriate by the technical committee, they are not necessarily those of the Transportation Research Board, the National Research Council, the National Academy of Sciences, or the program sponsors.

Each report is reviewed and processed according to procedures established and monitored by the Report Review Committee of the National Academy of Sciences. Distribution of the report is approved by the President of the Academy upon satisfactory completion of the review process.

The National Research Council is the principal operating agency of the National Academy of Sciences and the National Academy of Engineering, serving government and other organizations. The Transportation Research Board evolved from the 54-year-old Highway Research Board. The TRB incorporates all former HRB activities but also performs additional functions under a broader scope involving all modes of transportation and the interactions of transportation with society.

Published reports of the

NATIONAL COOPERATIVE HIGHWAY RESEARCH PROGRAM

are available from:

Transportation Research Board
National Academy of Sciences
2101 Constitution Avenue, N.W.
Washington, D.C. 20418

Printed in the United States of America.

FOREWORD

By Staff
Transportation
Research Board

This report contains the findings from an extensive laboratory investigation of fatigue effects in welded steel beams subjected to variable-amplitude loadings similar to those that occur in actual bridges. The report is recommended to engineers, researchers, and members of specification-writing bodies concerned with structural behavior under repeated loads.

Fatigue fractures observed in cover-plated steel-beam bridges during the AASHO Road Test, and more recently in similar structures in the field, emphasize the importance of understanding the factors that influence the life expectancy of highway bridges. Variables crucial to fatigue life include materials, structural details, quality of fabrication, and the loading history of the structure. NCHRP Project 12-12 was primarily concerned with the last of these factors—loading.

Fatigue design provisions adopted by the American Association of State Highway and Transportation Officials (AASHTO) are based on constant-amplitude fatigue data obtained in NCHRP Project 12-7, "Effect of Weldments on Fatigue Strength of Steel Beams," conducted at Lehigh University. Findings from this earlier study were published in *NCHRP Reports 102* and *147*. According to these AASHTO fatigue provisions, bridges are designed so that they can withstand a certain number of constant-amplitude cycles of stress induced by the design live load plus impact. The required constant-stress cycles were developed using Miner's law for cumulative damage to reflect the estimated volume of truck traffic causing variable-amplitude stress cycles that are usually well below the design live load plus impact stresses. These provisions are expected to result in conservative designs.

There are still gaps in the available information. Specifically, information is needed on (1) the magnitude and frequency of traffic loadings on bridges, (2) the actual stress caused by these traffic loadings, and (3) the fatigue life of various types of bridge members under variable-amplitude loadings. NCHRP Project 12-12 dealt with the third part of the problem. Its objectives were to acquire fatigue data on welded bridge members under variable-amplitude random-sequence stress spectrums, such as occur in actual bridges, and to develop an analytical method of predicting variable-amplitude fatigue behavior from constant-amplitude fatigue data.

This report is based on the results of an experimental program that included constant- and variable-amplitude fatigue tests of both small specimens and relatively large beams of various steels, with structural details similar to those tested in NCHRP Project 12-7. New fatigue provisions are suggested for incorporation into the AASHTO Standard Specifications for Highway Bridges.

CONTENTS

ACKNOWLEDGMENTS

The research reported herein was performed under Project 12-12 by the Research Section of United States Steel Corporation, Monroeville, Pa., with C. G. Schilling, Section Supervisor, and K. H. Klippstein, Senior Research Engineer, as co-principal investigators. They were assisted in preparation of the report by J. M. Barsom, Associate Research Consultant, and G. T. Blake, Research Engineer.

The authors acknowledge the important contribution of their colleagues, R. E. Droske, M. Humlan, C. E. Seigh, and E. J. Imhof, Jr., in developing the experimental procedures and performing the experimental work and G. E. Koons, D. E. Splitstone, and D. Chun in making statistical evaluations.

FATIGUE OF WELDED STEEL BRIDGE MEMBERS UNDER VARIABLE-AMPLITUDE LOADINGS

SUMMARY

Extensive test results showed that variable-amplitude random-sequence stress spectrums, such as occur in actual bridges, can be conveniently represented by a single constant-amplitude effective stress range that would result in the same fatigue life as the variable-amplitude stress range spectrum. Thus, the fatigue behavior of fabricated bridges under traffic loadings can be related to the extensive constant-amplitude fatigue data that are available for various types of structural details. Furthermore, the effective stress range concept can be used directly in the design of critical bridge members or in estimating the remaining fatigue life of existing bridges, and could eventually be incorporated in bridge-design specifications.

The effective stress range is defined by

$$S_{re}=\left[\sum \alpha_i S^B{}_{ri}\right]^{1/B}$$

in which S_{ri} is the midwidth of the ith bar, or interval, in a frequency-of-occurrence bar graph (histogram) defining the variable-amplitude spectrum and α_i is the fraction of stress ranges within that interval. If B is taken as 2, S_{re} from this equation is equal to the root mean square (RMS) of the stress ranges in the spectrum. If B is taken as the reciprocal of the slope of the constant-amplitude SN curve (plotted in the conventional way) for the particular detail under consideration, the equation is equivalent to Miner's Law. For most structural details, B is about 3. The values of S_{re} calculated for the two different values of B are only slightly different (usually less than 10 percent), the value of 3 being more conservative. The test results showed that both the RMS and Miner effective stress ranges satisfactorily represent the variable-amplitude spectrum, but the RMS method provides a slightly better representation.

A review of available field data on stresses in actual bridges showed that the passage of a truck across a bridge usually produces a single major stress cycle with small superimposed vibration stresses. For most types of bridges, these vibration stresses are so small that they do not significantly affect the fatigue life of the bridge. In cantilever (suspended-span) girder bridges, however, the single passage of a truck can cause many major stress cycles as a result of the vibration characteristics of the bridge. Since most of the available field data are on the main longitudinal member of girder bridges, it is possible that other types of members or bridges exist for which a single truck passage causes several major stress cycles. Such bridges or members would be considerably more susceptible to fatigue failures than other types. Consequently, it is suggested that future field studies be aimed at identifying such critical types of bridges and members and, if appropriate, including specification provisions for such cases.

The review of field data also showed that a family of Rayleigh probability-density curves, defined by a single mathematical expression, can be used to approximate the frequency of occurrence of major stress cycles in most highway-bridge

stress spectrums. A particular curve from the family is defined by two parameters: (1) the modal stress range, S_{rm}, which corresponds to the peak of the curve; and (2) a parameter S_{rd}, which is a measure of the width of the curve, or the dispersion of data.

As implied earlier, stress range and type of detail are the major parameters affecting the fatigue life of fabricated bridge members under variable-amplitude loadings as well as under constant-amplitude loadings. The effects of secondary parameters, such as minimum stress and type of steel, are similar to the effects reported in the NCHRP Project 12-7 study for constant-amplitude loadings.

Small-specimen crack-growth tests showed that the effect of a variable-amplitude spectrum on crack growth can be conveniently represented by an RMS method analogous to that discussed previously for the total fatigue life. The present study showed that small-specimen crack initiation and growth data can be useful in explaining the fatigue behavior of fabricated bridge members, but considerable uncertainty exists in predicting the total fatigue life of a fabricated member from such data. An extensive amount of fatigue crack data has been accumulated and should be very helpful in further theoretical studies to determine the initiation and propagation life of fatigue cracks near a weld. The data show that a significant part of the total fatigue life for certain details is expended in initiating the crack.

A possible new approach, based on the effective stress range concept, for bridge-design fatigue specifications is outlined in Chapter Three. This approach is simple, and realistically accounts for the loading conditions that actually affect the fatigue life of a bridge. It gives a realistic estimate of the minimum life of a bridge, and this estimate can be modified in the future if appropriate to account for changes in traffic volume. Furthermore, the method permits considerable flexibility in utilizing specific information on the volume and weight distribution for the bridge under consideration. For most cases, the new approach would be more liberal than the present AASHTO specifications.

Since full-lane loadings generally do not occur frequently enough to affect the fatigue life of a bridge, the new approach is based on a fatigue-design truck placed in realistic positions to calculate a design stress range. A standard weight is given for the fatigue-design truck, but a different weight corresponding to an expected spectrum of truck loads can be used as an alternative. Larger lateral distribution factors than are presently specified by AASHTO for static designs are used to account for the large difference between calculated and measured stresses in bridges. If the design stress range is below a limiting value that is different for each detail category, no further fatigue check is required. Otherwise, the estimated minimum life of the detail in years must be calculated from information on the expected average daily truck traffic and average number of stress cycles per truck passage, which is greater than one for transverse members and certain types of bridges.

To provide realistic fatigue specifications, the fatigue limit or the fatigue behavior at low stress ranges must be accurately known for various details. Therefore, it is suggested that comprehensive research be conducted to determine this information. The present study showed that the fatigue limit is very low for severe details, such as cover-plate ends. For less severe details, however, the fatigue limit is probably higher.

Effective methods of performing variable-amplitude random-sequence fatigue tests on large specimens were developed as a part of the program and are described herein.

CHAPTER ONE

INTRODUCTION AND RESEARCH APPROACH

INTRODUCTION

Highway bridges are subjected to a large number of repetitive loads of different magnitudes that are caused primarily by the passage of vehicles. In most types of short- and medium-span bridges, each vehicle, especially a truck, produces a major stress cycle with superimposed vibration stresses that are much smaller than the major cycle. In long-span bridges, individual vehicles produce only very small stress cycles in the main members, but larger cycles may be produced when the entire bridge is subjected to lane loading during peak traffic. Thus, bridges are subjected to variable-amplitude stress cycles that generally occur in a random sequence.

Such stress cycles can cause fatigue failures. Consequently, to insure that the bridge will not fail prematurely by fatigue, present (*1*) and past highway bridge specifications give allowable fatigue stresses based on extensive constant-amplitude fatigue tests of different types of simulated bridge members similar to those tested in NCHRP Project 12-7 (*2, 3*) and on earlier constant-amplitude tests (*4*).

Little information, however, exists on the fatigue behavior of bridge members under variable-amplitude random-sequence loadings that simulate traffic on a bridge. Many references are available on variable-amplitude fatigue, but very few are directly applicable to bridges. Most of the earlier variable-amplitude tests (*5*) utilized block loadings in which the sequence of loads was fixed in a pattern much different from the random pattern caused by traffic. Many of the more recent variable-amplitude tests (*6*) have been conducted by controlling the variation of stress by a tape obtained by recording the stresses during the operation of some particular aircraft or piece of equipment. Neither of these types of results is directly applicable to bridges. Furthermore, almost all of the available references are for tests conducted on (1) small specimens that do not realistically simulate bridge members, (2) specimens of materials not widely used in bridges, and/or (3) prototypes of particular pieces of equipment.

NCHRP Project 12-12, therefore, was initiated to study the behavior of bridge members under simulated traffic loadings. The ultimate goal of this work is to assist in improving, and possibly liberalizing, present design methods and specifications for fatigue in highway and other bridges. However, to reach this goal, additional information beyond that obtained in Project 12-12 is needed. Specifically, information is needed on (1) the number and variation of truck loads and resulting stresses that occur in actual bridges and (2) the fatigue limit for various types of bridge members. Toward this end, extensive studies are being conducted by the Federal Highway and Transportation Administration (FHWA) (*7*) and others (*8* through *18*).

OBJECTIVES

The main objectives of Project 12-12 were to develop fatigue data on welded bridge members under variable-amplitude random-sequence stress spectrums, such as occur in actual bridges, and to develop an analytical method of predicting the fatigue behavior under variable-amplitude stress spectrums from constant-amplitude fatigue data. Other objectives were to (1) determine the effect of type of detail, type of steel, and dead-load (minimum) stress on the variable-amplitude fatigue behavior; (2) determine the fatigue behavior for bridge members subjected to a very large number (above 30 million) of small variable-amplitude stress cycles; (3) study crack-growth behavior under variable-amplitude loadings and relate this behavior with the over-all fatigue life of bridge members; (4) make a preliminary evaluation of the effect of vibration stresses superimposed on the major stress cycles; (5) establish the effect of the number of different load levels and the sequence length used in controlling variable-amplitude tests; and (6) develop effective methods of performing variable-amplitude random-sequence fatigue tests on large specimens.

RESEARCH PLAN

Stress Spectrums

At the beginning of the program, all available results of field measurements of the stresses in highway bridges under traffic loadings were assembled. including 51 sets of data covering 37,000 truck passages from 6 sources. As will be discussed in detail in Chapter Two, these results showed that the passage of a truck over a bridge produces a single major stress cycle with superimposed vibration stresses that are usually small enough to be neglected. The major stress cycles are added to a constant minimum stress corresponding to the dead load. Thus each major stress cycle varies from the dead-load stress to a maximum that depends on the size of the truck. The difference between the maximum and minimum stress for a cycle is defined as the stress range, S_r. Therefore, the stress spectrums used in the fatigue tests were defined in terms of a constant minimum stress, $S_{\min}$, and the frequency of occurrence of stress ranges, S_r, of various magnitudes.

The frequency of occurrence was defined by two parameters: (1) the modal stress range, S_{rm}, which is the stress range that occurs most frequently and is slightly above the mean stress range for the spectrum, and (2) the dispersion ratio, S_{rd}/S_{rm}, which defines the dispersion. or variation, of the stress range in the spectrum. The dispersion ratio is a measure of the width of a frequency-of-occurrence graph.

Specimens

Stress spectrums defined by the three parameters—S_{min}, S_{rm}, and S_{rd}/S_{rm}—were applied to several different types of specimens. First, 84 plate specimens with a simulated cover plate were tested to aid in planning subsequent beam tests and to study several secondary test parameters. To obtain the approximate lower bound for the variable-amplitude fatigue strength of fabricated bridge members, 156 beams with partial-length cover plates were tested. Sixty-three welded beams without cover plates were tested to obtain the approximate upper bound. Wedge-opening-loading (WOL) specimens were tested to study fatigue crack growth under variable-amplitude loading. Two different structural steels (A514 and A36) encompassing the range of yield strengths of available bridge steels were used for the beam specimens. Only A514 steel was used for the plate and WOL specimens.

Originally, only one type of cover-plate beam detail was planned; however, the results of 27 sets of beams showed that the fabrication technique used (welding the cover plate to the flange plate before the assembly was welded to the web) for this detail produced unconservative results that differed from those of past studies (*2*). Consequently, after pilot tests were conducted on a few beams with two different cover-plate details, the remaining cover-plate beams were modified to obtain conservative results comparable with past experience (*2*). In addition, cover plates were added to some welded beams that had originally been intended to be tested without cover plates, and thus three different cover-plate beam details were tesed.

The following terminology will be used throughout the report to identify the different specimen and beam details. A complete description of these details is given later. "Cover-plate beams" refer to welded beams with partial-length cover plates. In cover-plate-beam detail A, the cover plates were welded to the flange plates by longitudinal fillet welds along both edges, but not across the cover-plate ends, and the assembly was then fillet welded to the web. This is the fabrication procedure that resulted in longer fatigue lives. (The longer lives apparently resulted from compressive residual stresses produced at the ends of the longitudinal fillet welds joining the cover plate to the flange plate, by shrinkage of the fillet welds that were made subsequently to join the assembly to the web.) In detail B, the flanges first were fillet welded to the web, and then the cover plates were welded to the flange plate by longitudinal fillet welds along both edges but not across the ends. Detail C beams were obtained either by cross-welding the cover-plate ends in detail A (that is, by placing a fillet weld across the cover-plate end) or by adding cover plates with welds across the ends to some welded beams. "Welded beams" refer to fabricated beams without cover plates. "Cover-plate specimens" (cover-plate S) refer to plate specimens with a simulated partial-length cover plate welded to one side only.

Experiment Design

The original plan for the main fatigue testing program is given in Table 1. Factorials of the three parameters—S_{min}, S_{rm}, and S_{rd}/S_{rm}—were planned for the different types of details and steels. In addition to these main factorial experiments, a few other tests, not shown in Table 1, were devised.

The original plan (see Table 1) was followed for the cover-plate specimens; however, because of the changes in cover-plate beams mentioned earlier, the plan for the beams was modified, as summarized in Table 2. Each set listed in the table represents three tests under the same stress spectrum. As in the original plan, the main part of the program consisted of factorials of S_{rm}, S_{rd}/S_{rm}, and S_{min} for different types of details and steels; but, in the modified plan, full

TABLE 1

SUMMARY OF ORIGINAL FACTORIAL TEST PLAN

Cover-Plate Specimens

A514 Steel		
S_{min}	S_{rm}	S_{rd}/S_{rm}
0	10	0
10	20	0.5
	30	1.0

Cover-Plate Beams

A514 Steel			A36 Steel		
S_{min}	S_{rm}	S_{rd}/S_{rm}	S_{min}	S_{rm}	S_{rd}/S_{rm}
0	10	0	0	10	0
10	20	0.5	10	20	0.25
	30	1.0			0.50

Welded Beams

A514 Steel			A36 Steel		
S_{min}	S_{rm}	S_{rd}/S_{rm}	S_{min}	S_{rm}	S_{rd}/S_{rm}
-10	20	0	-10	20	0
0	30	0.5	0	30	0.25
	40	1.0			0.50

All stresses S_{min} and S_{rm} are in ksi.

Conversion Factor

1 ksi = 6.89 MPa

TABLE 2

SUMMARY OF FINAL TEST PLAN

Detail	Steel	S_{min}	Factorials* S_{rm}	Factorials* S_{rd}/S_{rm}	Sets**	Experiment
Cover Plate C	A514	10	10,20,30*	0,0.5,1.0*	8	Main Factorial
Cover Plate C	A514	10	2,3	1.0	2	Long Life
Cover Plate C	A514	0	10	0,1.0	2	Different S_{min}
Cover Plate B	A514	0	10	0,1.0	2	Different Fabrication
Cover Plate C	A36	0	10,20	0,0.25,0.50	6	Main Factorial
Cover Plate C	A36	0	(5,40)	(0.50,0)	2	SN Curve Extensions
Cover Plate C	A36	10	10	0,0.50	2	Different S_{min}
Welded Beam	A514	0	20,30,40*	0,0.5,1.0*	8	Main Factorial
Welded Beam	A514	0	(10,80)	(1.0,0)	2	SN Curve Extensions
Welded Beam	A36	-10	20,30*	0,0.25,0.50*	5	Main Factorial
Welded Beam	A36	-10	(12,50)	(0.50,0)	2	SN Curve Extensions
Welded Beam	A36	0	20,30*	0,0.25,0.50*	5	Main Factorial
Cover Plate A	A514	10	10,20,30*	0,0.5,1.0*	8	Main Factorial
Cover Plate A	A514	10	(4,60)	(1.0,0)	2	SN Extensions
Cover Plate A	A514	40	10,30	0,0.5	4	High S_{min}
Cover Plate A	A514	0	10,20,30*	0,0.5,1.0*	8	Main Factorial
Cover Plate A	A36	10	10,20*	0,0.25,0.50*	5	Main Factorial

* All combinations of the listed factorials were tested except factorials identified by the asterisk. For example, in the first row of data, a test was not performed at S_{rm} = 30 and S_{rd}/S_{rm} = 1.0. Factorials of the parameters enclosed by parentheses were not tested; instead, one set was tested at first listed values of S_{rm} and S_{rd}/S_{rm} and a second set was tested at the second listed values of these parameters.

** Each set included three individual tests under the same stress spectrum. Stresses in ksi.

Conversion Factor

1 ksi = 6.89 MPa

factorials were not tested for each of two different values of S_{min}. Instead, partial factorials (identified as "Different S_{min}" in Table 2) were performed at some values of S_{min} that were originally intended to have full factorials. The factorial variations were selected to provide the widest possible range of the parameters within the limitations that (1) the highest nominal stress in the spectrum must be less than the yield strength, and (2) the minimum stress must be greater than $-S_{rm}/2$ to reduce the chances of premature fatigue failures in the wrong flange of the beam.

The two limitations greatly restrict the possible choices of stress spectrums, especially for the A36-steel beams. Nevertheless, an adequate variation of the main parameters was possible. The values of S_{min} selected for the program provide both positive and negative values, as well as a common value of zero for both cover-plate and welded beams. The use of a positive (tensile) S_{min} for the welded beams would have resulted in maximum stress values above the yield strength of A36 steel for most of the factorials.

Idealized SN curves for a typical factorial (for A514 cover-plate beams) are shown in Figure 1. The solid circles correspond to the stress spectrums for the main factorial experiment. The results for the different values of S_{rd}/S_{rm} at a single value of S_{rm} permit the direct calculation of the ratio of the fatigue life for constant-amplitude loading to the life for two different variable-amplitude spectrums, each defined by a particular value of S_{rd}/S_{rm}. Three values of S_{rm} were used for the A514 beams, but only the lower two were used for the A36 beams because of their lower yield strength.

In addition to the tests in the main factorial experiment, individual tests were made to extend the SN curve for $S_{rd}/S_{rm} = 0$ to a higher S_{rm} and to extend the curve for $S_{rd}/S_{rm} = 1.0$ or 0.5 (the highest value for the particular steel) to a lower S_{rm}. These tests were made at one of the two S_{min} values for most types of beams and steels. Open circles in Figure 1 represent these tests for the A514 beams.

One set of tests was made on the A514-steel cover-plate C beams at a stress spectrum approximating the highest spectrum observed in field measurements. $S_{min} = 10$ ksi (69 MPa), $S_{rm} = 2$ ksi (14 MPa), and $S_{rd}/S_{rm} = 1.0$. This set was tested in such a way that a second set of data was obtained from the other end of the cover plate at S_{min} and S_{rm} values 50 percent greater and at the same value of S_{rd}/S_{rm}. The results provide six data points at very long lives on the lowest SN curve in Figure 1, and thus show whether the curve for the main factorial experiment can be extrapolated to long lives. The tests were performed only on the cover-plate C beams because they have the most critical detail for fatigue loadings. Additional tests on the other details could not be included in the program because of the very long time required.

Because of previously mentioned limitations, the main factorial experiments were conducted at relatively low values of S_{min}, the highest value being 10 ksi. To further investigate the effect of S_{min}, a partial factorial experiment was duplicated at $S_{min} = 40$ ksi (275 MPa). These tests are identified as "High S_{min}" in Table 2.

In addition to the main factorial test for the cover-plate specimens, four sets of six specimens were used to study

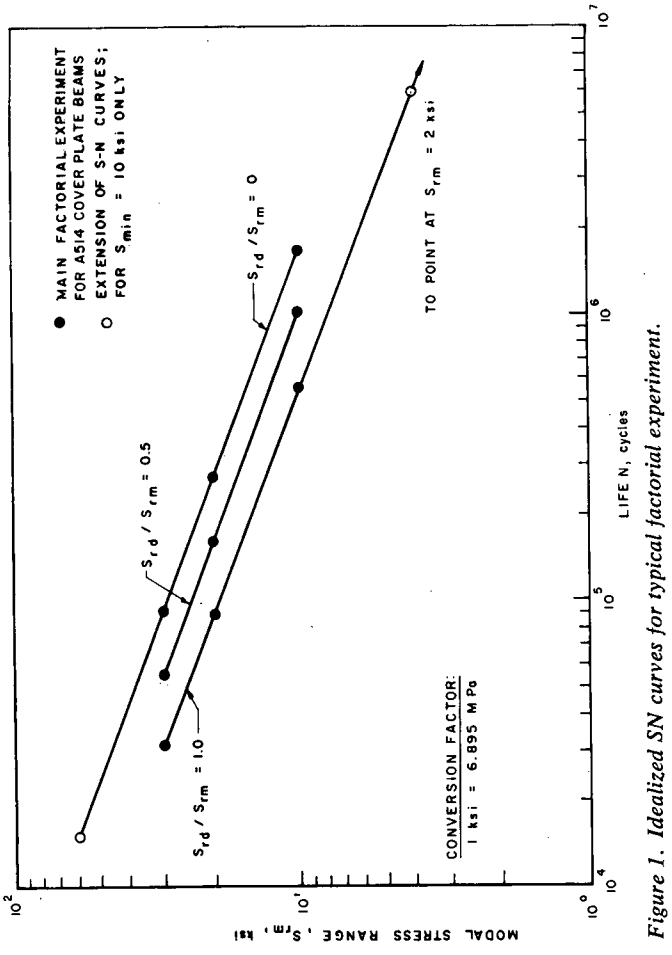

Figure 1. Idealized SN curves for typical factorial experiment.

the effects of a finite random-sequence length and the number of individual load levels that were used to simulate a continuous probability-density curve and a random sequence of infinite length. Also, two sets of three specimens were used to investigate the effect of small vibration stresses superimposed on major stress cycles.

Crack-growth tests were performed on WOL specimens of A514 steel under loadings outlined in Table 3, which are comparable to the loadings in the fatigue tests. The main objective of the crack-growth tests was to obtain curves of crack-growth rate, da/dN, versus the stress-intensity range, K_r. The stress-intensity range for this specimen increases

TABLE 3

CRACK-GROWTH TEST PLAN

Specimens	P_{min}, lb	P_{rm}, lb	P_{rd}/P_{rm}	Sequence	Range of K_{min}, ksi $\sqrt{in.}$	Range of K_r, ksi $\sqrt{in.}$
2	200	800	0	-	2.8 - 11.8	11.1 - 47.1
2	200	3800	0	-	2.8 - 6.4	52.7 - 122.5
2	3800	800	0	-	52.7 - 115.4	11.1 - 24.3
1	3800	3800	0	-	52.7 - 80.6	52.7 - 80.6
1	100	800	0.5	Random	1.4 - 4.2	11.1 - 33.2
1	500	800	1.0	Random	7.0 - 23.0	11.3 - 37.0
1	200	800	1.0	Ascending	3.0 - 6.5	11.9 - 25.8
1	200	800	1.0	Descending	2.8 - 6.5	11.1 - 27.6
1	200	800	1.0	asc/disc	2.8 - 6.8	11.1 - 27.3

* Symbols are explained in text.

Conversion Factors

1 lb = 4.448 N

1 ksi $\sqrt{in.}$ = 1.0998 MPa $\sqrt{m}$

as the crack length increases if the cyclic load amplitude is held constant. Thus, a single test provides data for a range of K_r values. In the present program, constant-amplitude data were obtained for K_r values from about 10 to 100 ksi$\sqrt{\text{in.}}$ (11 to 110 MPa$\sqrt{\text{m}}$) by testing two specimens at different load amplitudes. Such tests were performed at a high and low minimum load to show whether minimum load has a significant effect. P_{min} was held constant during a test, but K_{min} varied because it is a function of crack length. Variable-amplitude tests were performed under loading spectrums corresponding to the values of S_{rd}/S_{rm} used in the cover-plate specimen tests. Several different load sequences, including a random sequence, were used to determine the effect of sequence on the crack growth.

SPECIMENS AND BEAMS

The material properties and fabrication methods for the specimens and beams are summarized in this section. A detailed description is given in Appendix A and in a previous report (*19*). All specimens and beams were fabricated from material that satisfied the chemical- and mechanical-property requirements for either ASTM A36 or A514 steel. The fabrication methods generally followed normal bridge practice. The quality of workmanship was comparable to that required by state highway department specifications and was similar to that reported for Project 12-7.

Welding procedures conformed to the AWS bridge specifications (*20*), and the welders and welding operators were qualified in accordance with these specifications. All tack and manual welds were made with E7018 electrodes. AWS F71-EL12 wire-flux combination was used for all submerged-arc fillet welds on A36 steel, and F72-EM12K wire-flux combination was used on A514 steel.

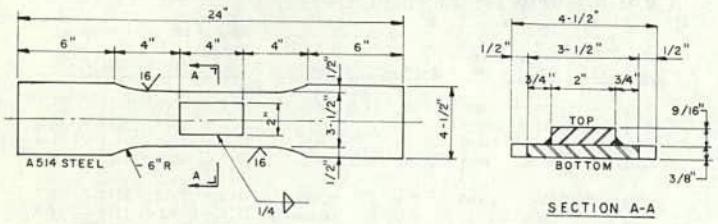

Nominal Section Modulus	Top:	0.337 in.^{3}	Bottom:	0.441 in.^{3}
Nominal Moment of Inertia		0.179 in.^{4}		
Mean Section Modulus	Top:	0.352 in.^{3}	Bottom:	0.461 in.^{3}
Mean Moment of Inertia		0.191 in.^{4}		

Conversion Factor:
1 in. = 25.4 mm

Figure 2. Cover-plate specimens.

Cover-Plate Specimens

A sketch and photograph of the cover-plate specimens are shown in Figure 2 The cover plate was submerged arc welded to the main plate (or simulated flange plate) along both longitudinal edges, but no welds were placed across the ends of the cover plate. The weld shrinkage caused a slight bowing of most of the specimens that was removed by straightening within the center 3½ in. (8.9 cm). This straightening had no significant effect on the fatigue behavior of the specimens. Visual and magnaflux inspections and sectioning did not reveal any cracking at the weld ends.

Wedge-Opening-Loading Specimens

A sketch of the WOL specimens is shown in Figure 3. The specimens were machined from ⅜-in.-thick (9.5-mm) plates of A514 steel, such that the crack propagation was transverse to the direction of plate rolling.

Welded Beams

A sketch and photograph of a welded beam are shown in Figure 4. The flange and web plates were oxygen cut from larger plates, assembled, tack welded, and then joined by submerged-arc fillet welds. Polished sections of these welds indicated that they are comparable in quality to welds normally found in bridges.

Cover-Plate Beams

A sketch and photograph of a cover-plate beam without welds across the cover-plate ends are shown in Figure 5. All original cover-plate beams were fabricated according to this sketch. Submerged-arc welding was used for all fillet welds. Since the fabrication specifications did not specify the assembly sequence (this is not specified in most bridge-fabrication specifications; in practice, cover plates are normally used only on rolled beams, which are not available in A514 steel, and thus there is no normal practice for attaching cover plates to welded beams), the fabricater chose to weld the cover plate to the flange plate first and then to weld this assembly to the web. Beams fabricated in this way are the cover-plate A beams referred to earlier. Visual and magnaflux inspections of weld ends did not reveal any cracking at the weld ends.

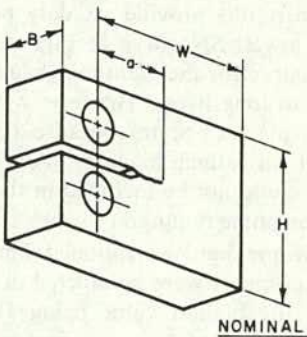

	NOMINAL DIMENSIONS
a - CRACK DEPTH	a = 1.0 inch (25.4 mm)
B - SPECIMEN THICKNESS	B = 0.37 inch (9.4 mm)
W - SPECIMEN WIDTH	W = 2.55 inches (64.77 mm)
H - SPECIMEN HEIGHT	H = 2.48 inches (62.99 mm)

Figure 3. Wedge-opening-loading (WOL) specimens.

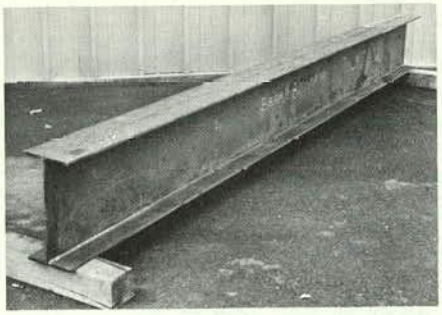

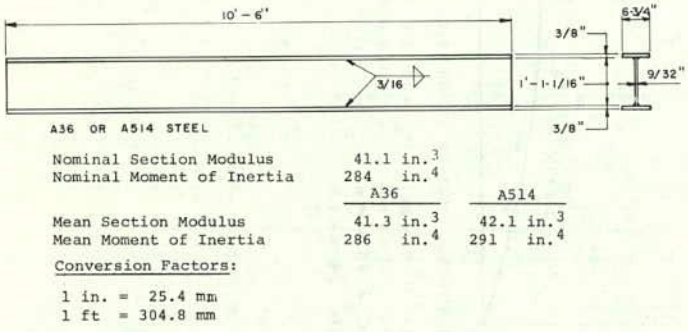

Nominal Section Modulus	41.1 in.^{3}		
Nominal Moment of Inertia	284 in.^{4}		
	A36	A514	
Mean Section Modulus	41.3 in.^{3}	42.1 in.^{3}	
Mean Moment of Inertia	286 in.^{4}	291 in.^{4}	

Conversion Factors:

1 in. = 25.4 mm
1 ft = 304.8 mm

Figure 4. Welded beams.

Because the fatigue results for these cover-plate A beams were not consistent with past results, as mentioned earlier, it was decided to modify some of these beams by placing manual fillet welds across the cover-plate ends. Also, some welded beams were modified by adding cover plates with welds across the ends. The cover plates were attached by submerged-arc fillet welds along both edges, but not across the cover-plate ends. Thus, these beams differ from the cover-plate A beams only in the assembly sequence. Both types of modified beams are the cover-plate C beams mentioned earlier. Two sets of welded beams were also modified by adding cover plates without welds across the ends. These are the cover-plate B beams mentioned earlier.

TEST PROCEDURES AND SETUP

The test procedures and setup summarized in this section are described in more detail in Appendix B and in a previous report (*21*). In all tests, a closed-loop electrohydraulic system was used to apply the desired load spectrum. A punched tape that defined 500 individual loads satisfying the desired probability-density curve and arranged in a random sequence controlled each test; the 500-load block was cycled continuously throughout a test. A load cell was used to measure the actual applied load so that the system could correct any difference between this load and the load specified by the control tape.

In all tests except the crack-growth tests, the nominal dynamic stress at some location was the main test parameter. This stress was directly proportional to the load, which was used to control the test, and the relationship between the two was established by a static calibration of each specimen or beam that was tested. (The stress caused by a given cyclic load is theoretically larger than the stress caused by a static load of the same magnitude, but for the test conditions in the present program the difference was very small and was neglected (*21, 22*).) Thus, the effects of any deviations of the actual beam dimensions and span from the nominal values were accounted for by the calibration. Electric-resistance strain gages were used to measure the strain during the calibration. The effect of residual stresses in the beams on the calibration was properly accounted for by using the unloading portion of the calibration curve to establish the relationship between stress and load. All specimens and beams were properly aligned before calibration.

In the crack-growth tests, the stress intensity at the crack tip was the main parameter and increased as the crack length increased, even though the load amplitude was held constant. The relationship between the load and stress intensity has been established theoretically (*23*) for given specimen geometries, and the specimens were accurately machined to the desired geometry. Therefore, no static calibration was required.

During each fatigue test the readout from the load cell was monitored periodically to check that the system was functioning properly. Near the beginning of the test, the readout from the strain gages was recorded for a 500-cycle loading block to provide a permanent record of the applied stress spectrum. Crack growth was recorded at convenient time intervals; visual observations, usually magnified, were made to determine the crack length. Flat white paint was sprayed on the specimen or beam at critical locations to highlight the cracks. The region containing the major crack was cut from the beam and retained after failure.

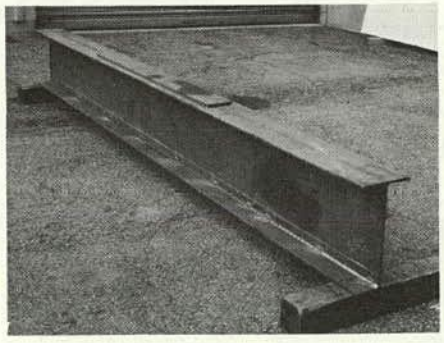

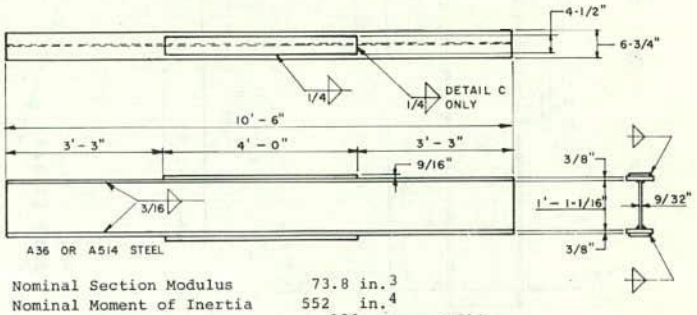

Nominal Section Modulus	73.8 in.^{3}		
Nominal Moment of Inertia	552 in.^{4}		
	A36	A514	
Mean Section Modulus	74.3 in.^{3}	75.7 in.^{3}	
Mean Moment of Inertia	556 in.^{4}	567 in.^{4}	

Conversion Factors:

1 in. = 25.4 mm
1 ft = 304.8 mm

Figure 5. Cover-plate beams.

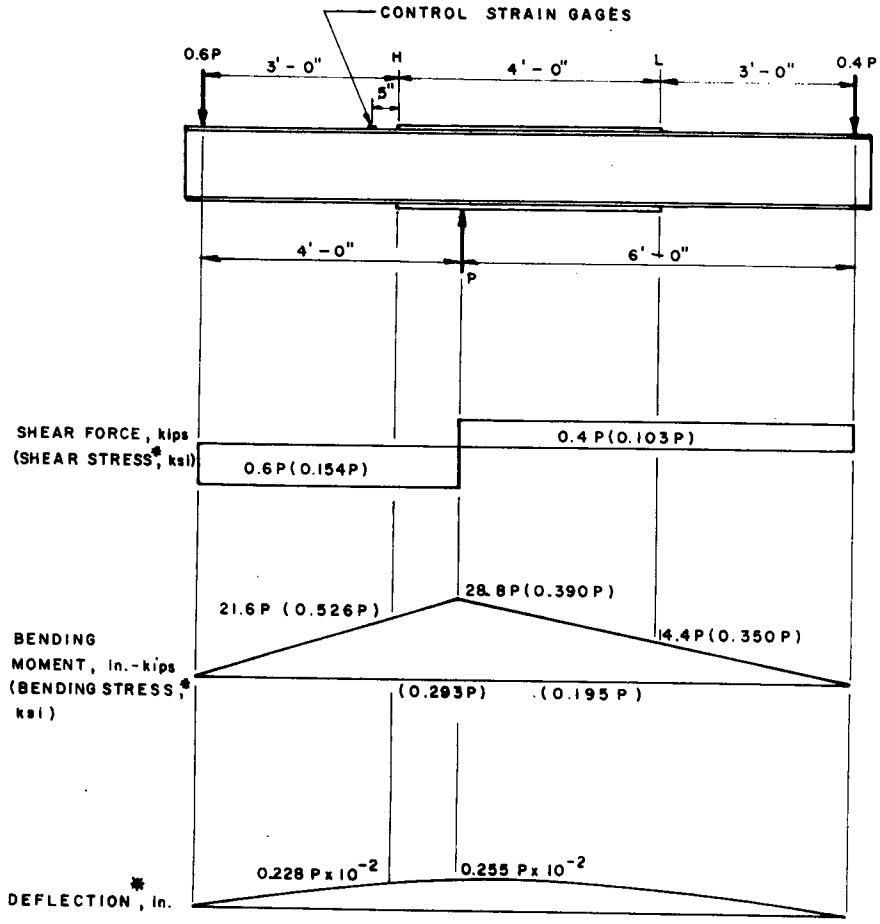

* BASED ON NOMINAL PROPERTIES

NOTES: LOAD P IN kips
1 ft = 304.8 mm
1 in. = 25.4 mm
1 kip = 4448.2 N

MODULUS OF ELASTICITY E = 29,000 ksi
1 ksi = 6.895 MPa
1 in.-kip = 113.0 N-m

Figure 6. Loading diagrams for cover-pate beams.

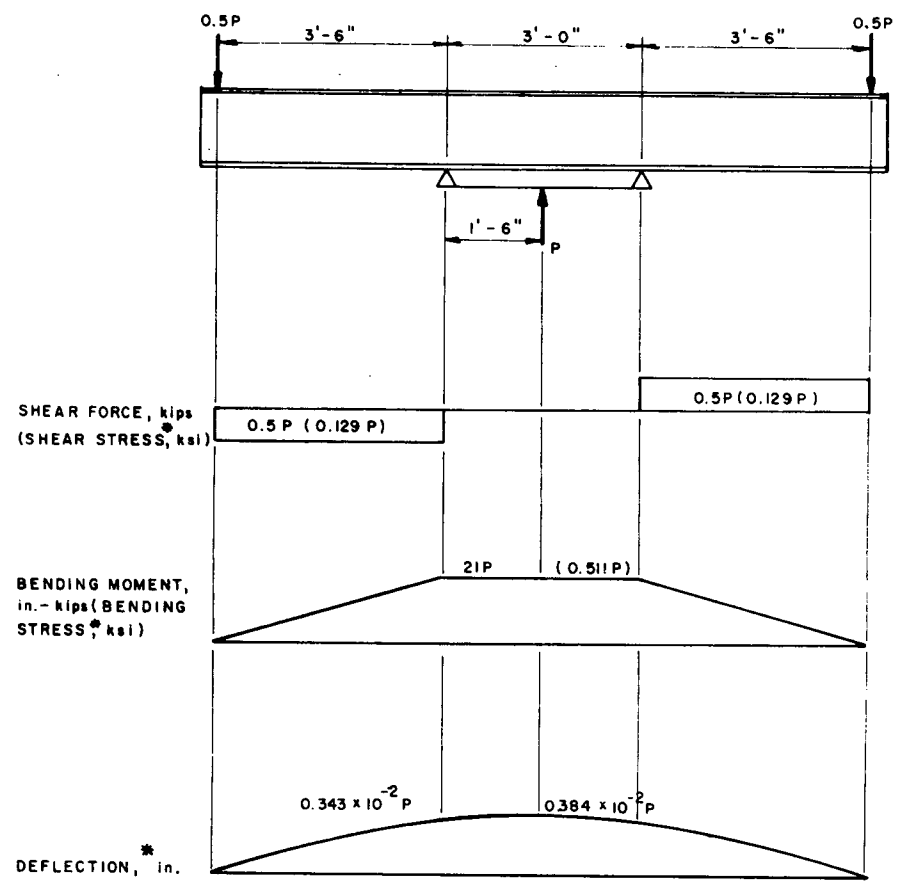

* BASED ON NOMINAL SECTION PROPERTIES

NOTES: LOAD P IN kips
1 ft = 304.8 mm
1 in. = 25.4 mm
1 kip = 4448.2 N

MODULUS OF ELASTICITY E = 29,000 ksi
1 ksi = 6.895 MPa
1 in.-kip = 113.0 N-m

Figure 7. Loading diagrams for welded beams.

Beam Tests

The beams were tested with a 10-ft (3-m) span as shown in Figures 6 and 7. For the cover-plate beams, the nominal bending stress at the end of the cover plate was the main test parameter. The stress at the test end, H, of the cover plate was 50 percent higher than the stress at the other end, L. For the welded beams, the nominal bending stress on the outer fibers of the beam in the central constant-moment portion of the span was the main test parameter. The bending stress in the flange-web fillet welds was about 5 percent less.

The beams were loaded upward in a test frame to facilitate observation of cracks on the tension flange and installation of the beams by an overhead crane. Three beams were tested simultaneously under the same stress spectrum. A separate jack and load cell was used for each beam. Automatic controls in the system assured that all three beams would reach their programmed peak loads. Usually, all three beams in a set were tested to failure before tests were started on any beam from the next set.

The average testing speed for a 500-cycle loading block depended on the stress spectrum being used for that test and ranged from about 1 to 8 Hz. The speed was slower for the higher values of S_{rm}. Within a variable-amplitude 500-cycle loading block the time for each cycle was roughly proportional to the maximum amplitude for that cycle, although cycles with very high amplitudes required even more time. The programmed stress cycles were sinusoidal in shape. The shape of the actual stress cycles was somewhat distorted from the programmed shape.

The test was stopped by a limit switch set about ¼ in. (6 mm) beyond the maximum deflection of the uncracked beams. When the limit switch was activated, a crack had propagated throughout the flange and into the web, usually to a depth of between ¼ and ½ of the web depth. After the crack extended over the entire flange, the beam could sustain only a relatively few cycles before the web cracked and the test stopped.

After the beams in the long-life tests had failed at the high-stress ends, H, of the cover plates, the remaining portion was placed in a new position in the test frame such that the low-stress ends, L, of the cover-plates were exposed to the same stress conditions as during the original test. The test was then continued and the total number of cycles to failure for the low-stress end of the cover plate was recorded. Thus, test results for two different values of S_{rm} were obtained from one set of beams.

Cover-Plate Specimen Tests

The cover-plate specimens were axially loaded in a 300-kip (1.33-MN) closed-loop testing machine (that is, the main plate of the specimen was concentrically gripped and loaded). However, the transfer of stress from the main plate into the cover plate and the eccentricity caused by a cover plate on only one side of the main plate resulted in a nonuniform stress over the cross section, as discussed in Appendix B and in Ref. (*24*). The tensile stress at the longitudinal centerline on the front face of the main plate, ⅛ in. (3 mm) from the end of the cover plate, was chosen to represent the nominal stress on the specimen. This stress corresponds roughly to the nominal stress at the end of the cover plate in the beams and is the main parameter in the test. This sress is about 40 percent greater than the stress at the same location on the opposite face.

The time for each cycle in a variable-amplitude test was approximately the same. The testing speed ranged from about 5 to 11 Hz for different spectrums, but was equal to 7.5 Hz for most spectrums. The stress cycles were sinusoidal in shape.

WOL-Specimen Tests

The WOL specimens were tested in a 50-kip (0.22-MN) closed-loop testing machine. Magnified visual observations, aided by calibrated indentations on the specimen, were used to measure crack length.

CHAPTER TWO

FINDINGS

STRESS SPECTRUMS

The review of field data, discussed in detail in Appendix C, showed that the passage of a vehicle over a bridge produces a single major stress cycle with superimposed vibration stresses as idealized in Figure 8a. The vibration stresses may continue after the vehicle has left the bridge. For most types of bridges, the vibration stresses are much smaller than illustrated in Figure 8a and can be neglected in fatigue design. Thus, the passage of a vehicle causes one major stress cycle that can be represented as shown in Figure 8b. However, for some types of bridges, especially cantilever (suspended-span) girder bridges, the passage of a vehicle may produce many large stress cycles as a result of the vibration characteristics of the bridge. This type of behavior, shown in Figure 8c, was not included in the testing program.

Each major stress cycle can be defined by two parameters: (1) the stress range, S_r, and (2) the minimum stress, S_{min}, corresponding to dead load. The stress range, of course, varies with the size of the vehicle, but the minimum stress corresponding to dead load remains essentially constant throughout the life of the bridge. Therefore, the stress spectrum, or stress history, for a particular point in a bridge can be defined in terms of the frequency of occurrence of stress ranges of different magnitudes and the magnitude of the constant minimum stress. As illustrated in Figure 9, the frequency of occurrence of the idealized stress

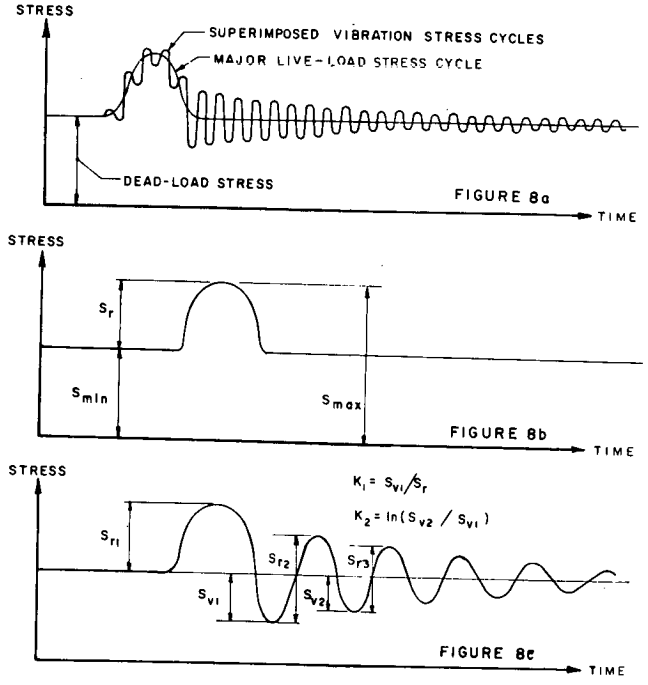

Figure 8. Idealized load traces for passage of a single vehicle.

ranges can be defined by a histogram, or bar graph, in which the height of the bar represents the percentage of stress ranges within an interval represented by the width of the bar. If the interval used to plot a given set of data were doubled, the height of the bar would also be approximately doubled. Hence, the shape of the histogram depends on the interval selected.

Frequency-of-occurrence data can be normalized by dividing the height of each bar by the width of the bar to obtain a probability-density curve, as shown at the bottom of Figure 9 and discussed in Appendix D. Thus, data plotted with different intervals can be related. The area under the probability-density curve between any two values of S_r represents the fraction of stress ranges within that interval. Since the probability-density curve represents the complete spectrum, the total area under the curve equals 1.0.

As discussed in Appendix C, available field data were used in selecting a single nondimensional mathematical expression that can be used to represent almost any highway-bridge stress histogram. Fifty-one sets of frequency-of-occurrence data from six sources were used for this purpose. Data covering 37,000 truck passages over 15 short-span bridges of 6 different types were included. All bridges are on Interstate or U.S. routes in semirural or metropolitan locations.

Two different mathematical expressions were considered: (1) a two-parameter Rayleigh probability-density function

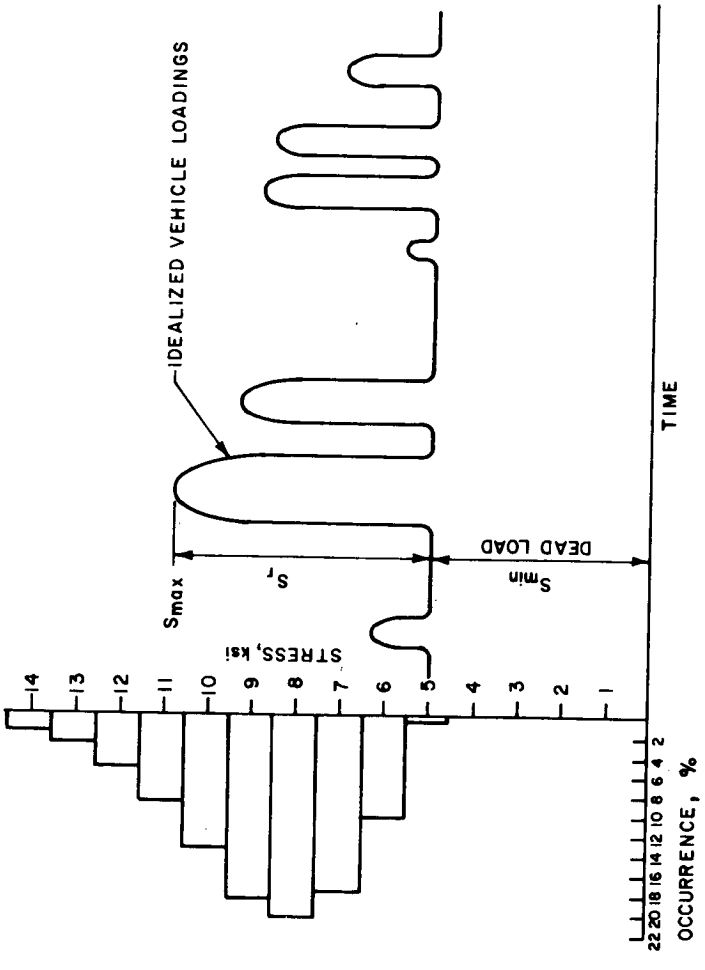

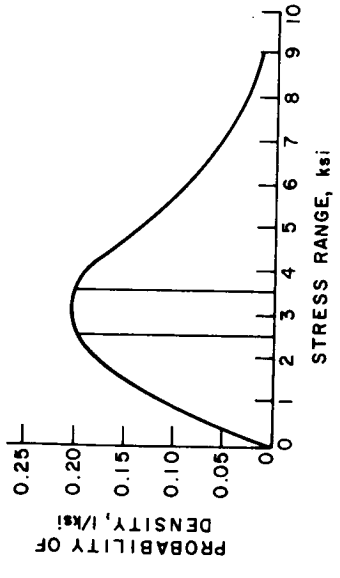

Figure 9. Frequency-of-occurrence data.

and (2) a three-parameter Erlang probability-density function. Curves of both types were fit to all 51 sets of data, and the sum of the squares of the residuals (algebraic difference between the actual and calculated frequency of occurrence) was calculated to indicate the closeness of fit. Although the three-parameter Erlang curve provided a slightly closer fit, the Rayleigh curve was selected for use in the test program because it is simpler and provides an adequate fit.

The single mathematical expression

$$p' = 1.011x' e^{-(\frac{1}{2})(x')^2} \quad (1)$$

defines the family of Rayleigh curves used in the testing program; in this equation

$$x' = \frac{S_r - S_{r\min}}{S_{rd}} \text{ and } p' = pS_{rd} \quad (2)$$

where p is the probability density (units of 1/ksi), e is the Napierian (2.7183) base, $S_{r\min}$ is the lowest stress range in the spectrum, and S_{rd} equals $S_{rm} - S_{r\min}$. In Figure 10, Eq. 1 is plotted both in terms of the nondimensional parameters p' and x' (see top portion) and in terms of the dimensional parameters p and S_r (see middle portion). As illustrated by this second plot, a particular curve from the family can be defined by two parameters: (1) the modal stress range, S_{rm}, which corresponds to the peak of the curve; and (2) the parameter S_{rd}, which is a measure of the width of the curve, or the dispersion of the data. By changing the value S_{rm}, the curve can be shifted sideways; and by changing S_{rd}, its width can be changed. Thus, a curve can be fit very closely to a great variety of actual frequency-of-occurrence data, although it may not closely fit a distribution with more than one peak. Since the Rayleigh curves have a positive skew, the values of the median, mean, and root mean square (RMS) of the spectrum are to the right of the modal value by the amounts shown in Figure 10. The RMS is the square root of the mean of the squares of the individual values of x' or S_r. The probability-density curves used in the testing program are defined by S_{rm} and S_{rd}/S_{rm}. A set of curves for a single value of S_{rm} and the four values of S_{rd}/S_{rm} from the testing program is shown at the bottom of Figure 10; $S_{rd}/S_{rm} = 0$ corresponds to constant-amplitude loading in which all cycles are at S_{rm}. The control tapes used in the fatigue testing program define 500 individual stress ranges that satisfy one of these Rayleigh probability-density curves and are arranged in a random sequence such as would occur on most actual bridges. Details of the development of these tapes are given in Appendix C.

FATIGUE-TEST RESULTS

The fatigue-test results are tabulated in Appendix E for the cover-plate specimens and the beams; the cycles to the first observed crack and to failure, as well as the size and location of observed cracks at various lives, are included. The distribution of failure locations for the welded beams of A36 and A514 steel is shown in Figures E-4 and E-5, respectively. The types of cracks in the beams are classified into five categories: (1) edge cracks in the flanges of welded or cover-plate beams, (2) intersection cracks spreading outward from the flange-web junction in the welded beams, (3) crescent-shaped cracks initiating at the ends of the welds in the cover-plate A and B beams and the cover-plate specimens, (4) long cracks occurring along the cross weld in the cover-plate C beams, and (5) peeling cracks propagating longitudinally along the throat of the fillet weld connecting the cover plate to the flange in the cover-plate beams. A photograph of each type of crack is included in Appendix E.

Except for the peeling cracks, the initiation and growth of all beam cracks were similar to those in the Project 12-7 study (*2*) and will not be described. The peeling cracks shown in Figure E-2 occurred only in a few cover-plate A beams tested at very high maximum stresses; apparently, the cracks resulted from the high shear in the fillet welds near the end of the cover plates as a result of the rapid buildup of force in the cover plate in that region. This type of crack initiated in the weld metal at the end of the longitudinal weld and propagated along this weld without entering either the flange or cover-plate material. Cover plates in bridges are normally extended a sufficient distance beyond the theoretical cutoff point to develop the full force in the cover plate without overstressing the fillet welds in shear. Therefore, this type of cracking is not likely to occur in bridges.

As discussed in Appendix E, fretting failures occurred at the load points in the first set of welded beams that were tested. Therefore, the test setup was modified by adding paper shims, and a duplicate set of beams (A36 steel, set 121) was tested under the same stress conditions. This duplicate set did not show any signs of fretting at the load points but had approximately the same life as the set with fretting failures. Only the results for the duplicate set are included in the tabulated test results. There was no evidence of fretting during any of the subsequent tests.

DISCUSSION OF RESULTS

The results of the fatigue and crack-growth tests are discussed as follows; details are given in Appendixes F and G. The statistical concepts used are explained in Appendix D.

SN Curves

Past studies (*2*) showed that fatigue data for simulated bridge members can be satisfactorily represented by a log SN curve in which the log of the number of cycles to failure, N, is plotted against the log of the stress range. Consequently, log SN curves were fit to the data for each of the different details in the testing program, except that the few available data for the cover-plate B beams were combined with the data for the cover-plate C beams because there was not a statistically significant difference between the two sets of data. Specifically, the modal stress range, S_{rm}, was used as the stress parameter, and a different curve was developed for each different value of S_{rd}/S_{rm}, or spectrum width.

The SN curves are defined in log form by

$$\log N = \log A - B \log S_{rm} \quad (3)$$

and in the normal form by

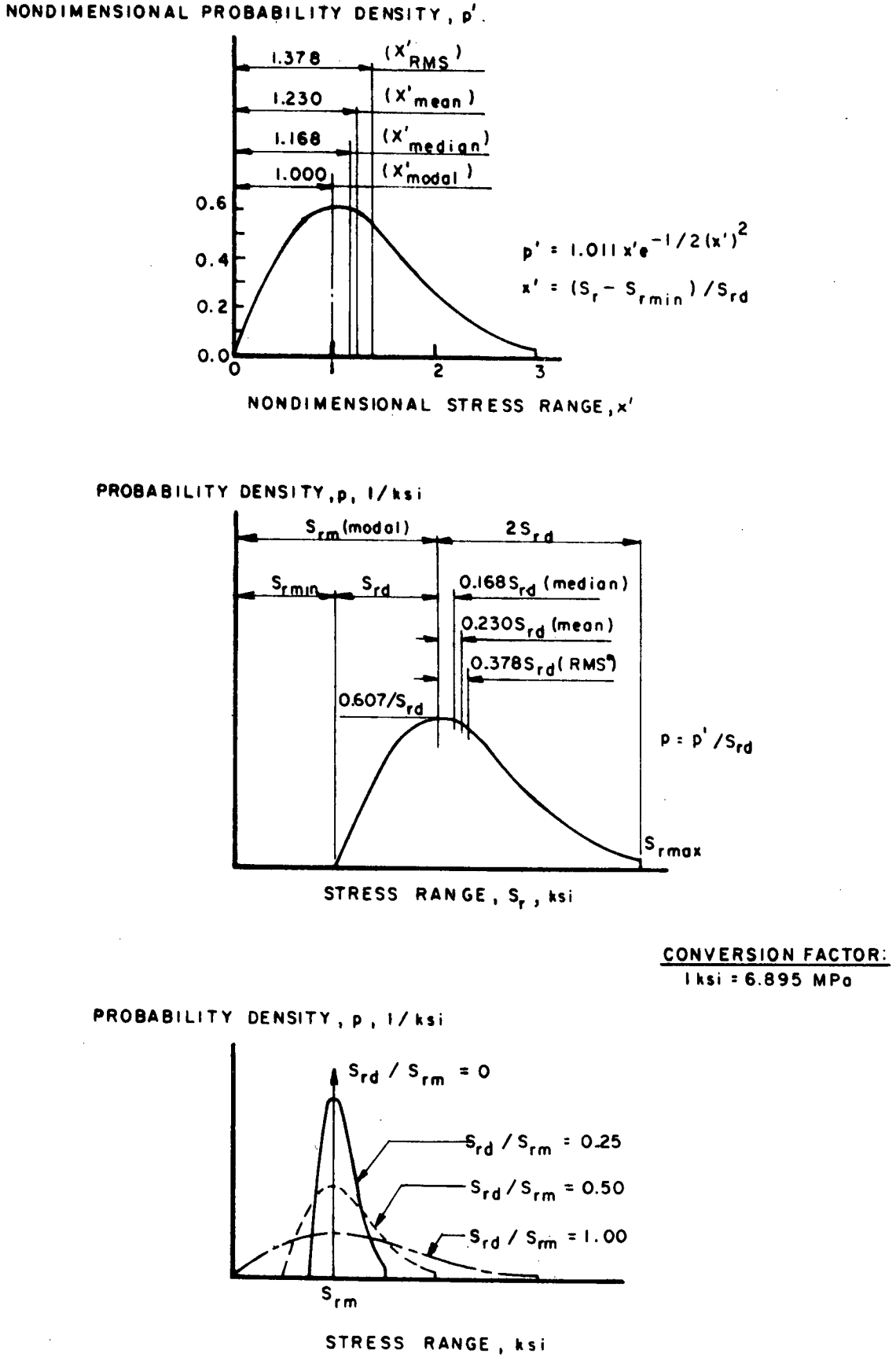

Figure 10. Characteristics of Rayleigh probability curves.

$$N = \frac{A}{S^B_{rm}} \quad (4)$$

As shown in Figure F-1, log A is the log-N-axis intercept of the log SN curve and B is the reciprocal of the slope of this curve (plotted conventionally).

Past studies (*2*) showed that the types of steel and minimum stress have a secondary effect on constant-amplitude fatigue results. Consequently, the results for both steels and for different minimum stress levels from −10 to +10 ksi (69 MPa) were grouped together in developing best-fit curves from Eq. 3. As discussed in Appendix F, a study showed that closeness of fit of the data represented by Eq. 3 could not be significantly improved by adding terms to Eq. 3 to account for the effects of secondary variables, and thus confirmed that it is reasonable to omit them. The few available data for cover-plate A beams with $S_{\min} = 40$ ksi (276 MPa), however, were not included with the other data for this detail because such a large $S_{\min}$ value was expected to have a significant effect. This expectation was confirmed for the cover-plate A beams, as detailed in Appendix F.

Best-fit log SN curves are shown in Figures 11 and 12 for the cover-plate C beams and welded beams, respectively, and represent the approximate lower and upper bounds, respectively, for the fatigue strength of fabricated bridge members. The SN curves for the other details and calculated values of the constants A and B are given in Appendix F. Generally, the scatter bands for the different values of S_{rd}/S_{rm} overlap. Therefore, to avoid clutter, individual data points and confidence limits for various curves were omitted. Furthermore, curves are shown within the range of test data only. The SN curves are roughly parallel and show that the life corresponding to a given S_{rm} decreases as S_{rd}/S_{rm} increases.

Semilog SN curves (log N vs. S_{rm}) were also fit to each set of data and showed that the log SN curves provide a slightly closer fit of the data than the semilog SN curves (see Appendix F).

Relationship Between Constant- and Variable-Amplitude Results

There are many ways of relating variable-amplitude fatigue data to constant-amplitude data; probably, the most convenient way for bridge applications is the effective stress range concept, which will permit the four separate lines in Figures 11 and 12 to be approximated by a single line relating the effective stress range, S_{re}, to the life, N. The effective stress range for a variable-amplitude spectrum is defined as the constant-amplitude stress range that would result in the same fatigue life as the variable-amplitude spectrum. Different methods of calculating S_{re} are discussed as follows and in more detail in Appendix F.

Effective Stress Range From Rayleigh Distribution

In the first method, which is based directly on the Rayleigh distribution described earlier, the effective stress range is given by

$$S_{re} = S_{rm} + C\,S_{rd} = S_{rm}\,(1 + C\,S_{rd}/S_{rm}) \quad (5)$$

in which the best-fit value of the correlation factor, C, is determined from available data. Thus, C defines a single stress range that has the same effect on fatigue behavior as the complete spectrum. If $C = 0.378$, S_{re} is the root mean square of the stress ranges in the spectrum; if $C = 0.230$, S_{re} is the mean of the stress ranges.

The variation of S_{re}/S_{rm} with the dispersion ratio, S_{rd}/S_{rm}, for these two values of C is shown in Figure 13. At a dispersion ratio of 0, which corresponds to constant-amplitude loading, $S_{re} = S_{rm}$ for both definitions of S_{re}. As the dispersion ratio increases—or, in other words, as the width of the spectrum becomes greater—S_{re} becomes increasingly larger than S_{rm}. At $S_{rd}/S_{rm} = 1.0$, the S_{re} corresponding to the RMS value is about 11 percent greater than the value corresponding to the mean.

Values of C were determined for various groups of test data by calculating the value of C that resulted in the best-fit SN curve for each group. Although C varies significantly for various cases (see Appendix F), the value of 0.378 (RMS) provides a reasonable approximation of C for practical purposes. The difference between this approximate value of C and the true value for a particular case has only a small effect on S_{re} and on the fatigue life.

Effective Stress Range by RMS

The root mean square (RMS) can be calculated for a spectrum defined by a stress-range histogram by fitting a Rayleigh probability-density curve to the histogram to get S_{rm} and S_{rd}, and then calculating S_{re} from Eq. 5 with $C = 0.378$. Alternatively, $S_{re\text{RMS}}$ can be calculated directly from the stress-range histogram by using the formula

$$S_{re\text{RMS}} = (\Sigma\alpha_i S^2_{ri})^{\frac{1}{2}} \quad (6)$$

in which S_{ri} is the ith stress range in the spectrum and α_i is the fraction of stress ranges of that magnitude.

Figures 14 and 15 show the best-fit SN curves and approximate 95-percent confidence limits for a single future test for the constant-amplitude tests of the cover-plate C beams and welded beams. (As indicated in Appendix D, these limits also approximate the 95-percent tolerance limits for the data.) Data points for both the constant- and variable-amplitude tests are also plotted; all variable-amplitude data points are transformed according to Eq. 5 with $C = 0.378$. The best-fit line and confidence limits are shown as solid and dashed lines, respectively, within the range of constant-amplitude data and are extended as dash-dot lines beyond this range. Similar curves for the other details are shown in Appendix F. The variable-amplitude data points generally fall within a scatter band bounded by the 95-percent confidence limits for the constant-amplitude data, which shows that the $S_{re\text{RMS}}$ satisfactorily relates constant- and variable-amplitude data. Furthermore, a statistical analysis generally did not show a statistically significant difference between the constant-amplitude data and the transformed variable-amplitude data.

Effective Stress Range by Miner's Law

Miner's Law has been widely used for many years to show the cumulative effect on fatigue life of stress cycles

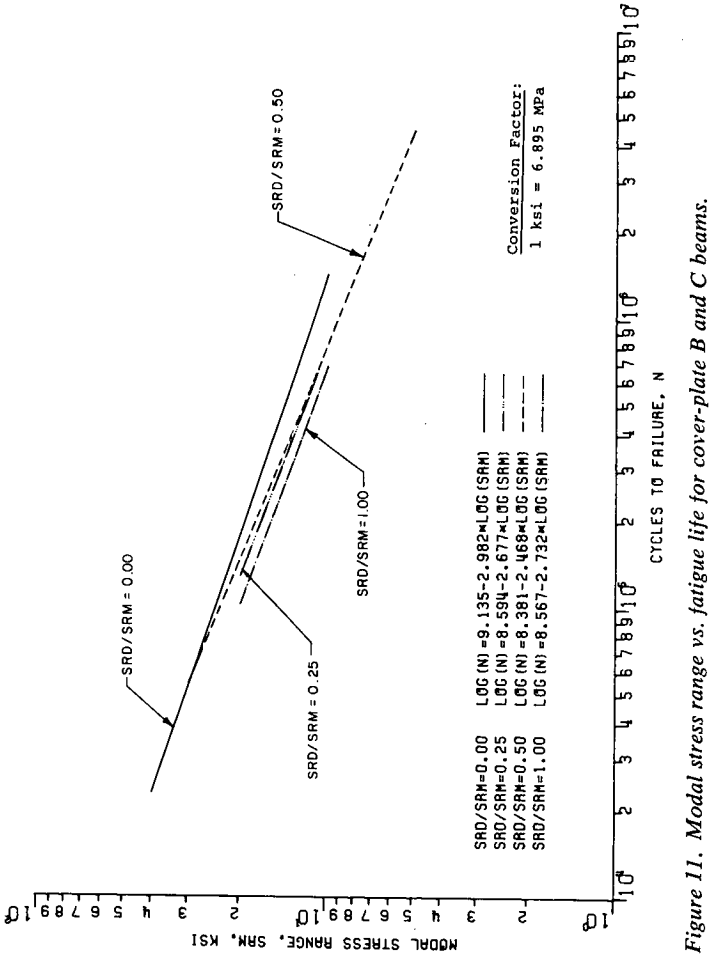

Figure 11. Modal stress range vs. fatigue life for cover-plate B and C beams.

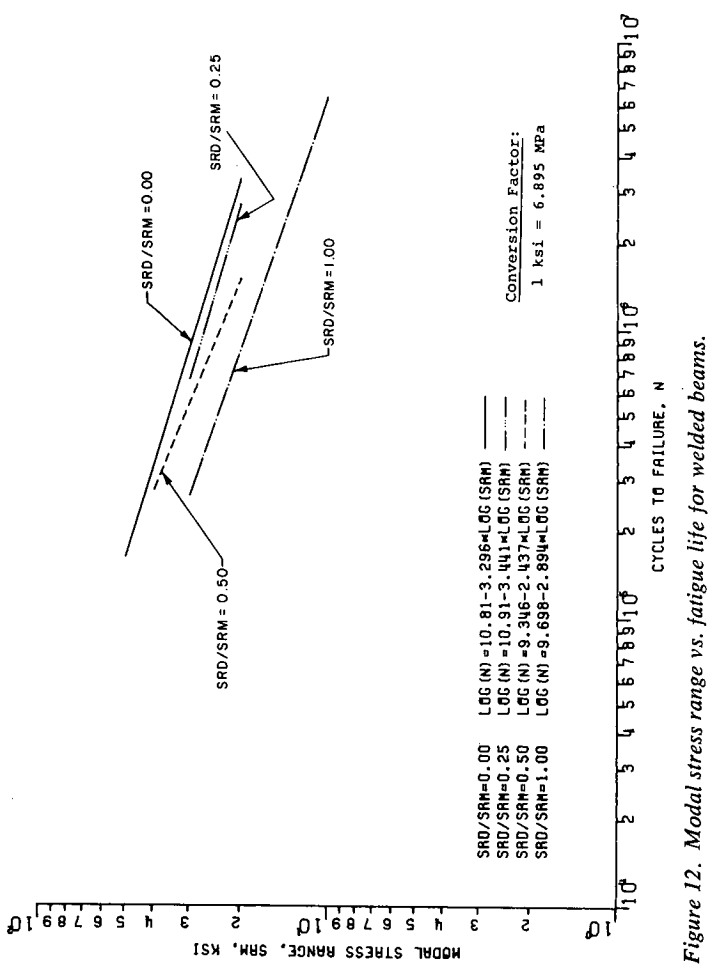

Figure 12. Modal stress range vs. fatigue life for welded beams.

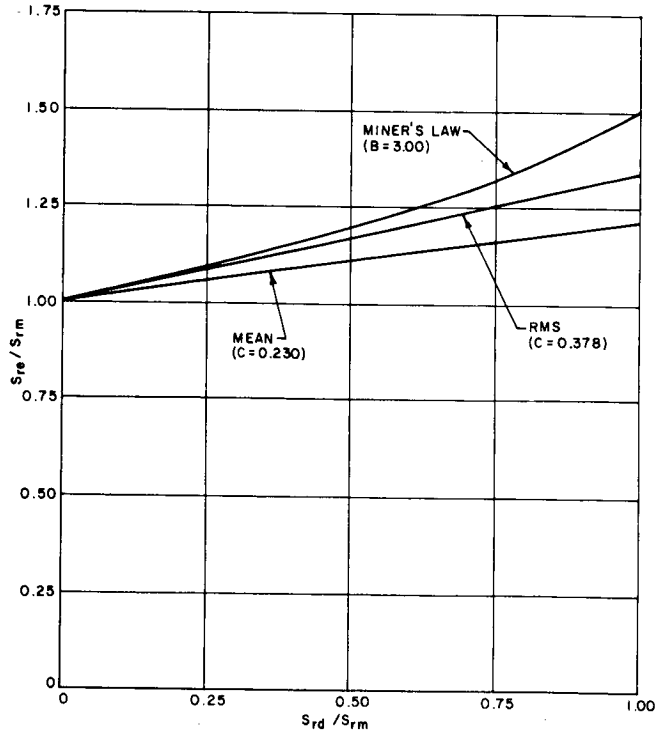

Figure 13. Variation of effective stress range with spectrum width.

of different magnitudes. Miner's Law can be used, as discussed in Appendix F, to derive the following equation for an effective stress range:

$$S_{re} = (\Sigma \alpha_i S^B_{ri})^{1/B} \tag{7}$$

where B is the reciprocal of the slope of the constant-amplitude log-SN curve of the detail under consideration and is about 3 for most structural details. Thus, Eq. 7 is similar to Eq. 6, which defines $S_{re\mathrm{RMS}}$, but the S_{ri} term is cubed rather than squared.

The variation of S_{re}/S_{rm} with S_{rd}/S_{rm} for a spectrum defined by a Rayleigh curve and for $B = 3$ is shown in Figure 13. This curve is always slightly higher than the curves for the other methods of calculating the effective stress range discussed herein. Thus, $S_{re\mathrm{MINER}}$ is somewhat more conservative than $S_{re\mathrm{RMS}}$, but the maximum difference between the two is only about 11 percent.

The $S_{re\mathrm{MINER}}$ for the variable-amplitude data was compared with S_r for the constant-amplitude data in the same way as $S_{re\mathrm{RMS}}$ was compared with S_r for the constant-amplitude data. The corresponding curves are given in Figures 16 and 17 for the cover-plate C beams and the welded beams, respectively, and in Appendix F for the other details. These figures show that the variable-amplitude data points in general fall within a scatter band bounded by the 95-percent confidence limits of the constant-amplitude

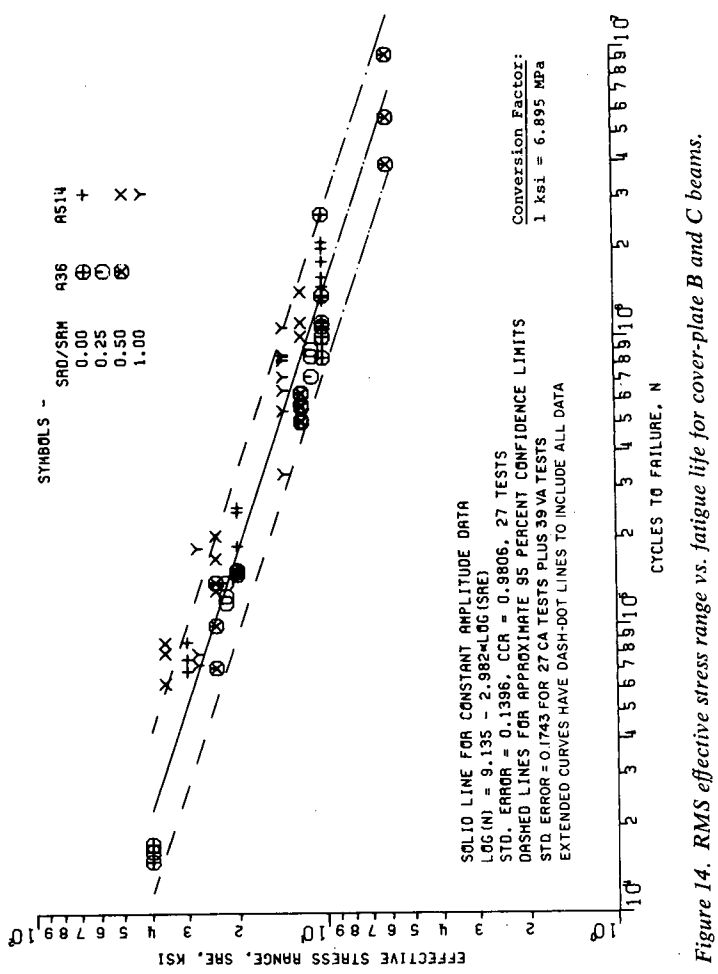

Figure 14. RMS effective stress range vs. fatigue life for cover-plate B and C beams.

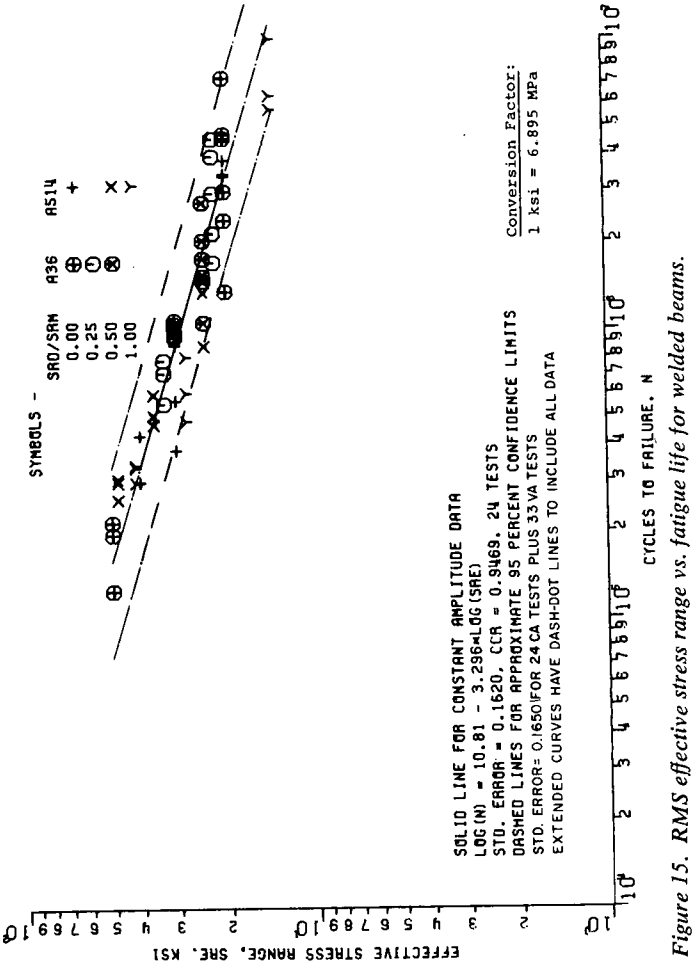

Figure 15. RMS effective stress range vs. fatigue life for welded beams.

data. Furthermore, the differences between the constant- and transformed variable-amplitude data in general were not statistically significant. Therefore, it is concluded that $S_{re\text{MINER}}$ satisfactorily relates variable- and constant-amplitude data.

A comparison of the standard errors of the estimate of the variable-amplitude data transformed by the two methods shows that the RMS method makes the transformed variable-amplitude data fit the constant-amplitude SN curve slightly better than the Miner method. Thus, the RMS method is a slightly more accurate way of relating variable- and constant-amplitude data than the Miner method.

Comparisons with AASHTO Specifications and Project 12-7 Results

The results for all cover-plate beams from the present study are compared with AASHTO allowable fatigue provisions (*1*) in Figure 18. Specifically, the cover-plate beam results—including details A, B, and C—are compared with the allowable fatigue stress line for AASHTO Category E (cover-plate ends) on the basis of $S_{re\text{RMS}}$. The allowable fatigue stress line was obtained by fitting a straight line defined by Eq. 3 to the allowable stress ranges for three categories of design life: 10,000, 500,000, and 2,000,000 cycles. This line closely approximates the lower limits (95-percent tolerance limit) of previous constant-amplitude test results on cover-plate end details (*2*).

The scatter in Figure 18 is reasonable, considering the fact that data for several different steels, minimum stresses, and details are included in a single plot. Almost all of the data points lie above the line; thus, the AASHTO allowable stress line provides an approximate lower limit for the variable- and constant-amplitude test results plotted on the basis of the RMS effective stress range.

Figure 19 gives a similar comparison of the welded-beam results with the AASHTO allowable fatigue-stress line for Category B, longitudinal flange-web fillet welds. Again the scatter is reasonable for this type of specimen, and almost all of the data points lie above the allowable stress line. Thus, the AASHTO allowable stress line provides an approximate lower limit for the variable- and constant-amplitude test results plotted on the basis of the RMS effective stress range.

Two details—cover-plate C beams and welded beams—used in the present study are comparable to the details used in NCHRP Project 12-7. Consequently, the present constant-amplitude data for these two details were compared with the corresponding Project 12-7 data (*2*). The comparison showed that the differences are not practically significant and, furthermore, would generally not be statistically significant.

The cover-plate B beams were also comparable to details in Project 12-7, but were not included in the analytical comparison because only six such beams were tested in

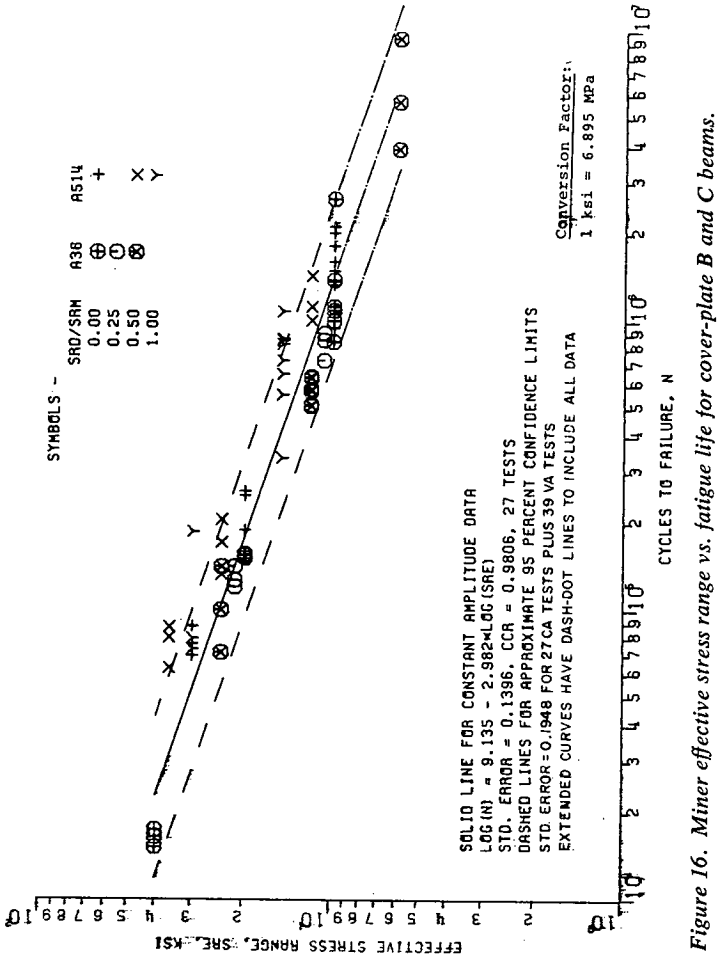

Figure 16. Miner effective stress range vs. fatigue life for cover-plate B and C beams.

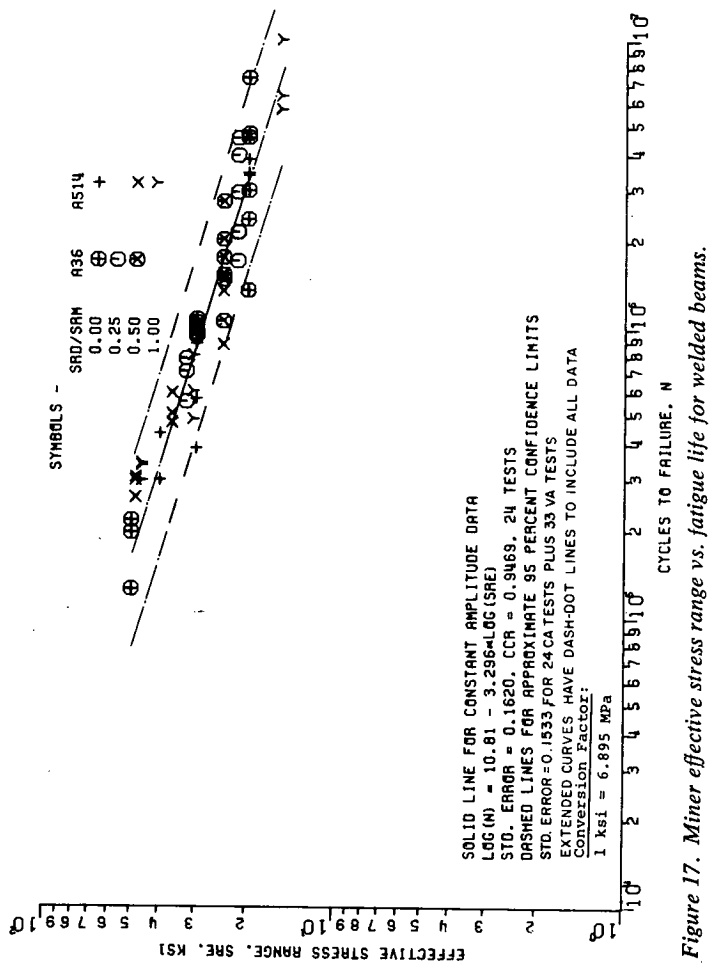

Figure 17. Miner effective stress range vs. fatigue life for welded beams.

the present study. The results for these six beams, however, appear to agree with the results from Project 12-7.

Long-Life Tests

The purpose of the long-life beam tests was to show whether SN curves for bridge members extend to very low stress range levels, such as occur in actual bridges, or, conversely, whether there is a fatigue limit or break in the SN curves. Consequently, the results of tests on A514-steel cover-plate C beams (set 21), conducted at $S_{rm} = 2$ and 3 ksi (14 and 21 MPa) with $S_{rd}/S_{rm} = 1.0$, are compared with the SN curves from previous tests on such beams at higher stress range levels, as shown in Figure 20. For the tests conducted at $S_{rm} = 2$ and 3 ksi, $S_{r\mathrm{RMS}} = 2.8$ and 4.1 ksi (19 and 28 MPa) and $S_{\min} = 10$ and 15 ksi (69 and 103 MPa), respectively. The best-fit line for the tests at $S_{rm} = 10$ ksi, or above, is shown as a solid line within the range of test data; similarly, approximate 95-percent confidence limits for a single future test (or approximate 95-percent tolerance limits) are shown as dashed lines within the range of the test data. Extensions of the best-fit line and confidence limits are shown as dash-dot lines.

The long-life data points for $S_{rm} = 3$ ksi are slightly to the right of the extension of the best-fit line, but are within the extensions of the confidence limits. Thus, it appears that these data do not indicate a fatigue limit, or significant break in the SN curve, but instead point out that the original SN curve should be adjusted slightly to better fit the wider range of data. Therefore, a new best-fit line was developed for the combined data including the long-life results at $S_{rm} = 3$ ksi and the previous results. This line is shown as a dash-dot-dot solid line in Figure 20.

One of the three long-life beams sustained about 104 million cycles without visible cracks at the low-stress end of the cover plate where $S_{rm} = 2$ ksi and $S_{r\mathrm{RMS}} = 2.8$ ksi. The other two beams failed at the low-stress end at lives of about 60 million and 104 million cycles. Thus, it appears that a fatigue limit, or break in the SN curve, occurs at an $S_{r\mathrm{RMS}}$ of about 3 ksi for this type of detail.

Crack-Growth Tests

As discussed in detail in Appendix G, the results of the crack-growth tests of the A514-steel WOL specimens are interpreted in terms of the stress intensity, K, at the crack tip and the crack growth rate, da/dN, in which a is the crack depth and N is the number of cycles (*25*). In Figure 21, the log da/dN is plotted as a function of the modal stress-intensity range, K_{rm}, for three values of K_{rd}/K_{rm} (0, 0.5, and 1.0) corresponding to three spectrum widths. These results are for a random sequence of loads. The lines representing the three values of K_{rd}/K_{rm} are ap-

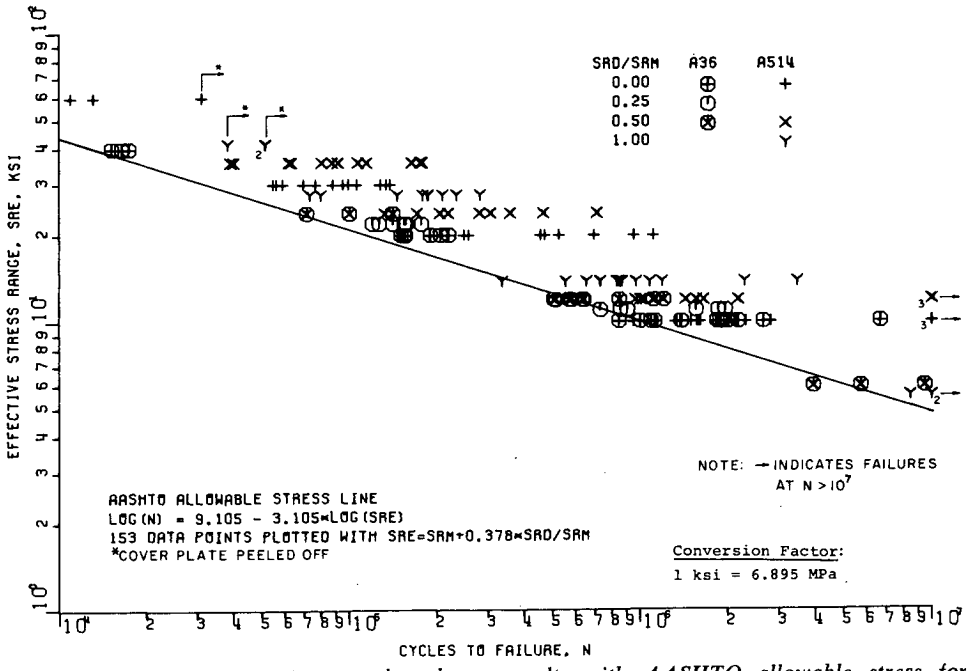

Figure 18. Comparison of cover-plate beam results with AASHTO allowable stress for Category E.

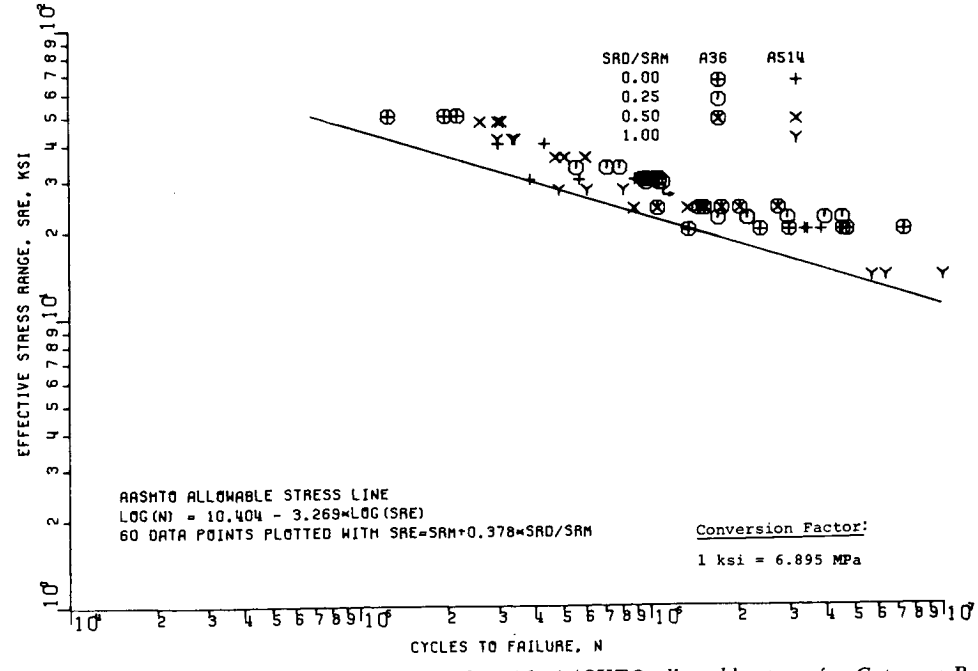

Figure 19. Comparison of welded beam results with AASHTO allowable stress for Category B.

proximately parallel and show that the crack-growth rate for a given K_{rm} increases as the spectrum width measured by K_{rd}/K_{rm} increases. This is consistent with the results for the fatigue tests.

The curves of the three spectrum widths can be shifted together by plotting $K_{r\mathrm{RMS}}$ instead of K_{rm} as the stress-intensity parameter, as shown in Figure 22. The line through the data is defined by equations similar to those for the SN curves. Specifically,

$$\log (da/dN) = \log A + B \log K_{r\mathrm{RMS}} \tag{8}$$

and

$$da/dN = AK^{B}_{r\mathrm{RMS}} \tag{9}$$

The values of log A, A, and B depend on the material properties and are equal to -9.11, 7.68×10^{-10}, and 2.60, respectively, for the data in Figure 22. Thus, the RMS method for relating variable- and constant-amplitude data

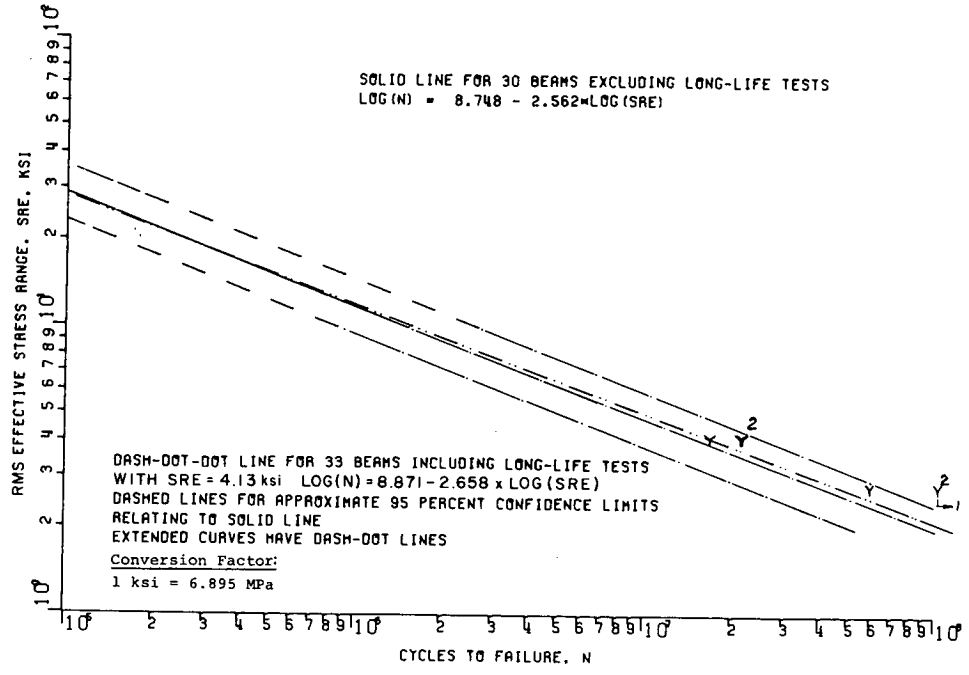

Figure 20. Long-life test results.

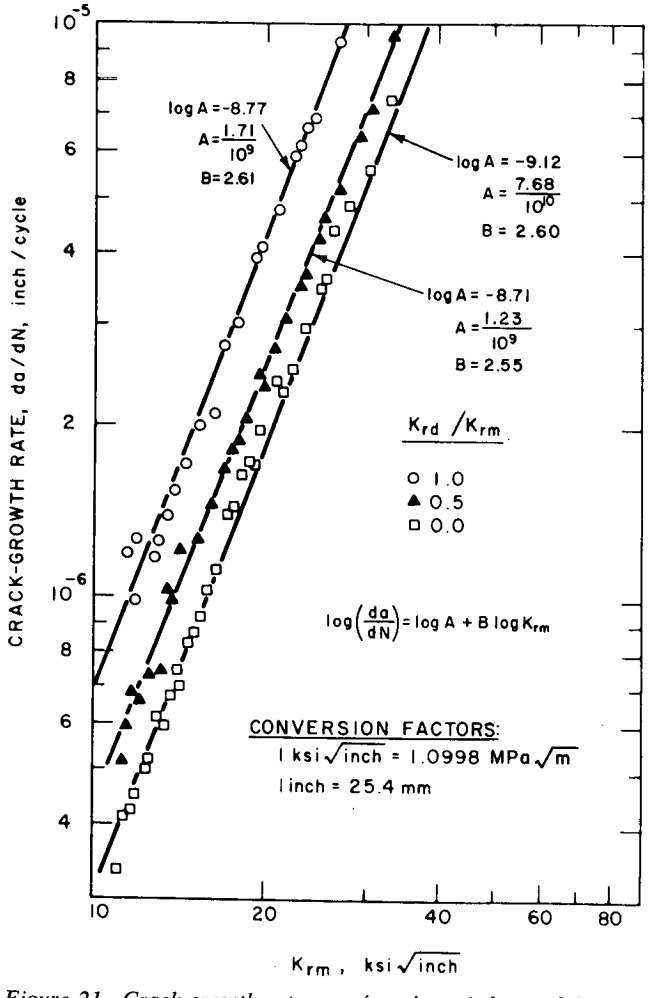

Figure 21. Crack-growth rate as a function of the modal stress intensity range.

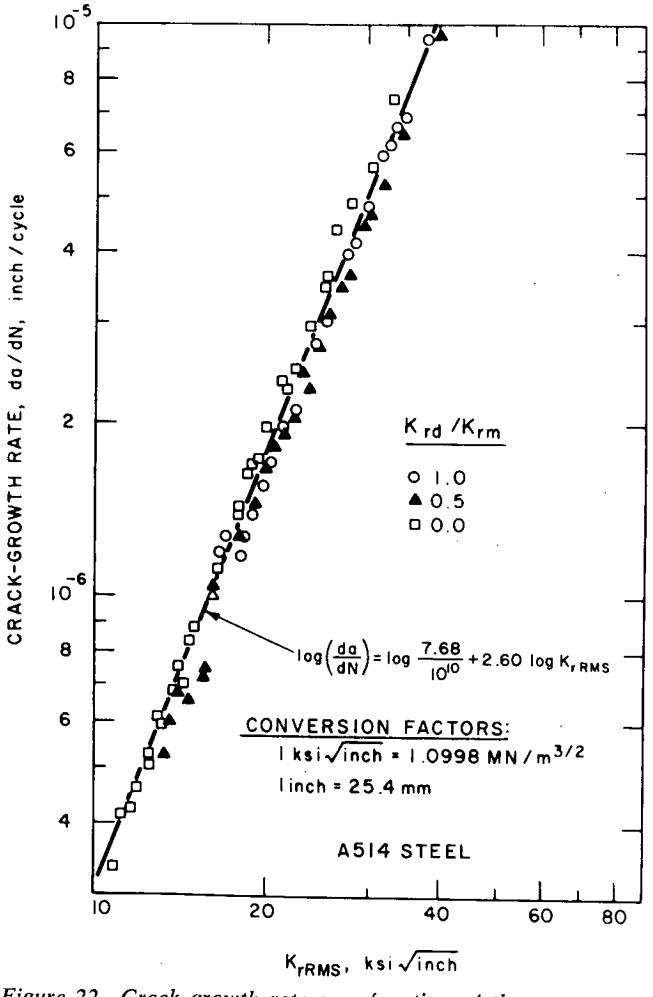

Figure 22. Crack growth rate as a function of the root-mean-square stress-intensity range.

applies to crack-growth rate as well as to the total fatigue life.

As explained in Appendix G, K_{min}, which is analogous to S_{min} in the fatigue tests, could not be held constant during the crack-growth tests. However, test results showed that large variations in K_{min} have little effect on the crack-growth rate. Test results for several different variable-amplitude loading sequences showed that the loading sequence has little effect on the crack-growth rate. Although crack-growth tests were performed only on A514-steel specimens, past work (*25*) suggests that the crack-growth rates for A36-steel would not be greatly different.

Crack-Growth Data from Cover-Plate Beam Tests

As discussed in greater detail in Appendix G, the crack-growth data from the beam tests could not be correlated with the basic crack-growth data from the WOL specimens. The crack-growth data from the beam tests, however, provide valuable information on the initiation and propagation phase of fatigue life for such beams. Specifically, these data were used to obtain the curves in Figure 23, which show the crack initiation and propagation phases of the fatigue life for A514-steel cover-plate C beams. These curves indicate that the crack initiation phase is an important part of the total fatigue life of this type of detail.

The ratio of crack length to crack depth, l/a, for semi-elliptical cracks in beams is an important parameter in crack propagation studies. Therefore, l/a was determined for the cover-plate A and B beams. The results showed that l/a was equal to approximately 4 for these beams.

Prediction of Beam Fatigue Lives From Basic Data

The fatigue life of a structural detail can be divided into two phases: (1) initiation and (2) propagation, or growth (*26*). Basic small specimen data are available for both the initiation and propagation phases (*25, 26*). These data were used in predicting the total fatigue lives of four sets of cover-plate C beams. Several different approaches of varying complexity were used in making these predictions to illustrate the uncertainties involved. These approaches are explained and compared with test data in Appendix G. The results showed that more information on several aspects of crack initiation and propagation is needed to consistently make accurate predictions of the fatigue life of fabricated members from basic crack initiation and propagation data.

Compression-Flange Cracking

A significant number of cracks occurred in the compression flange of the welded beams and the cover-plate C beams, which caused failure in a few beams, especially in those in which a reversal of stress occurred, so that some tensile stress was applied to the compression flange during a part of the stress cycle. As discussed in Appendix G, this compression-flange cracking was generally consistent with the results of the Project 12-7 study, and did not significantly affect the over-all results of the present program; however, the reason for a few of the compression-flange failures has not been convincingly explained.

Superimposed Vibration Stresses

Field measurements of stresses in bridges show that vibration stresses are superimposed on the major stress cycle produced by the passage of a vehicle. For most types of bridges, these vibration stress cycles have a much smaller amplitude but a higher frequency, f, than the major stress cycles. If the ratio of the frequency of the vibration cycles to that of the major cycles is an odd integer and the two types of cycles are in phase, the vibration cycles reinforce the positive and negative peaks of the major stress cycles. Thus, the over-all stress range, S_r, is the sum of the stress ranges for the two types of cycles. Both the amplitude ratio, S_{rv}/S_r, and frequency ratio, f_v/f, vary considerably with the type of bridge and vehicle, but the value of 7 appears to be fairly representative for the frequency ratio and the amplitude ratio is generally less than 0.2.

The effect of these vibrations on fatigue life can be estimated by Miner's Law. This was done, as detailed in Appendix F, by assuming that the over-all stress range cycles, S_r, and the vibration cycles, S_{rv}, have the same effect as if they had been applied at different times rather than simultaneously. The results showed that the reductions in fatigue life for a frequency ratio of 7 and amplitude ratios of 0.1 and 0.2 were 1.0 and 10.2 percent, respectively.

A few tests of cover-plate specimens were conducted at amplitude ratios of 0.1 and 0.2. These specimens had slightly longer lives than similar specimens tested without superimposed vibrations, but the differences were not statistically significant. Thus, the experimental and theoretical studies both suggest that the effect of superimposed vibrations of the magnitude usually encountered in bridges is small.

Number and Sequence of Loads in the Spectrum

The main fatigue tests were controlled by a 500-cycle tape in which the loads satisfy the desired continuous Rayleigh distribution and are arranged in a random sequence. The 500-cycle tape was continuously cycled throughout a test so that the same 500-cycle random sequence was repeated many times; thus, the loading was not truly random throughout the test. Four sets of 6 cover-plate specimens were tested at various combinations of number of load levels and sequence lengths to show the effect of these parameters on fatigue life. There was very little difference in the fatigue lives for the different sets, which included sets tested with 100-cycle, 500-cycle, and 5,000-cycle tapes. Therefore, it is concluded that the 500-load tape used in the main testing program adequately represents a continuous Rayleigh distribution and a truly random loading sequence. It appears that even a 100-cycle tape would have been adequate.

The standard Rayleigh curve used in the main fatigue testing program was also used to study the effects of the number of load levels and sequence length on fatigue life. This standard curve, as explained in Appendix C, was obtained by truncating the asymptotic tail of the theoretical Rayleigh distribution at a width of $3S_{rd}$. The effect of different widths, or clipping ratios, on fatigue life was not determined in the present study.

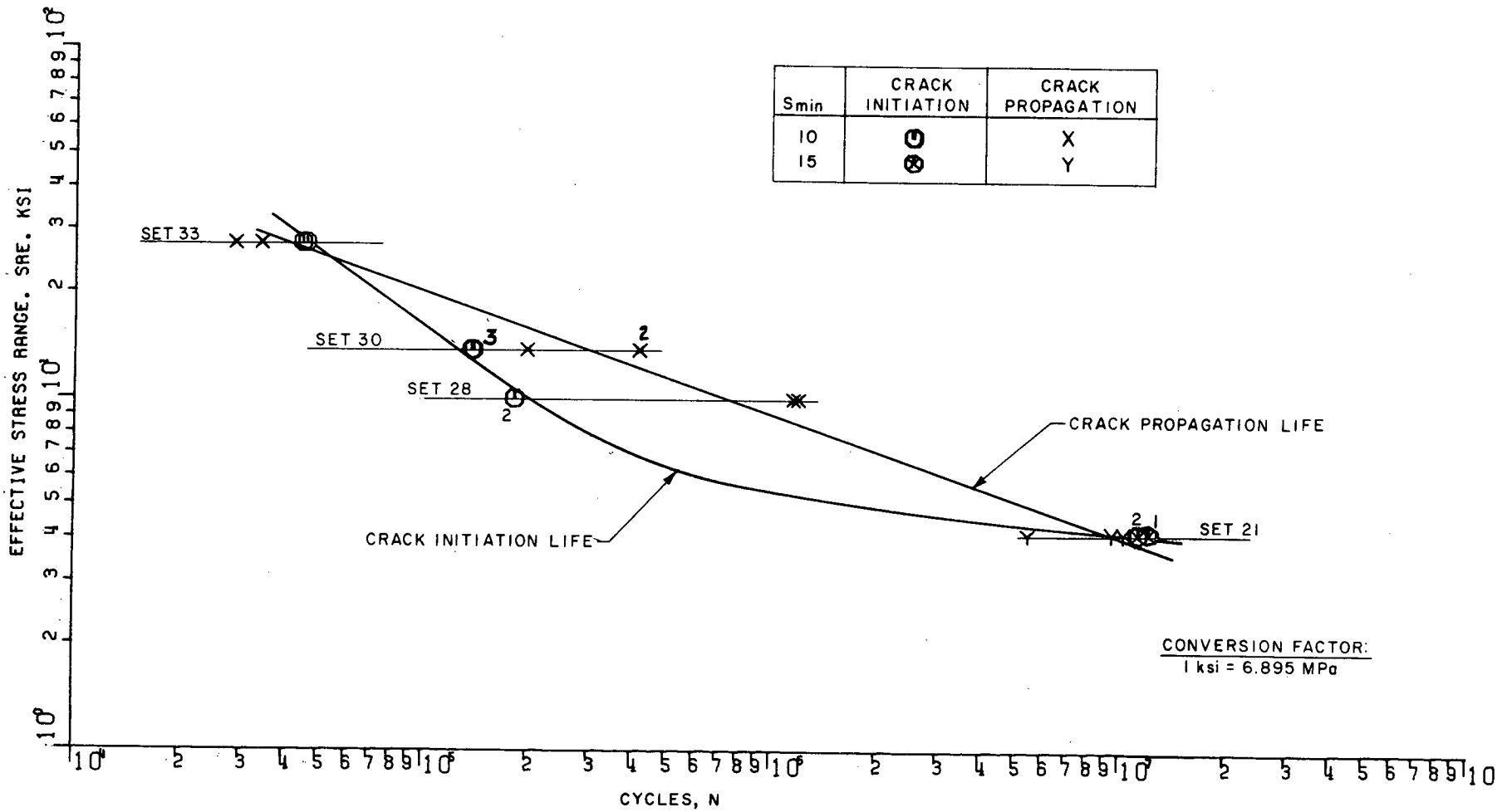

Figure 23. Crack initiation and propagation lives for A514-steel cover-plate A beams.

CHAPTER THREE

APPLICATIONS OF FINDINGS

The findings of the present study provide a link between the types of variable-amplitude random-sequence fatigue loadings that actually occur on bridges and the constant-amplitude fatigue data and allowable-stress values that are commonly used in designing such bridges. Consequently, the results should be useful to design engineers. specification writers, and researchers, and could eventually lead to AASHTO fatigue design methods based on more realistic loadings. Specific ways in which the findings can be used in design applications and in specifications are discussed as follows.

DESIGN APPLICATIONS

The findings can be used by bridge designers to calculate (1) the remaining life of existing bridges, especially old bridges that were originally designed for lighter loads or that contain undesirable design details, and (2) the design life of new bridges that are frequently subjected to unusual loading conditions.

Four steps are required in estimating the life of a bridge: (1) develop a histogram (frequency-of-occurrence bar graph) for the stress spectrum at each critical detail and an estimate of the number of cycles per day, (2) calculate the effective (constant-amplitude) stress range for the spectrum, (3) develop a curve or equation of the allowable constant-amplitude stress range vs. the numbers of cycles for each critical detail, and (4) calculate the fatigue life for each detail. In the following paragraphs, these steps are discussed in detail and are illustrated by an example problem. In this example (shown in Figure 24), the remaining life for an end detail of the hangers on a 10-year-old truss bridge is calculated. The example was selected to illustrate severe fatigue conditions not representative of the conditions in most highway bridges.

The cyclic stress range, which corresponds to the passage of a single truck, is the main parameter in the fatigue analysis (stress cycles caused by cars can be neglected). Consequently, the type of histogram (*9*) shown in Figure 24 is used; the height of each bar represents the percentage of stress ranges within the interval defined by the width of the bar. The most reliable method of obtaining such a histogram for an existing bridge is to make field measurements of the nominal stresses at critical details while the bridge is under normal traffic. (Because the available fatigue curves for various details are based on nominal stresses, the measured stresses that are related to these curves should also be based on nominal stresses. Consequently, the stresses should be measured far enough from a critical detail to eliminate local stress concentrations.) Although this method is expensive, it may be justified in a few critical cases. A second way to obtain the needed stress-range histogram is to estimate it from measured or predicted data on truck traffic at the location of the bridge. Field measurements have shown that the actual stresses due to live loads plus impact in bridges are almost always well below the corresponding design stresses because of various conservative factors in the design procedures. Consequently, realistic parameters based on past experience or available field measurements on similar bridges must be used to estimate the stress ranges corresponding to given trucks. An empirical method of doing this for certain types of bridges is given by Heins and Galambos (*14*). A third way to obtain the needed histogram is to estimate it directly from field data on similar bridges. If the histogram is expected to change during the life of the bridge, separate calculations must be made for the portion of the life covered by each histogram.

To predict the remaining or total life of a bridge in years, it is necessary to estimate the past and future traffic volumes, including any expected growth in traffic, for the bridge. Specifically, it is necessary to know the total number of daily occurrences of the stress ranges defined in the histogram. Passage of a truck usually causes a single major stress cycle; but in certain types of bridges, such as cantilever (suspended-span) girder bridges, such a passage has been found to produce a large number of stress cycles as a result of bridge vibrations. Consequently, the type of bridge must be considered when estimating the number of daily stress cycles from the expected traffic volume. In the example, the number of daily stress cycles is estimated to be 1,000 and is assumed to be constant throughout the life of the bridge.

The effective (constant-amplitude) stress range for the stress spectrum defined by a histogram can be taken as the root mean square of the stress ranges in the histogram and can be calculated from Eq. 6. The effective stress range for the example spectrum was calculated to be 4.38 ksi (30.2 MPa), as shown in Figure 24.

A curve or equation for the allowable constant-amplitude stress range for a particular detail can be obtained from the recently adopted AASHTO fatigue provisions (*1*) or from available test data (*2*). To obtain the best (most probable) estimate of the remaining life, a curve approximating the mean values of experimental data should be used; to obtain a conservative estimate, the lower 95-percent tolerance limit for the data should be used. The AASHTO allowable stress curves and equations approximate the lower limits (95-percent tolerance limit) of test results and, therefore, can be used to obtain a conservative estimate of the remaining life. To obtain a curve from the AASHTO provisions for Category E, the allowable stress ranges for three life categories (100,000, 500,000, and 2,000,000 cycles) are plotted and a straight line is drawn through

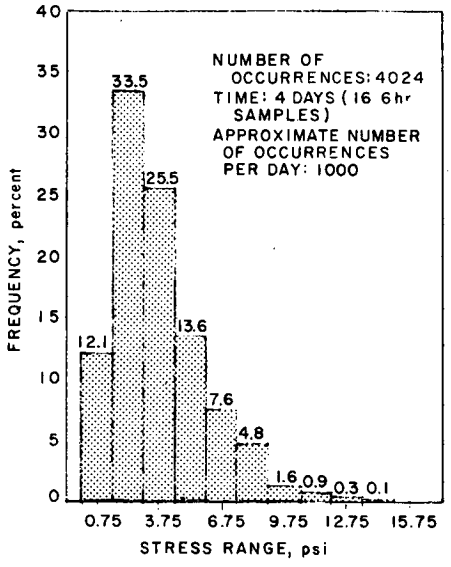

Histogram for Hanger End Detail

Stress Spectrum, ksi				
i	α_i	S_{ri}	$\alpha_i S_{ri}^2$	$(\alpha_i S_{ri}^2)^*$
1	0.121	0.75	0.07	-
2	0.335	2.25	1.70	-
3	0.255	3.75	3.59	-
4	0.136	5.25	3.75	3.75
5	0.076	6.75	3.46	3.46
6	0.048	8.25	3.27	3.27
7	0.016	9.75	1.52	1.52
8	0.009	11.25	1.14	1.14
9	0.003	12.75	0.49	0.49
10	0.001	14.25	0.20	0.20
	1.000		19.19	13.83

*Considering the Fatigue Limit

1 ksi = 6.895 MN/m^2

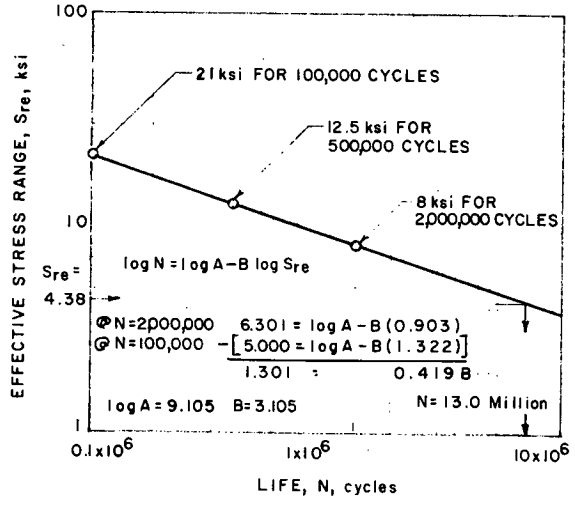

Allowable Effective Stress Range for Hanger End Detail (AASHTO Category E)

Without Considering the Fatigue Limit:

$$S_{re} = \sqrt{\sum \alpha_i S_{ri}^2} = \sqrt{19.19}$$

$$S_{re} = 4.38 \text{ ksi}$$

$$\log N = 9.105 - 3.105 \log (4.38)$$

$$N = 13.0 \times 10^6 \text{ cycles}$$

$$\text{Life, in years } Y = \frac{13.0 \times 10^6}{1000 \times 365} = 35.6$$

Remaining life: 35.6 - 10.0 = 25.6 years

Considering the Fatigue Limit:

$$S_{re} = \sqrt{\sum \alpha_i S_{ri}^2} = \sqrt{13.83}$$

$$S_{re} = 3.72 \text{ ksi}$$

$$\log N = 9.105 - 3.105 \log (3.72)$$

$$N = 21.6 \times 10^6 \text{ cycles}$$

$$\text{Life, in years } Y = \frac{21.6 \times 10^6}{1000 \times 365} = 59.0$$

Remaining life: 59.0 - 10.0 = 49.0 years

Figure 24. Example of the estimation of the minimum remaining life.

these points, as shown in Figure 24. An equation for this curve could be obtained in similar fashion.

A conservative estimate of the fatigue life for a particular detail can then be determined from the AASHTO allowable constant-amplitude stress-range (or effective stress-range) curve or equation for that detail; the value of N corresponding to the calculated effective stress range for the spectrum (4.38 ksi) is a conservative estimate of the total number of cycles to failure (13.0×10^6). The percentage of these cycles falling within any particular interval

of stress ranges is given by the histogram. The corresponding expected minimum life in years can be calculated by dividing the total number of cycles (13.0×10^6) by the estimated number of cycles per year ($365 \times 1{,}000$). Thus, in the example, the expected total life for the critical detail is 35.6 years and the minimum remaining life is 25.6 years. The term "minimum remaining life" if used to indicate that the estmated life is based on the lower limits of the scatter of fatigue data.

BRIDGE SPECIFICATIONS

Relationships between variable- and constant-amplitude fatigue data, such as were developed in the present program. are necessary to relate the large amount of available constant-amplitude fatigue data on various details (*2, 4, 27*) to actual variable-amplitude traffic loadings and, thereby, develop realistic fatigue specifications for bridges. There are, of course, many different ways of utilizing such relationships in improving bridge specfications. For example, Miner's Law was used to relate the specified number of constant-amplitude truck loadings in the new AASHTO fatigue specifications (*1*) to the corresponding average daily truck traffic (*28*). Although the development of new fatigue specifications for bridges is beyond the scope of the present project, the work performed during this study and work by others (*28, 29*) suggested a new approach that is described as follows. The discussion is intended only to illustrate the approach and not to give final recommendations for changes in any present specifications.

Lane Loading

The magnitude and position of the loads used in the static (nonfatigue) design of a bridge, according to the AASHTO specifications, are intended to represent the worst possible conditions (with an appropriate factor of safety) and do not occur frequently enough to affect the fatigue life of a bridge. For example, in designing a continuous-span bridge governed by lane loading, the loading is applied first over only certain portions of the bridge to obtain the maximum possible positive moment and then over different portions of the bridge to obtain the maximum negative moment. This type of loading, which results in large stress ranges, would occur very rarely, if ever, and consequently is overconservative for use in determining the fatigue life of the bridge. Therefore, the magnitude and position of loads used in estimating the fatigue life of a bridge member should be different from that used for the static (nonfatigue) design of that member.

Fatigue-Design Truck and Elimination of Lane Loading

The fatigue life of most bridge members is affected primarily, if not exclusively, by passages of single trucks of different weights (*29*). Although the weights of a few of these trucks are above the 72-kip (320-kN) weight of the AASHTO HS20 design truck, most are well below 72 kips. Consequently, the suggested new fatigue-design method uses a fatigue-design truck of weight W_F instead of the usual HS20 (or similar) truck or lane loading. W_F is an "average" weight chosen to represent actual traffic and, therefore, is well below 72 kips. Specifically, W_F is chosen so that a given number of passages of this truck will cause the same amount of fatigue damage as the same total number of passages of trucks of different weights in actual traffic. This same truck is used for bridges designed for static loadings less than H20, but the effect of the smaller amount of traffic that would normally cross such bridges is included later in the design method.

The fatigue-design truck is analogous to the effective stress range for variable-amplitude stress-range spectrums and can be calculated from the distribution of traffic by either the RMS or Miner method. The Miner method with $B = 3$ is used in the suggested design method because it is slightly more conservative than the RMS method. For convenience, the fatigue-design truck is related to the AASHTO HS20-44 truck. Thus,

$$W_F = [\Sigma \alpha_i W_i^3]^{\frac{1}{3}} = W_D[\Sigma \alpha_i \phi_i^3]^{\frac{1}{3}} \qquad (10)$$

in which α_i is the fraction of trucks with a weight W_i, W_D is the weight of the HS20-44 truck load, and ϕ_i equals W_i/W_D. It has been reported (*29*) that the value of $\Sigma \alpha_i \phi_i^3$ from various loadometer surveys varies from 0.3 to 0.5. If the Federal Highway Administration 1970 nationwide loadometer survey is used to define the distribution of truck traffic, $\Sigma \alpha_i \phi_i^3$ equals 0.35 (*28*) and W_F equals 0.705 W_D. In the new fatigue-design method, it is suggested that the first part of Eq. 10 be used to calculate W_F if the expected distribution of traffic is known; otherwise, W_F can be taken as about 0.7 W_D or 50 kips (222 kN). Eq. 10 is theoretically applicable only when all of the stress ranges caused by the distribution of traffic are above the fatigue-limit stress range; the effects of stress ranges below the fatigue limit will be incorporated later in the suggested design procedure.

Elimination of lane loadings from the fatigue-design procedures would practically eliminate fatigue from consideration for main members of relatively long-span bridges. The steady flow of traffic on such bridges during peak hours could be represented by an approximately constant lane loading, because individual trucks cause only minor fluctuations in stress. In urban areas, there are usually two periods of peak traffic daily and, consequently, only two cycles of lane loading daily. In 70 years, this would result in only about 50,000 cycles of lane loading. Therefore, it seems reasonable to eliminate lane loadings from consideration in fatigue design. However, experimental data should be obtained to support this conclusion. Lane-loading criteria could easily be added to the new design method if such data indicated that this is necessary.

Design Stress Range

The next step in the suggested fatigue-design method is to calculate the design stress range caused at a detail by the passage of a single fatigue-design truck across the bridge in the lane under consideration. The effects of trucks in other lanes and of additional trucks in the same lane are minor and are discussed later. The truck is first placed in the position that produces maximum tensile stress at the detail and then in the position that produces the maximum compressive stress as is done with present design pro-

cedures. The stress range is the sum of these maximum stresses—both being considered positive—times an impact factor. In a simple-span bridge, of course, there is no reversal of stress; consequently, the maximum compressive stress is zero and the design stress range equals the maximum tensile stress caused by the truck.

The present AASHTO impact factor is used in the suggested design method. The present AASHTO spacing and weight distribution of truck wheels and axles (Article 1.2.12) are also used. It has been proposed (*29*) that a single representative spacing of axles be used in fatigue design rather than the present variable spacing. Although this proposal is reasonable, it was not adopted in the suggested fatigue-design method (1) because it would mean that the maximum and minimum moment envelopes developed in the static design for truck loadings could not be utilized in the fatigue design, and (2) because the effect on the fatigue design would be relatively small.

Numerous field measurements (*9, 10, 15*) have shown that the actual stresses that occur in the longitudinal beams and stringers in bridges under traffic are much smaller than the live-load (plus impact) stresses calculated by present AASHTO methods. A large part, but probably not all, of the difference results from the lateral-distribution factor (S/5.5) specified by AASHTO for such beams and stringers. This factor is based on the worst possible loading conditions (that is, trucks are placed simultaneously in the worst positions in all lanes). Therefore, the factor is appropriate for static design, but not for fatigue design.

Lower factors based on a truck on only one lane are used in the suggested method to account for all of the differences between the actual and calculated stresses, even though part of these differences may be attributable to factors other than lateral distribution. According to theoretical calculations based on Ref. (*30*), the proportion of a wheel load carried by an exterior beam when one truck is in the outside lane is usually greater than the proportion of a wheel load carried by an interior beam when the truck is over that beam. Therefore, it appears that a larger distribution factor should be used for exterior beams than for interior beams. Although an extensive study of distribution factors was beyond the scope of the present investigation, a preliminary investigation based on available experimental and theoretical information (*14, 29, 30*) suggested that factors of S/7 and S/10 would be appropriate for exterior and interior beams, respectively. These factors apply when $S \leq 14$ ft (4.2 m); otherwise, the lateral distribution factor should be calculated by simple span distribution of a single truck. The factors of S/7 and S/10 are quite conservative compared with the average factor of S/14.7 determined from field measurements on 10 bridges (*29*). This factor, which gives the fraction of a wheel load (½ of a truck load) carried by a single beam, was determined in the following way. The stress range, S_i, produced in each beam by the passage of a truck was measured. It was assumed that all beams were similar, so that M_i is proportional to S_i. The fraction of the total truck moment carried by each beam is $M_i/\Sigma M_i$ or $S_i/\Sigma S_i$. The fraction of the wheel-load moment is twice this amount and is equal to the distribution factor, S/α, mentioned earlier. The α for the critical beam (interior or exterior) in each bridge was used in calculating the average value of 14.7 for the 10 bridges.

The preliminary study suggested that other parameters—such as the total number of longitudinal beams, or stringers, and the position of the beam under consideration—might be more appropriate than S for defining the lateral distribution when only one lane is loaded. These parameters should be considered in future studies aimed at developing lateral-distribution factors specifically for fatigue design.

Design SN Curve and Effect of Fatigue Limit

The next step in the suggested fatigue-design method requires a comparison of the design stress range with constant-amplitude SN curves corresponding to the present AASHTO design categories. Such curves, including approximate fatigue limits, are given by Fisher (*28*). The approximate fatigue limits correspond to the present AASHTO (*1*) allowable stress ranges for over 2,000,000 cycles. The curves represent the approximate lower limits (lower 95-percent tolerance limit) for available data and, therefore, give the minimum number of cycles to failure. The finite-life portion of the curves for all details, except AASHTO Category F, is defined by

$$N = \frac{A}{F_{sr}^3} \tag{11}$$

in which N is the fatigue life, F_{sr} is the stress range, and A is a constant that is different for each detail. Although the curve for Category F has a different slope from the other curves, the portion of this curve used in the suggested design method can also be adequately approximated by Eq. 11, so that a single equation can be used for all detail categories. Values of A for the various detail categories are given in Table 4.

As mentioned earlier, the method used to calculate the weight of the fatigue-design truck, and the corresponding design stress range, theoretically is applicable only when all stress ranges caused by the traffic are above the fatigue-limit stress range. Those stress ranges in the variable-amplitude spectrum that are below the fatigue limit do not cause fatigue damage; consequently, in Eq. 10, the $\alpha_i W_i^3$ terms corresponding to such stress ranges must be taken as zero. The weight of the fatigue-design truck calculated in this way is defined as W'_F, and the corresponding stress range is defined as F'_{sr}. The correct fatigue life, N', for this variable-amplitude traffic is given by an equation similar to Eq. 11, even when F'_{sr} is below the fatigue limit, since the stress ranges below the fatigue limit were assumed to cause no fatigue damage in the calculation of W'_F and F'_{sr}. Thus,

$$N' = \frac{A}{(F'_{sr})^3} \tag{12}$$

All variable-amplitude cycles, even those below the fatigue limit, are included in N'.

When any of the stress ranges in a spectrum is below the fatigue limit, W'_F is less than W_F. The ratio W'_F/W_F depends on the percentage of the stress-range distribution curve (probability-density curve) that is below the constant-amplitude fatigue limit and on the shape of the stress-range

TABLE 4

FATIGUE EQUATIONS AND CONSTANTS

$$N' = \frac{KA}{F_{sr}^3}$$

For $F_{sr}/F_{srL} \geq 3$: $K = 1$

For $F_{sr}/F_{srL} < 3$: $K = \frac{1}{2(F_{sr}/F_{srL} - 1)} + \frac{3}{4}$

N' = estimated minimum number of loading cycles to failure.

F_{sr} = design stress range based on W_F.

F_{srL} = maximum allowable stress range for infinite fatigue life.

A = constant listed below.

Category	F_{srL}, ksi	Constant A
A	12	240×10^8
B	8	105×10^8
C (stiffeners)	6	37×10^8
C (other attachments)	5	37×10^8
D	3.5	20×10^8
E	1.5	10×10^8
F	4	10×10^8

Conversion Factor

1 ksi = 6.89 MPa

distribution curve. For example, when half of the stress-range distribution curve corresponding to the 1970 loadometer survey is below the fatigue limit, as shown in Figure 25, $W'_F/W_F = 0.88$. If all of the stress-range distribution curve is below the fatigue limit, $W'_F/W_F = 0$.

Since fatigue life is inversely proportional to the stress range (or weight of the design truck) cubed,

$$\frac{N'}{N} = \left(\frac{W_F}{W'_F}\right)^3 \tag{13}$$

in which N' is the life calculated by assuming that the stress ranges below the fatigue limit cause no fatigue damage, and N is the fatigue life calculated by assuming that all stress ranges in the spectrum cause fatigue damage. Thus, in the example illustrated in Figure 25, the correct life, N', including all variable-amplitude cycles, is 1.46 times the life that would be calculated by ignoring the fatigue limit.

The effect of the fatigue limit could be incorporated into the design procedure in either of two ways: (1) by using W'_F in conjunction with constant-amplitude SN curves defined by Eq. 12 and (2) by using W_F in conjunction with constant-amplitude curves modified in line with Eq. 13. In the former method, a different value of W'_F would have to be used for each different detail because the fatigue limit, F_L, is different for each. Since this would be inconvenient, the second method was chosen for use in the suggested fatigue-design method.

To implement this second method, N'/N is plotted as a function of F_{sr}/F_L, in which F_{sr} is the design stress range corresponding to W_F, and F_L is the constant-amplitude fatigue limit. A typical calculation for one point on such a curve is shown in Figure 25 ($N'/N = 1.46$ for $F_{sr}/F_L = 0.87$). The curves shown in Figure 26 are for several different assumed distributions of traffic including Rayleigh distributions with $S_{rd}/S_{rm} = 1.0$ and 0.5 and a distribution corresponding to the 1970 loadometer survey. An empirical curve providing a conservative approximation of these curves is also shown.

Modified SN curves for use in conjunction with W_F were calculated by multiplying N from Eq. 11 by the correction factor N'/N from the empirical equation in Figure 26. These modified SN curves are plotted in Figure 27 for each AASHTO detail category and are used in the suggested fatigue-design method. The curves give the estimated minimum number of cycles to failure for the design stress range, F_{sr}, corresponding to W_F. A scale is given to show the average daily truck traffic that would cause this number of cycles in 50 years, if each passage caused one cycle. Equations for the SN curves are also given to facilitate computer calculations. To be consistent with the results of the long-life tests, F_L for cover-plate end details was taken as 3 ksi (21 MPa) rather than the 5 ksi (34 MPa) proposed by Fisher (*28*).

For the various distributions considered in Figure 27, all stress ranges are below the fatigue limit when $F_{sr}/F_L \leq 0.5$; consequently, the fatigue life, N', is infinite when $F_{sr}/F_L \leq 0.5$. Therefore, no further check is required in the suggested design method when the design stress range is below this limiting value of $F_{srL} = 0.5\ F_L$. Also, in line with the present AASHTO fatigue specifications, no further fatigue check is required if the stress at a detail due to combined dead, live, and impact loading is always compressive.

Design Life

In the suggested design method. if the design stress range exceeds the limiting value, F_{srL}, the estimated minimum life of the detail in years must be calculated from the following equation:

$$L = \frac{N'}{365TP}$$

in which T is the average daily truck traffic and P is the average number of loading cycles per truck passage.

Traffic Volume

For multiple-lane bridges, excluding two-lane bridges with traffic in both directions, T is taken as the total daily truck traffic in one direction. Actually, only a fraction of the traffic in one direction passes in the lane under consideration, and the rest pass in adjacent lanes. Because of lateral distribution of load, the passages in adjacent lanes cause stresses in the longitudinal members in the lane under consideration, but these stresses are considerably less than the stresses that would occur if the trucks had passed in the lane under consideration. Opposing traffic in adjacent lanes produces additional stress cycles, but usually of a relatively small magnitude. For multiple-lane bridges, therefore, it is conservative to take T as the total traffic in one direction. Some trucks pass across the bridge close enough to interact; the minor effects of such interactions are discussed later.

In two-lane bridges with traffic in both directions, all of

the traffic in one direction actually passes in the lane under consideration. Traffic in the opposite direction causes additional stress cycles of a smaller magnitude. Therefore, in the suggested design method, it is conservatively assumed that in such two-lane bridges, the total traffic in both directions passes in the lane under consideration.

In the preceding directions, it was assumed that all trucks passing over the bridge are far enough apart, either in the same lane or adjacent lanes, so that the peak stress caused by one is not significantly increased by the effect of another. For most truck passages this is true; but, for a few passages, the trucks are close enough to cause peak stresses somewhat larger than those that would occur if they were far apart (*29*). However, the conservative nature of the assumption that all traffic in one direction passes in the lane under consideration, and of various assumptions made in the suggested design method, is considered sufficient to account for the minor effects of these interactions.

Load Spectrum (1970 Loadometer Survey)

i	Wi, kips	α_i	$\alpha_i W_i^3$ for W_F	$\alpha_i W_i^3$ for W'_F
1	22.5	11.35	1,293	0
2	27.5	15.70	3,265	0
3	32.5	12.73	4,370	0
4	37.5	9.67	5,099	0
5	42.5	6.42	4,928	0
6	47.5	5.82	6,237	0
7	52.5	5.53	8,002	0
8	57.5	5.73	10,893	0
				$W_L = 60$
9	62.5	6.12	14,941	14,941
10	67.5	7.80	23,989	23,989
11	72.5	8.29	31,591	31,591
12	77.5	3.06	14,244	14,244
13	82.5	0.99	5,559	5,559
14	87.5	0.49	3,283	3,283
15	92.5	0.20	1,583	1,583
16	97.5	0.10	927	927
		1.000	140,204	96,117

$$W_F = \left[\sum \alpha_i W_i^3\right]^{1/3} = (140204)^{1/3} = 52.0 \text{ kips} \qquad W'_F = (96117)^{1/3} = 45.8 \text{ kips}$$

$$\frac{W'_F}{W_F} = \frac{45.8}{52.0} = 0.88 \qquad \frac{N'}{N} = \left(\frac{W_F}{W'_F}\right)^3 = \left(\frac{52.0}{45.8}\right)^3 = 1.46$$

$$\frac{F_{sr}}{F_L} = \frac{W_F}{W_L} = \frac{52.0}{60.0} = 0.87$$

Conversion Factor

1 kip = 4.448 kN

Figure 25. Typical calculation of the effect of fatigue limit on W_F and N.

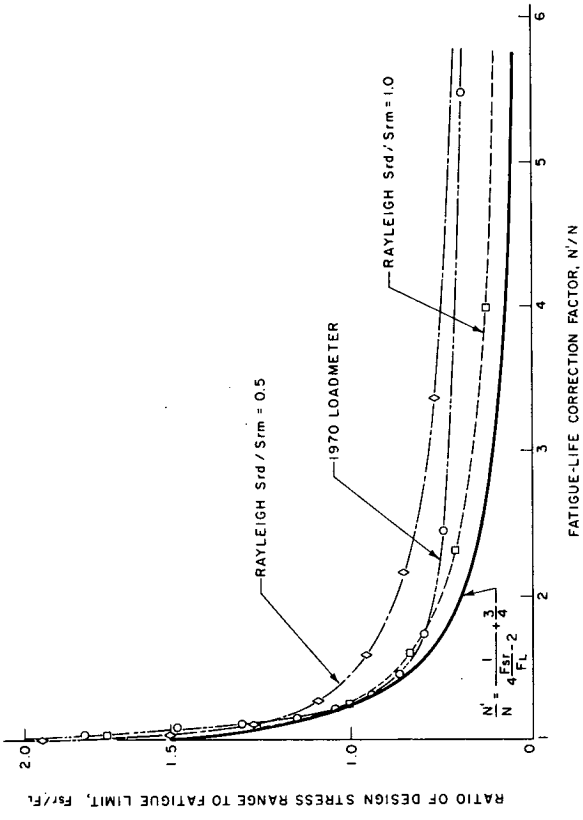

Figure 26. Relationship between fatigue-life correction factor and ratio of design stress range to fatigue limit.

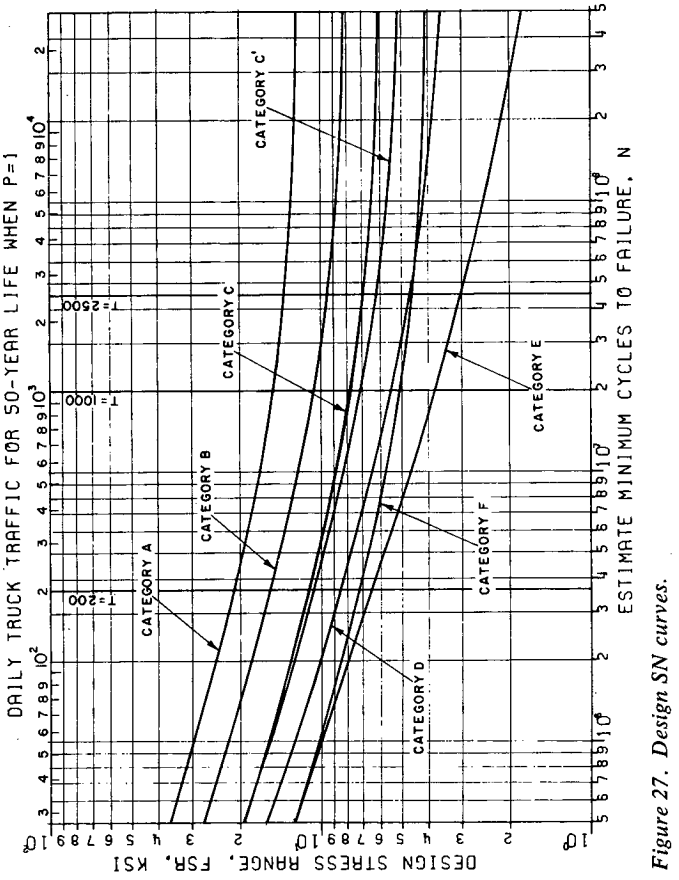

Figure 27. Design SN curves.

Stress Cycles per Truck Passage

The appropriate value of P to be used in Eq. 14 varies with the type of bridge, location on the bridge, and type of member under consideration. The passage of a truck across a simple-span bridge causes a single loading cycle in the longitudinal members. The passage of a truck across a continuous-span bridge theoretically causes several loading cycles that alternate between positive and negative amplitudes as the truck passes from one span to the next; also, the amplitudes increase in magnitude as the truck approaches the location under consideration. When the truck is more than one span away from the location under consideration, the stresses are small. Therefore, at most locations in a continuous-span bridge, it is assumed that the passage of a truck can be represented by a single cycle with the stress range calculated from the maximum and minimum live-load moments as discussed earlier. Therefore, P is taken as 1 for all portions of simple-span bridges and most portions of continuous-span bridges. At interior supports in continuous-span bridges, two approximately equal stress cycles occur as the truck passes across the two spans adjacent to the support. Therefore, P is assumed to equal 2 at locations within 10 percent of the span on either side of an interior support.

The vibration characteristics of some types of bridges, such as cantilever (suspended-span) girder bridges, cause several major stress cycles in the main longitudinal members for each passage of a truck. Experimental load trace number 5 in Figure C-1 shows these stress cycles for a cantilever suspended-span bridge composed of wide-flange beams. Consequently, P should be taken as some number above 1, say 5, for longitudinal members in such bridges.

For transverse members and details subject to wheel or axle loads, P must be taken as some effective value representing the average number of wheel or axle loads per truck passage. Since the heavier trucks contributing most of the fatigue damage have several axles, a value of about 3 appears reasonable for P. With this value of P, the allowable stress range for infinite life governs most practical designs of transverse members. Probability-density curves of wheel loads for normal traffic would be required to obtain a more refined value of P for transverse members.

It is suggested that the life, L, calculated from Eq. 14, be at least 50 years. It is also suggested that T be taken as at least 2,500 for all Interstate highways and for other major highways in urban areas; at least 1,000 for major highways in rural areas; and at least 200 for secondary roads, unless available traffic information indicates otherwise. This classification of highways corresponds roughly to the present AASHTO classification (Table 1.7.3A of the 1974 AASHTO Interim Specifications (*1*)). The suggested values of P, T, and L, of course, could be modified to provide any degree of safety desired by specification writers.

Incorporation into AASHTO Specifications

The foregoing approach could be incorporated into the AASHTO specifications as follows:

Fatigue Design of Steel Bridges

Fatigue-Design Truck. In the fatigue design of a bridge, the expected distribution of truck traffic shall be repre-

sented by a fatigue-design truck that is the same as the HS20-44 truck (Article 1.2.5), except that its gross weight, W_F, shall be selected so that the number of cycles to failure for the fatigue-design truck is the same as the total number of cycles to failure for the different trucks in the distribution. If specific information is available on the expected distribution of truck traffic, W_F shall be determined from the following equation:

$$W_F = [\Sigma \alpha_i W_i^3]^{\frac{1}{3}}$$

in which α_i is the fraction of trucks with a weight W_i. If specific information is not available on the expected distribution of truck traffic, W_F shall be equal to 50 kips (220 kN).

Design Stress Range. To determine the design stress range for a particular structural detail, a single fatigue-design truck shall first be placed in the position that produces the maximum tensile stress at the detail and then in the position that produces the maximum compressive stress. The design stress range is the sum of these maximum stresses, both being considered positive, times the impact factor from Article 1.2.12. The lateral-distribution factors and procedures in Article 1.3.1(B) shall be used without modification except that for interior and exterior longitudinal stringers and beams supporting a concrete deck; factors of S/10 and S/7, respectively, shall be used when S does not exceed 14 feet. When S exceeds 14 feet, the lateral distribution factor shall be calculated assuming that the deck acts as a simple span between adjacent beams and is loaded by a single truck.

Maximum Allowable Stress Range for Infinite Life. If the design stress range does not exceed the value of F_{SRL} listed in Table 4 for the details described in Table 1.7.3C (this table is given in the 1974 AASHTO Interim Specifications (*1*) and is not repeated herein), the fatigue life is infinite and no further fatigue check is required. Also, if a compressive dead-load stress greater than the maximum tensile stress due to the fatigue-design truck plus impact occurs at a detail, no further fatigue check is required.

Minimum Estimated Life. If a further check is required, the minimum estimated life shall be calculated from:

$$L = \frac{N'}{365TP}$$

in which L = estimated minimum life in years;
N' = estimated minimum number of loading cycles to failure from Figure 27 or Table 4;
T = average daily truck traffic (over 20 kips (89 kN) gross weight) on the bridge in one direction, except that for two-lane bridges with traffic in two directions T shall be the total traffic in both directions; and
P = average number of loading cycles per truck passage for that member.

Unless different values can be shown to apply, P shall be taken as 5 for main longitudinal members of cantilever (suspended-span) bridges, 2 for the portion of main longitudinal members within 0.1 of the span on both sides of an interior support of continuous-span bridges, 1 for all other portions of main longitudinal members of continuous-span bridges and for all portions of main longitudinal members of other bridges, and 3 for transverse members and details subject to wheel or axle loads. Unless traffic surveys, predictions of future traffic, or other considerations indicate otherwise, the average daily truck traffic on the bridge in one direction shall be taken as not less than 2,500 for all Interstate highways and for other major highways and streets in urban areas; 1,000 for major highways and streets in rural areas; and 200 for secondary roads and streets. The estimated minimum life for each structural detail in the bridge shall be not less than 50 years.

Advantages of New Method

The main advantages of thc suggested new method can be summarized as follows. First, the new method recognizes that the magnitude and position of the loadings that affect the fatigue life of a bridge are usually different from those used in the static design of the bridge. Thus, the new method fits well with the load-factor design method in which the fatigue design is based on service loads that are different from the overloads used in the static design of the bridge. Second, the calculated design stress ranges approximate the actual stress ranges that affect the fatigue life of a bridge and are usually less than 40 percent of the stress ranges calculated by present AASHTO procedures. Third, any specific information on the volume and weight distribution of truck traffic can be accurately reflected in the design. Fourth, for designs based on the maximum allowable stress range for infinite life, only one allowable value is given for each detail category. This stress range applies to different types of members (transverse and longitudinal) and bridges, including those seriously affected by vibration stresses, and to all present and future volumes of traffic. Fifth, for designs based on the estimated life, the degree of safety for a detail is indicated directly by the estimated life; if allowable fatigue stresses are given for different life categories, the degree of safety is obscured. Furthermore, the effects of any future changes in traffic volumes on the fatigue life in years can be immediately calculated. A check of the safety of the bridge under service loads in this manner follows the philosophy of load-factor design and would fit neatly into the present format of the load-factor specifications.

The new method might appear, at first glance, to involve more work than the present method, because a separate stress calculation must be made for the fatigue design. However, this is the only way to realistically reflect the true conditions affecting the fatigue life of the bridge. Furthermore, for simple-span members designed for truck or wheel loadings, the design stress range can be obtained from the static-design stresses by simply multiplying by the factor W_F/W_D. For continuous members, the design stress range can be calculated from the maximum and minimum moment envelopes for truck loading by using this factor. These calculations are similar to the check of truck-loading stresses that is presently required by the footnote in AASHTO Table 1.7.3A (*1*) for longitudinal members for which lane loading is used in the static design.

For main interior members in bridges governed by AASHTO truck-loading requirements, the design stress range (stress range produced in the bridge by the design truck) determined by the new design method is generally 38 percent ($50/72 \times 5.5/10$) of the stress range based on present AASHTO procedures. The allowable stress range of the new method is also less than the allowable stress range of the present method, but, as a rule, by a smaller amount, so that the new method is in the long run more liberal than the present method. This is illustrated in Table 5 for various details and magnitudes of traffic. Except for a daily truck traffic of 200, which applies only to secondary roads, the relative design stress range is always less than the relative allowable stress range. For bridge

designs governed by AASHTO lane-loading requirements, the new method is even more liberal compared with the present method.

A general comparison between the new method and present procedures cannot be made for exterior members because the lateral distribution to such members depends on the specific geometry of the bridge according to present procedures. Trial designs should be made to further assess the effect of the new method on the design of different details in various types and spans of bridges.

TABLE 5

COMPARISON OF PROPOSED NEW DESIGN METHOD WITH AASHTO METHOD FOR LONGITUDINAL INTERIOR BEAMS

	Present Method		Proposed Method		Comparison	
Detail Category	Life Category[1], cycles	Allowable Stress Range, ksi	Life Category, daily traffic	Allowable[2] Stress Range, ksi	Relative[3] Design Stress Range	Relative[4] Allowable Stress Range
A	Over 2,000,000	24	2500	14.0	0.38 (0.49)	0.58
	500,000	36	1000	17.5	0.38	0.49
	100,000	60	200	21.0	0.38	0.35
B	Over 2,000,000	16	2500	9.5	0.38 (0.49)	0.59
	500,000	27.5	1000	13.0	0.38	0.47
	100,000	45	200	16.0	0.38	0.36
C (Stiffeners)	Over 2,000,000	12	2500	7.0	0.38 (0.49)	0.58
	500,000	19	1000	8.0	0.38	0.42
	100,000	32	200	11.5	0.38	0.36
D	Over 2,000,000	7	2500	4.6	0.38 (0.49)	0.66
	500,000	16	1000	6.7	0.38	0.42
	100,000	27	200	8.6	0.38	0.32
E	Over 2,000,000	5	2500	3.0	0.38 (0.49)	0.60
	500,000	12.5	1000	4.8	0.38	0.38
	100,000	21	200	6.6	0.38	0.31
F	Over 2,000,000	8	2500	4.6	0.38 (0.49)	0.58
	500,000	12	1000	5.9	0.38	0.49
	100,000	15	200	7.2	0.38	0.48

(1) Life categories given in Table 1.7.3A of the 1974 AASHTO Interim Specifications for main members under truck loading.

(2) Allowable stress range for a 50-year life from Figure 29.

(3) Design stress range calculated by the new method divided by design stress range calculated by present AASHTO methods. This factor equals the ratio of design-truck weights divided by the ratio of lateral distribution factors (50/72) (5.5/10). The factor 0.49 shown in parenthesis is the factor that would apply if the proposed lateral distribution of S/7 is adopted by AASHTO for the over 2,000,000 cycle category (50/72)·(7/10).

(4) Allowable stress range by the new method divided by the allowable stress range by present AASHTO methods. If this factor is larger than the relative design stress range, the new method is more liberal than present AASHTO methods.

Conversion Factor

1 ksi = 6.89 MPa

CHAPTER FOUR

CONCLUSIONS AND SUGGESTED RESEARCH

CONCLUSIONS

Variable-amplitude random-sequence stress spectrums, such as occur in actual bridges, can be conveniently represented by a single constant-amplitude effective stress range, S_{re}, that would result in the same fatigue life as the variable-amplitude spectrum. The effective stress range is defined by

$$S_{re} = [\Sigma \alpha_i S^B{}_{ri}]^{1/B}$$

in which S_{ri} is the midwith of the ith interval in a histogram defining the variable-amplitude spectrum and α_i is the fraction of stress ranges within that interval. If B is taken as 2, S_{re} from this equation is equal to the root-mean-square (RMS) stress range. If B is taken as the reciprocal of the slope of the constant-amplitude SN curve for the particular detail under consideration, which is 3 for most structural details, the equation is equivalent to Miner's Law. The RMS and Miner values of S_{re} are only slightly different, and both satisfactorily represent the variable-amplitude spectrum. The RMS method provides a slightly better agreement with the test data, but is less conservative than the Miner method.

The passage of a truck across a bridge usually produces a single major stress cycle with superimposed vibration stresses that are small enough to be neglected. In cantilever (suspended-span) girder bridges, however, the single passage of a truck can cause many major stress cycles, apparently as a result of the vibration characteristics of the bridge. A family of Rayleigh probability-density curves, defined by a single mathematical expression (see Fig. 10), can be used to approximate the frequency of occurrence of major stress cycles in most stress spectrums observed in highway bridges. A particular curve from the family is defined by two parameters: (1) the modal stress range, S_{rm}, which corresponds to the peak of the curve; and (2) a parameter S_{rd}, which is a measure of the width of the curve, or dispersion of data.

Stress range and type of detail are the major parameters affecting the fatigue life of fabricated bridge members under variable-amplitude loadings as well as under constant-amplitude loadings. The effects of secondary parameters, such as minimum stress and type of steel, on the fatigue life under variable-amplitude loadings are similar to those reported in NCHRP Project 12-7 for constant-amplitude loading. A log-SN curve provides a slightly better fit of the variable-amplitude test data than a semilog-SN curve. A loading spectrum defined by a continuous Rayleigh probability-density curve and a random sequence of infinite length can be satisfactorily represented by a 500-cycle block of individual loads arranged in a random sequence that is repeated throughout a test.

Small-specimen (WOL) variable-amplitude crack-growth data can be conveniently related to constant-amplitude crack-growth data by an RMS effective stress range analogous to that used for the total fatigue life. Small-specimen crack initiation and growth data can be useful in explaining the fatigue behavior of fabricated bridge members; however, considerable uncertainty presently exists in predicting the total fatigue life of a fabricated member from such data.

SUGGESTED RESEARCH

Further research suggested by the present study is discussed in the following paragraphs under two categories. The first category covers research needed to improve present fatigue specifications, and the second category covers research aimed at obtaining a better understanding of the fatigue behavior of structural members and the correlation of this behavior with basic crack initiation and propagation data.

Improvement of Fatigue Specifications

The discussion of fatigue specifications presented earlier suggests several areas where research is needed to improve fatigue specifications for bridges. The fatigue limits need to be determined with greater confidence for various structural details, especially the more severe details. The fatigue limits for some of these details, such as cover-plate ends, probably depend significantly on the fabrication procedures. For example, the fatigue behavior, especially at low-stress ranges, of the cover-plate A beams in the present program was significantly affected by the sequence in which the cover plate, the flange plate, and the web were joined. Apparently, this effect was caused by differences in the residual stresses. Therefore, in determining the conservative fatigue limits for use in specifications, it is important to use fabrication procedures that result in the lowest fatigue limits.

As mentioned in the discussion of fatigue specifications, research is needed to determine whether lane-loading criteria are required for any type of bridge or span length. This research would involve field measurements of the stresses in members of such proportions that individual trucks would cause insignificant or, at least, small stresses. The objective would be to determine whether the variations in stresses that occur during continuous normal traffic, and the variations between peak and slack traffic during the day, would be of sufficient magnitude and frequency to be of concern.

Research would be desirable to better establish the relationship between gross truck weights and the corresponding magnitudes and spacing of wheel loads with the objective of developing a more representative idealized truck for use as the fatigue-design truck. The distribution of weight to the wheels and the spacing of the wheels for this idealized truck may differ from those for the present AASHTO

static-design trucks. The simplest representation would be a single concentrated load for designs based on truck loading, a smaller concentrated load for designs based on axle loads, and a still smaller concentrated load for designs based on wheel loads. Ratios representing the average number of wheel or axle loads per truck would be used in conjunction with these concentrated loads in estimating the fatigue life of the members in years.

Research on the effect of closely spaced trucks on the distribution of stress ranges in bridges would be desirable to determine whether this effect, referred to as headway (*29*), should be included when calculating the fatigue-design truck from a given distribution of traffic.

Some work has been done to establish realistic transverse distribution factors for girder bridges and longitudinal distribution factors for transverse members. Additional work is needed to obtain final values for these factors and for impact factors so that the stress range produced in the bridge by the passage of a given truck can be accurately calculated.

A considerable number of field measurements have been made on girder bridges to obtain stress and load spectrums caused by traffic. Additional field measurements are needed on different types of bridges and members to identify the types that are particularly susceptible to fatigue problems. For example, field measurements have shown that the passage of a truck over a cantilever (suspended-span) girder bridge produces many major stress cycles instead of only one major stress cycle as in most types of bridges. Obviously, such bridges are much more susceptible to fatigue problems than other types and may require special treatment in specifications. It is possible that other types of bridges or members that have not yet been identified are also particularly susceptible to fatigue problems. Therefore, field measurements on different types of bridges and members are more important than the further accumulation of data on one type, the girder bridge.

As discussed earlier, residual stresses caused by different fabrication procedures appear to have a significant effect on the fatigue behavior of fabricated members tested at low stress levels. Information on the effect of residual stresses would permit better correlations of crack initiation and propagation data with fatigue results for fabricated members. Also, this information would relate to design specifications because of the effects of residual stresses on the fatigue limit and fatigue cracking in compression regions.

Pilot studies have indicated that fatigue cracks initiating in regions of nominal compressive stress, as the result of local tensile residual stresses, propagate only within this local region of tensile stress. However, as discussed earlier, some beams tested at low stress levels in the present study developed cracks in the compression flange that propagated into the web and were the main cause of failure of the beam. These results are not necessarily inconsistent with previous results, but suggest that further studies of compression-flange cracking are needed.

According to the present AASHTO specifications (*1*), the full stress range is used in the design of members subjected to any tensile stress, even if it is very small; but fatigue need not even be considered if the tensile stress is 0. For example, if the stress varies from 0.1 ksi (0.7 MPa) in tension to 30 ksi (206.9 MPa) in compression, the full stress range of 30.1 ksi (207.6 MPa) must be used in design; however, if the 0.1-ksi tensile stress is reduced to 0, the design stress range is, in effect, 0. Furthermore, a variation from 30 ksi in compression to 0.1 ksi in tension is considered to have exactly the same effect as a variation from 30 ksi in tension to 0.1 ksi in compression. Additional research on compression-flange cracking would show whether this specification provision could be improved.

Fatigue Behavior of Bridge Members

Although a considerable amount of research has been conducted on the fatigue behavior of bridge members, several aspects merit further study.

To improve the correlation of crack initiation and growth data with beam results, the following additional information is needed: (1) a better understanding of the behavior for crack sizes below the crack-growth threshold, (2) more precise stress concentration factors, and (3) a better understanding of the effect of residual stresses on crack initiation and growth. Tests in which a single specimen is used to obtain basic data on both crack initiation and propagation would be especially useful in resolving inconsistencies between initiation and propagation data obtained from different specimens.

A limited amount of work on small specimens would be desirable to evaluate the RMS and Miner methods for probability-density curves other than the Rayleigh curves used in the present study; curves with more than one peak and curves that continuously increase to a maximum should be included. Similarly, the application of the RMS and Miner methods to spectrums that include stress ranges below the presently assumed fatigue limit should be evaluated. Small specimen tests on the effects of superimposed vibration stresses would be desirable to confirm the theoretical conclusions presented herein.

REFERENCES

1. "Standard Specifications for Highway Bridges, 1973" and "Interim Specifications, 1974." American Assn. of State Highway and Transportation Officials (1973, 1974).

2. FISHER, J. W., FRANK, K. H., HIRT, M. A., and MCNAMEE, B. M., "Effect of Weldments on the Fatigue Strength of Steel Beams." *NCHRP Report 102* (1970) 114 pp.

3. FISHER, J. W., ALBRECHT, P. A., YEN, B. T., KLINGERMAN, D. J., and MCNAMEE, B. M., "Fatigue Strength of Steel Beams With Welded Stiffeners and Attachments." *NCHRP Report 147* (1974) 85 pp.
4. MUNSE, W. H., "Fatigue of Welded Steel Structures." Welding Res. Council (1964).
5. ALDER, J. F., "Cumulative Damage in Fatigue of Welded Structures." *Brit. Welding J.* (Oct. 1964).
6. CONOVER, J. C. JAECKEL, H. R., and KIPPOLA, W. J., "Simulation of Field Loading in Fatigue Testing." *Reprint 660102,* Automotive Eng. Congress, Detroit, Jan. 10-14, 1966.
7. GALAMBOS, C. F., and ARMSTRONG, W. L., "Loading History of Highway Bridges." *Highway Research Record 295,* Highway Research Board (1969).
8. CUDNEY, G. R., "The Effects of Loadings on Bridge Life." *Res. Rep. No. R-638,* Michigan Dept. of State Highways (Jan. 1968).
9. CUDNEY, G. R., "Stress Histories of Highway Bridges." *J. Struct. Div.,* ASCE, Vol. 94, No. ST12 (Dec. 1968) pp. 2725-2737.
10. HEINS, C. P., and SARTWELL, A. D., "Tabulation of Dynamic Strain Data on Three-Span Continuous Bridge Structures." *Civil Eng. Res. Rep. No. 33,* Univ. of Maryland (Nov. 1969).
11. HEINS, C. P., and SARTWELL, A. D., "Tabulation of 24-Hour Dynamic Strain Data on Four Simple-Span Girder-Slab Bridge Structures." *Civil Eng. Res. Rep. No. 29,* Univ. of Maryland (June 1969).
12. HEINS, C. P., and SARTWELL, A. D., "Tabulation of Dynamic Strain Data on a Girder-Slab Bridge Structure During Seven Continuous Days." *Civil Eng. Res. Rep. No. 31,* Univ. of Maryland (Sept. 1969).
13. CHRISTIANO, P., GOODMAN, L. E., and SUN, C. N., "Bridge Stress Range History and Diaphragm Stiffening Investigation." Dept. of Civil Eng. and Hydraulics, Univ. of Minnesota (June 1970).
14. HEINS, C. P., and GALAMBOS, C. F., "Bridge Fatigue Due to Daily Traffic." *Transportation Research Record 507* (1974).
15. GOBLE, G. G., MOSES, F., and PAVIA, A., "Field Measurements and Laboratory Testing of Bridge Components." Dept. of Solid Mechanics, Structures, and Mechanical Design, Case Western Reserve Univ. (Jan. 1974).
16. TURNER, H. T., and MANNING, T. A., "A Loading History Study of Selected Highway Bridges in Louisiana." Div. of Eng. Res., Louisiana State Univ. (Apr. 1, 1972).
17. CICCI, F., and CSAGOLY, "Assessment of the Fatigue Life of a Steel Girder Bridge." Ontario Ministry of Transportation and Communications, *Res. and Dev. Div. Rep. RR192* (Sept. 1974).
18. MCKEEL, W. T., MADDOX, C. E., KINNIER, H. L., and GALAMBOS, C. F., "Loading History Study of Two Highway Bridges in Virginia." *Highway Research Record N382,* Highway Research Board (1972).
19. KLIPPSTEIN, K. H., and SCHILLING, C. G., "NCHRP Project 12-12—Materials Properties and Fabrication Methods for Beams and Specimens." U.S. Steel Corp., *Res. Lab. Rep. 76.019-001(1)* (Nov. 15, 1971).
20. "Specifications for Welded Highway and Railway Bridges." American Welding Society, *AWS D2.0-69,* 1969, and April 1971 Rev.
21. BLAKE, G. T., KLIPPSTEIN, K. H., and SCHILLING, C. G., "NCHRP Project 12-12—Test Setup and Procedures for Beam and Plate Specimen Tests." U.S. Steel Corp., *Res. Lab. Rep. 76.019-001(2)* (June 30, 1972).
22. KLIPPSTEIN, K. H., "NCHRP Project 12-12—Evaluation of Test-Performance Parameters." U.S. Steel Corp., *Res. Lab. Rep. 76-H-004(019-3)* (Apr. 7, 1975).
23. WILSON, W. K., "Review of Analysis and Development of WOL Specimen." *67-7D7-BTLPV-R1,* Westinghouse Res. Lab. (Mar. 8, 1967).
24. KLIPPSTEIN, K. H., "NCHRP Project 12-12—Stress Distributions in Specimens With Cover Plates That Simulate Bridge Details." U.S. Steel Corp., *Res. Lab. Rep. 76-H-004(019-2)* (Jan. 2, 1975).
25. BARSOM, J. M., "Fatigue-Crack Propagation in Steels of Various Yield Strengths." *Trans. ASME, J. Basic Eng.,* Series B, Vol. 93, No. 4 (Nov. 1971).
26. BARSOM, J. M., "Fatigue Behavior of Pressure-Vessel Steels." *WRC Bulletin 194* (May 1974).
27. HAAIJER, G., "Design Data for High-Yield-Strength Alloy Steel." *ASCE Struct. J.* (Aug. 1966).
28. FISHER, J. W., "Guide to 1974 AASHTO Fatigue Specifications." American Institute of Steel Construction (1974).
29. MOSES, F. M., GOBLE, G. M., and PAVIA, A., "Truck Loading Model for Bridge Fatigue." Specialty Conference on Metal Bridges, ASCE (Nov. 1974).
30. SANDERS, W. W., JR., and ELLEBY, H. A., "Distribution of Wheel Loads on Highway Bridges." *NCHRP Report 83* (1970) 56 pp.
31. "American National Standard—Surface Texture." American National Standards Institute, *ASA B46.1-1962.*
32. VELETSOS, A. S., and HUANG, T., "Analysis of Dynamic Response of Highway Bridges." *J. Struct. Div.,* ASCE, Vol. 96, No. EM5 (Oct. 1970) pp. 617-619.
33. SCHILLING, C. G., and KLIPPSTEIN, K. H., "NCHRP Project 12-12—Stress Spectrums." U.S. Steel Corp., *Res Lab. Rep. 76.019-001(3)* (Sept. 25, 1972).
34. LINDGREN, B. W., *Statistical Theory.* Macmillan (1962).
35. DIXON, W. J., and MASSEY, F. J., *Introduction to Statistical Analysis.* McGraw-Hill (1957).
36. Columbia University Statistical Research Group, *Selected Techniques of Statistical Analysis.* McGraw-Hill (1947).
37. WILLIAMS, E. J., *Regression Analysis.* John Wiley (1957).
38. MADDOX, S. J., "Assessing the Significance of Flaws in Welds Subject to Fatigue." *Welding Res. Supplement,* Vol. 53 (Sept. 1974).
39. PARIS, P. C., and SIH, G. C., "Stress Analysis of Cracks." *Fracture Toughness Testing and Its Applications,* ASTM STP 381 (Apr. 1965).
40. SCHILLING, C. G., KLIPPSTEIN, K. H., BARSOM, J. M.,

NOVAK, S. R., and BLAKE, G. T., "Low-Temperature Tests of Simulated Bridge Members." *J. Struct. Div.*, ASCE, Vol. 101, No. ST1 (Jan. 1975) pp. 31-48.

41. ALBRECHT, P., and FISHER, J. W., "An Engineering Analysis of Crack Growth at Transverse Stiffeners." *Publications,* IABSE, Vol. 35-I (1975).

APPENDIX A

SPECIMENS AND BEAMS

Sketches showing nominal dimensions and photographs of the specimens and beams are given in Figures 2 through 5.

MATERIALS

All specimens and beams were fabricated from plates obtained from Homestead Works of U.S. Steel Corporation. Two different steels were used: ASTM A36 steel and ASTM A514 Grade B steel. A sketch was made of each plate to identify the location of each part cut from the plate, and an identification number was assigned to the parts (*19*).

The results of mill tests of the chemical (ladle analysis) and mechanical properties of the plates, together with the results of a check analysis made at the Research Laboratory on the material used in the WOL specimens, are given in Table A-1. All results satisfied ASTM specification requirements.

To determine the mechanical properties more precisely, a set of six or more specimens for each combination of plate thickness and steel was tested in tension at the Research Laboratory. Each specimen from a set was cut from a different plate, except when fewer than six plates were available for a particular thickness-steel combination. The location from which the specimen was cut was shown on the plate sketch. The longitudinal axis of each specimen was in the direction of final rolling of the plate. All specimens conformed to standard ASTM strap specimens and were tested in accordance with standard ASTM procedures (*21*). The loading rate in the elastic range was approximately 80 ksi/min (552 MPa/min). The static yield stress was obtained for all the specimens by stopping the crosshead movement while the strain was in the plastic region before strain hardening. The crosshead was held fixed for several minutes until stress and strain reached equilibrium. This procedure results in cusps in the stress-strain curve, with the bottom of the lowest cusp representing the static yield stress. Three such cusps were obtained during each test. The full stress-strain curve was determined for one specimen from each set. The results are summarized in Table A-2 and in a previous report (*19*). Also given are the results of separate tests made on the material used in the WOL specimens. The scatter in the results, including those for plates from different heats, as indicated by the test data, was small.

The thickness of each plate was measured at two locations (recorded on the plate sketch) by the fabricator. The average of all measurements on the plates of one nominal thickness is given in Table A-3.

The surface condition of all plates was inspected visually and found to be normal. On some plates, stamped die marks were observed, and the location of these marks was recorded on the plate sketch. During fabrication, the parts were arranged so that these die marks occurred at noncritical locations, such as in the compression flanges of the beams.

FABRICATION

All beams and cover-plate specimens were fabricated by Kutz Engineering, Inc., Pittsburgh. Pa. The quality of workmanship was comparable to that required by state highway department specifications for steel bridges and was similar to that reported for Project 12-7. U.S. Steel Corporation personnel, including a welding engineer, conducted inspections during fabrication.

As mentioned earlier, a sketch was made of each plate received from the mill to record the location of any surface defect or die mark, and the position of each component part was cut from the plate. The plates and parts were marked with a crayon. The long direction of all fabricated parts was oriented in the direction of final rolling. All plates, specimens, and beams were fabricated and stored indoors.

Beams

The beams were fabricated to the following specified tolerances:

Description	*Tolerance, in. (mm)*
Maximum sweep	1/16 (1.6)
Maximum camber	1/8 (3.2)
Over-all depth	±1/16 (±1.6)
Over-all width	±1/16 (±1.6)
Flanges out of square	1/16 max (1.6 max)
Web off center	±1/16 (±1.6)
Fillet-weld size	±1/16, −0 (±1.6, −0)

These tolerances, which are more restrictive than required in normal bridge fabrication, were specified to reduce alignment problems during testing. The toleranecs were not expected to affect the fatigue results. After fabrication, each beam was checked for conformance to these tolerances, and an inspection record was maintained. Some of the beams exceeded the specified tolerances, especially with respect to flanges out of square, but were considered acceptable for testing. No beam was straightened.

TABLE A-1

MILL-TEST AND CHECK-ANALYSIS RESULTS

Component	Steel	Plate No.	Heat No.	Yield Stress,* ksi	Tensile Strength, ksi	Reduction Area, %	Elongation, % 2 in.	Elongation, % 8 in.	Composition, % C	Mn	P	S	Si	Cu	Ni	Cr	Mo	V	B	Ti
Web	A36	1-29	74A918	46.2	69.7			28.0	0.22	0.84	0.010	0.024	0.045	0.02	0.02		0.02			
		30-41	66A795	46.8	68.1			25.0	0.23	0.72	0.010	0.025	0.028	0.02	0.02		0.01			
Flange	A36	1-29	71A954	45.1	73.4			22.0	0.22	1.01	0.011	0.024	0.026	0.04	0.02	0.04	0.01			
		30	66B035	46.0	68.1			26.0	0.22	0.88	0.008	0.035	0.025	0.03	0.02	0.02	0.01			
		31-32	65B066	46.1	72.2			27.0	0.21	0.98	0.010	0.025	0.030							
Cover Plate	A36	1-5	71A954	41.7	69.5			29.0	0.22	1.01	0.011	0.024	0.026	0.04	0.02	0.04	0.01			
		6-16	71B314	43.8	71.9			27.0	0.21	0.90	0.008	0.023	0.028	0.05	0.07	0.05	0.01			
Web	A514	1-50	70A909	122	129	49.9	22.1		0.20	0.82	0.009	0.029	0.23			0.46	0.15	0.04	0.003	0.02
Flange and Specimen	A514	1-46	70A909	120	128	48.6	23.3		0.20	0.82	0.009	0.029	0.23			0.46	0.15	0.04	0.003	0.02
		47-50	70B059	116	124	48.0	32.0		0.20	0.83	0.010	0.021	0.26	0.03	0.04	0.58	0.20	0.05	0.002	0.02
		51-54	70A909	122	130	45.0	28.0		0.20	0.82	0.009	0.029	0.23			0.46	0.15	0.04	0.003	0.02
Cover Plate	A514	1-10	70A909	117	124	49.0	20.0		0.20	0.82	0.009	0.029	0.23			0.46	0.15	0.04	0.003	0.02
		11-32	73B132	112	121	57.5	32.0		0.20	0.82	0.009	0.029	0.23			0.46	0.15	0.04	0.003	0.02
									Research Laboratory Check Analysis											
WOL Specimen									0.21	0.91	0.009	0.023	0.26	-	-	0.56	0.19	0.048		0.017

* Denotes yield point for A36 steel and yield strength (0.2% offset) for A514 steel.

Conversion Factors

1 ksi = 6.89 MPa

1 in. = 0.025 m

TABLE A-2

MECHANICAL PROPERTIES

Component	Steel	Yield Stress,* ksi Mean	Yield Stress,* ksi Std Dev	Static Yield Stress, ksi Mean	Static Yield Stress, ksi Std Dev	Tensile Strength, ksi Mean	Tensile Strength, ksi Std Dev	Reduction of Area, % Mean	Reduction of Area, % Std Dev	Elongation, % In 2 in. Mean	Elongation, % In 2 in. Std Dev	Elongation, % In 8 in. Mean	Elongation, % In 8 in. Std Dev
Web	A36	42.3	0.6	41.5	0.7	69.1	1.2	61.9	1.7	45.5	2.9	25.8	1.8
Flange	A36	42.2	0.5	41.1	1.2	70.5	1.8	65.1	1.5	47.0	2.9	26.1	1.3
Cover Plate	A36	38.5	2.6	35.6	1.3	71.4	1.8	60.0	7.8	45.6	4.0	24.5	3.4
Web	A514	121.9	3.6	120.1	1.9	126.3	3.5	49.2	4.5	22.3	0.5	-	-
Flange and Specimen	A514	119.6	2.0	115.1	2.4	128.2	1.6	47.8	2.8	24.8	1.2	-	-
Cover Plate	A514	112.7	3.9	110.2	6.3	122.4	2.9	55.7	5.1	30.0	2.1	-	-
WOL Specimens	A514	129	-	-	-	136	-	64	-	16*	-	-	-

* Denotes yield point for A36 steel and yield strength (0.2% offset) for A514 steel.

** Elongation in 1 inch.

Conversion Factors

1 ksi = 6.89 MPa
1 in. = 0.0254 m

Assembly

The flanges, webs, and cover plates were oxygen cut from the plates to a tolerance of ±1/16 in. (1.6 mm) and a surface finish of 1,000 microinches (arithmetic average—1,000 microinches are equivalent to 0.025 mm) (*31*) or better; both edges were cut simultaneously, as shown in Figure A-1, to reduce distortions. The edges of the web plates were then blast cleaned, and the center of the flange plates was cleaned by grinding in the longitudinal direction of the plate, as shown in Figure A-2. The flange plates for cover-plate beams and the edges of the cover plates were wire brushed along the axis of the cover-plate fillet welds before welding.

In fabricating the cover-plate A beams, and some of the cover-plate C beams, the cover plates were first welded to the flanges. Tack welds between the cover plate and flange were usually confined to the center third of the cover plate. The flanges and web were then assembled in a jig and tack welded by using properly dried E7018 electrodes, as shown in Figure A-3. Tack-weld locations were marked on the web. For the cover-plate C beams, a manual 1/4-in. (6.4-mm) fillet weld was later placed across the cover-plate ends, around the corners, and feathered into the existing longitudinal edge welds. Cover-plate B beams were fabricated in the same way as the A beams except that the cover plate was welded to the flange plate after it had been welded to the web. The remaining cover-plate C beams were fabricated similarly to the cover-plate B beams except that the ends of the cover plates were also welded across each end.

TABLE A-3

PLATE THICKNESS MEASUREMENTS

Component	Steel	Thickness, in. Nominal	Thickness, in. Mean	Thickness, in. Std Dev	No. of Measurements
Web	A36	0.281	0.286	0.0005	60
Flange	A36	0.375	0.377	0.0006	64
Cover Plate	A36	0.563	0.567	0.0007	12
Web	A514	0.281	0.293	0.0008	100
Flange	A514	0.375	0.383	0.0007	100
Specimen	A514	0.375	0.381	0.0025	8
Cover Plate	A514	0.563	0.577	0.0009	20

Conversion Factor

1 in. = 0.0254 m

The beams without cover plates were assembled in the same jig as was used for the cover-plate beams, and in the same way.

Welding

The welders and welding operators were qualified in accordance with the AWS bridge specifications (*20*); the welding procedures also conformed to this specification. All welds, with the exception of the cross welds mentioned earlier, were placed by the automatic submerged-arc process. The size tolerance for the 3/16- and 1/4-in. (4.8- and 6.4-mm) fillet welds was +1/16 and —0 in. (1.6 and —0 mm). Any visually apparent defects were gouged out and repaired

by welding. The location of the repairs was marked on the web.

The two welds connecting one flange with the web plate were placed simultaneously; however, to avoid interference of the two opposite arcs, one welding head preceded the opposite head by up to 6 in. (150 mm) (see Fig. A-4). The two welds connecting the cover plates with the flange plates were placed simultaneously in the same direction, with no gap between opposite heads. The ends of these welds were not touched up. The cross welds for cover-plate C beams were made by Research Laboratory welders using the shielded-metal-arc process with E7018 electrodes.

The A36-steel beams were welded with the AWS F71-EL12 wire-flux combination (Lincoln L-60 5/64-in.-diameter (2-mm) wire and L-780 flux). The A514-steel beams were welded with the AWS F72-EM12K wire-flux combination (Lincoln L-61 5/64-in.-diameter wire and L-780 flux). All 3/16-in. (4.8-mm) submerged-arc fillet welds were placed at 23 in. (584 mm)/min, and all 1/4-in. (6.4-mm) submerged-arc fillet welds at 16 in. (406 mm)/ min. The electric current and potential were 350 amp and 30 V, respectively. No preheat was used. The tack welds were made with 1/8-in. (3.2-mm) ASTM E7018 electrodes. All electrodes and fluxes were stored in accordance with the AWS specification (*20*), immediately upon removal from hermetically sealed containers.

The quality of the flange-web welds for the A514-steel beams was checked by fabricating 10 polished weld sections from one beam without cover plates. A typical section is shown in Figure A-5a. A slightly larger heat-affected zone is apparent for the left fillet weld, because this weld was

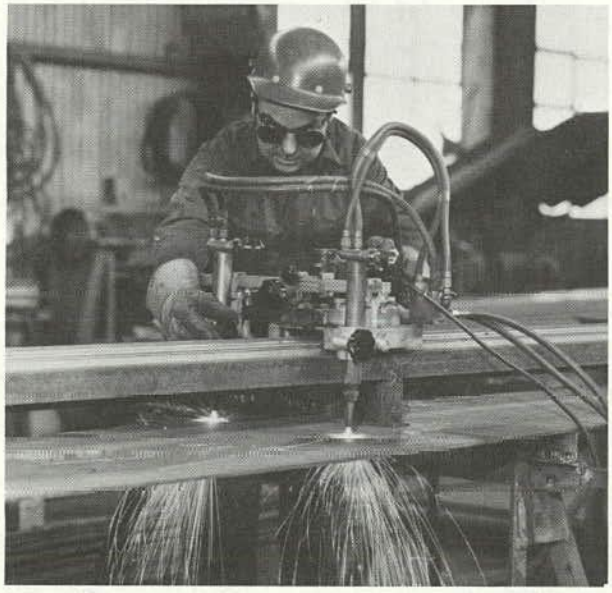

Figure A-1. Oxygen cutting.

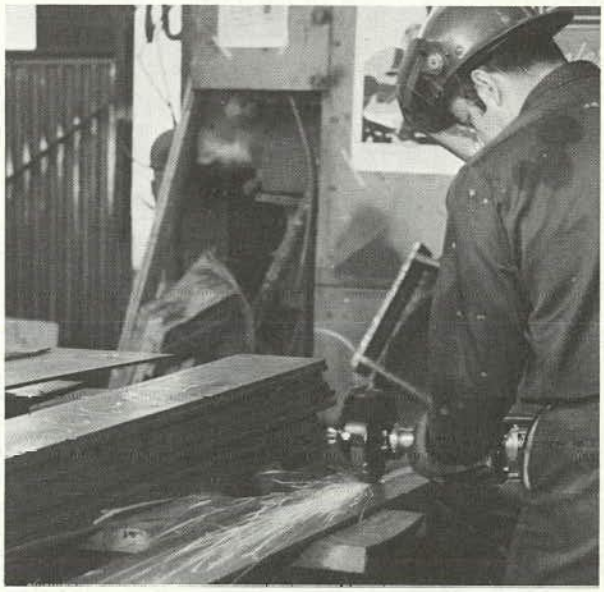

Figure A-2. Grinding.

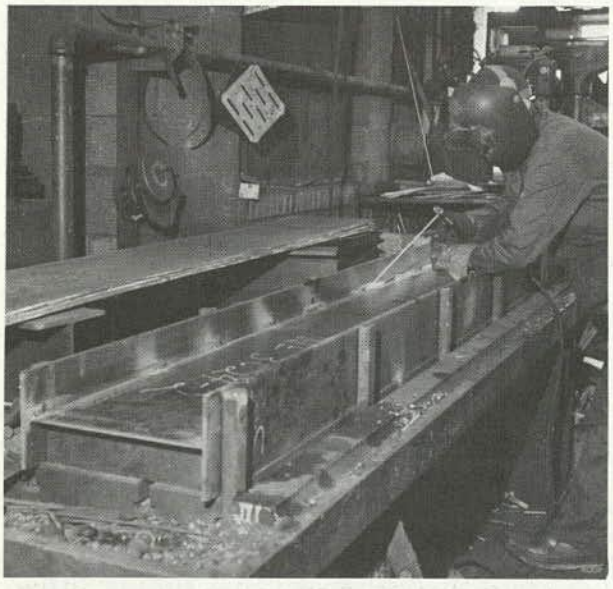

Figure A-3. Tack welding.

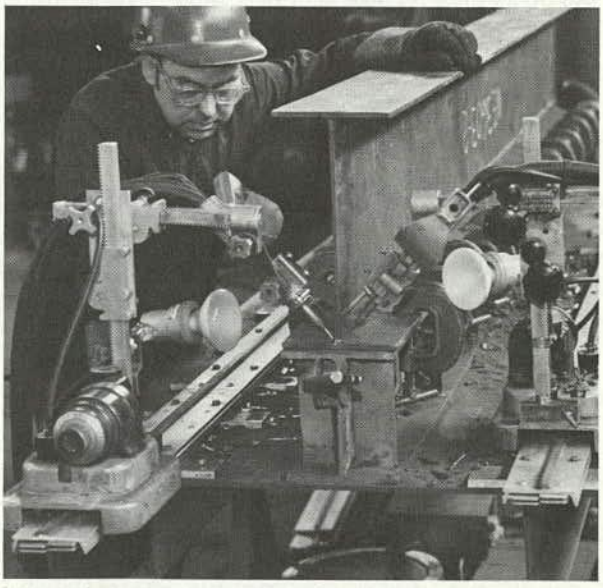

Figure A-4. Submerged-arc welding.

produced by the trailing welding head and the material was slightly preheated by the leading (right) weld. Specimen 9, shown in Figure A-5b, was the only section in which a below-surface crack was observed. The quality of the welds was rated by welding engineers as comparable to the quality of welds normally found in bridge structures.

Cover-Plate Specimens

The cover plate was clamped to the flange plate after both were oxygen cut. Submerged-arc welds were placed one at a time and in opposite directions. No tack welds were used. The end of each weld was touched up manually by shielded-metal-arc welding with E7018 electrodes to fill the end craters. The welding procedures for the cover-plate specimens were the same as for the A514-steel beams. The reduced width of the specimen was then machined to a tolerance of ±0.002 in. (0.0508 mm), as shown in Figure A-6, and polished to an edge-surface finish of 16 (*31*) or better. The tolerances on all other dimensions were ±1/16 in. (1.6 mm).

Even though the specimens were clamped during welding, the shrinkage of the welds caused a slight curvature of the specimen (concave on the cover-plate side) in the region of the cover plate; the end portions beyond the cover plate, however, remained straight. The resulting camber was measured over the specimen length of 24 in. (610 mm) along both sides of the specimen and was recorded for each specimen. In general, the camber was about 1/8 in. (3.2 mm), but was 3/16 in. (4.8 mm) in some specimens. Since such a camber would cause undesirable bending stresses in the axial-load fatigue tests, when the camber exceeded 1/64 in. (0.4 mm), the specimen was straightened to within 1/64 in. To minimize the effects of straightening on fatigue behavior, the specimens were straightened only within the center 3½ in. (88.9 mm) of the cover plate. Thus, the ends of the welds, where fatigue failures occur, were approximately ½ in. (12.7 mm) beyond the straightened region.

Figure A-7 shows the straightening fixture. The hand-operated hydraulic jack has a capacity of 50 T (445 kN). The supports of the fixture were spaced 3½ in. A force of approximately 30 to 40 T (267 to 356 kN) was required to straighten the specimens, depending on the initial camber. A record was kept of the initial and final camber of each specimen.

COVER-PLATE END DETAILS

Since the cover-plate end details control the fatigue strength, these details are described, as follows, for the cover-plate A beams and for the cover-plate specimens.

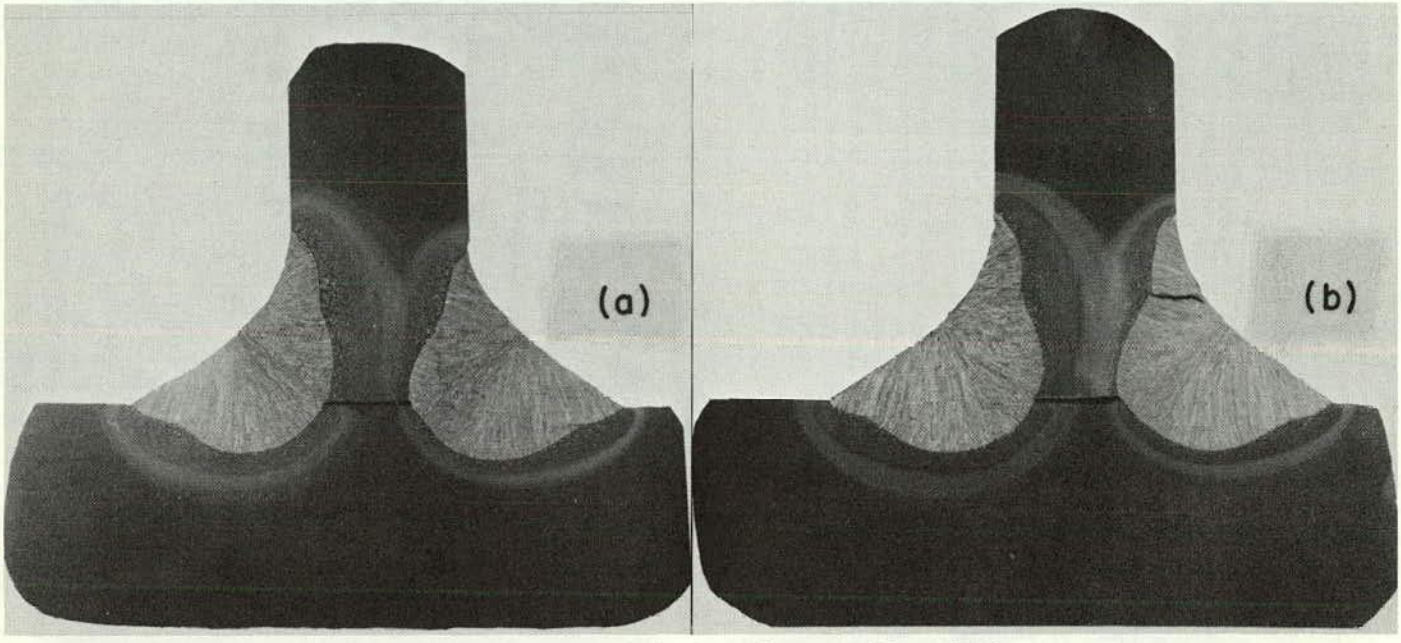

Figure A-5. Fillet-weld sections: (a) typical weld section, X3; (b) weld section with crack, X3

Cover-Plate A Beams

For the cover-plate end beams, the start and the end of the fillet welds connecting the cover plate to the flange plate are shown in Figure A-8. The start of the welds (Fig. A-8a) had a more consistent geometry than the end of the welds (Fig. A-8b); in other words, there was more variation in the geometry at the weld ends. The fillet-weld extension beyond the end of the cover plate was approximately ¼ in. (6.4 mm) at the start and up to ½ in. (13 mm) at the end of the weld.

Visual inspection of the end details and inspection by the magnaflux method did not reveal any cracks near the end of the fillet weld.

Cover-Plate Specimens

For cover-plate specimens, Figure A-9 shows close-up top views of a specimen with the fillet welds connecting the flange plate to the cover plate. The lower-left and the upper-right end details of Figure A-9a represent the start of the fillet welds, and the upper-left and lower-right end details represent the end of the fillet welds. Figure A-9b

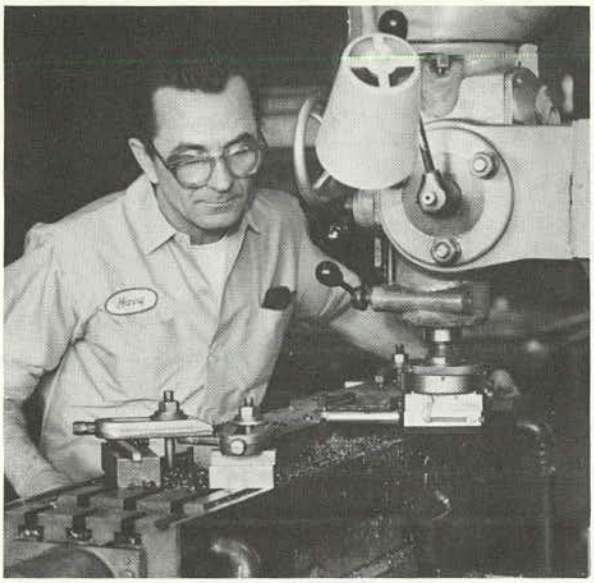

Figure A-6. Machining of specimens.

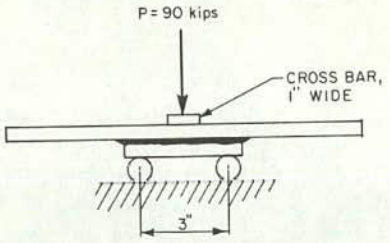

Load and Support Layout

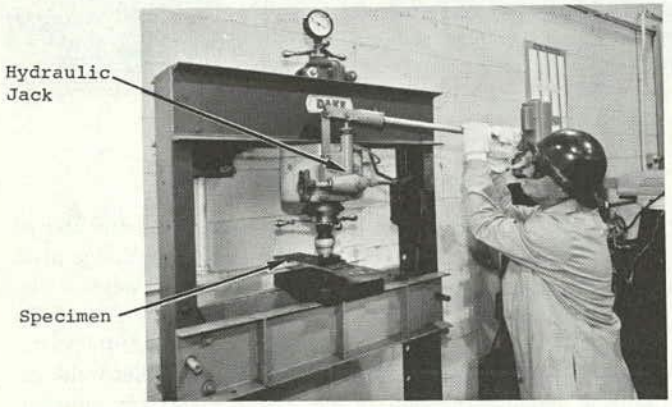

Fixture

Conversion Factors:
1 kip = 4.45 kN
1 in. = 25.4 mm

Figure A-7. Straightening setup for cover-plate specimen.

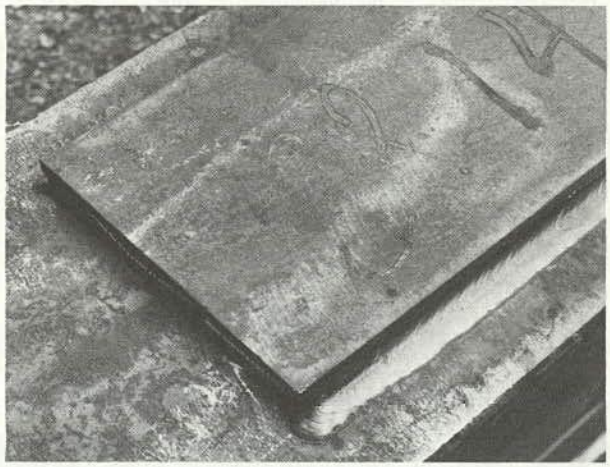

a) Start of fillet weld.

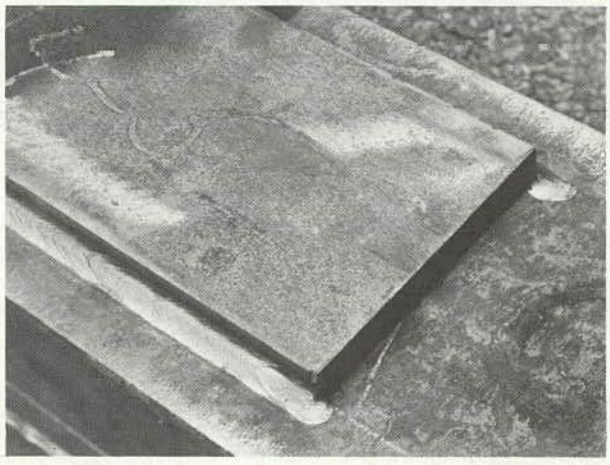

b) End of fillet weld.

Figure A-8. Start and end of fillet welds connecting cover plate to flange plate.

shows the rear weld of the specimen. The craters at the end of all fillet welds were filled by using the shielded-metal-arc process and E7018 electrodes to avoid undercuts or end defects.

Visual and magnaflux inspections revealed no cracks near the weld ends. To further check for cracks, one sample specimen was sectioned, as shown in Figure A-10a. Sections 3 and 4 were macroetched (see Figs. A-10b and A-10c), and when these sections were observed at a magnification of $\times 500$ no cracks were visible. It is apparent that cracks did not occur along the toe of the fillet-weld ends or starts, since such cracks would be perpendicular to the cut section and would therefore be visible in the cut section.

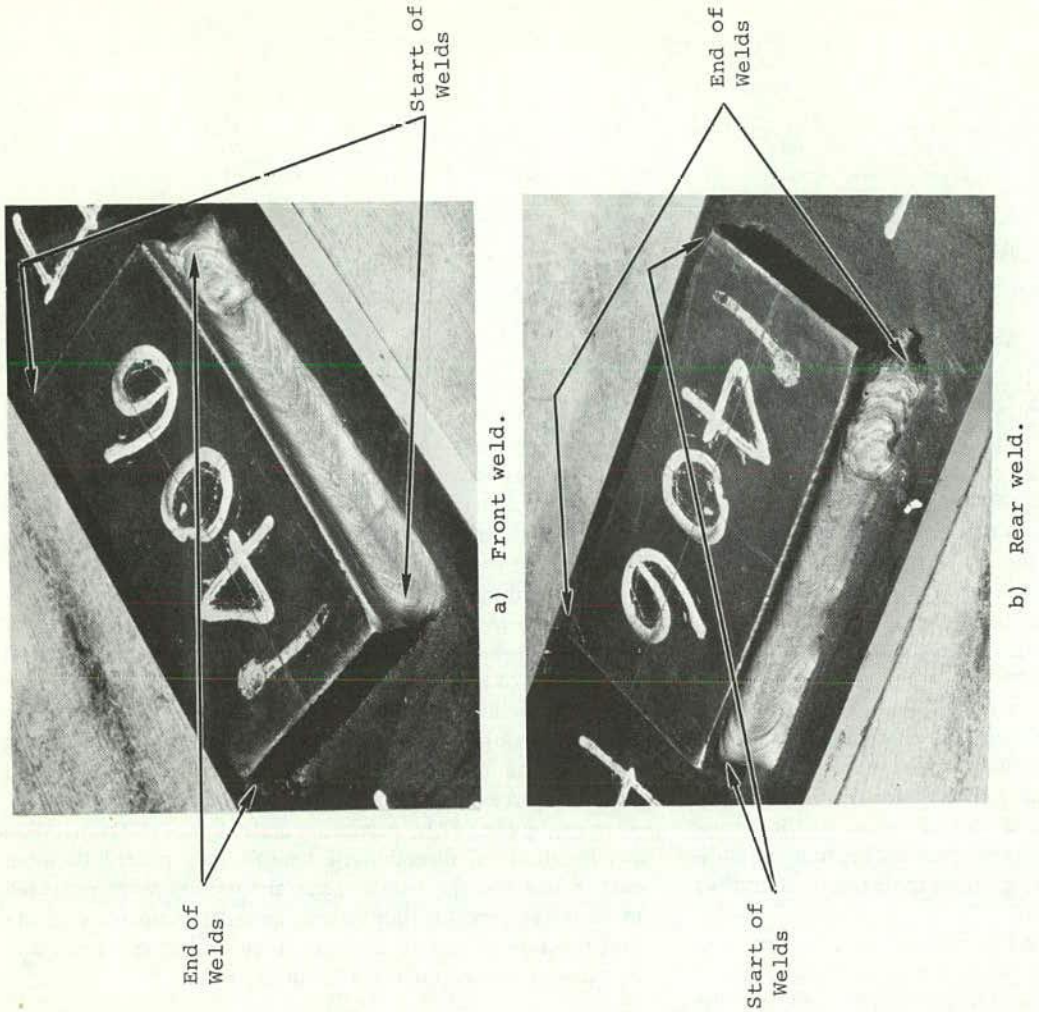

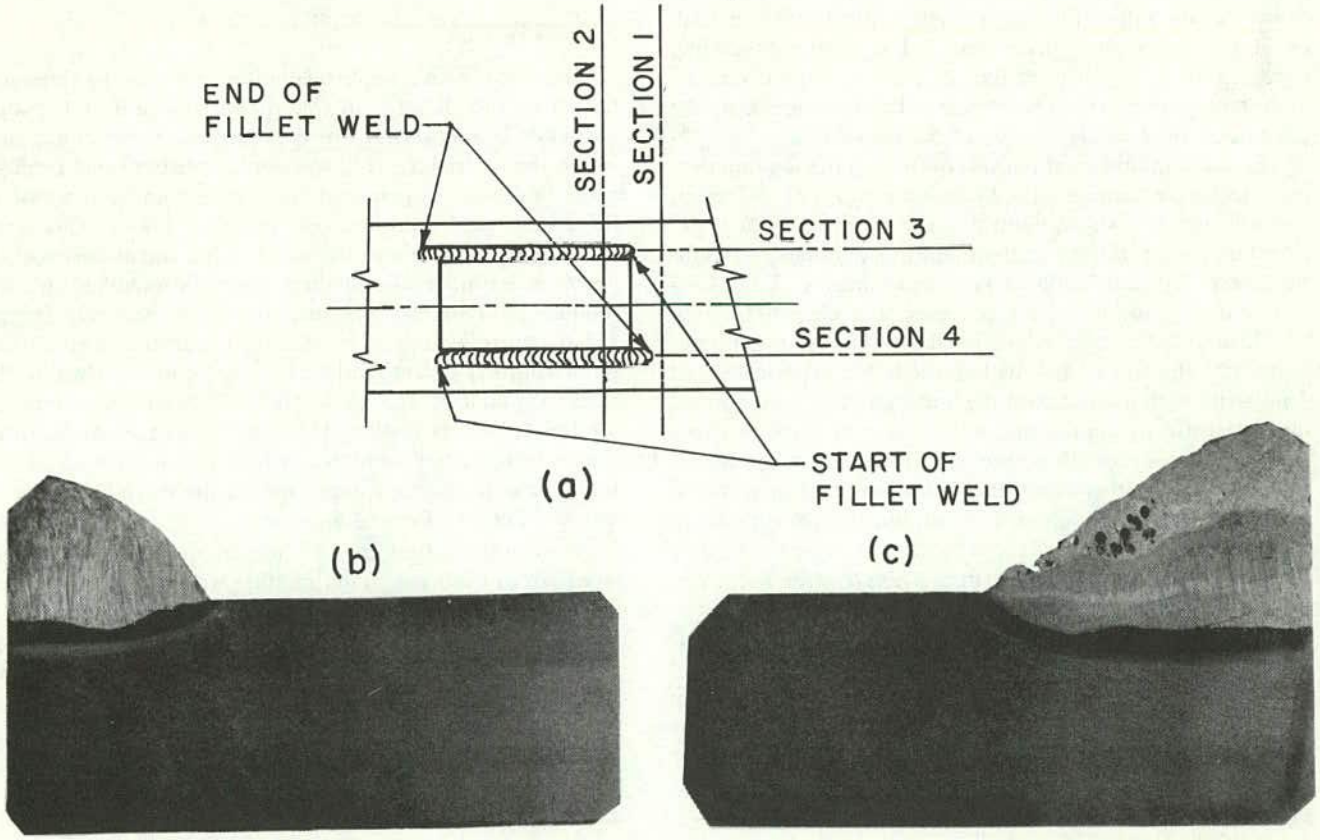

Figure A-10. Weld sections cut from specimen: (a) sectioning schematic; (b) section 3, start of weld, X3; (c) section 4, end of weld. X3.

APPENDIX B

TEST PROCEDURES AND SETUP

BEAM-TEST SETUP

All beams, with the exception of the beams tested in the second phase of the long-life tests, were tested on a 10-ft (3.05-m) span. The critical cross section for the cover-plate beams (as shown in Fig. 6) was at the high-stress end (location H) of the cover plate, and the nominal stress in this location was used as the main test parameter. Specifically, this nominal stress was the bending stress, excluding stress concentrations, on the outer fibers of the flange of the beam without a cover plate. For the cover-plate A beams, the weld geometry was more severe and consistent at the end of the cover plate, where the welds were started, than at the opposite end. Therefore, the end of the cover-plate with the starting weld was placed at the high-stress location in the test frame. The load was placed away from midspan to reduce the chance of failure at the wrong end of the cover plate and to permit acquisition of additional data (if desirable) by retesting the low-stress ends of beams (*21*).

A spreader beam was used to provide a region of constant bending stress in the welded beams without cover plates (see Fig. 7). Thus, these beams were tested over the center region rather than at a single critical cross section, as in the cover-plate beam tests. The nominal bending stress on the outer fibers of the beam in this region was the main test parameter. The nominal bending stress in the flange-web fillet welds was about 5 percent less.

Three alternative methods of controlling the loading during a test were considered: (1) load control, (2) deflection control, and (3) strain control. Any of these control parameters can be related to the main test parameter—nominal stress—by static calibration or other means. Load control, utilizing commercial load cells, was chosen because (1) load cells have excellent reliability and long-term stability, (2) the researchers had considerable experience and familiarity with load-control methods, and (3) load control more realistically approximates the effects of truck passages after a beam or girder has cracked. In the deflection-control method, on the other hand, the deflection amplitude would remain constant throughout the test, but the corresponding loads would change as the cracks progressed. Similar changes in load would occur in a strain-control test. The possibility of long-term drift for strain gages applied to the beam was another important disadvantage of the strain-control method.

Three beams were tested simultaneously, but each was controlled individually. Usually, all three beams in a set were tested to failure before tests were started on any of the beams from the next set. Photographs of the cover-plate beam-test setup are shown in Figures B-1 and B-2.

Test Frame

Figure B-3 shows a schematic of the beam-test frame. The figure specifically shows the setup for cover-plate beams; the setup for welded beams is similar, but spreader beams are used to distribute the jack loads. The beams are gripped at load and reaction points to permit reversals of loads. The loading was upwards except during load reversals. The upward-loading feature of the setup facilitated crack inspections of the tension flange and installation of the beams by an overhead crane. Rubber pads were inserted between the bottom of the beam and the top of the frame at reaction points to facilitate bolt tightening and reduce chatter due to elastic elongation of the bolts. Rollers were provided at load and reaction points to eliminate end-fixity moments and catenary forces; tests showed that these moments and forces were negligible (*22*). A bearing plate, 6 in. (152 mm) wide (in longitudinal direction of beam), was placed between each roller and the beam. Lateral supports were provided at load (at jack location when spreader beams are used) and reaction points to assist in aligning the specimen and to prevent lateral buckling at high loads.

Loading System

Cyclic loads were applied simultaneously to the three test beams by the closed-loop eletcrohydraulic test system diagrammed in Figure B-4. In the system, a tape corresponding to the desired S_{rd}/S_{rm} was continuously cycled through a single digital programmer that fed a command signal to three command modules, one for each beam. This command signal, which was usually a cyclic signal corresponding to a desired cyclic loading, could be modified in each module by reducing the magnitude of the cyclic signal (span control) and/or by adding a constant signal (set-point control) corresponding to a static load. Thus, a different cyclic-load amplitude and a different superimposed minimum (static) load could be applied to each of the three beams being tested simultaneously to account for small differences in the section properties of the three beams or to test at different values of S_{rm} and $S_{\min}$ for each beam.

An electronic summing junction compared the command signal from each command module with a feedback signal from its corresponding load cell attached to each hydraulic jack. The difference (error signal) between the two signals was amplified by a gain (sensitivity) control and fed to a servo valve controlling the double-acting jack for that beam. The servo valve opened in proportion to the magnitude (voltage) of the error signal. Oil flowed from a single hydraulic pump through the servo valve into the jack and thereby caused the jack to apply the programmed load.

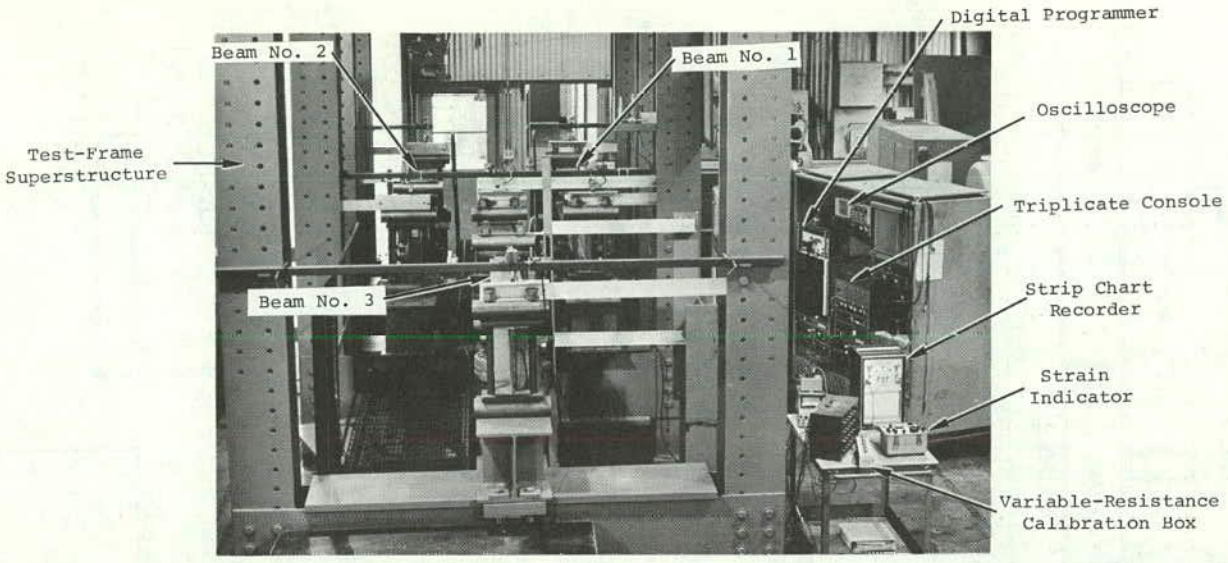

Figure B-1. Beam-test setup.

The feedback signal from the load cell was also displayed on various readout devices to provide a precise check on the applied load for each of the three beams.

A cycle counter in each command module recorded the number of cycles applied to each particular beam. Several automatic electronic-control devices were included in the system to assure that the correct loads were applied and to prevent damage due to malfunctions. Most important of these was a peak-load control that automatically delayed the programmer signal, when one beam reached its programmed peak load slightly before the others, as a result of differences in stiffness among the three beams. When all three beams had reached their peak loads, the programmer signal started again and the test continued. This peak-load control permited the system to take whatever time was required to reach the programmed peak loads for each cycle, regardless of the programmed testing speed, and assured that all three beams reached their programmed loads.

During cyclic loading the system operated at the maximum speed permitted by its hydraulic characteristics, which was usually less than the programmed speed (*21*). With three beams being tested simultaneously, the rate of loading was generally controlled by the maximum oil flow provided by the pump and, consequently, equaled a constant value that was independent of the stress amplitude unless this amplitude exceeded about 75 ksi (517 MPa). The maximum amplitudes for most stress cycles in the testing program were below this value. Therefore, the total time for each cycle was approximately proportional to the maximum amplitude for that cycle. If the amplitude increased above 75 ksi, the loading rate decreased rapidly and the total time for the cycle was correspondingly greater.

Because of these hydraulic characteristics, the average testing speed for a 500-cycle loading block varied with the stress spectrum and number of beams being tested simultaneously, and ranged from about 1 to 8.5 Hz. The time for each cycle within a variable-amplitude spectrum was roughly proportional to the maximum amplitude for that cycle, although cycles with very high amplitudes required even more time. The testing speed was generally higher

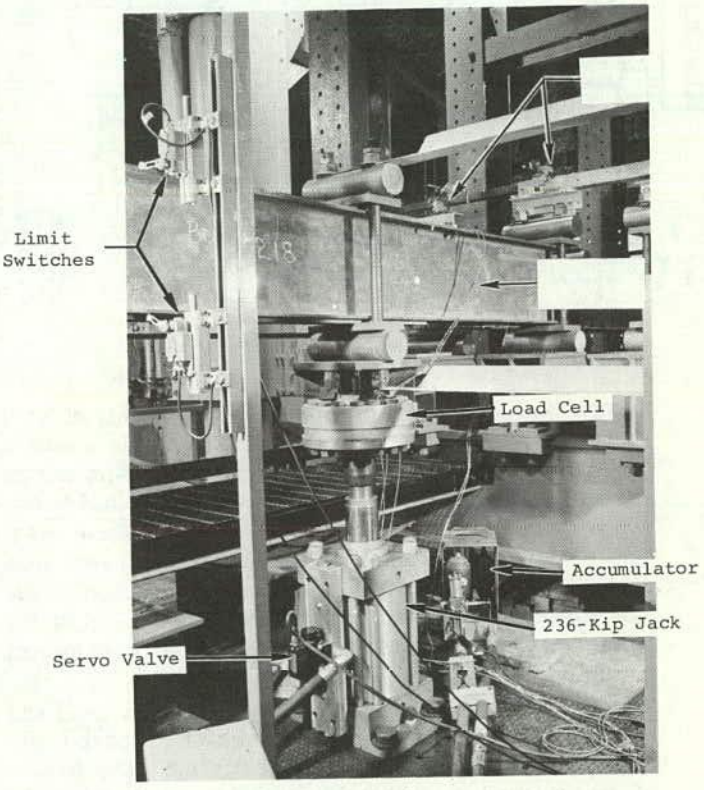

Figure B-2. Individual beam-test setup.

when only one or two beams were being tested than it was when all three beams were being tested simultaneously. The stress cycles were roughly sinusoidal in shape (*21*).

The various components of the system are described in more detail in Ref. (*21*).

BEAM-TEST PROCEDURES

Preparation of Specimens

Each beam was first inspected visually, and the flange to be loaded in tension was selected. The better of the two

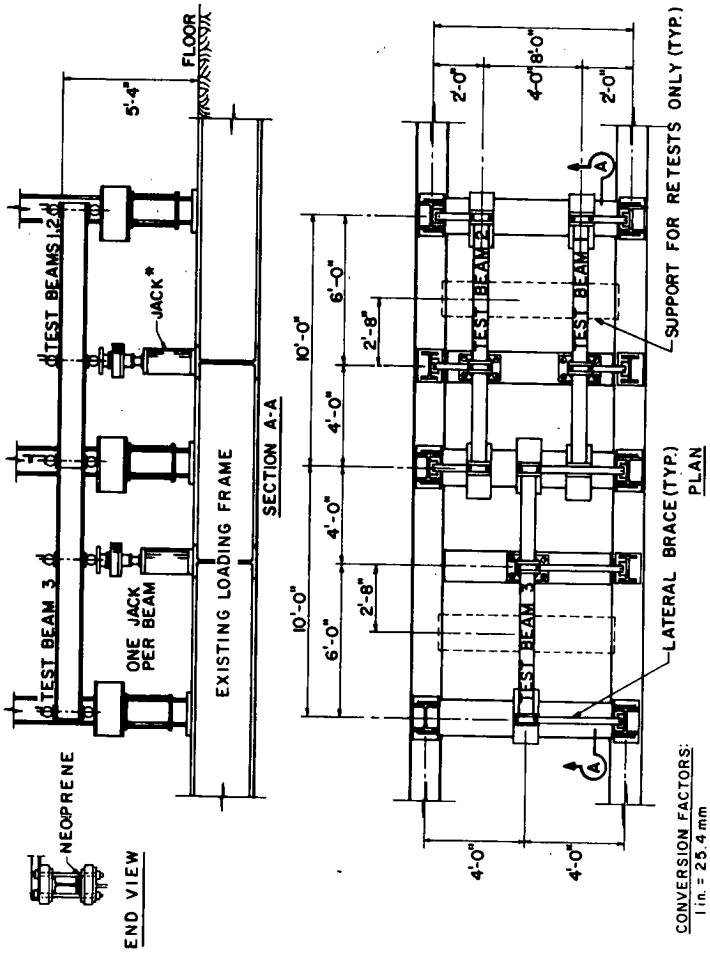

Figure B-3. Beam-test frame.

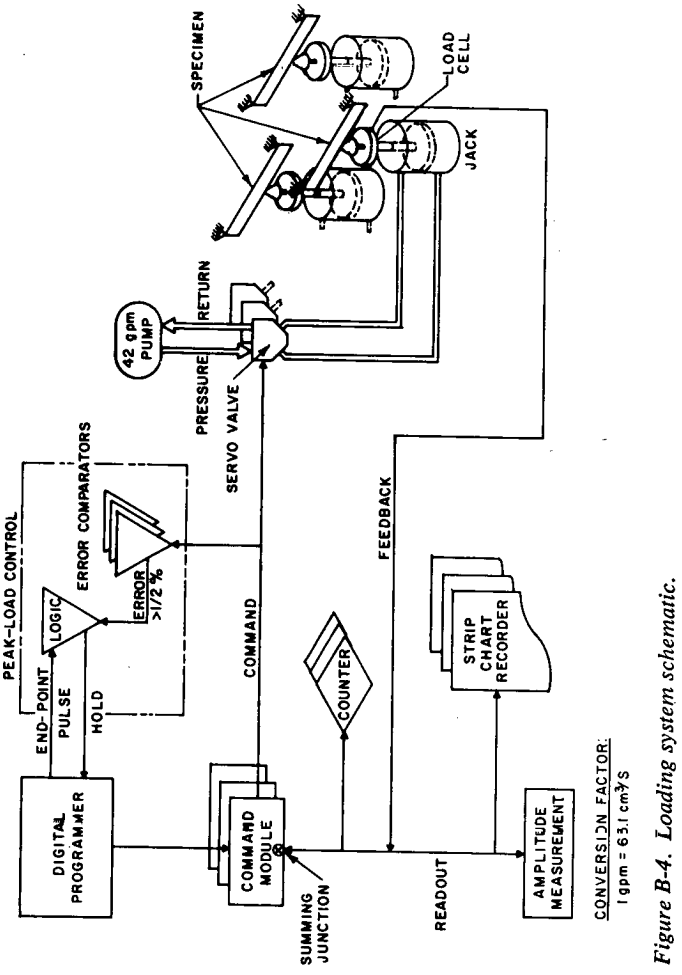

Figure B-4. Loading system schematic.

flanges, with respect to edge roughness and quality of web-flange welds in the vicinity of the cover-plate ends, was used in tension. Two ½-in. (12-mm), electrical-resistance, temperature-compensated strain gages were attached to this flange to facilitate alignment and calibration. These strain gages were located ¾ in. (19 mm) from each flange edge and 31 in. (787 mm) from the maximum reaction of the cover-plate beams (5 in. (127 mm) from the end of the cover plate). For the welded beams, the gages were located at midspan.

Reference lines indicating the locations of the loads and reactions were marked on the edge of each flange to facilitate installation of the beam in the frame. The tension flange was spray painted in the vicinity of anticipated cracks to highlight these cracks. For beams with cover plates, a mylar microscale was attached across the tension flange near the end of the fillet welds to facilitate crack-length measurements. The scale had 0.005-in. (0.127-mm) increments and was attached to the beam with double-sided pressure-sensitive tape. The dimensions of the beams were measured at the cross section of the beam near the gages. These measurements were used in a computer program to calculate the section properties of the beams and the preliminary load-control settings to be used during alignment. Wood blocks were forced between the flanges at the locations of reactions if the measurements indicated that the tension flange was more than 1/16-in. (1.6-mm) out of square. This blocking squared the beam cross section and thereby simplified alignment.

Installation and Alignment

The beams were accurately positioned in the test frame, and the tie-down rods and lateral braces at the reaction points (but not at the load points) were installed. Rubber pads were placed under the beams at the reaction points. The reaction tie-down nuts were tightened ¼ to ½ turn beyond the hand-tight position. Reference lines marked on the beam assured accurate longitudinal positioning of the beam with respect to the reactions and loads. Lateral braces assured accurate lateral positioning. The strain gages were read before and after the reaction tie-downs and braces were installed to assure that installation of tie-downs did not induce significant stresses in the beam. If the average of the two gages exceeded 30 microstrain or the difference was greater than 10 microstrain, the tie-down nuts were re-adjusted to meet these requirements.

After the beams were installed, the precalibration procedure detailed in Ref. (*21*) was followed. As part of this procedure, the beam was loaded to its calculated maximum load and the alignment of the beam was checked by comparing the readings of the two strain gages. If these two readings and the stress ranges for the two gages were within

10 percent of each other, the alignment was considered satisfactory; otherwise, the beam was unloaded and adjusted until this criterion was met. Thus, the stress range throughout the flange was within 5 percent of the average stress range.

Static Calibration

After the beam was properly aligned, the static calibration, also detailed in Ref. (*21*), was made to determine the loads and command settings (set point and span) corresponding to the desired maximum and minimum stresses for the fatigue tests. During the calibration, the set-point control was varied until the observed strain (average of the two gages) corresponded to the desired minimum stress. The corresponding load-cell reading was measured precisely with the amplitude-measurement module of the testing system. A modulus of elasticity of 29×10^3 ksi (200 GPa) was used to relate strain to stress. The span control was then used in a similar manner to determine the load corresponding to the desired maximum stress. By using this static calibration method, inaccuracies in calculating sectional properties and in establishing the effective span were eliminated, but the accuracy of the experimental stresses depended on the accuracy of the assumed value of the modulus of elasticity.

Residual stresses due to welding and flame cutting caused a nonlinear relation between the load and the measured strain (or stress) during the first cycle of loading, and a residual strain in the gages was caused after unloading. If the gages are rezeroed after unloading, the relation between load and measured strain is linear on all subsequent cycles in which the original load is not exceeded. The precalibration procedure discussed earlier served to preload the beam and eliminate the nonlinear effect of the residual stresses on the static calibration; the gages were rezeroed after the beam was unloaded. Thus, the applied stress was the main test parameter. Residual stresses present at any point on the cross section after the precalibration were superimposed on the applied stresses, but these did not change the stress range imposed at that point.

The stress caused in the beam by a given cyclic loading is larger than the stress caused by a static load of the same magnitude by an amount that depends on the ratio of the frequency of the cyclic loading to the natural frequency of the beam. However, for the constant-amplitude tests in the present program, this ratio was less than 1/10, and the corresponding difference in stress theoretically was less than 1 percent. For the variable-amplitude tests, in which the frequency varies, a theoretical analysis of the dynamic effect is very complex, but the average frequency can probably be used to approximate the true effect. Thus, the dynamic effect was theoretically very small for all test conditions in the present program. Furthermore, dynamic strain-gage readings taken at the beginning of each fatigue test showed that the dynamic effect was negligible (*22*). Therefore, static calibration was satisfactory for the present program.

Fatigue Tests

The beams were tested in sets of three. The set-point and span-control settings determined in the static calibration were used in the fatigue tests. The amplitude-measurement module was used to monitor the load cell throughout the tests to assure that the correct loading was maintained. Since the system is equipped with the peak-load control, only minor adjustments of the gain setting were necessary to assure that the desired load peaks (and valleys) were obtained throughout the test. Adjustments were made only if measured loads differed from the desired loads by an amount exceeding 1 percent of the testing-system load range. The load on each beam was observed periodically, and any adjustment that was made in the gain settings was recorded. The digital programmer was set at a speed slightly faster than the actual speed of the system, which was limited by its hydraulic characteristics. Near the beginning of the test, the readout from the strain gages was recorded for a 500-cycle loading block to provide a permanent record of the applied stress spectrum.

Crack-Growth Observations

When the fatigue test loads were checked, the beam was also inspected for fatigue cracks with a 15× portable reflector-type microscope or with a 50× microscope with built-in illumination. If a crack was present, the number of cycles, the time of the observation, and the location and length of the crack were recorded. To determine the location of the ends of the crack relative to the edge of the flange or to the web-flange juncture, the operator sometimes stopped the fatigue loading temporarily and applied a static load equal to or less than the minimum load plus ½ the difference between minimum and maximum loads.

Failure

The test of a beam was stopped by a limit switch set ¼ in. (6 mm) beyond the maximum deflection of the uncracked beam. The limit switches were located 2.5 ft (762 mm) from the unloaded end. By this time, the crack had propagated throughout the tension flange and into the web, usually to a depth of between ¼ and ½ of the web depth. After the crack extended over the entire flange, the beam sustained only a relatively few additional cycles before the web cracked and the test stopped.

After the test was finished, the region near the critical crack was cut from the surrounding beam and retained. For cover-plate beams, the long portion of the beam was also retained for possible retests. Photographs were taken of typical failure planes.

COVER-PLATE-SPECIMEN TEST SETUP AND LOADING SYSTEM

In all tests of cover-plate specimens, axial loads were applied by a 30-kip (1335-kN) MTS closed-loop fatigue machine (that is, the main plate of the specimen was concentrically gripped and loaded). However, because the specimen had a cover plate on only one side, transverse bending occurred, especially in the region of the cover plate. As a result, the tensile stress at the longitudinal centerline on the front (cover plate) face of the main plate at the ends of the cover plate was about 20 percent above the average axial stress (axial force divided by the area of the main plate), and the stress on the back face was

about 20 percent less than the average axial stress. In addition, the tensile stress at the front face of the main plate in front of the ends of the weld for the cover plate was about 50 percent higher than the stress at the longitudinal centerline because of the transfer of stress from the main plate into the cover plate through the welds. The tensile stresses at the two edges of the specimen were essentially the same when the specimen was properly aligned. Details of the stress distribution in the specimen are given in a previous report (*24*).

The tensile stress at the longitudinal centerline on the front face of the main plate ⅛ in. (3 mm) from the end of the cover plate was used as the main test parameter. This stress corresponds roughly to the nominal stress at the end of the cover plate in the beams and is linearly related to the applied load after initial loading during calibration.

The loading system is shown in Figure B-5. It consisted of a 300-kip (1335-kN) loading frame; an integral pump and jack system; a tape-controlled digital programmer; a command module; safeguard and readout equipment, such as a precise amplitude-measurement module; and a two-channel memory oscilloscope. Functionally, the system operated similarly to the system used to test the beams, but it did not include a peak-load control because only one specimen was tested at a time. The system used the same control tapes as the system used for the beam tests.

Sufficient pump capacity was available to permit the loading system to operate at its programmed speed in all tests. Usually, this programmed speed was 7.5 Hz, but in some tests it was as low as 5 Hz and as high as 11 Hz. The time for each cycle in a variable-amplitude test was approximately the same.

COVER-PLATE-SPECIMEN TEST PROCEDURES

Specimen Preparation

To permit measurement of the strain during alignment, static calibration, and the initial stages of fatigue testing, three ⅛-in. (3-mm) strain gages were attached to each specimen, as shown in Figure B-6. Each gage number (1 for front gage at top, 2 for back gage at top, and 3 for front gage at bottom) refers to the same location for all specimens.

Four mylar microscale tapes were mounted near the four ends of the welds. These tapes, which had 0.005-in. (0.127-mm) divisions, facilitated measurement of cracks that initiated at the ends of the welds and propagated transversely across the specimen. The ends of the welds were numbered T1 through T4.

Before testing, each specimen was sprayed with flat white paint at the ends of welds to highlight subsequent cracks.

Installation and Alignment

To facilitate specimen alignment, the swivel head and grips of the testing machine were positioned before a series of specimens was tested. As detailed in a previous report (*21*), this was accomplished by gripping a straight alignment bar, tensioning it while the swivel head was unlocked, and locking the swivel head when the bar was at maximum tension. This procedure assured that the centerlines of the grips in the upper and lower heads were in line.

The longitudinal centerline was marked on the specimen and used to assure satisfactory lateral alignment during installation of the specimen. The specimen was first inserted and gripped at the top, and then the bottom grips were closed. Readings of the strain gages were observed while the top and bottom grips were closed. If the gripping process produced strains exceeding 100 microstrains, the gripping process was discontinued and the heads were realigned. If the gripping caused strains less than 100 microstrains and the difference between the top and bottom grapping strains (gages 1 and 3) was less than 50 microstrains, the alignment was considered satisfactory. Any strains locked into the specimen by gripping and alignment were included in the static calibration as discussed later.

Static Calibration

After the specimen was properly aligned, the static calibration detailed in Ref. (*21*) was made to determine the loads corresponding to the desired maximum and minimum stresses for the fatigue tests. During the calibration, the specimen was loaded by using the bias control until the observed strain (average of gages 1 and 3) corresponded to the desired maximum stress. The maximum load was held for 5 min. to permit stabilization of any local yielding. The specimen was then unloaded until the strain corresponded to the desired minimum stress. The range setting for the fatigue tests was the difference between the bias settings corresponding to maximum and minimum strains. A modulus of elasticity of 29×10^3 ksi (200 GPa) was used to relate strain to stress.

Local yielding at points of stress concentration, and straightening of slightly bent specimens, sometimes caused a slight curvature of the load-stress curve during loading. During unloading and on subsequent reloading, the load-stress curve was essentially straight. By using the calibration loads obtained during unloading, the correct stress range was obtained for the test. Since the strain gages were zeroed before installation and alignment and were not subsequently rezeroed, any stresses locked into the specimen as the result of alignment were included in the maximum and minimum stresses applied during calibration and throughout the fatigue tests.

Fatigue Tests and Crack-Growth Observations

The initial bias and range settings for fatigue tests were determined from the static calibration. The testing speed (usually 7.5 Hz) and the haversine wave forms were set on the programmer, and the program tape was inserted. The load-cell readout was monitored on the amplitude-measurement module to determine whether the desired peaks and valleys were being reached; in addition, the output of strain gage No. 1 was continuously recorded on the strip chart recorder for the first 500 cycles (or less for constant-amplitude tests) to provide a permanent record of the strains. Figure B-7 shows a portion of a typical strain record.

To assure that the peak loads were reached, the system was dynamically adjusted (overprogrammed) by changing the range and bias settings slightly (up to 4 percent) from the static-calibration settings. Specifically, the control settings were changed until the dynamic load-cell readings

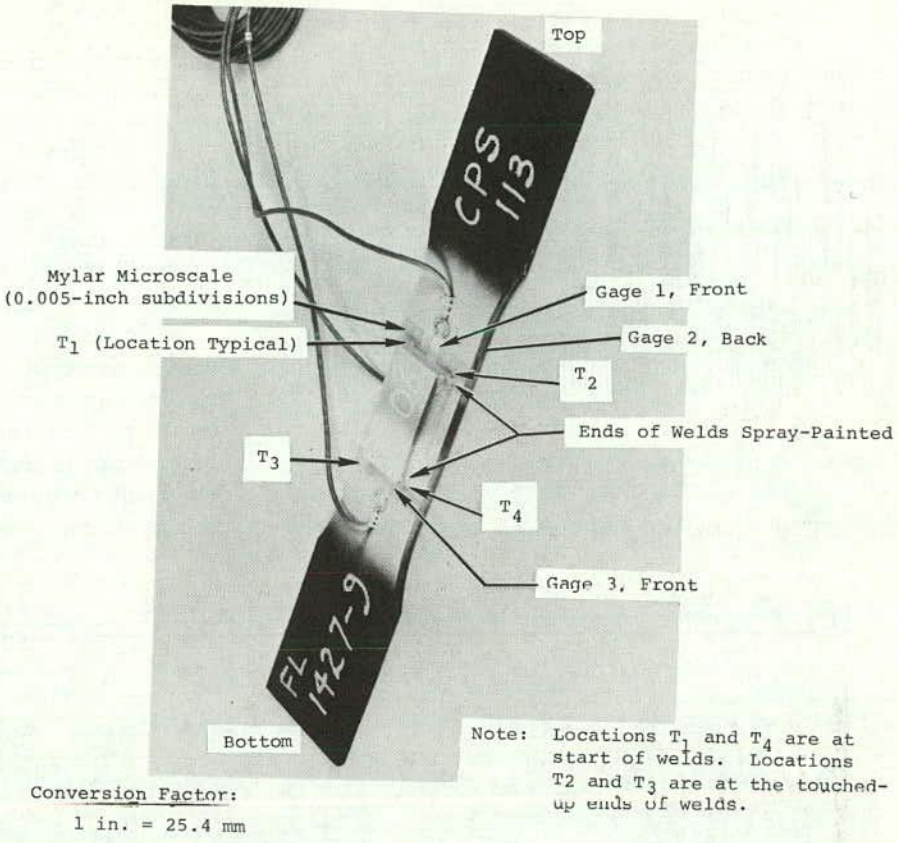

Figure B-5. Specimen-test setup.

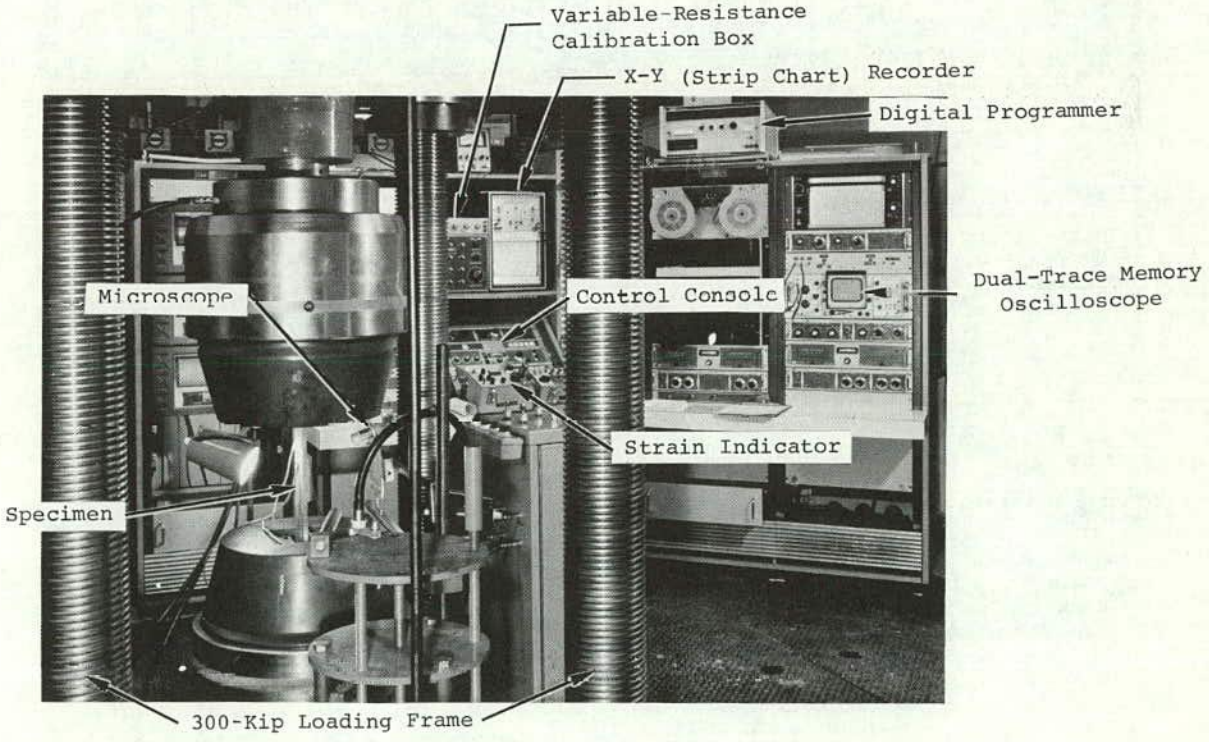

Figure B-6. Cover-plate specimen ready for testing.

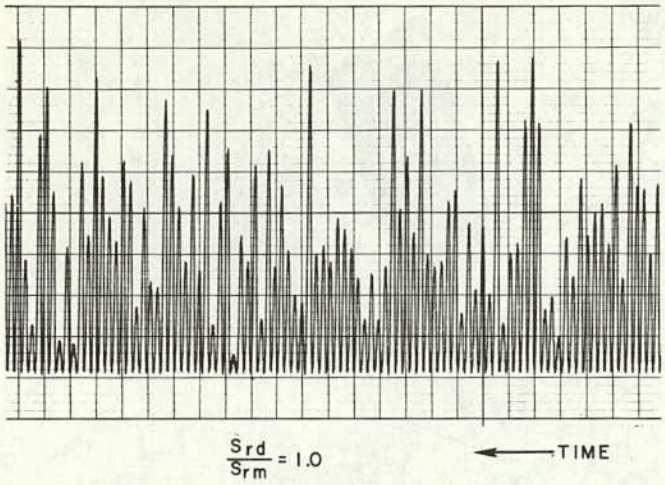

Figure B-7. Portion of a typical strain record.

indicated by the amplitude-measurement module equaled the static-calibration loads. For variable-amplitude loadings, the maximum load in the spectrum was used to make the dynamic adjustments. The dynamic loads were observed periodically, and dynamic adjustments were made if the peak (or valley) load was off by more than 1 percent of the system load range. A record was maintained of all such adjustments.

The fatigue test was terminated when the fatigue crack separated the specimen into two parts.

A 25× microscope attached to a supporting fixture was used to observe cracks. The number of observations varied for each specimen; however, morning-noon-afternoon observations were standard procedure unless short-life tests necessitated observations at shorter time intervals. Each observation consisted of a record of the distance from the edge of the specimen to the left and the right end of a crack.

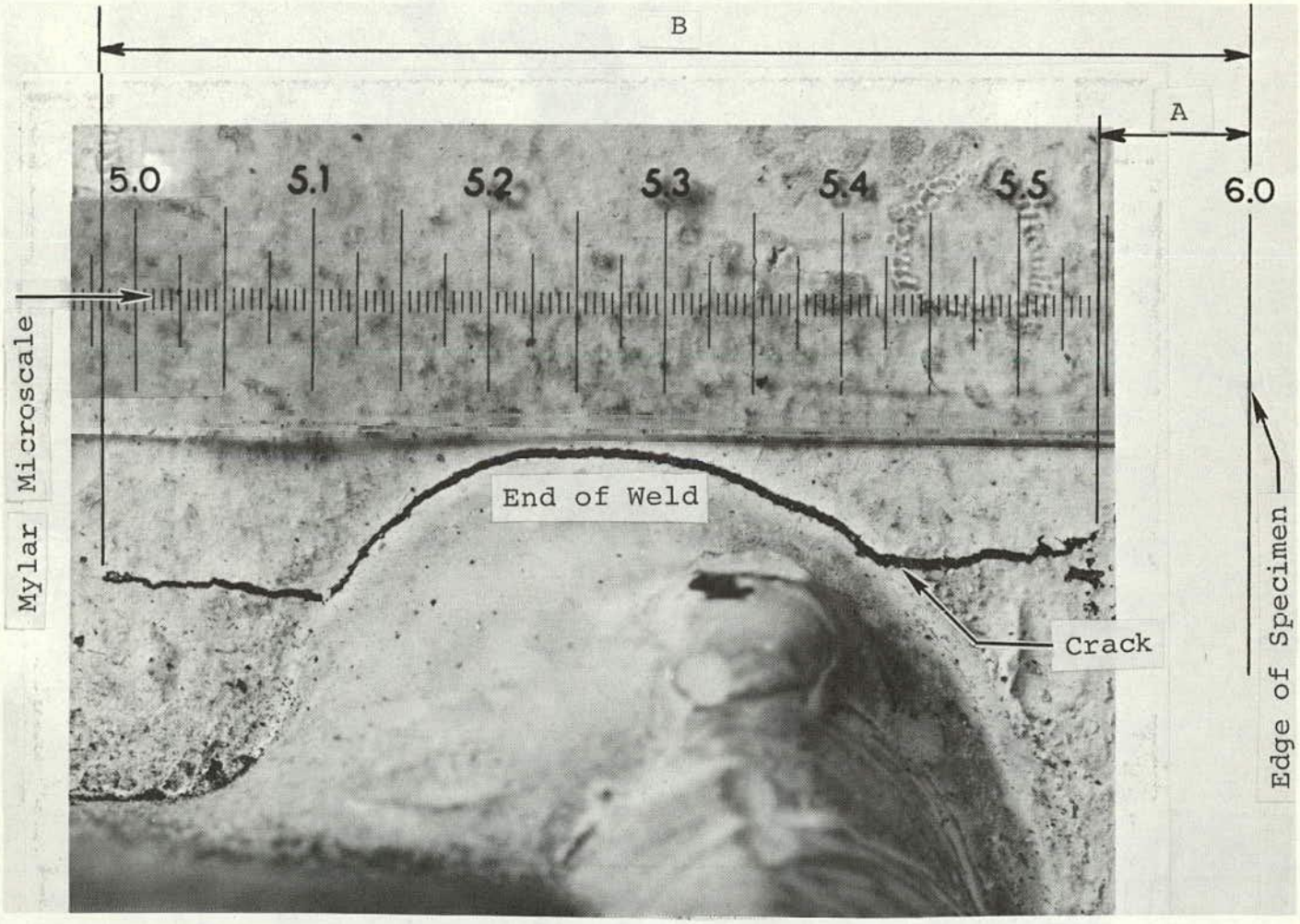

Specimen: CPS-108
Location: T2
A = 6.000 - 5.545 = 0.455 in.
B = 6.000 - 4.980 = 1.020 in.
Crack Length = B - A = 0.565 in.

No. of Cycles = 96,195
Bias = -0.40
Range = 5.37
Date = 4/17/72
Time = 1:30 p.m.

Conversion Factor:

1 in. = 25.4 mm

Figure B-8. Crack observed at end of weld in a cover-plate specimen, X10.

The location of the crack and the number of cycles at the time of the observation were also recorded. Figure B-8 shows a crack at the end of a weld (location T2 of specimen CPS-108) observed through the microscope. The figure also shows the data that were recorded. During the observation of a crack, the operator sometimes stopped the fatigue loading and applied a static load not exceeding ½ of the maximum cyclic load. This procedure permitted an accurate recording of the crack length.

WOL-SPECIMEN SETUP AND PROCEDURES

All WOL tests were performed in a 50-kip (222-kN) MTS closed-loop fatigue machine at a uniform speed of 5 Hz. The load cycles were sinusoidal in shape. Proper alignment was obtained by carefully machining specimens and other auxiliary parts and by using universal joints to load the specimens. In each test, the fatigue crack was initiated and propagated under the same loading spectrum. Crack-length measurements, which were begun when the total crack length, a, was 1.0 ± 0.001 in. (25.4 ± 0.0254 mm), were always made at the end of a 500-cycle loading block.

Crack lengths were measured optically with a type M-101 Gaertner microscope mounted in a micrometer slide. To improve the accuracy of measuring the crack length, series of hardness indentations were made on the surface (with a Vickers Pyramid Hardness Testing Machine) along a line parallel to the plane of the initial crack and in the direction of expected crack extension, as shown in Figure B-9.

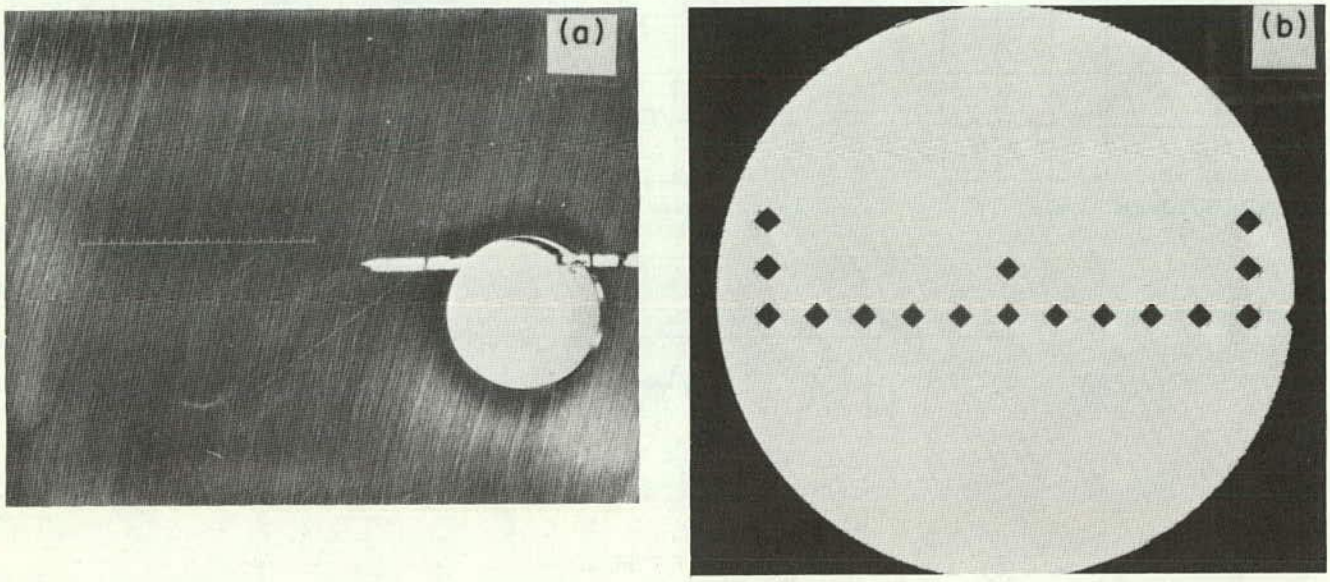

Figure B-9. Hardness indentations used to measure crack length in WOL specimens: (a) location of hardness indentation, X1; (b) close-up of hardness indentation, X25.

APPENDIX C

STRESS SPECTRUMS

Available field measurements of stresses in short-span bridges under traffic were used to develop the stress spectrums used in the testing program. These field data and the stress spectrums developed from them are described in this appendix.

FIELD MEASUREMENTS

Individual Vehicle Passages

The response of a bridge to the passage of a vehicle depends on the type of bridge; the weight, the speed, and the dynamic characteristics of the vehicle; the roughness of the pavement preceding the bridge; and many other factors (*32*). Therefore, the exact shapes of stress-time curves from available field measurements (*8, 9, 10*) vary considerably, as shown in Figure C-1 for seven different bridges. Most of the available curves, however, can be characterized as illustrated in Figure 8.

Without a vehicle on the bridge, dead weight produces a static stress that is not recorded during field measurements because it existed when the strain gages were installed. The passage of a vehicle produces a single major cycle of additional stress that is controlled primarily by the weight of the vehicle. Smaller vibration stress cycles, which depend on the dynamic characteristics of the bridge and vehicle, are superimposed on the major stress cycle. Vibration stress cycles also occur after the major stress cycle is complete and the vehicle has left the bridge (*8*). These

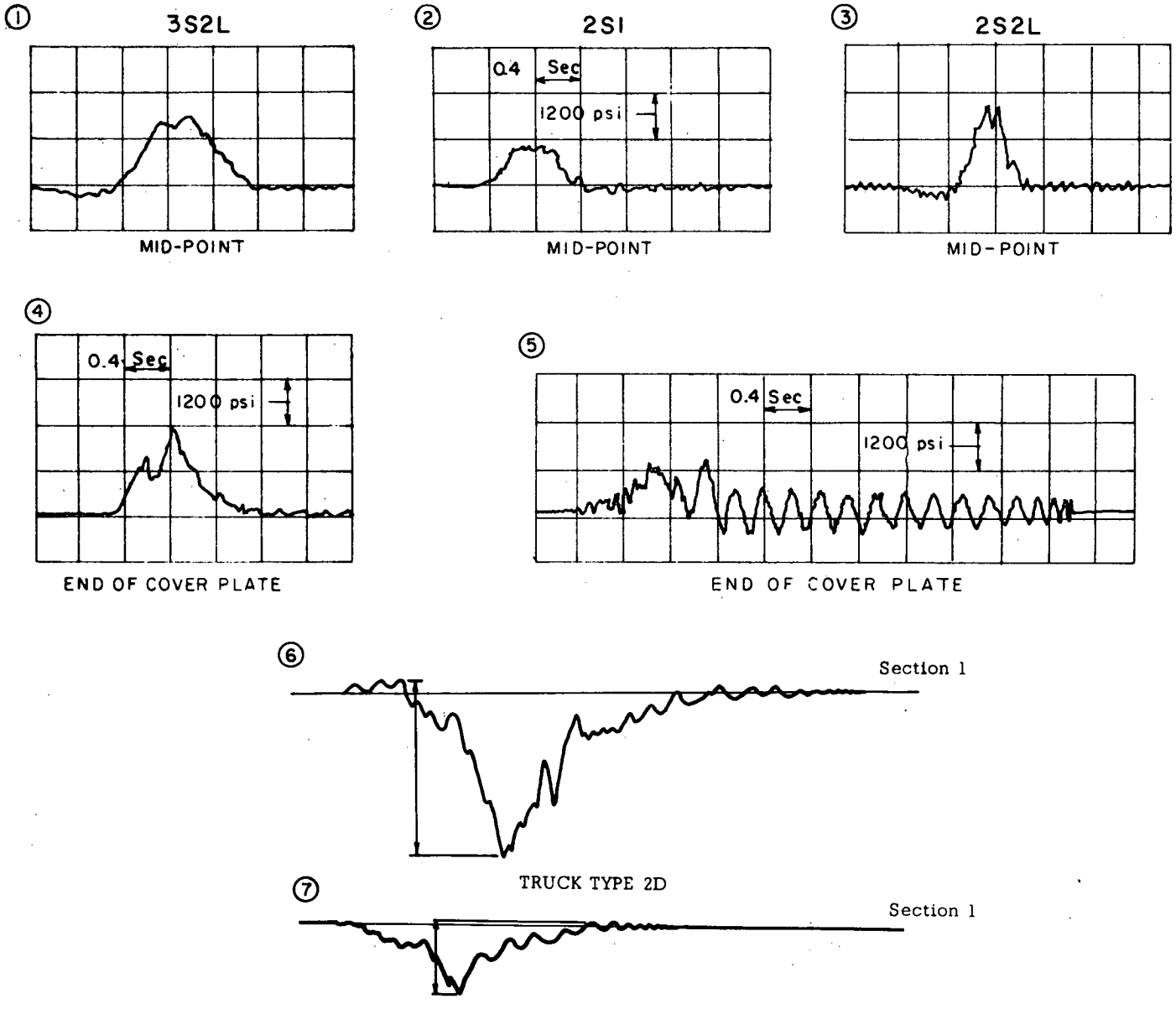

Conversion Factor:

1 psi = 6.895 kPa

Figure C-1. Experimental load traces for passage of a single vehicle.

vibration stress cycles occur at the natural frequency of the bridge and usually decrease logarithmically because of viscous damping. (Viscous damping, in which a force proportional to the velocity opposes motion, causes a progressive decrease in the peak amplitudes, such that the logarithm of the ratio of any two consecutive peaks (the smaller divided by the larger) is a constant.)

In most of the available stress-time curves, the vibration stress cycles are small compared with the major stress cycle, so that the stress caused by the passage of a vehicle can be approximated by a single cycle (see Fig. 8b) defined by any two of the three parameters: (1) the maximum stress, S_{max}; (2) the minimum stress, S_{min}; and (3) the stress range, S_r.

In a few stress-time curves, particularly curves for a cantilever (suspended-span) girder bridge, large vibration stress cycles occur after the major cycle. This type of curve is illustrated by the fifth load trace in Figure C-1 and can be approximated as shown in Figure 8c. Two parameters, in addition to those defining the major cycle, are required to define this curve: (1) the ratio of the peak amplitude for the first cycle of vibration stress to the stress range for the major cycle, $k_1 = S_{v1}/S_r$; and (2) the natural logarithm of the ratio of the peak amplitude of any vibration cycle to the peak amplitude of the preceding cycle, $k_2 = \ln(S_{v2}/S_{v1})$. The parameter k_2 is commonly referred to as the logarithmic decrement and is a function of the damping in the bridge. Both parameters depend primarily on the dy-

namic characteristics of the bridge; k_2 depends to a lesser extent on the dynamic interaction of the vehicle and bridge.

Frequency of Occurrence

The stress spectrum, or stress history, for a particular location in a bridge can be conveniently defined in terms of the frequency of occurrence of maximum (peak) stresses in the major stress cycles mentioned earlier. Usually, frequency-of-occurrence data are presented as a histogram showing the percentage of recorded maximum stresses that fall within a certain stress interval (see Fig. 9). The stress-time curve (upper portion of Fig. 9) records the passage of a few individual vehicles of different weights; normally such a record would be continued until many more passages were recorded. The frequency of occurrence of the corresponding maximum stresses is plotted to the left in the figure. (For example, 20.2 percent of the maximum stresses are within the interval between 7.5 and 8.5 ksi (52 to 59 MPa).) The frequency of occurrence of stress ranges can be represented by a similar plot with the vertical scale changed according to the relationship between S_{max}, S_{min}, and S_r. Since stress range is the most important stress parameter controlling the fatigue strength of bridge members (*2*), stress range is used to define the major stress cycles in the present program.

As explained in Appendix D, the frequency-of-occurrence data can be presented in a more general form by dividing the percentage of occurrence for each interval in Figure 9 (upper portion) by the interval width to obtain a probability-density curve (see lower portion of Fig. 9; note also that the points representing each interval are connected by a smooth curve). The probability density is independent of the interval used in classifying the data. Thus, data from sources that use different stress-range intervals can be compared by using the probability-density curve. The area under the curve between any two values of stress range represents the percentages of the stress ranges that are within this interval. For example, 20.2 percent of the stress ranges are between 2.5 and 3.5 ksi (17 to 24 MPa); the area is approximately equal to the ordinate, 0.202 ksi^{-1} (0.029 MPa^{-1}), times the interval, 1 ksi 6.9 MPa).)

Also as explained in Appendix D, probability-density curves can be plotted in nondimensional form, and a single nondimensional mathematical expression can be found to represent a family of different probability-density curves.

In bridges where vibration stresses are significant, such as cantilever suspended-span) girder bridges, the stress spectrum can be conveniently defined in terms of the probability density of major stress cycles and constant values of k_1 and k_2—the two parameters defining the vibration stress cycles. This method of defining stress spectrums that include vibration stress cycles has several advantages. First, the number of vibration stress cycles following each major stress cycle, which theoretically is infinite, need not be defined. Hence, distortions in the shape of the probability-density curve resulting from different cutoff points for the vibration stress cycle do not occur. Second, the sequential relationship of the vibration stress cycles in following the major stress cycle is correctly defined. Third, the minimum stresses for both the major and vibration cycles are correctly defined. The major cycle is added to the minimum stress due to dead load, whereas the vibration cycles oscillate about the dead-load stress.

Available Field Data

To determine a suitable nondimensional probability-density expression to represent the frequency of occurrence of stress ranges in short-span highway bridges, all available field measurements on such bridges under traffic were compiled. Fifty-one sets of frequency-of-occurrence data were included from six sources (*7, 8, 10, 11, 12, 13*). (Many other references dealing with stress measurements in bridges were reviewed but did not contain suitable data, usually because the measurements were made under artificial loadings rather than under normal traffic. Also, measurements that were made after this study of stress spectrums was completed in 1972 are not included.)

The available data cover a total observation period of 850 hr; a total of 37,000 truck passages occurred during this period. All of the stress-range data plus a description of each data set were recorded on computer cards.

Each data set represents the frequency of occurrence of stress ranges at a particular location in a bridge—usually at a critical location, such as the end of a cover plate. (Stress measurements were made far enough away from stress-concentration points to avoid high local stresses, and, therefore, the measurements indicate the nominal stresses.) Data were collected on 15 different, short-span steel bridges of the following types:

1. Rolled-beam simple-span bridge with noncomposite concrete deck.
2. Rolled-beam simple-span bridge with composite concrete deck.
3. Welded-girder simple-span bridge with composite concrete deck.
4. Rolled-beam cantilever (suspended-span) bridge with composite concrete deck.
5. Welded-girder cantilever (suspended-span) bridge with composite concrete deck.
6. Rolled-beam continuous-span bridge with noncomposite concrete deck.

For the cantilever girder (suspended-span) bridges, readings were taken in both suspended and end-anchored spans. All bridges are on Interstate or U.S. routes in semirural or metropolitan locations.

Since the available data were obtained from different sources, there were several differences in the methods of accumulating and presenting these data. In most of the studies, only the stress range for the major stress cycle was recorded. In a few studies, however, vibration stress cycles occurring after the major stress cycle were also recorded. The smallest stress range that was recorded in a particular study varied from 0 to 435 psi (3.00 MPa); all investigators stated that stress cycles caused by automobiles were too small to be recorded.

The inclusion or exclusion of vibration stress cycles and the magnitude of the lowest recorded stress range may have a major effect on the shape of the probability-density curve, or histogram, for the field data. Since the vibration stress cycles following each major stress cycle decrease loga-

rithmically, and since most of the vibration stress cycles are small compared with the major stress cycle, inclusion of these vibration stress cycles results in a high frequency of occurrence of small stress cycles. For example, in one study (7), where an average of two to three stress cycles per vehicle passage was recorded, the frequency-of-occurrence values steadily decrease from a peak as the stress range increases. In contrast, the data from studies, in which only one cycle per vehicle passage was recorded, increase to a peak and then decrease. If additional vibration stress cycles had been included in the aforementioned study, the frequency of occurrence (in percent) of small stress cycles would have further increased, and the influence of the major stress cycles on the frequency-of-occurrence data would have declined. Since the small vibration stress cycles have a very small effect on fatigue life, their inclusion may distort the meaningful representation of stress spectrums.

Curve Fitting

Two mathematical expressions were considered for use in representing the frequency of occurrence of stress ranges: (1) a two-parameter Rayleigh probability-density function and (2) a three-parameter Erlang probability-density function. The Rayleigh function is defined for $x' \geq 0$ by

$$p' = x' e^{-(\frac{1}{2})(x')^2} \qquad \text{(C-1)}$$

In this equation, p' is the nondimensional probability density, e is the Napierian base (2.7183), and

$$x' = \frac{S_r - S_{r\min}}{S_{rd}} \qquad \text{(C-2)}$$

in which S_r is the independent variable (stress range) and $S_{r\min}$ and S_{rd} are parameters (constants) that define any particular probability-density curve from the family represented by Eq. C-1. (In both the Rayleigh and Erlang functions, $S_{r\min}$ represents the distance from the origin to the starting point of the function; S_{rd} represents the distance from the starting point to the modal value in the Rayleigh function and from the starting point to the mean value in the Erlang function.) The Erlang function is defined for $x' \geq 0$ by

$$p' = \frac{k^k}{\Gamma(k)} (x')^{k-1} e^{-kx'} \qquad \text{(C-3)}$$

in which x' is defined by Eq. C-2, k is a nondimensional parameter greater than 0, and $\Gamma(k)$ is the gamma function defined by

$$\Gamma(k) = \int_0^\infty z^{k-1} e^{-z} dz \qquad \text{(C-4)}$$

The Rayleigh curve always starts with zero probability density at the lowest S_r. In contrast, the Erlang curve starts with the highest probability density at $S_r = 0$ and steadily decreases if the parameter k is equal to 1.0. If the parameter k is greater than 1, the Erlang curve has a shape similar to that of the Rayleigh curve. If $k < 1.0$, the Erlang curve is asymptotic to a vertical line at $S_{r\min}$.

Eqs. C-1 and C-3 were fitted to each of the 51 sets of frequency-of-occurrence data by using a curve-fitting computer program selected from a group of available programs. Specifically, the program determines optimum values for the two or three parameters defining an individual probability-density curve of each type. Using trial values of these parameters, the computer program calculates the theoretical frequency of occurrences (in percent) of stress ranges within each experimental interval. The algebraic difference between the experimental frequency of occurrence and the corresponding theoretical value is the residual. The computer program automatically changes the parameters and recalculates the residuals until a minimum value of the sum of the squares of the residuals is obtained. When the difference in the sum of the squares between two successive iterations is less than 0.01 percent, it is assumed that the minimum value has been reached. Thus, the selected parameters give the best possible fit (according to the least-squares criterion) over the range of experimental S_r values.

Table C-1 summarizes the results of the curve fitting. For convenience in comparing the Rayleigh and Erlang curves for a given set of data, the mean, $S_{r\text{mean}}$, and the minimum, $S_{r\min}$, instead of $S_{r\min}$ and S_{rd} are given to define a particular probability-density curve. The mean is equal to $S_{r\min} + 1.23\, S_{rd}$ for the Rayleigh curve and $S_{r\min} + S_{rd}$ for the Erlang curve. The parameter k is given to complete the definition of the Erlang curve. The sum of the squares of the residuals, which is a measure of the closeness of fit, is also given.

As expected, the sum of the squares for the three-parameter Erlang curve is less than the corresponding sum for the two-parameter Rayleigh curve for most of the 51 sets of data. The Erlang curve provides a much closer fit than the Rayleigh curve for data (classified as "descending" in Table C-1) that starts with the highest probability density at $S_r = 0$ and steadily decreases; as discussed earlier, such a probability-density curve results if the small vibration stress cycles are included in the data.

The closer fit provided by the Erlang curves, of course, results primarily from the use of the third parameter, k, which varied from 1.0 to 8.2 for the 51 sets of data. Two-parameter Erlang curves—obtained by using a k value of either 2, 3, or 4—were also fit to each of the 51 sets of data. These results are given in Table C-2. If the 16 sets of descending data are not considered, the best fit is provided by the Erlang curve with $k = 2$ in 13 cases, by the Rayleigh curve with $k = 2$ in 13 cases, by the Erlang curve with $k = 3$ in 7 cases, and by the Erlang curve with $k = 4$ in 2 cases. Thus, both the Rayleigh curve and the Erlang curve with $k = 2$ appear to provide a good two-parameter representation of traffic loadings.

The Rayleigh curve was chosen for use in the test program because it has been more widely used than a two-parameter Erlang curve to approximate physical phenomena involving skewed data. A two-parameter curve rather than a three-parameter curve was chosen (1) because two parameters were found to be sufficient to represent a wide variation of skewed data (as may be seen in Table C-1), and (2) because many more fatigue tests would have been required to establish the fatigue strength in terms of three parameters than in terms of two parameters.

TABLE C-1

RAYLEIGH AND ERLANG CURVE RESULTS

Data Set	Type of Curve	Rayleigh Curve			Erlang Curve			
		S_{rmin}, ksi	S_{rmean}, ksi	Fit Parameter, $(ksi)^2$	S_{rmin}, ksi	S_{rmean}, ksi	k	Fit Parameter, $(ksi)^2$
1	D	0.52	0.79	12.1	0.56	0.81	1.87	2.8
2	P	0.23	2.24	29.1	0.22	2.35	3.30	18.7
3	D	0.46	0.80	59.6	0.60	0.90	1.10	0.6
4	P	0.20	1.94	18.0	0.00	1.99	4.06	30.2
5	P	0.00	1.36	42.0	0.25	1.50	1.84	2.2
6	P	0.14	1.52	80.9	0.45	1.71	1.61	8.3
7	D	0.42	0.97	13.7	0.48	1.00	2.91	2.3
8	P	0.47	2.04	157.0	0.00	2.10	5.85	180.8
9	D	0.52	0.81	28.7	0.60	0.84	1.05	1.0
10	P	0.32	1.28	20.0	0.34	1.34	3.08	5.8
11	D	0.43	0.89	34.3	0.55	0.96	2.03	2.8
12	P	0.21	2.37	17.2	0.25	2.49	2.96	12.4
13	P	0.07	1.54	3.5	0.00	1.60	3.55	4.0
14	P	0.11	1.47	29.3	0.03	1.52	3.54	28.8
15	P	0.00	1.01	55.2	0.35	1.15	1.11	0.6
16	P	0.05	1.33	68.2	0.38	1.49	1.48	2.6
17	P	0.52	1.84	208.5	0.00	1.86	6.86	225.9
18	P	0.30	0.95	14.1	0.41	0.82	2.02	2.1
19	P	0.09	1.37	20.2	0.08	2.02	3.22	12.4
20	P	0.17	0.95	80.2	0.07	1.00	4.11	81.6
21	P	0.12	0.35	0.1	0.00	0.34	8.18	0.2
22	P	0.22	0.74	19.2	0.16	0.78	3.99	10.6
23	P	0.15	1.05	59.8	0.30	1.18	1.97	31.6
24	P	0.23	1.00	56.0	0.26	1.03	2.93	49.5
25	P	0.14	0.68	30.8	0.17	0.71	2.86	25.5
26	P	0.20	1.02	35.3	0.22	1.07	2.86	28.7
27	P	0.23	1.91	6.8	0.00	1.97	4.11	9.2
28	P	0.20	1.56	37.2	0.00	1.59	4.28	35.4
29	P	0.01	1.02	48.1	0.16	1.16	2.04	19.0
30	P	0.23	1.61	48.8	0.38	1.71	2.33	36.6
31	P	0.08	0.88	118.4	0.40	1.00	1.05	43.7
32	P	0.00	1.26	72.8	0.35	1.47	1.42	31.6
33	D	0.50	0.96	9.8	0.48	0.95	4.19	9.0
34	P	0.31	1.15	4.3	0.21	1.16	4.29	4.6
35	P	0.40	1.14	0.0	0.00	1.15	7.82	2.1
36	D	0.31	0.88	6.1	0.33	0.92	3.61	1.8
37	D	0.37	0.79	2.8	0.36	0.81	3.80	0.6
38	P	0.28	1.08	4.9	0.25	1.12	3.76	6.1
39	D	1.33	1.69	3.0	1.33	1.70	3.51	0.4
40	P	0.82	2.37	5.7	0.44	2.39	5.15	9.6
41	D	0.80	1.79	123.3	0.92	1.86	2.70	79.2
42	P	0.46	1.26	18.2	0.51	1.28	2.95	6.0
43	D	0.00	1.07	151.4	0.43	1.34	0.98	5.9
44	D	0.05	1.01	42.4	0.57	1.28	1.08	8.9
45	D	0.26	0.78	22.9	0.33	0.80	2.19	9.6
46	P	0.21	1.20	4.6	0.40	1.29	2.46	0.0
47	D	0.16	0.81	110.6	0.35	0.88	1.08	36.7
48	D	0.00	1.19	70.3	0.40	1.38	1.63	31.6
49	P	0.27	1.17	3.9	0.15	1.21	4.52	7.1
50	P	0.32	1.20	3.6	0.30	1.23	3.78	0.6
51	D	0.31	0.75	15.8	0.43	0.76	1.11	13.8

Notes: (1) 1 ksi = 6.895 MPa

(2) Curves that start at a peak and steadily decrease are referred to as descending curves and are identified by a D; curves that increase to a peak and then decrease are called peak curves and are identified by a P.

(3) S_{rmin} is the minimum stress range in the spectrum; S_{rmean} is the mean stress range for the spectrum; k is the nondimensional shape parameter; and the fit parameter is the sum of the squares of the residuals; lower values of the fit parameter indicate a closer fit.

TABLE C-2

SEVERAL TWO-PARAMETER ERLANG CURVE RESULTS

Data Set	Type of Curve	k = 2.00			k = 3.00			k = 4.00			Optimum k
		S_{rmin}, ksi	S_{rmean}, ksi	Fit Parameter, $(ksi)^2$	S_{rmin}, ksi	S_{rmean}, ksi	Fit Parameter, $(ksi)^2$	S_{rmin}, ksi	S_{rmean}, ksi	Fit Parameter, $(ksi)^2$	
1	D	0.56	0.80	3.0	0.52	0.80	5.8	0.49	0.79	7.1	1.87
2	P	0.66	2.44	19.4	0.31	2.35	18.9	0.03	2.31	19.1	3.30
3	D	0.54	0.85	15.8	0.48	0.84	27.7	0.43	0.83	34.9	1.10
4	P	0.50	2.13	48.8	0.22	2.04	33.0	0.00	2.00	30.0	4.06
5	P	0.22	1.49	2.4	0.01	1.43	9.2	0.00	1.34	59.7	1.84
6	P	0.36	1.65	13.1	0.15	1.59	34.1	0.00	1.54	52.6	1.61
7	D	0.58	1.05	0.4	0.46	1.01	3.4	0.39	0.99	5.6	2.91
8	P	0.66	2.23	270.8	0.41	2.16	224.9	0.25	2.13	201.6	5.85
9	D	0.56	0.81	7.9	0.51	0.80	13.0	0.48	0.80	16.6	1.05
10	P	0.49	1.38	15.4	0.35	1.34	5.8	0.22	1.32	8.3	3.08
11	D	0.55	0.96	2.7	0.46	0.93	10.4	0.39	0.91	18.0	2.03
12	P	0.66	2.59	15.5	0.24	2.49	12.5	0.00	2.42	15.7	2.96
13	P	0.28	1.69	24.7	0.08	1.64	6.5	0.06	1.44	83.6	3.55
14	P	0.33	1.60	38.9	0.13	1.52	29.0	0.00	1.50	32.7	3.54
15	P	0.14	1.10	6.1	0.01	1.01	25.0	0.00	0.96	117.9	1.11
16	P	0.27	1.44	7.4	0.08	1.40	22.6	0.05	1.25	86.6	1.48
17	P	0.70	1.96	332.6	0.48	1.92	284.2	0.32	1.88	257.9	6.86
18	P	0.41	0.99	2.2	0.31	0.97	4.0	0.22	0.96	5.8	2.02
19	P	0.30	1.49	19.4	0.11	1.44	12.5	0.00	1.40	18.1	3.22
20	P	0.30	1.05	96.7	0.18	1.01	83.0	0.08	1.00	81.6	4.11
21	P	0.15	0.36	16.9	0.12	0.36	7.3	0.00	1.10	3565.2	8.18
22	P	0.30	0.81	27.6	0.23	1.15	12.8	0.16	0.78	10.6	3.99
23	P	0.29	1.18	31.6	0.16	1.11	37.4	0.03	1.09	43.5	1.97
24	P	0.38	1.06	53.2	0.25	1.03	49.5	0.14	1.00	51.5	2.93
25	P	0.24	0.72	27.6	0.16	0.71	25.7	0.08	0.70	27.8	2.86
26	P	0.34	1.10	33.5	0.21	1.06	28.8	0.09	1.05	31.6	2.86
27	P	0.49	2.09	19.2	0.24	2.01	10.8	0.02	1.96	9.2	4.11
28	P	0.43	1.73	53.5	0.21	1.65	38.9	0.04	1.60	35.7	4.28
29	P	0.16	1.15	19.1	0.01	1.08	24.4	0.00	1.06	52.6	2.04
30	P	0.45	1.74	37.2	0.24	1.66	39.0	0.05	1.63	44.0	2.33
31	P	0.26	0.94	63.7	0.12	0.92	79.6	0.00	0.88	91.7	1.05
32	P	0.20	1.40	38.2	0.00	1.32	45.1	0.00	1.20	85.9	1.42
33	D	0.66	0.97	8.4	0.57	0.97	8.8	0.51	0.95	11.3	4.19
34	P	0.52	1.23	7.9	0.37	1.20	4.6	0.24	1.16	4.5	4.29
35	P	0.57	1.21	11.0	0.42	1.18	7.3	0.32	1.16	3.5	7.82
36	D	0.50	0.95	1.7	0.38	0.93	1.8	0.29	0.93	2.1	3.61
37	D	0.51	0.84	0.8	0.39	0.81	1.1	0.34	1.27	1.7	3.80
38	P	0.49	1.15	8.4	0.34	1.12	5.9	0.22	1.10	6.3	3.76
39	D	1.42	1.72	2.7	1.35	1.70	2.8	1.25	1.69	0.8	3.51
40	P	1.19	2.55	14.9	0.91	2.47	10.2	0.67	2.43	9.3	5.15
41	D	1.06	1.91	66.2	0.89	1.86	83.1	0.73	1.83	96.5	2.70
42	P	0.64	1.29	3.5	0.50	1.28	7.8	0.38	1.28	8.2	2.95
43	D	0.18	1.06	28.9	0.01	1.00	44.6	0.00	1.02	78.5	0.98
44	D	0.31	1.19	13.9	0.13	1.12	20.0	0.00	1.08	25.6	1.08
45	D	0.34	0.81	8.6	0.27	0.81	12.9	0.20	0.80	16.4	2.19
46	P	0.49	1.30	0.2	0.30	1.27	0.2	0.15	1.25	1.1	2.46
47	D	0.38	0.89	1.4	0.30	0.87	4.1	0.22	0.86	6.5	1.08
48	D	0.30	1.35	34.7	0.08	1.28	45.5	0.02	1.18	78.4	1.63
49	P	0.53	1.25	10.1	0.36	1.23	7.4	0.22	1.22	6.9	4.52
50	P	0.57	1.26	0.5	0.40	1.25	0.4	0.27	1.23	0.8	3.78
51	D	0.37	0.77	8.6	0.31	0.76	11.3	0.25	0.75	13.0	1.11

Notes: (1) 1 ksi = 6.895 MPa

(2) Curves that start at a peak and steadily decrease are referred to as descending curves and are identified by a D; curves that increase to a peak and then decrease are called peak curves and are identified by a P.

(3) S_{rmin} is the minimum stress range in the spectrum; S_{rmean} is the mean stress range for the spectrum; k is the nondimensional shape parameter; and the fit parameter is the sum of the squares of the residuals; lower values of the fit parameter indicate a closer fit.

(4) The optimum k is the value of k listed in Table C1.

Extreme-Value Probability

The curve-fitting procedure provides the best fit within the range of experimental data only. Although the selected mathematical expression can be used to extend the curve beyond the limits of the data, especially in the direction of higher S_r values, the extended portion does not necessarily represent the true probability for the variable S_r. An accurate definition of the probability of extreme values of the variable requires a very large number of data—much larger than the number of field data that were available for this study.

For the testing program, the asymptotic tail of the theoretical probability-density curve was truncated. Specifically, a standard Rayleigh curve having a width of $3S_{rd}$ was used ("standard Rayleigh curve" is used herein to refer to the family of truncated Rayleigh curves that were used as the standard probability-density curves for the testing program); 100 percent of the S_r values fall within the range of $3S_{rd}$. This width was chosen to permit a reasonable factorial experiment within the limitation that the peak loads must not exceed the yield load. As indicated earlier, there are insufficient data to establish an accurate representation of the probability of extreme values of S_r ($3S_{rd}$ and above) in actual bridges. Therefore, it is not possible to determine whether an extension of the Rayleigh curve beyond $3S_{rd}$ would result in a better or worse fit of field data. The fact that the probability of S_r values above $3S_{rd}$ is only 1.1 percent according to the Rayleigh function, however, suggests that the cutoff at $3S_{rd}$ is of little practical significance. Furthermore, the value of $S_{r\text{RMS}}$, is shifted only 2.6 percent by truncating a Rayleigh curve at $3S_{rd}$.

Sequence of Loads

To fully define a stress spectrum, the sequence and the frequency of occurrence of stresses must be given. In general, the sequence of vehicles passing over a bridge, and that of the resulting major stress cycles, is random. The vibration stress cycles that occur after the major stress cycle in some types of bridges (*8*) are arranged in descending order as defined by the log decrement. Therefore, in the main testing program, in which the vibration stress cycles were not considered, the stresses defined by the standard Rayleigh probability-density curve were arranged in a random sequence.

CHARACTERISTICS OF THE STANDARD RAYLEIGH PROBABILITY-DENSITY CURVES

The characteristics of the family of standard Rayleigh probability-density curves that were used in the testing program are shown in Figure 10. The curves are truncated at $x' = 3$. A full Rayleigh curve extends to infinity, and 1.1 percent of the total area under the curve is beyond $x' = 3$. Therefore, the constant 1.011 has been inserted into the mathematical expression defining the curve to make the area under the truncated curve equal to 1.000. Thus,

$$p' = 1.011x'e^{-(\frac{1}{2})(x')^2} \qquad \text{(C-5)}$$

Each particular probability-density curve from the family can be defined by any two of the following three parameters: S_{rm}, S_{rd}, and $S_{r\min}$. In the testing program, the curves are defined in terms of S_{rm} and S_{rd}/S_{rm}. Probability-density curves for the four values of S_{rd}/S_{rm} used in the testing program are shown in the bottom sketch in Figure 10.

The modal, median, mean, and root-mean-square values of x' for the standard truncated curve are also shown in the figure. These values are slightly different from the corresponding x' values for a full curve, which are equal to 1.000, 1.177, 1.253, and 1.414, respectively. The root-mean-square (RMS) value is equal to the square root of the mean of the squares of the individual values. The RMS of the x' values ($x'_{r\text{RMS}}$) is a constant for all curves from the Rayleigh family, but the RMS of the S_r values ($S'_{r\text{RMS}}$) varies slightly with the ratio $S_{r\min}/S_{rd}$. However, the maximum difference between the two RMS values, which occurs when $S_{r\min}/S_{rd}$ is between 1 and 2, is less than 3 percent.

CONTROL TAPES FOR FATIGUE TESTS

The punched tapes used to control the fatigue tests were generated by a computer program. This program calculates 500 individual loads that satisfy the standard Rayleigh probability-density curve, arranges them in a random sequence, and punches a control tape defining these loads in ASC II code. A separate tape is required for each different value of S_{rd}/S_{rm}, but different levels of S_{rm} and $S_{\min}$ are set manually on the testing-machine controls. The program, written in FORTRAN IV, is included in a previous report (*33*).

The 500 individual loads are calculated by dividing the area below the nondimensional probability-density curve, Eq. C-1, into 500 vertical segments (bars) of equal area. The width of the bars varies to provide equal areas. The midwidth (or more precisely the value of x' that bisects the bar into two equal areas) of each of these bars corresponds to a load with a frequency of occurrence of 1/500. The value x'_n corresponding to the midwidth of the nth bar is calculated by integrating the nondimensional probability-density curve from 0 to x'_n and equating the result to the desired area, $(n - \frac{1}{2})/500$. The result of the integration is $1.011\ (1 - e^{-(\frac{1}{2})(x'_n)^2})$. Thus,

$$x'_n = \sqrt{-2\ \text{ln}[1 - 0.001978(n - 0.5)]} \qquad \text{(C-6)}$$

The resulting values of x'_n vary from slightly greater than 0 to slightly less than 3. In generating the tapes for the main testing program, the values of x'_n corresponding to the right side of the bars rather than to midwidths were used for convenience. This procedure is equivalent to omitting the 0.5 in Eq. C-6 and is permissible because the x' interval is very small. The resulting increase in $S'_{r\text{RMS}}$ does not exceed 0.3 percent. Eq. C-6 was used without modification to prepare the tapes for secondary tests involving 100 individual loads because larger x' intervals are involved.

For convenience in operating the fatigue-testing equipment, the corresponding stress ranges, S_{rn}, on the control tapes were expressed as a percentage of the maximum stress range, $S_{r\max}$. Since $x'_n = (S_{rn} - S_{r\min})/S_{rd}$, $S_{r\max} = S_{rm} + 2S_{rd}$, and $S_{r\min} = S_{rm} - S_{rd}$,

$$\frac{S_{rn}}{S_{r\max}} = \frac{1 + (x'_n - 1)S_{rd}/S_{rm}}{1 + 2S_{rd}/S_{rm}} \qquad \text{(C-7)}$$

Thus, the values of $S_{rn}/S_{r\max}$ vary from a minimum to a maximum value that approaches 1 . The minimum value depends on $S_{r\bar{a}}/S_{rm}$, but is always greater than 0. When $x'_n = 3$, $S_{rn}/S_{r\max} = 1$ regardless of the value of $S_{r\bar{a}}/S_{rm}$.

The computer program arranges the calculated $S_{rn}/S_{r\max}$ values in a random sequence by generating 500 random-sequence numbers, consecutively assigning these sequence numbers to the 500 $S_{rn}/S_{r\max}$ values, and finally rearranging the $S_{rn}/S_{r\max}$ values according to the assigned sequence numbers. The same sequence numbers are used for all tapes (corresponding to different values of $S_{r\bar{a}}/S_{rm}$) for the main testing program; hence, the nth value of $S_r/S_{r\max}$ always appears at the same location in the sequence for these tapes. The random numbers are generated by an available CDC (Control Data Corporation) computer subroutine and are based on a seed number of —1.

The control tape defines both the peak and valley of each load cycle; the valley is equal to 0, and the peak equals the calculated value of $S_{rn}/S_{r\max}$. Because the tape reader accepts only 3-digit numbers, the peak and valley values are truncated beyond 0.1 percent and result in 3-digit numbers ranging from 000 to 999. In a previous report (*33*), the 500 values of $S_{rn}/S_{r\max}$ are listed in proper sequence for each different variable-amplitude

To assure that the tapes satisfy the desired probability-density curves, the $S_{rn}/S_{r\max}$ range between 0 and 1 was divided into 20 equal-width intervals, the number of occurrences in each interval was counted, and the corresponding frequency of occurrence was compared with the value calculated from the probability-density curve defined by Eq. C-5. The results (*33*) confirmed that the tapes satisfy the desired probability-density curves.

APPENDIX D

STATISTICAL CONCEPTS

This appendix is intended primarily to explain the statistical concepts used in this study.

EXPLANATION OF PROBABILITY CURVES

The development of histograms and probability-density curves representing the observed frequency of occurrence of events is described as follows and in Figure D-1.

Frequency-of-Occurrence Graphs

The top sketch in Figure D-1 shows histograms and curves that give the percent of occurrences that falls within each interval of a variable x. Both of the curves are for the same set of data. The percent of occurrences that falls within any interval depends on the size of the interval; specifically, the frequency of occurrence, f, is proportional to the interval, Δx. (For example, 18 percent of the occurrences are between 21 and 23, and 9 percent are between 21.5 and 22.5.)

Probability-Density Curve

By dividing the frequency of occurrence, f, by the interval, Δx, a single curve representing a set of data is obtained. The ordinate of this curve is the probability density, $y = f/\Delta x$. The area $(y \cdot \Delta x)$ under the curve between any two values of x is the percentage of occurrences (frequency of occurrence) that falls within that interval of x. The total area under the curve equals 1 since the curve covers 100 percent of the occurrences; the area is dimensionless since y has the dimensions of $1/x$.

The heavy line in the middle sketch in Figure D-1 is the probability-density curve corresponding to the frequency-of-occurrence graphs in the top sketch. The light line in the middle sketch is the probability-density curve for a different set of data. For the shape of the probability-density curve shown in Figure D-1—a normal distribution curve—the mean, or average, value is the same as the modal value, which is the value of x corresponding to the highest value of y. Thus, the mean (and modal) values, x_m, for the heavy and the light curves are equal to 20 and 18, respectively; hence, the light curve peaks to the left of the heavy curve. In addition, the light curve has a greater width than the heavy curve, which indicates a greater dispersion, or scatter, of data. The width of the curve, or dispersion, can be defined as the distance from x_m to $x_{\bar{a}}$, with $x_{\bar{a}}$ defined as the value of x corresponding to a value y that is a certain percent of the maximum y, $y_{\max}$, associated with x_m. For the shape of the probability-density curve in Figure D-1—a normal distribution curve—the standard deviation, σ, is used to define the width; then $x_{\bar{a}} = x_m + \sigma$ and $y_{\bar{a}} = 0.606y_{\max}$.

Nondimensional Probability-Density Curve

Probability-density curves for different sets of data can be plotted as a single nondimensional curve if they have the same general shape. The bottom sketch in Figure D-1 shows the nondimensional curve for the two probability-density curves in the middle sketch. The x_m values for the curves are shifted horizontally to a single point by plotting the deviation from the mean, $x - x_m$, or from some other constant value of x, rather than the actual values of x. Curves of different widths are compressed or expanded to a single width by dividing $x - x_m$ by the standard deviation, σ, or by some other measure of dispersion. Thus, the deviation from the mean divided by the standard deviation is used as the horizontal axis. Since the area under the curve between any two values of x (frequency of occurrence) must remain the same in the nondimensional plot, the prob-

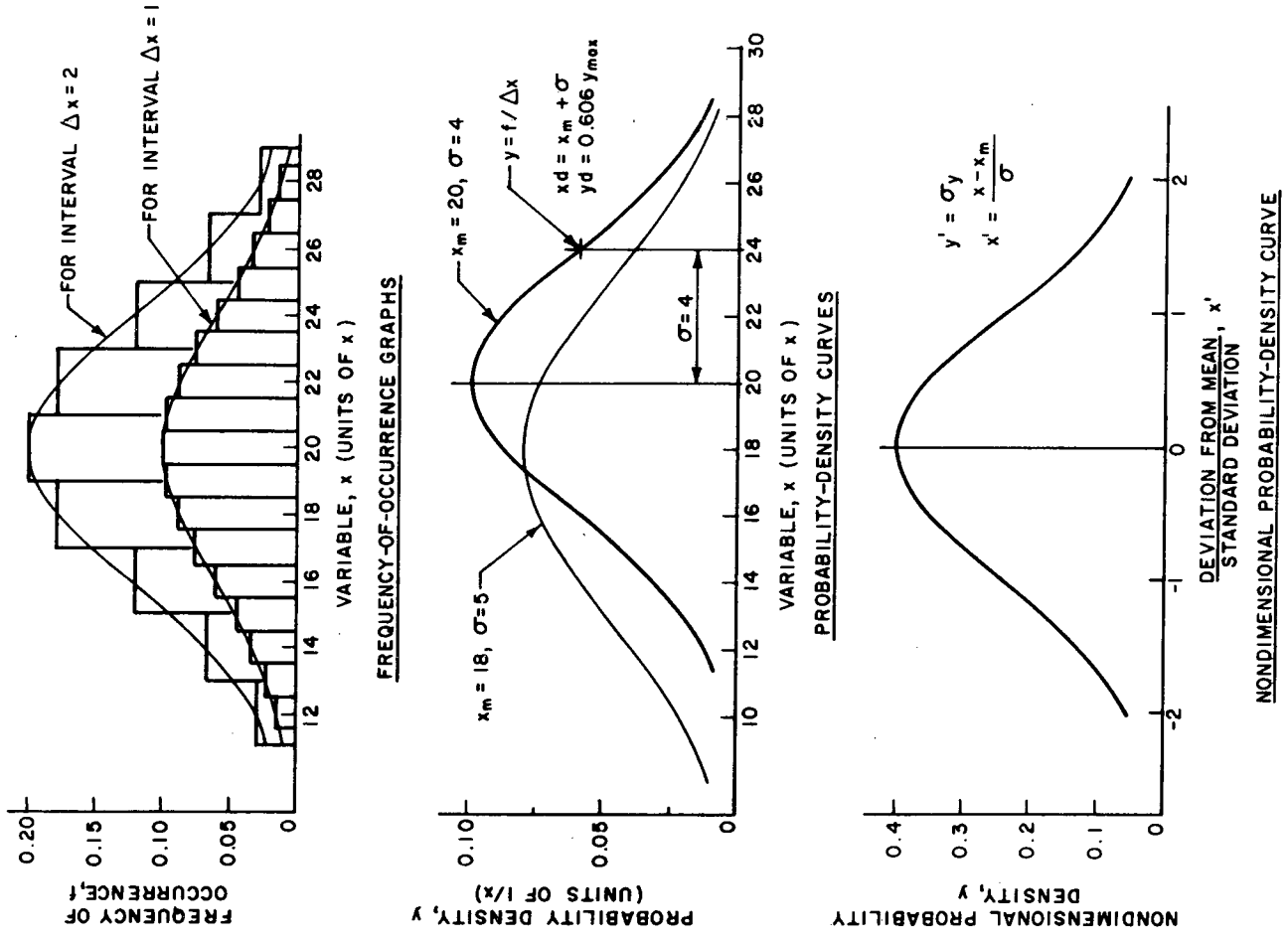

Figure D-1. Typical probability curves.

ability density, y, must be multiplied by σ to obtain the nondimensional probability density.

For convenience, a mathematical expression is usually used to approximate nondimensional probability-density curves obtained from actual data. For example, a symmetric curve, such as is shown in Figure D-1, can be represented by a normal distribution curve that has been shown to apply to a wide range of physical phenomena. The basic mathematical expression for this curve is

$$y' = \frac{1}{\sqrt{2\pi}} e^{-(\frac{1}{2})(x')^2} \qquad \text{(D-1)}$$

The factor $1/\sqrt{2\pi}$ makes the total area under the curve between plus and minus infinity equal to 1.0.

Physical phenomena involving a variable that has a lower limit but no upper limit, such as flow in a river or traffic on a bridge, can frequently be represented by a skewed curve defined for $x' \geq 0$ by the expression

$$y' = x' e^{-(\frac{1}{2})(x')^2} \qquad \text{(D-2)}$$

The characteristics of this expression, which is called a Rayleigh function, are shown in Figure 10.

Each of these mathematical expressions represents a nondimensional probability-density curve that can be expanded into a family of probability-density curves, each of which is defined by the modal value (or a similar fixed point) and the standard deviation (or a similar measure of curve width). Histograms with any interval, Δx, can be obtained from each frequency-density curve. Thus, a large variety of different sets of data can be approximated by a single mathematical expression.

SAMPLING ERROR

The results of a testing program on a finite number of specimens represent only a sample of the data (population) that would result if an infinite number of similar tests were performed. The average results obtained from such a finite sample usually differ from the average results that would be obtained from an infinite population. The magnitude and significance of this difference, which is referred to as sampling errors, is discussed in statistical terms, as follows.

Variation Among Samples

If a large number of samples (groups of individual data) are taken from a population (a very large or infinite number of compatible data), the means and standard deviations of the samples will be scattered about the true population mean and standard deviation. Nevertheless, the sample mean, $\bar{x}$, represents the best (unbiased) estimate of the population mean that can be obtained from the single sample. The best (unbiased) estimate of the variance (square of the standard deviation) of the population that can be obtained from the single sample equals the variance of the sample times a factor $n/(n-1)$. Hence,

$$S^2 = \frac{\Sigma(x - \bar{x})^2}{n - 1} \qquad \text{(D-3)}$$

in which x is an individual test result or data point, n is the number of test results or different values of x, and S^2 is the unbiased variance.

The standard deviation of the sample means is called the standard error of the mean and can be estimated by

$$S_{\bar{x}} = \frac{S}{\sqrt{n}} \qquad \text{(D-4)}$$

Similarly, the standard deviation of the standard deviations of the samples is called the standard error of the standard deviation, which is expressed as

$$S_s = \frac{S}{\sqrt{2n}} \qquad \text{(D-5)}$$

Confidence Limits

If the samples are relatively large (say 100), the sample means are approximately normally distributed. Hence, the probability that the population mean is within one standard error from the sample mean is about 68 percent. Similarly, the probability that the population mean is within any other number, t, of standard errors from the sample mean can be obtained from normal distribution curves (although statisticians usually use the symbol Z for this number if the probability is obtained from a normal distribution and the symbol t if the probability is obtained from the Student's t distribution, the symbol t is used herein for both cases). As an example, the probability that the population mean is within $t = 3$ standard errors from the sample mean is 99.7 percent.

If the samples are relatively small (say less than 30), the probability corresponding to a given t value is somewhat smaller than given by the normal distribution because the distribution of differences between the sample and population means for small samples does not follow a normal distribution. Instead, the samples follow a distribution called Student's t, which approaches the normal distribution when the sample size becomes large. Statistical tables (*34*) give t values corresponding to various probability levels and degrees of freedom; the number of degrees of freedom depends primarily on the number of data. For example, in determining the probability that the population mean is within t standard errors from the sample mean, the degrees of freedom are equal to the number of data in the sample minus 1.

Use of the t table can be conveniently illustrated by an example. Suppose that the mean for a sample of 11 items is 101 and that the standard error of the mean calculated by Eq. D-4 is 10. Because of sampling errors, the true population mean probably differs from 101. The range of values within which the true population mean can be expected to lie with a certain degree of probabilty, say 90 percent, can be determined by entering the tables (*35*) with the degrees of freedom (10) and desired probability (90 percent) to get a t value of 1.81. There is a 90-percent probability that the true population mean lies within $1.81 \times 10 = 18.1$ (t times the standard error) from the sample mean; or, in other words, between 82.9 and 119.1. These limits are called the 90-percent confidence limits for the mean. If a large number of 11-item samples were taken from the population and the mean, standard error—and confidence limits of each sample were determined—in 90 percent of the cases the true value for the population would be located between the calculated upper and lower confidence limits for each sample. If the sample mean and standard error were the same as noted previously, but the sample size was 30 instead of 11, the t value would be 1.70 and the 90-percent confidence limits would be slightly closer to the sample mean, or between 84 to 118. As the number of data increases, the confidence interval (distance between the two limits) approaches 0 because $S_{\bar{x}}$ approaches 0.

Tolerance Limits

Limits that define the scatter band, or a range of values that includes a certain percent, P, of the population with a certain degree of confidence (probability), are called tolerance limits. These limits are defined in terms of a factor K that is similar to the t value discussed earlier; K times the standard deviation is the distance from the mean to the tolerance limits. Tables of K values are available for normally distributed data (*36*). If $n = 10$, $P = 75$ percent, and $\alpha = 90$ percent, such tables indicate that $K = 1.99$. This means that if a large number of 10-item samples were taken from a normal population and the tolerance limits were calculated for each sample, at least 75 percent of the population would be within the calculated limits in 95 percent of the cases. Because the sample may not exactly represent the population, the value of K is always greater than the number of standard deviations, K', that include P percent of the area under a normal distribution curve. However, K approaches K' as the sample size increases. For example, with $P = 75$ percent and $\alpha = 95$ percent, $K = 1.99$ for a 10-item sample; $K = 1.31$ for a 100-item sample; and $K = K' = 1.15$ for an infinite sample.

The best estimate of the limits that include P percent of the population that can be determined from a sample of that population is $K'S$. The distance $(K - K')S$ defines a confidence interval about this best-estimate line that is analogous to the confidence interval about the mean determined from a sample, as discussed earlier. As the number of data in the sample increases, this interval approaches 0 and K approaches K' as previously illustrated. The limits $K'S$ can also be interpreted as tolerance limits for P percent of the population with a 50-percent confidence level.

Comparison of Two Samples

If a large number of pairs of samples are taken from the same population and the mean of each sample is calculated, the differences in the means of the pairs of samples will be normally distributed. The standard deviation of the differences is called the standard error of the difference and can be estimated by

$$S_{\bar{x}_1 - \bar{x}_2} = \sqrt{\frac{S_1^2}{n_1} + \frac{S_2^2}{n_2}} \qquad \text{(D-6)}$$

in which the subscripts 1 and 2 denote the first and second sample. Again, the probability that the difference in means

of any pair of samples from the population would be within any specified number, t, of standard errors from the true value of 0 can be obtained from a t table.

T-Test

The standard error of the difference can be used to test whether an observed difference between the means of two samples either was likely to have occurred merely by chance (that is sampling variability) or indicates a real difference between the two samples. To make this test of statistical significance, the observed difference is divided by the standard error of the difference to determine t. Thus,

$$t = \frac{\text{observed diff.}}{\text{std. error of diff.}} \qquad \text{(D-7)}$$

The probability that a difference that occurred merely by chance would be smaller than the observed difference can then be determined from a t table. For example, if t equals 1.96 for the pair of large samples being compared, there is only a 5-percent chance that such a large difference would occur if the two samples were from the same population; and it would be reasonable to conclude that a real difference exists.

The probability that a chance difference would be less than the observed difference is referred to as the confidence level, because it is a measure of the confidence that can be placed in the conclusion that there is a real, or statistically significant, difference between the two samples. In the example, the confidence level is 95 percent. Usually, if the confidence level is less than 95 percent, the difference between the two samples is not considered to be statistically significant; in other words, it has not been shown conclusively that a real difference exists between the samples.

F-Test

The t value indicates the significance of a difference in the means of two samples. A similar value—called the variance ratio, or F statistic—indicates the significance of a difference in the variances (standard deviation squared) of the two samples. Specifically, F equals the greater estimate of the population variance divided by the lesser estimate of the population variance. Thus,

$$F = \left(\frac{S_G^2}{S_L^2}\right) \qquad \text{(D-8)}$$

in which the subscripts G and L refer to the samples with the greater and lesser variance, respectively. If the two samples are from the same population, F approaches 1.0 as the size of the samples increases. The probability associated with various values of F and degrees of freedom is given in F tables (*35*). If the probability corresponding to the calculated F value for a given pair of sample variances is less than 95 percent, it is usually concluded that the data do not show a statistically significant difference between the standard deviations of the two samples and, therefore, that the samples were drawn from the same population.

Comparison of Two Regression Lines

The standard error of the estimate for a regression (best-fit) line is analogous to the standard error of the mean of a sample and can be calculated from Eq. 2. This is accomplished by using the deviations from the regression line instead of the deviations from the mean in calculating S. Similarly, confidence limits can be calculated for a linear regression line as well as for a sample mean. These limits have the closest spacing (in the Y direction) at the mean value of the independent variables observed in the experiment, $\overline{X}$. The spacing is equal to t times the standard error of the estimate at that location. As the value of X moves away from $\overline{X}$, the confidence interval for Y increases because there is less certainty about the true value of Y. Thus, the confidence limits are hyperbolic and are closest to the regression line at $\overline{X}$. In many practical cases, however, the curvature is small and the confidence limits can be approximated by straight lines that are parallel with the regression line. Similarly, tolerance limits from a regression line are hyperbolic, but are often approximated by straight lines parallel to the regression line.

The probability that there is a real difference between regression lines estimated from independent sets of data can be assessed in the following way (*37*). The regression lines are of the form

$$Y = A + BX \qquad \text{(D-9)}$$

To test whether there is a statistically significant difference between the slopes, B, of the two lines, the data are first coded to eliminate the constant term, A. This is accomplished by subtracting the average of all X values in a set, $\overline{X}$, from each individual X value, and performing a similar operation with the Y values. Thus,

$$(Y - \overline{Y}) = B(X - \overline{X}) \qquad \text{(D-10)}$$

The least-squares slope estimate is then determined for each set, and the regression sum of squares—a measure of the variation in the dependent variable that is explained by the independent variable—is determined for each set. A combined estimate of the slope is calculated by combining the two sums of the squared deviations used to estimate the individual slopes. The regression sums of squares are then calculated by using the combined slope estimate. The difference between the over-all regression sum of squares based on the individual slope estimates and the over-all regression sum of squares based on using the combined estimate is compared to the unexplained variation about the individual lines. This is done by an F test (Eq. D-8). The degree of freedom for the numerator is equal to one, and the degree of freedom for the denominator is equal to the total number of data points minus one.

To test whether there is a statistically significant difference in the values of A, it is assumed that the slopes are not statistically different and the over-all mean values for both sets, $\overline{X}'$ and $\overline{Y}'$, are subtracted from each individual X or Y in both sets. Best-fit lines that have the same slope—the best-fit slope, B, for the combined data—are calculated for both sets of data. The increase in the unexplained variation about the over-all line relative to the unexplained variation in the combined data is compared to the inherent variability in the data by a variance ratio, and the probability for A is obtained from F tables as discussed earlier for B.

APPROXIMATE CONFIDENCE AND TOLERANCE LIMITS

Approximate 95-percent confidence limits are used in the present study. These limits were obtained by plotting lines parallel with the best-fit line a distance equal to 1.96 times the standard error of the estimate above and below the best-fit line. These particular approximate limits have several different meanings. First, they approximate the 95-percent confidence limits for a single future test result. If a set of tests is repeated a large number of times, confidence limits for a single future test are calculated for each set, and a single additional test is performed in conjunction with each set; each additional test result will fall within the calculated limits for that repetition in 95 percent of the repetitions. The limits also represent the best estimate of the true 95-percent tolerance limits for the population in the sense discussed in the section on sampling errors. The limits would contain at least 95 percent of the sample data in 50 percent of the cases in which the experiment was repeated to obtain replicate samples.

To show the difference between the straight-line approximate confidence limits and the true hyperbolic limits, the true limits were calculated for one large and one small set of data. The first set consisted of 36 variable-amplitude results (Project 12-12) for cover-plate C beams fitted to 85 constant-amplitude results (from both Project 12-12 and 12-7) for cover-plate C beams. The second set included 6 results of constant-amplitude tests from Project 12-12 on cover-plate A beams.

For both sets of data, the hyperbolic 95-percent confidence limits were calculated first for the true value of the dependent variable at some value of the independent variable:

$$\log(N) = \log(N_0) \pm t_{n-2,\,1-\gamma/2}\sqrt{v_0} \qquad \text{(D-11)}$$

and second for a single future test result:

$$\log(N) = \log(N_0) \pm t_{n-2,\,1-\gamma/2}\sqrt{s^2 + v_0} \qquad \text{(D-12)}$$

N_0 is the predicted (best-fit) value of the dependent variable, and v_0 is the estimate of variance, both at the point of estimation, X_0. The term $t_{n-2,\,1-\gamma/2}$ is the value of the Student's t distribution for n-2 degrees of freedom and a $(1-\gamma)$ confidence level. The estimate of variance is given by

$$v_0 = S^2\left[\frac{1}{n} + \frac{(X_0 - \overline{X})^2}{\sum(X_i - \overline{X})^2}\right] \qquad \text{(D-13)}$$

in which X_i is the ith value (data point) of the independent variable ($\log S_r$), $\overline{X}$ is the mean value of the independent variable for the sample, and S is the standard error of the estimate times the square root of the number of data, n. Thus, the term S^2/n is the square of the standard error of the estimate.

The results are shown in Figures D-2 and D-3 for the large and small sets of data, respectively. For the large set, the approximate and exact confidence limits for the population mean are almost identical, and, even for the small set, the difference is small enough to be neglected.

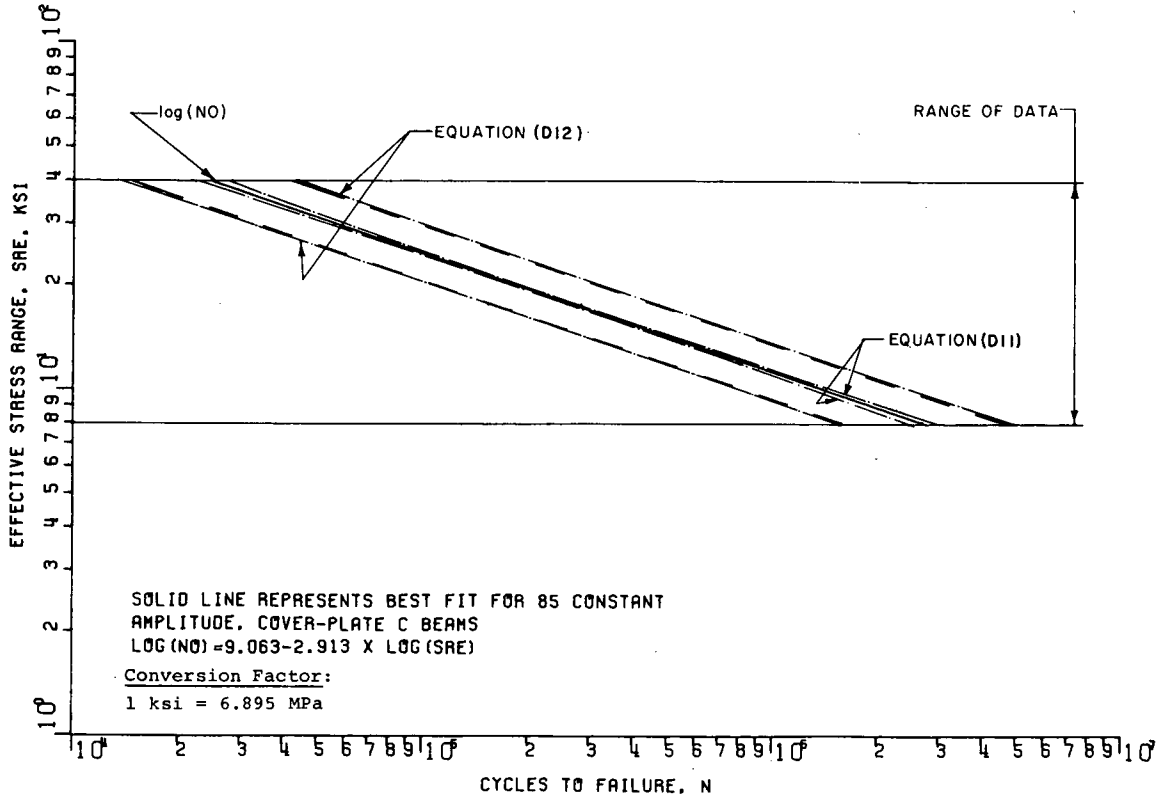

Figure D-2. Exact and approximate confidence and tolerance limits for large set of data.

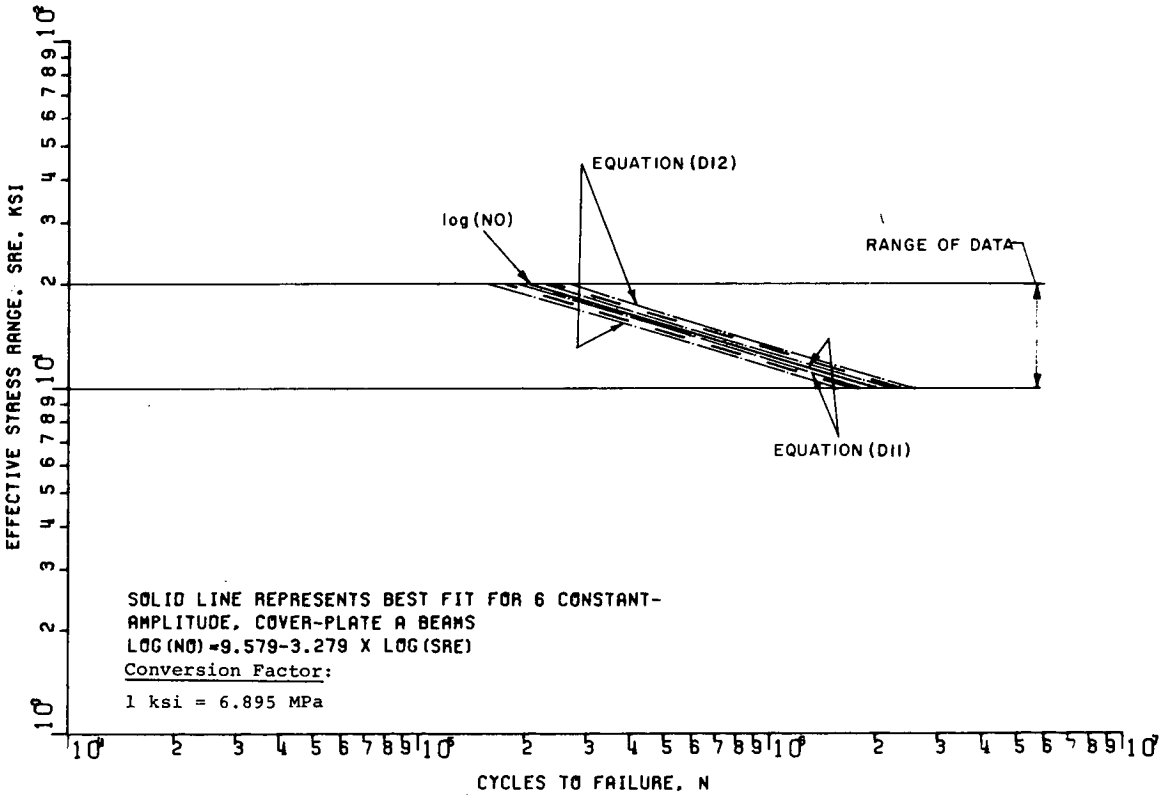

Figure D-3. Exact and approximate confidence and tolerance limits for small set of data.

APPENDIX E

FATIGUE-TEST RESULTS

The fatigue test results—including data on applied stresses, life, and observed cracks—are summarized in Tables E-1 through E-5 and Figures E-1 through E-5.

ORGANIZATION OF TABLES

Table E-1 gives the results for A514-steel cover-plate specimens, and Table E-2 gives the results for A514-steel cover-plate beams. The results for A514-steel welded beams are given in Table E-3. Tables E-4 and E-5 include the results for A36-steel cover-plate beams and A36-steel welded beams.

Each set of three beams or specimens tested under identical stress conditions has a set number that is used whenever reference to a specific set is made in the text. The sets of beams and specimens are numbered separately, but sets for different types of beams are not numbered separately. Thus, there is one beam set 31 and one specimen set 31. Within each table, the data are listed consecutively by set number. To find any set of data referred to in the text, the reader must look in the appropriate table for that type of beam or specimen. For example, set 31 is a cover-plate beam of A514 steel and, therefore, is listed in Table E-2. If the type of beam is not known, it is necessary to look through Tables E-2 through E-5 until the desired set number is found.

Each of the three beams or specimens within a set has a specific specimen name consisting of three letters followed by several numbers and another letter. These individual names are listed in the tables and are used in the text whenever it is necessary to distinguish among the three beams or specimens in a set. However, the set number is used as the main identification for the test results.

EXPLANATION OF TABLE COLUMN HEADINGS

An explanation of the headings for the beam tables (Tables E-2 through E-5) follows. The headings of the first eight columns in the specimen table (Table E-1) are identical with those in the beam tables. The headings for columns 9 through 12 (crack locations) of Table E-1 are explained in Figure B-6.

Column No.

(1) Set number.

(2) Beam designation with beam number and type of detail.

TABLE E-1

A514-STEEL COVER-PLATE SPECIMENS

COVER-PLATE SPECIMENS

SET	SPECIMEN NAME	SMIN, KSI	SRM, KSI	S_{RD}/S_{RM}	SRRMS, KSI	KILOCYCLES LOG.-AVG.	KILOCYCLES COUNT	CRACK LENGTH, IN. FOR LOCATIONS T1	T2	T3	T4	NOTES
(1)	(2)	(3)	(4)	(5)	(6)	(7)	(8)	(9)	(10)	(11)	(12)	(13)
1	CpS- 91A	0.00	10.00	0.00	10.00	18100	2799.15	.000	.000	.000	.000	
							3400.13	.000	.080	.000	.025	
							3659.61	.000	.080	.000	.025	
							4269.27	.000	.080	.000	.125	
							12889.84	.000	.080	.000	.125	
							25601.67	.000	.080	.000	.125	DISCONTINUED
	CpS- 25A						2584.49	.000	.000	.000	.000	
							4026.04	.000	.000	.085	.000	
							4273.67	.000	.000	.085	.000	
							5082.00	.000	.000	.360	.000	
							8108.78	.000	.000	.470	.000	
							8389.04	.000	.000	.495	.000	
							9067.79	.000	.000	.850	.000	
							9243.60			3.500	3.500	FAILED AT T3-T4
	CpS-104A						25005.26	.000	.000	.000	.000	DISCONT.--MISCALIBRATED
2	CpS- 84A	0.00	10.00	.50	11.89	3950	791.17	.000	.000	.000	.000	
							1244.01	.000	.000	.315	.000	
							1883.33	.000	.000	.425	.000	
							1938.11	.000	.000	.470	.000	
							3093.84	.000	.425	.000	.000	
							3179.15			3.500	3.500	FAILED AT T3-T4
	CpS-116A						481.87	.000	.000	.000	.000	
							758.60	.000	.120	.000	.000	
							978.06	.000	.135	.000	.000	
							1379.89	.000	.185	.100	.000	
							2338.95	.000	.250	.290	.000	
							2524.09	.175	.270	.290	.000	
							3164.49	.300	.310	.335	.000	
							3831.85	.420	.435	.400	.000	
							4878.52	.835	.850	.600	.000	
							5010.35	3.500	3.500			FAILED AT T1-T2
	CpS-109A						765.89	.000	.000	.000	.000	
							1210.82	.000	.000	.060	.000	
							1405.30	.000	.090	.065	.000	
							2920.41	.000	.560	.620	.000	
							3545.32	.000	.765	.960	.000	
							3776.21	.000	.945	1.325	.000	
							3854.92			3.500	3.500	FAILED AT T3-T4, T2

3	CpS-102A	0.00	10.00	1.00	13.78	2390	140.00	.000	.000	.000	.000	
							592.87	.000	.130	.120	.000	
							930.33	.274	.212	.215	.178	
							1039.80	.269	.230	.235	.180	
							1111.50	.295	.230	.255	.225	
							1533.94	.450	.320	.515	.320	
							2445.01	3.500	3.500			FAILED AT T1-T2
	CpS- 98A						20.00	.000	.000	.000	.000	
							500.90	.110	.000	.235	.000	
							690.54	.150	.000	.270	.125	
							1151.42	.255	.245	.325	.219	
							1335.11	.290	.280	.320	.230	
							1794.03	.365	.310	.520	.290	
							1984.43	.375	.335	.605	.310	
							2432.57	.610	.400	1.825	.445	
							2443.01			3.500	3.500	FAILED AT T3-T4
	CpS- 35A						38.00	.000	.000	.000	.000	
							1480.58	.320	.540	.575	.390	
							2051.12	.345	.650	.625	.385	
							2240.46	.485	.965	.955	.550	
							2294.49			3.500	3.500	FAILED AT T2-T3-T4
4	CpS- 33A	0.00	30.00	0.00	30.00	244	10.00	.000	.000	.000	.000	
							66.00	.185	.210	.280	.000	
							101.00	.275	.340	.355	.130	
							275.55	3.500	3.500			FAILED AT T1-T2
	CpS-115A						5.00	.000	.000	.000	.000	
							52.00	.000	.270	.000	.000	
							98.00	.155	.325	.265	.000	
							249.07	3.500	3.500			FAILED AT T1-T2, T3
	CpS-101A						5.00	.000	.000	.000	.000	
							10.00	.000	.000	.140	.000	
							25.00	.000	.000	.115	.175	
							61.00	.215	.375	.325	.120	
							195.37			3.500	3.500	FAILED AT T3-T4
5	CpS- 76A	0.00	30.00	.50	35.67	182	.50	.000	.000	.000	.000	
							5.00	.000	.180	.000	.000	
							67.34	.445	.345	.185	.205	
							142.81	.525	.500	.365	.260	
							186.95	3.500	3.500			FAILED AT T1-T2
	CpS- 34A						2.00	.000	.000	.000	.000	
							200.83			3.500	3.500	FAILED AT T3-T4
	CpS- 80A						12.00	.000	.000	.000	.000	
							58.62	.205	.340	.295	.000	
							105.41	.315	.455	.430	.200	
							141.48	3.500	3.500			FAILED AT T1-T2
6	CpS- 7A	0.00	30.00	1.00	41.34	136	5.50	.125	.135	.065	.095	
							10.00	.130	.145	.185	.115	
							25.00	.130	.145	.185	.115	
							50.00	.230	.360	.370	.265	
							75.00	.230	.360	.370	.265	
							100.00	.260	.450	.545	.345	
							125.00	.285	.550	.685	.360	
							167.36			3.500	3.500	FAILED AT T3-T4

TABLE E-1 (continued)

SET	SPECIMEN NAME	SMIN, KSI	SRM, KSI	SRD/SRM	SRRMS, KSI	KILOCYCLES LOG.-AVG.	KILOCYCLES COUNT	CRACK LENGTH, IN, FOR LOCATIONS T1	T2	T3	T4	NOTES
(1)	(2)	(3)	(4)	(5)	(6)	(7)	(8)	(9)	(10)	(11)	(12)	(13)
	CPS- 43A						5.00	.100	.000	.230	.085	
							21.50	.145	.220	.300	.175	
							110.01			3.500	3.500	FAILED AT T3-T4
	CPS- 82A						1.50	.000	.000	.000	.000	
							3.00	.175	.225	.265	.000	
							10.00	.255	.315	.350	.150	
							25.00	.265	.310	.450	.290	
							50.00	.315	.325	.450	.310	
							138.02			3.500	3.500	FAILED AT T3-T4
7	CPS- 2A	10.00	10.00	0.00	10.00	4400	2212.38	.000	.320	.200	.200	
							2340.29	.000	.340	.200	.200	
							3209.29	.000	.537	.200	.200	
							4069.29	.875	1.075	.200	.200	
							4354.25	3.500	3.500			FAILED AT T1-T2
	CPS- 4A						153.36	.000	.000	.000	.000	
							764.18	.000	.790	.700	.000	
							913.77	.000	.800	.700	.000	
							1000.00	.000	.805	.680	.000	
							5307.77			3.500	3.500	FAILED AT T3-T4
	CPS- 57A						737.50	.000	.000	.000	.000	
							1209.25	.000	.375	.438	.000	
							1530.25	.000	.387	.475	.000	
							1709.25	.000	.400	.500	.200	
							3335.60	.000	.600	.900	.275	
							3209.25	.000	.600	.900	.255	
							3696.12			3.500	3 500	Failed at T3-T4
8	CPS- 20A	10.00	10.00	.50	11.80	3560	50.00	.140	.000	.000	.175	
							1790.04	.140	.290	.000	.175	
							1897.03	.140	.290	.000	.175	
							1972.17	.140	.290	.000	.175	
							2421.00	.215	.290	.000	.175	
							2527.17	.390	.290	.000	.175	
							2594.76	.390	.290	.175	.175	
							3060.43	.460	.340	.185	.175	
							3242.32	.415	.400	.340	.175	
							3697.52	.445	.435	.375	.175	
							3880.13	.675	.450	.405	.315	
							4248.68	.515	.490	.455	.315	
							4408.47	.540	.500	.575	.325	
							5413.98	3.500	3.500			FAILED AT T1-T2

	CpS- 78A						5.00	.000	.000	.300	.000	
							521.00	.000	.000	.360	.000	
							715.94	.000	.000	.360	.000	
							1073.69	.000	.330	.465	.000	
							1251.99	.000	.360	.515	.000	
							1856.45	.000	.520	.805	.265	
							2447.55			3 500	3.500	Failed at T3-T4
	CpS- 14A						453.65	.000	.250	.280	.000	
							566.49	.000	.250	.290	.000	
							640.53	.000	.250	.290	.000	
							1087.05	.000	.250	.320	.000	
							1277.54	.000	.250	.345	.000	
							1727.90	.160	.250	.425	.000	
							1912.47	.160	.255	.465	.000	
							2362.32	.250	.260	.585	.000	
							2472.36	.260	.270	.625	.280	
							2531.68	.260	.270	.640	.280	
							3396.29			3.500	3.500	Failed at T3-T4
9	CpS- 21A	10.00	10.00	1.00	13.78	2080	5.00	.000	.000	.000	.000	
							66.47	.000	.175	.200	.225	
							137.26	.000	.175	.200	.325	
							574.78	.250	.475	.400	.325	
							674.64	.250	.475	.425	.325	
							743.78	.250	.475	.425	.325	
							1093.20	.250	.525	.450	.325	
							1187.46	.250	.550	.450	.325	
							1254.91	.250	.600	.450	.325	
							1511.76	.250	.800	.500	.375	
							1617.97	.250	.925	.525	.375	
							1679.39	.250	.925	.550	.375	
							1906.89	3.500	3.500			Failed at T1-T2
	CpS- 51A						73.45	.000	.000	.000	.000	
							140.90	.000	.075	.150	.125	
							609.10	.300	.350	.475	.275	
							1859.20	.575	.675	.650	.500	
							1992.00	.725	.725	.750	.550	
							2312.90			3.500	3.500	Failed at T3-T4
	CpS- 70A						452.02	.000	.000	.000	.000	
							896.02	.285	.410	.000	.000	
							1082.00	.312	.450	.600	.375	
							1856.00	.400	.625	.700	.425	
							2001.35	.487	.849	.750	.450	
							2031.85	3.500	3.500			FAILED AT T1-T2
10	CpS- 8A	10.00	30.00	0.00	30.00	240	.50	.000	.000	.000	.000	
							1.00	.000	.000	.192	.000	
							5.00	.000	.000	.000	.000	
							10.00	.000	.000	.000	.000	
							50.00	.171	.177	.316	.248	
							230.53			3.500	3.500	FAILED AT T3-T4

TABLE E-1 (continued)

SET	SPECIMEN NAME	SMIN, KSI	SRM, KSI	SRD/SRM	SRRMS, KSI	KILOCYCLES LOG.-AVG.	KILOCYCLES COUNT	CRACK LENGTH, IN. FOR LOCATIONS T1	T2	T3	T4	NOTES
(1)	(2)	(3)	(4)	(5)	(6)	(7)	(8)	(9)	(10)	(11)	(12)	(13)
	CPS- 11A						1.00	.000	.000	.000	.000	
							5.00	.000	.000	.135	.000	
							10.00	.000	.000	.160	.000	
							50.00	.000	.000	.330	.000	
							100.00	.000	.310	.388	.000	
							135.17	.235	.365	.420	.250	
							150.00	.235	.365	.420	.250	
							283.29			3.500	3.500	FAILED AT T3-T4
	CPS- 29A						11.06	.000	.150	.000	.125	
							76.45	.200	.150	.225	.200	
							136.88	.300	.375	.225	.325	
							161.94	.400	.550	.225	.350	
							212.51	3.500	3.500			Failed at T1-T2
11	CPS- 18A	10.00	30.00	.50	35.67	184	10.00	.000	.000	.000	.000	
							50.00	.000	.770	.270	.000	
							170.56			3.500	3.500	FAILED AT T3-T4
	CPS- 37A						5.00	.000	.000	.000	.000	
							10.00	.190	.000	.270	.000	
							50.00	.180	.000	.475	.000	
							203.67			3.500	3.500	FAILED AT T3-T4
	CPS- 22A						5.00	.000	.165	.193	.000	
							10.00	.000	.225	.275	.000	
							50.00	.000	.300	.305	.000	
							180.56	3.500	3.500			FAILED AT T1-T2
12	CPS- 6A	10.00	30.00	1.00	41.34	123	46.00	.000	.000	.100	.020	
							49.00	.000	.020	.100	.020	
							127.97	3.500	3.500			FAILED AT T1-T2
	CPS- 16A						81.00	.000	.000	.532	.000	
							99.00	.000	.532	.532	.000	
							116.00	.000	.609	1.062	.000	
							123.43	3.500	3.500			FAILED AT T1-T2
	CPS- 56A						10.00	.288	.087	.250	.050	
							15.00	.325	.250	.275	.200	
							20.00	.325	.300	.375	.225	
							30.00	.325	.313	.400	.225	
							90.00	.325	.575	.525	.250	
							100.00	.350	.650	.600	.250	
							110.00	.350	.750	.750	.375	
							118.61	3.500	3.500			FAILED AT T1-T2

13	CpS-114A	10.00	60.00	0.00	60.00	35.7	1.00	.000	.275	.000	.000	
							10.00	.200	.325	.150	.000	
							31.35			3.500	3.500	FAILED AT T3-T4
	CpS- 28A						.50	.000	.000	.000	.000	
							1.00	.000	.000	.060	.000	
							5.00	.000	.290	.195	.215	
							10.00	.175	.365	.200	.265	
							20.00	.250	.420	.265	.290	
							41.24			3.500	3.500	FAILED AT T3-T4
	CpS- 96A						.50	.000	.000	.000	.000	
							1.00	.000	.275	.000	.000	
							5.00	.000	.285	.000	.000	
							10.00	.205	.330	.000	.090	
							35.16	3.500	3.500			FAILED AT T1-T2
14	CpS-XXXA	10.00	4.00	1.00	5.51		.00	.000	.000	.000	.000	NOT TESTED BECAUSE
	CpS-XXXA						.00	.000	.000	.000	.000	OF VERY HIGH LIFE
	CpS-XXXA						.00	.000	.000	.000	.000	EXPECTANCY
15	CpS- 93A	40.00	10.00	0.00	10.00	5510	20.00	.000	.000	.000	.000	
							624.62	.049	.240	.074	.118	
							770.19	.000	.000	.000	.000	
							851.00	.095	.250	.220	.130	
							1422.20	.200	.292	.264	.187	
							1576.10	.000	.000	.000	.000	
							2279.65	.310	.386	.308	.207	
							3157.50	.478	.520	.375	.247	
							3420.00	.507	.612	.385	.268	
							4209.81	3.500	3.500			FAILED AT T1-T2
	CpS- 69A						50.00	.000	.000	.000	.000	
							134.56	.000	.210	.100	.000	
							739.18	.000	.345	.130	.000	
							996.36	.000	.355	.140	.000	
							1447.11	.000	.380	.140	.000	
							1618.24	.000	.400	.155	.000	
							2238.55	.000	.425	.185	.000	
							2491.35	.000	.460	.190	.000	
							3093.07	.000	.505	.215	.000	
							3349.75	.000	.510	.220	.000	
							4596.71	.000	.625	.260	.000	
							4843.32	.000	.655	.280	.000	
							5450.18	.000	.755	.330	.000	
							5695.02	.000	.835	.345	.000	
							6190.28	3.500	3.500			FAILED AT T1-T2
	CpS- 26A						203.57	.000	.000	.000	.000	
							812.45	.170	.030	.040	.110	
							1041.37	.190	.050	.065	.115	
							1667.61	.200	.270	.100	.120	
							1915.64	.210	.290	.120	.130	
							4271.39	.300	.350	.205	.150	

TABLE E-1 (continued)

SET	SPECIMEN NAME	SMIN, KSI	SRM, KSI	SRD/SRM	SRRMS, KSI	LOG.-AVG.	KILOCYCLES COUNT	CRACK LENGTH, IN. FOR LOCATIONS T1	T2	T3	T4	NOTES
(1)	(2)	(3)	(4)	(5)	(6)	(7)	(8)	(9)	(10)	(11)	(12)	(13)
							4510.77	.305	.365	.210	.150	
							5121.04	.335	.435	.235	.160	
							5323.45	.340	.465	.260	.165	
							5970.12	.375	.550	.275	.200	
							6759.86	3.500	3.500			FAILED AT T1-T2
16	CpS- 73A	40.00	10.00	.50	11.80	2460	34.12	.000	.000	.000	.000	
							488.19	.000	.235	.265	.165	
							597.26	.000	.285	.310	.235	
							1439.43	.285	.410	.560	.405	
							1525.37	.300	.410	.395	.440	
							1976.23	.335	.525	.900	.675	
							2036.29			3.500	3.500	FAILED AT T3-T4
	CpS- 54A						2.00	.000	.000	.240	.000	
							452.33	.115	.255	.340	.115	
							640.10	.125	.340	.355	.155	
							1084.40	.185	.445	.550	.190	
							1278.26	.195	.470	.595	.200	
							1725.65	.245	.670	.845	.300	
							1894.39	.275	.740	1.005	.335	
							1907.71	.300	.745	1.080	.345	
							2046.63	.310	.835	1.310	.365	
							2094.66			3.500	3.500	FAILED AT T3-T4
	CpS- 64A						5.00	.000	.000	.000	.000	
							479.56	.000	.225	.200	.000	
							573.03	.000	.225	.200	.000	
							1037.47	.000	.390	.225	.230	
							1217.43	.000	.415	.230	.235	
							1702.00	.180	.420	.240	.350	
							3501.79			3.500	3.500	FAILED AT T3-T4
17	CpS- 80A	40.00	30.00	0.00	30.00	234	5.00	.000	.000	.000	.000	
							10.00	.125	.000	.000	.125	
							58.56	.315	.000	.120	.295	
							215.94			3.500	3.500	FAILED AT T3-T4
	CpS- 17A						5.00	.000	.000	.000	.000	
							10.00	.000	.185	.000	.000	
							95.94	.330	.325	.190	.240	
							183.45	.400	.600	.350	.405	
							240.87	3.500	3.500			FAILED AT T1-T2
	CpS- 36A						10.00	.000	.000	.000	.000	
							20.00	.120	.000	.210	.000	
							101.85	.330	.400	.420	.290	
							247.63			3.500	3.500	FAILED AT T3-T4

18	CpS- 30A	40.00	30.00	.50	35.67	139	.50	.000	.000	.000	.000	
							1.00	.000	.300	.245	.055	
							2.00	.000	.320	.260	.055	
							3.00	.000	.320	.260	.055	
							6.00	.000	.320	.360	.130	
							20.00	.000	.320	.360	.130	
							55.15	.000	.360	.370	.140	
							109.18	3.500	3.500			Failed at T1-T2
	CpS- 88A						1.00	.000	.000	.000	.000	
							151.57	3.500	3.500			FAILED AT T1-T2
	CpS- 68A						90.50	.000	.000	.000	.000	
							161.69	3.500	3.500			FAILED AT T1-T2
19	CpS- 42A	0.00	30.00	1.00	41.34	103	5.00	.165	.000	.000	.175	Set used tape with 100 cycles
							20.00	.225	.500	.170	.230	and 100 load levels
							50.00	.350	.535	.455	.255	
							85.55	3.500	3.500			FAILED AT T1-T2
	CpS- 97A						5.00	.070	.050	.000	.185	
							14.05	.350	.350	.000	.185	
							40.00	.350	.445	.005	.270	
							88.84			3.500	3.500	FAILED AT T3-T4
	CpS- 87A						15.00	.285	.000	.000	.100	
							55.00	.340	.000	.000	.250	
							155.14	3.500	3.500			FAILED AT T1-T2
	CpS- 23A						5.00	.000	.000	.000	.000	
							10.00	.080	.000	.000	.075	
							60.24	.300	.325	.340	.240	
							96.53	3.500	3.500			FAILED AT T1-T2
	CpS-105A						2.00	.000	.000	.000	.000	
							5.00	.070	.000	.000	.090	
							45.00	.025	.350	.310	.340	
							100.47	3.500	3.500			FAILED AT T1-T2
	CpS-107A						40.00	.225	.000	.400	.225	
							75.00	.260	.225	.200	.260	
							103.47			3.500	3.500	Failed at T3-T4
20	CpS- 3A	0.00	30.00	1.00	41.34	103	10.00	.000	.000	.000	.000	Set used tape with 500
							50.00	.000	.215	.375	.150	cycles and 100 load levels
							99.30			3.500	3.500	Failed at T3-T4
	CpS- 67A						2.00	.000	.000	.000	.000	
							5.00	.000	.125	.225	.040	
							40.00	.000	.415	.395	.200	
							60.00	.000	.440	.405	.165	
							126.22	3.500	3.500			FAILED AT T1-T2
	CpS- 92A						5.00	.065	.200	.075	.135	
							15.00	.295	.365	.105	.120	
							45.00	.395	.415	.400	.285	
							110.65	3.500	3.500			FAILED AT T1-T2
	CpS-118A						1.50	.000	.000	.000	.000	
							4.82	.000	.155	.300	.050	
							11.85	.000	.280	.300	.110	
							16.86	.045	.335	.300	.190	
							32.00	.305	.375	.365	.255	
							57.61	.340	.405	.340	.320	
							84.30			3.500	3.500	Failed at T3-T4

TABLE E-1 (continued)

SET	SPECIMEN NAME	SMIN, KSI	SRM, KSI	SRD/SRM	SRRMS, KSI	LOG.-AVG.	KILOCYCLES COUNT	CRACK LENGTH, IN. FOR LOCATIONS T1	T2	T3	T4	NOTES
(1)	(2)	(3)	(4)	(5)	(6)	(7)	(8)	(9)	(10)	(11)	(12)	(13)
	CpS-106A						4.00	.000	.075	.100	.000	
							10.00	.000	.115	.185	.070	
							20.00	.000	.175	.260	.085	
							45.00	.035	.240	.325	.085	
							105.07			3.500	3.500	Failed at T3-T4
	CpS-108A						3.00	.000	.000	.000	.000	
							4.00	.000	.000	.000	.000	
							8.68	.175	.000	.000	.000	
							13.00	.175	.000	.000	.000	
							18.57	.255	.110	.305	.170	
							24.00	.260	.235	.315	.195	
							59.80	.275	.370	.360	.275	
							96.20			3.500	3.500	FAILED AT T3-T4
21	CpS-113A	0.00	30.00	1.00	41.34	99.9	5.00	.000	.000	.000	.000	Set used tape with 5000
							10.00	.000	.280	.000	.020	cycles and 100 load levels
							55.00	.125	.400	.250	.115	
							92.45			3.500	3.500	FAILED AT T3-T4
	CpS- 50A						5.00	.000	.000	.000	.000	
							65.00	.350	.465	.435	.000	
							81.40	3.500	3.500			FAILED AT T1-T2
	CpS- 72A						5.00	.150	.000	.325	.000	
							55.00	.265	.300	.455	.310	
							86.39	3.500	3.500			Failed at T1-T2
	CpS-112A						2.00	.000	.000	.000	.000	
							5.00	.135	.000	.135	.000	
							65.00	.325	.240	.145	.000	
							136.21	3.500	3.500			FAILED AT T1-T2
	CpS- 85A						5.00	.060	.000	.205	.000	
							102.46			3.500	3.500	FAILED AT T3-T4
	CpS- 63A						5.00	.055	.000	.060	.040	
							75.00	.255	.425	.095	.255	
							109.62	3.500	3.500			FAILED AT T1-T2
22	CpS-111A	0.00	30.00	1.00	41.34	103	5.00	.000	.000	.000	.000	Set used tape with 500
							98.47	.385	.580	.595	.175	cycles and 500 load levels
							109.49	3.500	3.500			FAILED AT T1-T2
	CpS- 61A						5.00	.000	.000	.000	.000	
							107.30			3.500	3.500	FAILED AT T3-T4
	CpS- 47A						2.50	.000	.000	.000	.000	
							102.12			3.500	3.500	FAILED AT T3-T4
	CpS- 32A						5.00	.000	.000	.000	.000	
							45.00	.300	.250	.145	.125	
							116.43			3.500	3.500	FAILED AT T3-T4
	CpS- 48A						5.00	.000	.000	.000	.000	
							50.00	.280	.400	.315	.285	
							80.58			3.500	3.500	FAILED AT T3-T4

	CpS- 38A						5.00	.000	.000	.000	.000	
							51.14	.325	.300	.350	.270	
							108.12			3.500	3.500	FAILED AT T3-T4
23	CpS- 24A	0.00	30.00	0.00	30.00	266	21.66	.000	.000	.000	.000	Set with superimposed vibrations S_{rv}/S_r = 0.1
							28.81	.000	.000	.000	.000	
							94.44	.090	.410	.290	.110	
							126.11	.190	.420	.305	.210	
							186.87	.250	.595	.335	.320	
							255.55	.380	.325	.660	.625	
							262.11	3.500	3.500			FAILED AT T1-T2
	CpS-120A						.53	.000	.000	.000	.000	
							1.71	.000	.000	.000	.000	
							66.13	.310	.419	.400	.220	
							93.65	.435	.490	.490	.345	
							189.39	.675	.700	.780	.540	
							212.82			3.500	3.500	FAILED AT T3-T4
	CpS- 83A						73.59	.000	.000	.000	.000	
							93.07	.000	.000	.000	.000	
							322.56	.095	.420	.300	.070	
							336.21			3.500	3.500	FAILED AT T3-T4
24	CpS- 9A	0.00	30.00	0.00	30.00	335	1.54	.000	.000	.000	.000	Set with superimposed vibrations S_{rv}/S_r = 0.2
							64.49	.190	.280	.105	.000	
							187.40	.530	.490	.365	.450	
							203.77	.570	.605	.395	.515	
							276.75			3.500	3.500	FAILED AT T3-T4
	CpS- 44A						16.34	.000	.000	.000	.000	
							83.69	.200	.060	.045	.730	
							144.69	.245	.060	.245	.100	
							229.67	.435	.260	.320	.190	
							303.51	.540	.340	.340	.205	
							400.29	.605	.800	.395	.280	
							455.84	3.500	3.500			FAILED AT T1-T2
	CpS- 39A						57.81	.135	.265	.255	.000	
							83.78	.235	.335	.390	.000	
							298.27	3.500	3.500			FAILED AT T1-T2
25	CpS- 90A	0.00	30.00	0.00	30.00	207	.01	.000	.000	.000	.000	Set with stress-relieved specimens
							204.35	.375	.355	.425	.000	
							301.85	3.500	3.500			FAILED AT T1-T2
	CpS- 40A						168.27			3.500	3.500	FAILED AT T3-T4
	CpS- 95A						211.05	.660	.260	.150	.315	
							213.12			3.500	3.500	FAILED AT T3-T4

Note: The locations T1, T2, T3, and T4 are shown in Figure B6.

TABLE E-2

A514-STEEL COVER-PLATE BEAMS

A514-STEEL COVER-PLATE BEAMS

SET	SPECIMEN NAME	SMIN, KSI	SRM, KSI	SRD/SRM	SRRMS, KSI	KILOCYCLES LOG.-AVG.	KILOCYCLES COUNT	CRACK DESCRIPTION: DISTANCE FROM SUPPORT, IN.	CRACK DESCRIPTION: TYPE	CRACK DESCRIPTION: TOP OR BOTTOM	CRACK SIZE IN: FLANGES IN.	CRACK SIZE IN: FLANGES IN.	CRACK SIZE IN: WEB IN.	NOTES
(1)	(2)	(3)	(4)	(5)	(6)	(7)	(8)	(9)	(10)	(11)	(12)	(13)	(14)	(15)
1	WBC-1440A	0.00	10.00	0.00	10.00		9976.6			T	.00	.00	.00	DISCONTINUED, NO CRACK
							9976.6	36.00	C	B	.00	1.25	.00	IN TENSION FLANGE
							9976.6	84.00	C	B	.00	.13	.00	
	WBC-1441A						11600.0			T	.00	.00	.00	DISCONTINUED, NO CRACK
							11600.0			B	.00	.00	.00	IN TENS. OR COMP. FLANGE
	WBC-1442A						2050.6	36.00	C	T	.00	.00	.00	
							2460.1		C		.25	.66	.00	UNDER COVER PLATE
							3195.0		C		.51	.66	.00	
							6337.2		C		.53	.74	.00	UNDER COVER PLATE
							10169.1		C		.82	1.90	.00	
							15130.9		L		6.75	6.75		FAILED THROUGH FLANGE
2	WBC-1449A	0.00	10.00	.50	11.89		81.0	36.00	C	T	.44	.48	.00	
							956.5		C		.62	.42	.00	
							1453.1		C		.62	.42	.00	
							2824.8		C		.62	.42	.00	
							11500.0		C		.62	.42		DISCONTINUED
	WBC-1450A						279.6	36.00	C	T	.67	.47	.00	
							973.2		C		.67	.47	.00	
							2144.8		C		.67	.47	.00	
							2922.1		C		.67	.47	.00	
							11500.0		C		.67	.47		DISCONTINUED
	WBC-1451A						71.8	36.00	C	T	.75	.52	.00	
							616.7		C		.75	.52	.00	
							2766.8		C		.75	.52	.00	
							4292.3		C		.75	.52	.00	
							11364.4		C		.75	.52		DISCONTINUED
3	WBC-1452A	0.00	10.00	1.00	13.78	2110	306.3	36.00	C	T	.41	.44	.00	
							487.8		C		.51	.44	.00	
							782.2		C		.99	.44	.00	
							978.4		C		1.26	.52	.00	
							1187.6		L		6.75	6.75		FAILED THROUGH FLANGE
	WBC-1453A						214.1	36.00	C	T	.27	.27	.00	BASE OF WELD
							576.3		C		.54	.40	.00	
							1271.9		C		1.04	.58	.00	
							1596.0		C		1.08	.61	.00	
							2280.1		L		6.75	6.75		FAILED THROUGH FLANGE

	WBC-1454A					252.7	36.00	C	T	.00	.00	.00	BASE OF WELD
						339.3		C		.44	.30	.00	BASE OF WELD
						1689.1		C		.51	.50	.00	
						2310.0		C		.58	.56	.00	
						3116.8		C		.65	.97	.00	
						3462.9		L		6.75	6.75		FAILED THROUGH FLANGE
4	WBC-1443A	0.00	20.00	0.00	20.00	900	30.0	36.00	C	T	.00	.00	.00	
							208.5		C		.15	.00	.00	
							536.2		C		1.09	.29	.00	
							852.0		C		1.38	.37	.00	
							915.2		C		1.46	.38	.00	
							1106.7		L		6.75	6.75		FAILED THROUGH FLANGE
	WBC-1444A						32.9	36.00	C	T	.33	.20	.00	BASE OF WELD
							819.5		C		.79	.67	.00	
							884.6		C		.87	.77	.00	
							949.0		L		6.75	6.75		FAILED THROUGH FLANGE
	WBC-1445A						73.6	36.00	C	T	.00	.00	.00	
							279.7		C		.56	.68	.00	
							331.7		C		.63	.82	.00	
							531.8		C		.72	1.12	.00	
							573.9		C		.77	1.21	.00	
							693.3		L		6.75	6.75		FAILED THROUGH FLANGE
5	WBC-1458A	0.00	20.00	.50	23.78	490	357.8	36.00	L	T	6.75	6.75		FAILED THROUGH FLANGE
	WBC-1459A						130.5	36.00	C	T	.48	.45	.00	UNDER COVER PLATE
							255.3		C		.76	.53	.00	BASE OF WELD
							308.6		C		.82	.63	.00	
							437.9		C		1.24	.65	.00	
							464.9		L		6.75	6.75		FAILED THROUGH FLANGE
	WBC-146 A						276.0	36.00	C	T	.58	.44	.00	
							350.9		C		.69	.54	.00	
							404.1		C		.75	.62	.00	
							528.9		C		.80	.67	.00	
							709.1		L		6.75	6.75		FAILED THROUGH FLANGE
6	WBC-1455A	0.00	20.00	1.00	27.56	198	127.9	36.00	C	T	.44	.38	.00	UNDER COVER PLATE
							151.6		C		.48	.48	.00	
							282.1		L		6.75	6.75		FAILED THROUGH FLANGE
	WBC-1456A						64.4	36.00	C	T	.20	.44	.00	ACROSS WELD
							90.0		C		.20	.44	.00	BASE METAL
							146.4		L		6.75	6.75		FAILED THROUGH FLANGE
	WBC-1457A						62.8	36.00	C	T	.65	.35	.00	ACROSS WELD
							80.4		C		.65	.35	.00	
							187.4		L		6.75	6.75		FAILED THROUGH FLANGE
7	WBC-1446A	0.00	30.00	0.00	30.00	122	44.3	36.00	C	T	.56	.61	.00	
							127.7		L		6.75	6.75		FAILED THROUGH FLANGE
	WBC-1447A						45.6	36.00	C	T	.45	.37	.00	
							133.8		L		6.75	6.75		FAILED THROUGH FLANGE
	WBC-1448A						106.2	36.00	L	T	6.75	6.75		FAILED THROUGH FLANGE

TABLE E-2 (continued)

SET	SPECIMEN NAME	SMIN, KSI	SRM, KSI	SRD/SRM	SRRMS, KSI	KILOCYCLES LOG.-AVG.	KILOCYCLES COUNT	CRACK DESCRIPTION: DISTANCE FROM SUPPORT, IN.	CRACK DESCRIPTION: TYPE	CRACK DESCRIPTION: TOP OR BOTTOM	CRACK SIZE IN: FLANGES IN.	CRACK SIZE IN: WEB IN.	NOTES
(1)	(2)	(3)	(4)	(5)	(6)	(7)	(8)	(9)	(10)	(11)	(12)	(13)	(14)	(15)
8	WBC-1467A	0.00	30.00	.50	35.67	173	7.0	36.00	C	T	.37	.36	.00	AT WELDS
							150.1		C		.42	.76	.00	UNDER COVER PLATE
							164.1		L		6.75	6.75		FAILED THROUGH FLANGE
	WBC-1468A						91.2	36.00	C	T	.63	.37	.00	UNDER COVER PLATE
							113.3		C		.63	.37	.00	
							178.2		L		6.75	6.75		FAILED THROUGH FLANGE
	WBC-1469A						36.2	36.00	C	T	.32	.48	.00	UNDER COVER PLATE
							134.2		C		.45	.67	.00	
							175.8		L		6.75	6.75		FAILED THROUGH FLANGE
9	XA	0.00	30.00	1.00	41.34									SET WAS NOT TESTED BECAUSE OF ANTICIPATED DELAMINATION
	XA													
	XA													
10	WBC-1401A	10.00	10.00	0.00	10.00		875.0	36.00	C	T	.00	.00	.00	
							1208.3	36.00	C	T	.87	.43	.00	
							1454.7	36.00	C	T	1.11	.45	.00	
							1808.1	36.00	C	T	1.31	.48	.00	
							2122.1	36.00	C	T	1.75	.63	.00	
							2306.2	36.00	L	T	6.75	6.75		FAILED
	WBC-1402A						875.0	36.00	C	T	.00	.00	.00	
							1209.3	36.00	C	T	.39	.41	.00	
							1693.1	36.00	C	T	.52	.51	.00	
							1918.4	36.00	C	T	.60	.59	.00	
							2326.3	36.00	C	T	.76	.70	.00	
							2808.8	36.00	L	T	6.75	6.75		FAILED
	WBC-1403A													DISCONTINUED, NO VISIBLE CRACK IN TENSION FLANGE. SMALL HAIR CRACK IN COMPRESSION FLANGE. SEE NOTE A.
11	WBC-1425A	10.00	10.00	.50	11.89	1770	28.5	36.00	C	T	.00	.00	.00	
							263.7		C		.00	.12	.00	BASE OF WELD
							948.1		C		.67	.38	.00	UNDER COVER PLATE
							1014.6		C		.89	.43	.00	
							1189.8		C		1.15	.49	.00	
							1257.5		C		1.21	.50	.00	
							1433.6		C		1.25	.53	.00	
							1557.2		L		6.75	6.75		FAILED THROUGH FLANGE

	WBC-1426A					23.5	36.00	C	T	.00	.00	.00		
						28.5		C		.00	.16	.00	BASE OF WELD	
						263.6		C		.00	.30	.00		
						948.2		C		.71	.84	.00		
						1014.6		C		.76	.98	.00		
						1192.8		C		.81	1.01	.00		
						1261.4		C		.85	1.06	.00		
						1437.5		C		1.02	1.40	.00		
						1501.8		C		1.26	1.67	.00		
						1650.8		L		6.75	6.75		FAILED THROUGH FLANGE	
	WBC-1427A					24.0	36.00	C	T	.00	.00	.00		
						209.1		C		.00	.15	.00	BASE OF WELD	
						264.1		C		.00	.17	.00		
						948.6		C		.63	.32	.00		
						1015.3		C		.65	.41	.00	UNDER COVER PLATE	
						1193.3		C		.75	.43	.00		
						1261.9		C		.80	.47	.00		
						1438.0		C		.85	.51	.00		
						1502.3		C		.87	.53	.00	UNDER COVER PLATE	
						1719.8		C		1.03	.57	.00		
						1825.9		C		1.13	.70	.00		
						2170.2		L		6.75	6.75		FAILED THROUGH FLANGE	
12	WBC-1413A	10.00	10.00	1.00	13.78	842	162.8	36.00	C	T	.25	.18	.00		
							202.1		C	T	.27	.39	.00		
							427.8		C	T	.47	.77	.00		
							603.0		C	T	.76	1.12	.00		
							658.2		C	T	.83	1.24	.00		
							731.5		L	T	6.75	6.75		FAILED	
	WBC-1414A						162.2	36.00	C	T	.53	.22	.00		
							201.4		C	T	.53	.25	.00		
							371.1		C	T	.74	.37	.00		
							657.6		C	T	1.27	.60	.00		
							843.9		L	T	6.75	6.75		FAILED	
	WBC-1415A						160.7	36.00	C	T	.35	.29	.00		
							200.0		C	T	.41	.39	.00		
							425.8		C	T	.65	.51	.00		
							656.2		C	T	.90	.65	.00	UNDER COVER PLATE	
							968.3		L	T	6.75	6.75		FAILED	
13	WBC-1404A	10.00	20.00	0.00	20.00	484	101.6	36.00	C	T	.00	.00	.00	SEE NOTE A.	
							174.1		C	T	.26	.00	.00	ACROSS WELD	
							289.4		C	T	.54	.75	.00		
							325.0	36.00	C	T	.67	.79	.00		
							398.6		C	T	.84	.93	.00		
							469.1	36.00	L	T	6.75	6.75		FAILED	
	WBC-1405A						101.6		C	T	.00	.14	.00		
							175.6		C	T	.49	.26	.00		
							290.8		C	T	.82	.39	.00		
							320.5		C	T	.94	.44	.00		
							400.1		C	T	1.10	.53	.00		
							525.4	36.00	L	T	6.75	6.75		FAILED	
	WBC-1406A						132.5		C	T	.00	.00	.00		
							159.5		C	T	.35	.38	.00		
							247.7		C	T	.45	.49	.00		
							283.3		C	T	.50	.50	.00		
							356.9		C	T	.61	.67	.00		
							454.3		L	T	6.75	6.75		FAILED	

TABLE E-2 (continued)

SET	SPECIMEN NAME	SMIN, KSI	SRM, KSI	SRD/SRM	SRRMS, KSI	KILOCYCLES LOG.-AVG.	KILOCYCLES COUNT	CRACK DESCRIPTION: DISTANCE FROM SUPPORT, IN.	CRACK DESCRIPTION: TYPE	CRACK DESCRIPTION: TOP OR BOTTOM	CRACK SIZE IN FLANGES IN.	CRACK SIZE IN FLANGES IN.	CRACK SIZE IN WEB IN.	NOTES
(1)	(2)	(3)	(4)	(5)	(6)	(7)	(8)	(9)	(10)	(11)	(12)	(13)	(14)	(15)
14	WBC-1422A	10.00	20.00	-.50	16.22	266	305.9	36.00	L	T	6.75	6.75	.00	FAILED THROUGH FLANGE
	WBC-1423A						280.8	36.00	L	T	6.75	6.75	.00	FAILED THROUGH FLANGE
	WBC-1424A						14.8	36.00	C	T	.30	.29	.00	BASE OF WELDS
							60.9		C		.46	.59	.00	UNDER COVER PLATE
							94.2		C		.60	.53	.00	
							219.3		L		6.75	6.75		FAILED THROUGH FLANGE
15	WBC-1415A	10.00	20.00	1.00	27.56	207	10.8	36.00	C	T	.00	.00	.00	
							21.4		C		.01	.22	.00	END OF WELDS
							234.5		L		6.75	6.75		FAILED THROUGH FLANGE
	WBC-1417A						5.0	36.00	C	T	.00	.00	.00	
							10.3		C		.26	.16	.00	ACROSS WELD
							20.7		C		.22	.30	.00	
							163.3		C		.31	.30	.00	UNDER WELD + COVER PLATE
							174.6		C		.53	.30	.00	
							209.9		L		6.75	6.75		FAILED THROUGH FLANGE
	WBC-1418A						5.2	36.00	C	T	.00	.00	.00	
							10.1		C		.00	.48	.00	
							36.3		C		.27	.39	.00	THROUGH WELD
							102.5		C		.44	.43	.00	
							125.0		C		.47	.69	.00	
							179.3		L		6.75	6.75		FAILED THROUGH FLANGE
16	WBC-1407A	10.00	30.00	0.00	30.00	109	16.6	36.00	C	T	.25	.33	.00	
							95.3		L	T	6.75	6.75		FAILED
	WBC-1408A						8.1	36.00	C	T	.25	.19	.00	
							99.2		L	T	6.75	6.75		FAILED
	WBC-1409A						16.9	36.00	C	T	.00	.00	.00	SEE NOTE A.
							138.1		L	T	6.75	6.75		FAILED
17	WBC-1419A	10.00	30.00	.50	35.67	104	91.5	36.00	L	T	6.75	6.75	.00	FAILED ACROSS FLANGE
	WBC-1420A						91.7	36.00	C	T	.62	.54	.00	UNDER COVER PLATE
							114.7		L		6.75	6.75		FAILED THROUGH FLANGE
	WBC-1421A						91.7	36.00	C	T	.69	.42	.00	WELD PEELING
							107.2		L		6.75	6.75		FAILED THROUGH FLANGE
18	WBC-1410A	10.00	30.00	1.00	41.34		38.3	36.00	P	T				DISCONTINUED ENTIRE SET,
	WBC-1411A						51.5	36.00	P	T				COVER PLATES DELAMINATED
	WBC-1412A						51.7	36.00	P	T				FOR ALL BEAMS IN SET
19	WBC-1464A	10.00	60.00	0.00	60.00		.9	36.00	L	T	.00	.00	.00	HAIRLINE CRACK AT WELD
							10.9		C		6.75	6.75		FAILED THROUGH FLANGE
	WBC-1465A						.9	36.00	P	T	.00	.00	.00	
							31.1		P		6.75	6.75		PEELING C.P., DISCONT.
	WBC-1466A						13.3	36.00	L	T	6.75	6.75		FAILED THROUGH FLANGE

20	WBC-14614	10.00	4.00	1.00	5.51		2144.3	36.00	C	T	.00	.00	.00	
							2253.0		C		.00	.63	.00	
							19813.3		C		.00	.63	.00	DISCONTINUED
	WBC-14624						1713.5	36.00	C	T	.00	.00	.00	
							1758.8		C		.37	.20	.00	
							5001.1		C		.58	.32	.00	
							10015.3		C		.69	.42	.00	
							14791.9		C		.72	.49	.00	
							21821.8		C		.88	.85	.00	DISCONTINUED
	WBC-14634						1868.2	36.00	C	T	.00	.00	.00	
							1960.0		C		.00	.47	.00	
							3978.9		C		.31	.69	.00	UNDER COVER PLATE
							5772.5		C		1.20	.85	.00	
							7447.8		C		1.71	1.15	.00	
							8439.9		L		6.75	6.75	.00	FAILED THROUGH FLANGE
21	WBC-14106C	15.00	3.00	1.00	4.13	20100	11350.4	36.00	L	T	.00		.00	HIGH-STRESS END OF
							11745.4		L		1.30		.00	COVER PLATE
							15021.2		L		1.68		.00	
							18901.0		L		3.53		.00	
							21657.8		L		6.75		12.00	FAILED THROUGH TOP FLANGE
	WBC-14107C						12073.7	36.00	L	T	.00		.00	
							12458.6		L		.57		.00	
							13697.0		L		.88		.00	
							15065.2		L		1.02		.00	
							18617.1		L		1.75		.00	
							21944.0		L		6.75		8.00	FAILED THROUGH TOP FLANGE
	WBC-14108C						11314.3	36.00	L	T	.00		.00	
							11709.6		L		1.82		.00	
							11883.5		L		2.46		.00	
							14985.2		L		3.93		.00	
							16986.4		L		6.75		11.00	FAILED THROUGH TOP FLANGE
	WBC-14106C	10.00	2.00	1.00	2.76		77528.0	36.00	L	T	.00		.00	LOW-STRESS END OF
							77669.4		L		.38		.00	COVER PLATE
							87883.3		L		.93		.00	FIRST HAIRLINE CRACKS
							94143.6		L		1.92		.00	OBSERVED AT 66 MILLION
							97183.7		L		2.40		.00	CYCLES
							102143.9		L		4.13		.38	
							103719.3		L		6.75		5.75	FAILED THROUGH TOP FL.
	WBC-14107C						56970.5	36.00	L	T	.00		.00	HAIRLINE CRACKS OBSERVED
							103719.9		L		.00		.00	DISCONTINUED
	WBC-14018C						31657.6	36.00	L	T	.00		.00	
							33598.8		L		1.75		.00	
							38191.5		L		2.30		.00	
							60224.3		L		6.75		12.00	FAILED THROUGH TOP FL.
22	WBC-14284	40.00	10.00	0.00	10.00	1480	333.2	36.00	C	T	.00	.20	.00	BASE OF WELD
							383.9		C		.20	.13	.00	
							350.9		C		.41	.38	.00	BASE OF WELD
							445.3		C		.49	.40	.00	
							685.4		C		.63	.54	.00	
							1363.8		L		6.75	6.75		FAILED THROUGH FLANGE

TABLE E-2 (continued)

SET	SPECIMEN NAME	SMIN, KSI	SRN, KSI	SRD/SRM	SRMS, KSI	KILOCYCLES LOG.- AVG.	KILOCYCLES COUNT	CRACK DESCRIPTION: DISTANCE FROM SUPPORT, IN.	TYPE	TOP OR BOTTOM	CRACK SIZE IN: FLANGES IN.	CRACK SIZE IN: FLANGES IN.	CRACK SIZE IN: WEB IN.	NOTES
(1)	(2)	(3)	(4)	(5)	(6)	(7)	(8)	(9)	(10)	(11)	(12)	(13)	(14)	(15)
	WBC-1429A						33.3	36.00	C	T	.15	.17	.00	BASE OF WELD
							345.9		C		.25	.26	.00	BASE OF WELD
							445.9		C		.30	.28	.00	BASE METAL
							685.6		C		.38	.36	.00	
							1584.3		L		6.75	6.75		FAILED THROUGH FLANGE
	WBC-1430A						33.7	36.00	C	T	.00	.00	.00	
							84.5		C		.00	.08	.00	BASE OF WELD
							287.2		C		.32	.20	.00	BASE OF WELD
							382.1		C		.33	.22	.00	
							716.2		C		.45	.36	.00	UNDER COVER PLATE
							1319.8		L		6.75	6.75		FAILED THROUGH FLANGE
23	WBC-1431A	40.00	10.00	.50	11.89	1040	221.6	36.00	C	T	.43	.36	.00	
							469.8		C		.63	.43	.00	
							558.1		C		.70	.54	.00	
							913.9		C		1.17	.87	.00	
							1125.2		L		6.75	6.75		FAILED THROUGH FLANGE
	WBC-1432A						221.2	36.00	C	T	.42	.00	.00	
							256.3		C		.43	.00	.00	
							557.6		C		.77	.00	.00	
							913.4		C		1.28	.00	.00	
							1026.2		L		6.75	6.75		FAILED THROUGH FLANGE
	WBC-1433A						222.6	36.00	C	T	.37	.27	.00	
							257.6		C		.37	.31	.00	
							558.8		C		.51	.43	.00	
							826.9		C		.80	.55	.00	UNDER COVER PLATE
							963.9		L		6.75	6.75		FAILED THROUGH FLANGE
24	WBC-1437A	40.00	30.00	0.00	30.00	57	40.6	36.00	C	T	.57	.55	.00	BASE METAL
							56.2		L		6.75	6.75		FAILED THROUGH FLANGE
	WBC-1438A						40.1	36.00	C	T	.00	.73	.00	ACROSS WELD
							54.8		L		6.75	6.75		FAILED THROUGH FLANGE
	WBC-1439A						40.2	36.00	C	T	.72	.50	.00	UNDER COVER PLATE
							59.2		L		6.75	6.75		FAILED THROUGH FLANGE
25	WBC-1434A	40.00	30.00	.50	35.67	46	23.9	36.00	C	T	.43	.64	.00	ACROSS WELD
							40.8		L		6.75	6.75		FAILED THROUGH FLANGE
	WBC-1435A						24.1	36.00	C	T	.51	.41	.00	UNDER COVER PLATE
							39.1		L		6.75	6.75		FAILED THROUGH FLANGE
	WBC-1436A						26.7	36.00	C	T	.45	.44	.00	ACROSS WELD
							61.2		C		.85	.73	.00	UNDER WELD
							62.3		L		6.75	6.75		FAILED THROUGH FLANGE

26	WBC-1470B	0.00	10.00	0.00	10.00	1860	55.7	36.00	C	T	.00	.00	.00	
							253.7		C		1.12	.00	.00	
							300.1		C		1.12	.48	.00	
							529.7		C		1.13	.63	.00	
							640.2		C		1.14	.77	.00	
							957.3		C		1.22	.92	.00	
							995.3		C		1.31	1.04	.00	
							1338.2		C		1.38	1.25	.00	
							1479.1		C		1.43	1.53	.00	
							2020.2		L		6.75	6.75		FAILED THROUGH FLANGE
	WBC-1471B						1019.7	36.00	C	T	.99	.57	.00	
							1146.6		C		1.02	.61	.00	
							1324.9		C		1.14	.68	.00	
							1371.9		C		1.20	.68	.00	
							1600.8		C		1.39	.83	.00	
							1711.3		C		1.56	.92	.00	
							1957.3		C		2.24	1.04	.00	
							2122.0		L		6.75	6.75		FAILED THROUGH FLANGE
	WBC-1472B						1063.1	36.00	C	T	1.21	.53	.00	UNDER COVER PLATE
							1123.5		C		1.34	.60	.00	
							1321.9		C		1.95	.63	.00	
							1440.5		C		2.33	.98	.00	
							1491.1		L		6.75	6.75		FAILED THROUGH FLANGE
27	WBC-1473B	0.00	10.00	1.00	13.78	928	208.1	36.00	C	T	.47	.33	.00	UNDER COVER PLATE
							469.9		C		.58	.40	.00	UNDER COVER PLATE
							740.1		C		.71	.50	.00	UNDER COVER PLATE
							992.1		C		1.04	.73	.00	UNDER COVER PLATE
							1078.6		L		6.75	6.75		FAILED THROUGH FLANGE
	WBC-1474B						204.1	36.00	C	T	.14	.40	.00	BASE OF WELD
							470.2		C		.66	.45	.00	UNDER COVER PLATE
							524.6		C		.71	.45	.00	
							740.4		C		1.15	.83	.00	
							855.8		L		6.75	6.75		FAILED THROUGH FLANGE
	WBC-1475B						66.2	36.00	C	T	.45	.40	.00	BASE OF WELD, UNDER
							148.9		C		.45	.40	.00	COVER PLATE
							298.5		C		.45	.42	.00	
							616.8		C		.45	.55	.00	UNDER COVER PLATE
							847.1		L		6.75	6.75		FAILED THROUGH FLANGE
28	WBC-1482C	10.00	10.00	0.00	10.00	1270	296.8	36.00	L	T	2.38		.00	
							392.4		L		3.84		.00	
							690.6		L		4.79		.00	
							834.7		L		5.00		.00	
							1128.1		L		6.75		12.20	FAILED THROUGH FLANGE
	WBC-1483C						87.3	36.00	L	T	.00		.00	
							385.4		L		2.73		.00	
							529.9		L		4.28		.00	
							824.5		L		4.95		.00	
							982.7		L		5.15		.00	
							1334.6		L		6.75		5.13	FAILED THROUGH FLANGE
	WBC-1484C						86.1	36.00	L	T	.00		.00	
							384.3		L		2.77		.00	
							528.8		L		4.33		.00	
							823.5		L		4.94		.00	
							980.3		L		5.02		.00	
							1370.1		L		6.75		8.75	FAILED THROUGH FLANGE

TABLE E-2 (continued)

SET	SPECIMEN NAME	SMIN, KSI	SRM, KSI	SRD/SRM	SRRMS, KSI	KILOCYCLES LOG.-AVG.	KILOCYCLES COUNT	CRACK DESCRIPTION: DISTANCE FROM SUPPORT, IN.	CRACK DESCRIPTION: TYPE	CRACK DESCRIPTION: TOP OR BOTTOM	CRACK SIZE IN: FLANGES IN.	CRACK SIZE IN: WEB IN.	NOTES
(1)	(2)	(3)	(4)	(5)	(6)	(7)	(8)	(9)	(10)	(11)	(12)	(13) (14)	(15)
29	WBC-1494C	10.00	10.00	.50	11.89	1170	919.1	36.00	L	T	1.68	.00	
							1030.8		L		4.45	.00	
							1301.5		L		5.26	.00	
							1431.2		L		6.75	7.25	FAILED
	WBC-1495C						919.4	36.00	L	T	5.52	.00	
							1004.8		L		6.75	.00	FAILED
	WBC-1496C						919.5	36.00	L	T	5.45	.00	
							1031.3		L		5.88	.00	
							1119.7		L		6.75	12.25	FAILED
30	WBC-14100C	10.00	10.00	1.00	13.78	469	67.6	36.00	L	T	.00	.00	
							285.0		L		3.56	.00	
							386.9		L		4.98	.00	
							555.3		L		6.75	3.00	FAILED
	WBC-14101C						67.2	36.00	L	T	.00	.00	
							279.6		L		5.16	.00	
							335.6		L		6.75	.00	FAILED
	WBC-14102C						67.0	36.00	L	T	.00	.00	
							279.4		L		4.62	.00	
							386.3		L		4.83	.00	
							554.6		L		6.75	3.50	FAILED
31	WBC-1485C	10.00	20.00	0.00	20.00	230	111.8	36.00	L	T	5.24	.00	THROUGH FILLET
							162.1		L		5.36	.00	
							248.4		L		6.75	3.00	FAILED
	WBC-1486C						112.1	36.00	L	T	4.98	.00	THROUGH FILLET
							162.4		L		5.25	.00	
							189.1		L		6.75	2.00	FAILED
	WBC-1487C						111.1	36.00	L	T	4.98	.00	THROUGH FILLET
							161.4		L		5.15	.00	
							257.4		L		6.75	11.00	FAILED
32	WBC-1497C	10.00	20.00	.50	23.78	167	23.7	36.00	L	T	1.08	.00	
							80.9		L		5.08	.00	
							132.6		L		6.75	6.50	FAILED
	WBC-1498C						17.3	36.00	L	T	.70	.00	
							79.7		L		4.97	.00	
							131.4		L		5.38	.00	
							171.3		L		6.75	4.50	FAILED
	WBC-1499C						16.4	36.00	L	T	3.25	.00	
							73.9		L		5.32	.00	
							125.7		L		5.52	.00	
							205.2		L		6.75	11.50	FAILED

33	WBC-1476C	10.00	20.00	1.00	27.56	103	16.2	36.00	L	T	3.47	.00	
							22.0		L		3.47	.00	
							186.2		L		6.75	4.18	FAILED THROUGH FLANGE
	WBC-1477C						27.2	36.00	L	T	.00	.00	
							73.4		L		6.75	6.75	FAILED THROUGH FLANGE
	WBC-1478C						26.3	36.00	L	T	.00	.00	
							80.0		L		6.75	11.90	FAILED THROUGH FLANGE
34	WBC-1488C	10.00	30.00	0.00	30.00	78	87.9	36.00	L	T	6.75		FAILED
	WBC-1489C						76.6	36.00	L	T	6.75		FAILED
							76.6		L	B	1.13		FAILED
	WBC-1490C						69.6	36.00	L	T	6.75	5.00	FAILED
							69.6		L	B	4.43		FAILED
35	WBC-1479C	10.00	30.00	.50	35.67	76	9.5	36.00	L	T	4.24	.00	
							29.5		L		5.25	.00	
							87.4		L		6.75	9.50	FAILED THROUGH FLANGE
	WBC-1480C						6.7	36.00	L	T	3.50	.00	
							72.7		L		5.51	.00	
							80.5		L		6.75	8.25	FAILED THROUGH FLANGE
	WBC-1481C						10.0	36.00	L	T	3.66	.00	
							28.8		L		4.40	.00	
							63.2		L		6.75	12.10	FAILED THROUGH FLANGE
36	WBC-1491C	0.00	10.00	0.00	10.00	1400	385.6	36.00	L	T	4.06	.00	
							947.8		L		6.75	8.00	FAILED
	WBC-1492C						99.5	36.00	L	T	.00	.00	
							779.9				3.09	.00	
							1377.8		L		5.58	.00	
							1550.1		L		5.71	.00	
							1819.8		L		6.75	9.50	FAILED
	WBC-1493C						384.9	36.00	L	T	2.95	.00	
							1406.0		L		6.75	10.75	FAILED
37	WBC-14103C	0.00	10.00	1.00	13.78	735	194.8	36.00	L	T	3.27	.00	
							284.5		L		3.99	.00	
							483.2		L		4.79	.00	
							578.7		L		5.09	.00	
							831.8		L		6.75	7.25	FAILED
							831.8		L	B	3.00	.00	FAILED
	WBC-14104C						193.8	36.00	L	T	1.57	.00	
							283.5		L		4.59	.00	
							482.3		L		5.12	.00	
							572.8		L		5.19	.00	
							729.1		L		6.75	13.75	FAILED
							709.6		L	B	6.75	.00	
							729.1		L		6.75	3.25	FAILED
	WBC-14105C						193.6		L	T	3.70	.00	
							283.3		L		4.81	.00	
							482.1		L		5.22	.00	
							572.5		L		5.54	.00	
							654.4		L		6.75	3.25	FAILED
							572.5		L	B	2.25	1.00	
							654.4		L		6.75	3.38	Failed

Note A: Discontinued because of equipment problems

TABLE E-3

A514-STEEL WELDED BEAMS

A514-STEEL WELDED BEAMS

SET	SPECIMEN NAME	SMIN, KSI	SRM, KSI	SRD/SRM	SRRMS, KSI	KILOCYCLES LOG.-AVG.	KILOCYCLES COUNT	CRACK DESCRIPTION: DISTANCE FROM SUPPORT, IN.	CRACK DESCRIPTION: TYPE	CRACK DESCRIPTION: TOP OR BOTTOM	CRACK SIZE IN: FLANGES IN.	CRACK SIZE IN: WEB IN.	NOTES
(1)	(2)	(3)	(4)	(5)	(6)	(7)	(8)	(9)	(10)	(11)	(12)	(13)	(14)	(15)
41	W8P-1413D	0.00	20.00	0.00	20.00	3540	2924.5	32.30		T	.00	.00	
							3376.9	32.30	L	T	6.75	7.25	FAILED
							3376.9	87.30	I	B	.38	.38	ADD. CRACK AFTER FAILURE
	W8P-1414D						3059.5	48.80		T	.00	.00	
							3212.1	48.80	I	T	.38	.38	
							3397.9	48.80	I	T	2.50	.63	
							3431.6	48.80	L	T	6.75	8.50	FAILED
							3431.6	41.10	I	T	1.38	.81	ADD. CRACK AFTER FAILURE
							3431.6	95.60	I	B	.38	.38	ADD. CRACK AFTER FAILURE
	W8P-1415D						3625.4	56.00		T	.00	.00	
							3829.1	56.00	L	T	6.75	10.50	FAILED
							3829.1	72.40	I	B	1.25	.75	ADD. CRACK AFTER FAILURE
42	W8P-1416D	0.00	20.00	.50	23.78	1220	1419.9	54.80		T	.00	.00	
							1542.4	54.80	L	T	6.75	1.88	FAILED NEAR TACK WELD
	W8P-1417D						814.6	51.40		T	.00	.00	
							878.3	51.40	L	T	6.75	12.00	FAILED AT TACK WELD
	W8P-1418D						1254.1	49.30		T	.00	.00	
							1341.1	49.30	L	T	6.75	9.50	FAILED AT TACK WELD
							1341.1	83.80	I	B	5.13	1.63	ADD. CRACK AFTER FAILURE
							1341.1	79.70	I	B	.88	.50	ADD. CRACK AFTER FAILURE
43	W8P-1401D	0.00	20.00	1.00	27.56	619	7253.8	48.00		T	.00	.00	
							8060.0	48.00	L	T	6.75	10.00	FAILED
	W8P-1402D						291.8	72.50		T	.00	.00	
							485.5	72.50	L	T	6.75		FAILED AT TACK WELD
							485.5	42.10	I	B	.50	.50	ADD. CRACK AFTER FAILURE
							485.5	43.20	I	B	.50	.50	ADD. CRACK AFTER FAILURE
	WPP-1403D						605.7	73.00	L	T	6.75	9.75	FAILED AT TACK WELD
44	W8P-1419D	0.00	30.00	0.00	30.00	579	91.6	49.00		T	.00	.00	
							384.3	49.00	L	T	6.75	4.13	FAILED AT TACK WELD
	W8P-1420D						787.6	59.00		T	.00	.00	
							860.8	59.00	I	T	1.25	.50	
							884.8	59.00	L	T	6.75	10.56	FAILED NEAR TACK WELD
	W8P-1421D						532.6	50.10		T	.00	.00	
							570.2	50.10	L	T	6.75	11.00	FAILED NEAR TACK WELD

45	W8P-1407D	0.00	30.00	.50	35.67	523	460.3	51.00		T	.00	.00
							472.2	51.00	L	T	6.75	10.50 FAILED IN TACK WELD
							472.2	43.60	I	B	2.50	1.00 ADD. CRACK AFTER FAILURE
							472.2	47.60	I	B	.94	.50 ADD. CRACK AFTER FAILURE
	W8P-1408D						593.1	48.10		T	.00	.00
							597.6	48.10	L	T	6.75	11.00 FAILED
							597.6	41.80	I	B	4.13	1.50 ADD. CRACK AFTER FAILURE
							597.6	46.30	I	B	1.94	1.06 ADD. CRACK AFTER FAILURE
							597.6	55.30	I	B	1.63	.88 ADD. CRACK AFTER FAILURE
							597.6	63.40	I	B	3.13	1.25 ADD. CRACK AFTER FAILURE
							597.6	68.60	I	B	3.38	1.38 ADD. CRACK AFTER FAILURE
							597.6	76.50	I	B	3.88	1.69 ADD. CRACK AFTER FAILURE
							597.6	83.20	I	B	2.75	1.00 ADD. CRACK AFTER FAILURE
							597.6	84.30	I	B	1.50	.50 ADD. CRACK AFTER FAILURE
							597.6	48.00	I	B	.38	.44 ADD. CRACK AFTER FAILURE
	W8P-1409D						4998.2	45.80		T	.00	.00
							5071.5	45.80	L	T	6.75	10.75 FAILED
							417.5	41.80	I	B	2.50	1.44 ADD. CRACK AFTER FAILURE
							417.5	48.00	I	B	2.88	1.56 ADD. CRACK AFTER FAILURE
							5071.5	62.40	I	B	.69	.25 ADD. CRACK AFTER FAILURE
							5071.5	64.00	I	B	.38	.38 ADD. CRACK AFTER FAILURE
							5071.5	66.50	I	T	2.63	1.00 ADD. CRACK AFTER FAILURE
46	W8P-1404D	0.00	30.00	1.00	41.34	325	270.9	59.80		T	.00	.00
							335.4	59.80	L	T	6.75	10.25 FAILED AT TACK WELD
							335.4	50.00	I	B	.69	.44 ADD. CRACK AFTER FAILURE
	W8P-1405D						228.6	77.50		T	.00	.00
							298.1	77.50	L	T	6.75	10.75 FAILED
							298.1	41.50	I	B	3.13	1.13 ADD. CRACK AFTER FAILURE
							298.1	49.10	I	B	1.88	1.00 ADD. CRACK AFTER FAILURE
							298.1	54.60	I	B	.32	.25 ADD. CRACK AFTER FAILURE
							298.1	65.80	I	B	.25	.38 ADD. CRACK AFTER FAILURE
							298.1	68.80	I	B	.32	.38 ADD. CRACK AFTER FAILURE
							298.1	78.60	I	B	.32	.31 ADD. CRACK AFTER FAILURE
							298.1	83.00	I	B	.32	.44 ADD. CRACK AFTER FAILURE
							298.1	81.00	I	B	.25	.44 ADD. CRACK AFTER FAILURE
							298.1	66.80	I	B	.32	.38 ADD. CRACK AFTER FAILURE
	W8P-1406D						322.6	76.50		T	.00	.00
							342.3	76.50	L	T	6.75	9.25 FAILED AT TACK WELD
							342.3	41.30	I	B	3.75	1.19 ADD. CRACK AFTER FAILURE
							342.3	49.00	I	B	2.88	1.31 ADD. CRACK AFTER FAILURE
							342.3	54.90	I	B	3.00	1.44 ADD. CRACK AFTER FAILURE
							342.3	58.80	I	B	2.63	1.25 ADD. CRACK AFTER FAILURE
							342.3	65.40	I	B	1.25	.63 ADD. CRACK AFTER FAILURE
							342.3	71.30	I	B	3.25	1.69 ADD. CRACK AFTER FAILURE
							342.3	83.10	I	B	3.25	1.25 ADD. CRACK AFTER FAILURE
							342.3	78.60	I	B	.32	.56 ADD. CRACK AFTER FAILURE

TABLE E-3 (continued)

SET	SPECIMEN NAME	SMIN, KSI	SRM, KSI	SRD/SRM	SRRMS, KSI	KILOCYCLES LOG.- AVG.	KILOCYCLES COUNT	CRACK DESCRIPTION: DISTANCE FROM SUPPORT, IN.	CRACK DESCRIPTION: TYPE	CRACK DESCRIPTION: TOP OR BOTTOM	CRACK SIZE IN: FLANGES IN.	CRACK SIZE IN: WEB IN.	NOTES
(1)	(2)	(3)	(4)	(5)	(6)	(7)	(8)	(9)	(10)	(11)	(12)	(13) (14)	(15)
47	WBP-1422D	0.00	40.00	0.00	40.00	338	412.8	79.90		T	.00	.00	
							432.7	79.90	L	T	6.75	10.56	FAILED
							432.7	58.50	I	T	3.88	.00	ADD. CRACK AFTER FAILURE
	WBP-1423D						174.0	47.00		T	.00	.00	
							298.5	47.00	L	T	6.75	8.38	FAILED
	WBP-1424D						255.3	60.60		T	.00	.00	
							299.5	60.60	L	T	6.75	9.75	FAILED
48	WBP-1410D	0.00	40.00	.50	47.56	288	151.2	80.10		T	.00	.00	
							260.0	80.10	L	T	6.75	10.25	FAILURE
							260.0	41.00	I	B	3.63	1.44	ADD. CRACK AFTER FAILURE
							260.0	42.40	I	B	1.25	.00	ADD. CRACK AFTER FAILURE
							260.0	53.40	I	B	2.13	1.06	ADD. CRACK AFTER FAILURE
							260.0	59.40	I	B	1.88	.88	ADD. CRACK AFTER FAILURE
							260.0	68.60	I	B	2.63	1.19	ADD. CRACK AFTER FAILURE
							260.0	71.90	I	B	2.13	1.25	ADD. CRACK AFTER FAILURE
							260.0	83.10	I	B	.75	.00	ADD. CRACK AFTER FAILURE
							260.0	84.10	I	B	2.38	1.13	ADD. CRACK AFTER FAILURE
							260.0	55.60	E	T	.75	.00	ADD. CRACK AFTER FAILURE
	WPB-1411D						254.3	42.10		T	.00	.00	
							306.3	42.10	L	T	6.75	10.25	FAILED NEAR TACK WELD
							306.3	40.90	I	B	3.00	1.56	ADD. CRACK AFTER FAILURE
							306.3	50.80	I	B	2.38	1.13	ADD. CRACK AFTER FAILURE
							306.3	53.10	I	B	2.38	1.13	ADD. CRACK AFTER FAILURE
							306.3	57.90	I	B	2.50	1.25	ADD. CRACK AFTER FAILURE
							306.3	64.10	I	B	3.38	1.25	ADD. CRACK AFTER FAILURE
							306.3	69.10	I	B	2.56	1.13	ADD. CRACK AFTER FAILURE
							306.3	72.90	I	B	2.63	1.19	ADD. CRACK AFTER FAILURE
							306.3	75.20	I	B	2.00	1.00	ADD. CRACK AFTER FAILURE
							306.3	77.40	I	B	2.50	1.13	ADD. CRACK AFTER FAILURE
							306.3	85.30	I	B	3.56	1.38	ADD. CRACK AFTER FAILURE
							306.3	60.20	I	B	.38	.38	ADD. CRACK AFTER FAILURE

							306.3	89.50	I	B	.19	.19 ADD. CRACK AFTER FAILURE
							306.3	90.00	I	B	.38	.38 ADD. CRACK AFTER FAILURE
							306.3	90.60	I	B	.38	.38 ADD. CRACK AFTER FAILURE
							306.3	91.10	I	B	.38	.38 ADD. CRACK AFTER FAILURE
	WBP-1412						221.3	55.40		T	.00	.00
							298.6	55.40	L	T	6.75	9.75 FAILED
							298.6	43.40	I	B	6.25	.25 ADD. CRACK AFTER FAILURE
							298.6	51.80	I	B	1.81	.25 ADD. CRACK AFTER FAILURE
							298.6	52.00	I	B	.75	1.13 ADD. CRACK AFTER FAILURE
							298.6	56.00	I	B	.38	.13 ADD. CRACK AFTER FAILURE
							298.6	56.90	I	B	.63	.38 ADD. CRACK AFTER FAILURE
							298.6	61.40	I	B	2.44	1.19 ADD. CRACK AFTER FAILURE
							298.6	68.60	I	B	1.88	1.00 ADD. CRACK AFTER FAILURE
							298.6	78.10	I	B	.50	.44 ADD. CRACK AFTER FAILURE
							298.6	82.50	I	B	.88	.38 ADD. CRACK AFTER FAILURE
49		XD	0.00	40.00	.50	47.56						.00 SET CANNOT BE TESTED
		XD										.00 BECAUSE OF YIELDING
		XD										.00
50		XD	0.00	80.00	0.00	80.00						.00 SET
		XD										.00 NOT
		XD										.00 TESTED
51	WBP-1425D		0.00	10.00	1.00	13.78	7170	6037.1	78.60		T	.00 .00
								6113.2	78.60	I	T	.50 .50
								6383.4	78.60	L	T	6.75 3.63 FAILED
								6383.4	77.50	I	T	.38 .38 ADD. CRACK AFTER FAILURE
								6383.4	73.60	I	T	.63 .38 ADD. CRACK AFTER FAILURE
								6383.4	47.80	I	T	.38 .38 ADD. CRACK AFTER FAILURE
								6383.4	83.80	I	B	2.25 1.38 ADD. CRACK AFTER FAILURE
	WBP-1426D							5405.2	53.90		T	.00 .00
								5481.6	53.90	I	T	3.75 .75
								5634.9	53.90	I	T	4.75 1.31
								5680.1	53.90	I	T	5.38 1.88
								5700.7	53.90	I	T	5.38 1.88
								5723.6	53.90	L	T	6.75 5.00 FAILED
								5723.6	84.30	L	B	6.75 4.75 ADD. CRACK AFTER FAILURE
	WBP-1427D							9563.7	65.50		T	.00 .00
								10086.2	65.50	L	T	6.75 4.13 FAILED AT TACK WELD
								10086.2	72.80	L	B	6.75 9.00 ADD. CRACK AFTER FAILURE

TABLE E-4

A36-STEEL COVER-PLATE BEAMS

A36-STEEL COVER-PLATE BEAMS

SET	SPECIMEN NAME	SMIN, KSI	SRM, KSI	SRD/SRM	SRRMS, KSI	KILOCYCLES LOG.- AVG.	KILOCYCLES COUNT	CRACK DESCRIPTION: DISTANCE FROM SUPPORT, IN.	TYPE	TOP OR BOTTOM	CRACK SIZE IN FLANGES IN.	CRACK SIZE IN WEB IN.	NOTES
(1)	(2)	(3)	(4)	(5)	(6)	(7)	(8)	(9)	(10)	(11)	(12) (13)	(14)	(15)
101	WBC-3619C	0.00	10.00	0.00	10.00	1600	716.2	36.00	L	T	.00	.00	
							1122.0		L		.00	.00	
							1122.0		L	B	6.75	3.00	FAILED
	WBC-3620C						1386.2	36.00	L	T	.00	.00	
							1386.2		L	B	6.75	3.50	FAILED
	WBC-3621C						2644.0	36.00	L	T	.00	.00	
							2644.0		L	B	6.75	6.00	FAILED
102	WBC-3628C	0.00	10.00	.25	10.94	826	59.9	36.00	L	T	.00	.00	
							234.1		L	T	.74	.00	
							491.4		L	T	2.23	.00	
							568.4		L	T	2.76	.00	
							885.6		L	T	6.75	4.75	FAILED
	WBC-3629C						50.1	36.00	L	T	.00	.00	
							224.3		L	T	.52	.00	
							481.5		L	T	1.93	.00	
							559.3		L	T	2.13	.00	
							904.5		L	T	6.75	5.50	FAILED
	WBC-3630C						49.9	36.00	L	T	.00	.00	
							224.0		L		1.15	.00	
							481.3		L		3.93	.00	
							728.2		L		6.75	4.81	FAILED
103	WBC-3634C	0.00	10.00	.50	11.89	614	175.7	36.00	L	T	.00	.00	
							403.6		L		3.41	.00	
							634.4		L		6.75	4.25	FAILED
	WBC-3635C						175.3	36.00	L	T	.00	.00	
							403.2		L		2.28	.00	
							570.4		L		6.75	3.50	FAILED
	WBC-3636C						123.0	36.00	L	T	.00	.00	
							400.8		L		1.89	.00	
							639.5		L		6.75	4.75	FAILED
104	WBC-3622C	0.00	20.00	0.00	20.00	154	155.8	36.00	L	T	6.75		FAILED
	WBC-3623C						150.8	36.00	L	T	6.75		FAILED
	WBC-3624C						150.1	36.00	L	T	6.75		FAILED

105	WBC-3631C	0.00	20.00	.25	21.89	129	76.5	36.00	L	T	2.03		.00	
							126.9		L		6.75		3.63	FAILED
	WBC-3632C						74.4	36.00	L	T	1.00		.00	
							126.7		L		4.54		.00	
							141.2		L		6.75		3.25	FAILED
	WBC-3633C						74.8	36.00	L	T	3.15		.00	
							120.2		L		6.75		2.75	FAILED
106	WBC-3646C	0.00	20.00	.50	23.78	100	13.9	36.00	L	T	.00		.00	
							24.1		L		3.18		.00	CRACK THROUGH FILLET
							28.8		L		3.41		.00	
							71.5		L		6.75		.25	FAILED
	WBC-3647C						14.1	36.00	L	T	.00		.00	
							24.2		L		1.95		.00	CRACK THROUGH FILLET
							28.9		L		3.33		.00	
							141.1		L		6.75		.25	FAILED
	WBC-3648C						28.6	36.00	L	T	.00		.00	
							100.2				6.75		.25	FAILED
107	WBC-3604A	10.00	10.00	0.00	10.00	1990	437.4	36.00	C	T	.00	.00	.00	
							498.9		C		.23	.00	.00	
							1011.9		C		.25	.09	.00	
							1286.2		C		1.11	.18	.00	
							1574.3		C		1.28	.53	.00	
							1690.9		C		1.72	1.27	.00	
							1833.6		L		6.75	6.75		FAILED
	WBC-3605A						272.3	36.00	C	T	.00	.00	.00	
							505.7		C		.46	.28	.00	
							1570.6		C		.49	.68	.00	
							2054.9		C		1.90	1.07	.00	
							2168.4		L		6.75	6.75		FAILED
	WBC-3606A						272.2	36.00	C	T	.00	.00	.00	AT TIP OF WELD
							505.7		C		.34	.30	.00	
							1492.5		C		.47	.64	.00	
							1761.8		C		.72	.67	.00	
							1989.9		L		6.75	6.75		FAILED
108	WBC-3607A	10.00	10.00	.25	10.94	1780	56.8	36.00	C	T	.00	.00	.00	
							849.1		C		.56	.42	.00	
							1101.1		C		.86	.50	.00	
							1361.2		C		1.33	.63	.00	
							1496.2		L		6.75	6.75	.00	
							1555.0		L		6.75	6.75		FAILED
	WBC-3608A						61.0	36.00	C	T	.00	.00	.00	
							803.3		C		.39	.30	.00	
							1174.0		C		.51	.40	.00	
							1500.0		C		.87	.58	.00	
							1759.0		C		1.78	.74	.00	
							1960.0		L		6.75	6.75		FAILED

TABLE E-4 (continued)

SET	SPECIMEN NAME	SMIN, KSI	SRM, KSI	SRD/SRM	SRRMS, KSI	KILOCYCLES LOG.-AVG.	KILOCYCLES COUNT	CRACK DESCRIPTION: DISTANCE FROM SUPPORT, IN.	CRACK DESCRIPTION: TYPE	CRACK DESCRIPTION: TOP OR BOTTOM	CRACK SIZE IN: FLANGES IN.	CRACK SIZE IN: FLANGES IN.	CRACK SIZE IN: WEB IN.	NOTES
(1)	(2)	(3)	(4)	(5)	(6)	(7)	(8)	(9)	(10)	(11)	(12)	(13)	(14)	(15)
	WBC-3609A						56.4	36.00	C	T	.00	.00	.00	
							723.7		C		.42	.22	.00	
							1044.4		C		.54	.32	.00	
							1370.4		C		.87	.47	.00	
							1851.7		L		6.75	6.75		FAILED
109	WBC-3601A	10.00	10.00	.50	11.89	1040	42.8	36.00	C	T	.00	.00	.00	
							106.6		C		.21	.26	.00	
							811.9		C		.60	.51	.00	
							896.7		C		.67	.57	.00	
							1202.0		L		6.75	6.75		FAILED
	WBC-3602A						40.5	36.00	C	T	.00	.00	.00	
							104.3		C		.00	.03	.00	
							809.0		C		.79	.75	.00	
							894.0		C		.92	.98	.00	
							1107.2		L		6.75	6.75		FAILED
	WBC-3603A						104.2	36.00	C	T	.00	.00	.00	
							804.7		C		3.22	.86	.00	FLANGE CRACKING UNDER CP
							848.7		L		6.75	6.75		FAILED
110	WBC-3613A	10.00	20.00	0.00	20.00	205	190.2	36.00	C	T	6.75	6.75		FAILED
	WBC-3614A						220.1	36.00	C	T	6.75	6.75		FAILED
	WBC-3615A						206.2	36.00	C	T	6.75	6.75		FAILED
111	WBC-3610A	10.00	20.00	.25	21.89	163	16.9	36.00	C	T	.42	.09	.00	
							32.7		C		.45	.43	.00	
							130.0		C		.72	.80	.00	
							177.2		L		6.75	6.75		FAILED
	WBC-3611A						18.0	36.00	C	T	.06	.19	.00	
							33.8		C		.19	.23	.00	
							131.1		C		.84	.47	.00	
							154.9		L		6.75	6.75		FAILED
	WBC-3612A						17.9	36.00	C	T	.21	.19	.00	
							33.2		C		.28	.27	.00	
							131.0		C		.97	.90	.00	
							156.8		L		6.75	6.75		FAILED
112	XA	10.00	20.00	.50	23.78									SET CAN NOT BE TESTED BECAUSE OF YIELDING
	XA													
	XA													

113	WBC-3637C	0.00	40.00	0.00	40.00	16	3.8	36.00	L	T	.00	.00	
							16.4		L		6.75	2.00	FAILED
	WBC-3638C						2.4	36.00	L	T	.00	.00	
							17.4		L		6.75	1.50	FAILED
	WBC-3639C						2.2	36.00	L	T	.00	.00	
							15.2		L		6.75	1.63	FAILED
114	WBC-3643C	0.00	5.00	.50	5.94	5970	9453.4	36.00	L	B	6.75	8.75	FAILED
	WBC-3644C						1570.5	36.00	L	T	.00	.00	
							1877.4		L		2.43	.00	
							2654.3		L		3.03	.00	
							3170.1		L		4.03	.00	
							3790.5		L		5.40	.00	
							3924.2		L		6.75	5.75	FAILED
	WBC-3645C						1568.8	36.00	L	T	.00	.00	
							2651.5		L		1.10	.00	
							3560.0		L		2.19	.00	
							4598.3		L		3.11	.00	
							5723.9		L		6.75	4.25	FAILED
115	WBC-3616A	0.00	10.00	0.00	10.00		229.4	36.00	C	T	.35	.23	.00	
							511.9		C		.42	.36	.00	
							951.8		C		.51	.40	.00	
							1873.2		L		6.75	6.75		FAILED
	WBC-3617A						229.3	36.00	C	T	.00	.00	.00	
							294.5		C		.33	.00	.00	
							3758.4		C		.33	.00	.00	
							4029.0		C		.33	.15	.00	
							4814.0		C		.33	.18	.00	
							6662.6		C		.33	.18		DISCONTINUED
	WBC-3618A						223.8	36.00	C	T	.29	.39	.00	
							1254.2		C		1.38	.95	.00	
							1338.6		C		1.48	.95	.00	
							1380.9		L		6.75	6.75		Failed
116	WBC-3625C	10.00	10.00	0.00	10.00	973	254.7	36.00	L	T	.00	.00		
							1087.6		L	T	6.75			FAILED
	WBC-3626C						254.6	36.00	L	T	.00	.00		
							999.6		L	T	6.75			FAILED
	WBC-3627C						254.6	36.00	L	T	.00	.00		
							846.1		L	T	6.75			FAILED
117	WBC-3640C	10.00	10.00	.50	11.89	533	485.7	36.00	L	T	5.10	.00		
							580.3		L		6.75	2.50		FAILED
	WBC-3641C						485.0	36.00	L	T	5.16	.00		
							511.4		L		6.75	2.00		FAILED
	WBC-3642C						484.7	36.00	L	T	5.12	.00		
							506.4		L		6.75	2.13		FAILED

TABLE E-5

A36-STEEL WELDED BEAMS

A36-STEEL WELDED BEAMS

SET	SPECIMEN NAME	SMIN, KSI	SRM, KSI	SRD/SRM	SRRMS, KSI	KILOCYCLES LOG.-AVG.	KILOCYCLES COUNT	CRACK DESCRIPTION: DISTANCE FROM SUPPORT, IN.	CRACK DESCRIPTION: TYPE	CRACK DESCRIPTION: TOP OR BOTTOM	CRACK SIZE IN FLANGES IN.	CRACK SIZE IN WEB IN.	NOTES
(1)	(2)	(3)	(4)	(5)	(6)	(7)	(8)	(9)	(10)	(11)	(12)	(13) (14)	(15)
121	W8P-3604D	-10.00	20.00	0.00	20.00	2660	4699.5			T	.00	.00	
							4699.5	39.00	L	B	6.75	8.25	FAILED NEAR LOAD POINT
	W8P-3605D						2978.3			T	.00	.00	
							2978.3	42.25	L	B	6.75	11.25	FAILED NEAR LOAD POINT
	W8P-3606D						1345.5	46.75	L	T	6.75	6.25	FAILED NEAR LOAD POINT
122	W8P-3610D	0.00	20.00	.25	21.89	2830	2518.6			T	.00	.00	
							2944.2		L		6.75	4.00	FAILED NEAR BEAM CENTER
	W8P-3611D						1555.6			T	.00	.00	
							1605.3		I		.38	.38	
							1701.5		L		6.75	5.50	FAILED NEAR BEAM CENTER
	W8P-3612D						4539.8			T	.00	.00	
							4539.8	36.5	L	B	6.75	12.50	FAILED NEAR LOAD POINT
123	W8P-3616D	-10.00	20.00	.50	23.78	1580	1468.8			T	.00	.00	
							1468.8	41.5	L	B	6.75	10.75	FAILED NEAR LOAD POINT
	W8P-3617D						1391.2			T	.00	.00	
							1750.3		I		4.75	1.50	
							1750.7		L		6.75	4.75	FAILED NEAR BEAM CENTER
	W8P-3618D						1465.2			T	.00	.00	
							1521.3		L		6.75	5.00	FAILED NEAR BEAM CENTER
124	W8P-3619D	-10.00	30.00	0.00	30.00	989	922.6			T	.00	.00	
							922.9		I		.25	.75	
							928.5		I		2.00	1.00	
							936.6		I		3.50	1.50	
							938.3		L		6.75	5.00	FAILED NEAR BEAM CENTER
	W8P-3620D						963.2			T	.00	.00	
							963.2	40.75	L	B	6.75	6.75	FAILED NEAR LOAD POINT
	W8P-3621D						1063.8			T	.00	.00	
							1072.0		L		6.75	6.50	FAILED NEAR BEAM CENTER
125	W8P-3622D	-10.00	30.00	.25	32.83	676	517.5			T	.00	.00	
							555.8		L		6.75	5.25	FAILED NEAR LOAD POINT
	W8P-3623D						784.1			T	.00	.00	Failed in center region
							784.1	50.00	L	B	6.75	10.00	
	W8P-3624D						674.0			T	.00	.00	
							707.9		L		6.75	3.75	FAILED NEAR LOAD POINT
126	XD	-10.00	30.00	.50	35.67								SET CANNOT BE TESTED BECAUSE OF YIELDING
	XD												
	XD												

127	WBP-3607D	0.00	20.00	0.00	20.00	4290	4486.1			T	.00	.00	
							4549.3	57.0	L	T	6.75	3.25	FAILED AT BEAM CENTER
	WBP-3608D						2371.0			T	.00	.00	
							2371.0	41.5	L	B	6.75	3.56	FAILED NEAR LOAD POINT
	WBP-3609D						7173.0			T	.00	.00	
							7257.6		I		.50	.38	
							7337.1		L		6.75	3.38	FAILED NEAR BEAM CENTER
128	WBP-3613D	0.00	20.00	.25	21.89	2630	1718.5			T	.00	.00	
							2144.5		I		3.65	1.60	
							1146.9		I		4.90	1.80	
							2147.6		I		6.10	3.30	
							2148.0		L		6.75	3.80	FAILED NEAR BEAM CENTER
	WBP-3614D						2562.5			T	.00	.00	
							2634.7		L		6.75	2.20	Additional Crack
							3939.7			B	.00	.00	
							3905.3		L		6.75	3.50	
							3939.7		L		6.75	6.75	FAILED NEAR BEAM CENTER
	WBP-3615D						1957.0			T	.00	.00	
							2137.8		I		5.75	1.10	
							2138.8		L		6.75	4.50	FAILED NEAR LOAD POINT
129	WBP-3625D	0.00	20.00	.50	23.78	1800	1007.2			T	.00	.00	
							1055.8		I		6.75	3.75	FAILED NEAR LOAD POINT
	WBP-3626D						2678.6			T	.00	.00	
							2728.4		E		3.00	.00	
							2731.4		E		6.75	4.63	FAILED NEAR BEAM CENTER
	WBP-3627D						1585.1		I	T	.00	.00	
							2023.5	42.25	L		6.75	4.13	FAILED NEAR TIEDOWNS
							2023.5	54.50	I	T	2.50	1.00	ADD. CRACK AFTER FAILURE
130	WBP-3628D	0.00	30.00	0.00	30.00	1000	733.0			T	.00	.00	
							952.9		L		6.75	8.00	FAILED NEAR BEAM CENTER
							952.9	29.50	I	T	3.00	.00	ADD. CRACK AFTER FAILURE
	WBP-3629D						906.4			T	.00	.00	
							1007.2		L		6.75	4.00	FAILED NEAR LOAD POINT
	WBP-3630D						1016.0			T	.00	.00	
							1043.7		L		6.75	6.75	FAILED NEAR LOAD POINT
131	WBP-3631D	0.00	26.70	.25	29.22	1010	1044.3			T	.00	.00	
							1064.9		E		3.25	.25	
							1066.7		L		6.75	3.25	FAILED NEAR BEAM CENTER
	WBP-3632D						1100.0			T	.00	.00	DISCONTINUED BECAUSE SYSTEM MALFUNCTIONED
	WBP-3633D						907.9			T	.00	.00	
							963.8		L		6.75	3.75	FAILED NEAR BEAM CENTER
132	XD	0.00	30.00	.50	35.6								SET CANNOT BE TESTED BECAUSE OF YIELDING
	XD												
	XD												
133	WBP-3634D-1	0.00	50.00	0.00	50.00	175	144.5			T	.00	.00	
							196.4		L		6.75	4.00	FAILED NEAR LOAD POINT
	WBP-3635D						125.4		L	T	6.75	4.00	FAILED NEAR BEAM CENTER
	WBP-3636D						121.2			T	.00	.00	
							216.8		L		6.75	3.75	FAILED NEAR BEAM CENTER

Conversion Factors: 1 ksi = 6.895 MPa, 1 in. = 25.4 mm

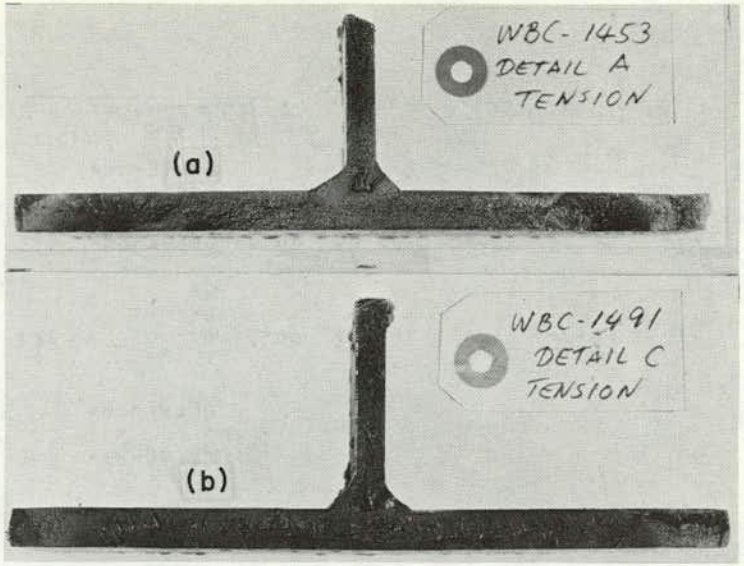

Figure E-1. Typical crack types: (a) crescent crack, designation type C; (b) long crack, designation type L.

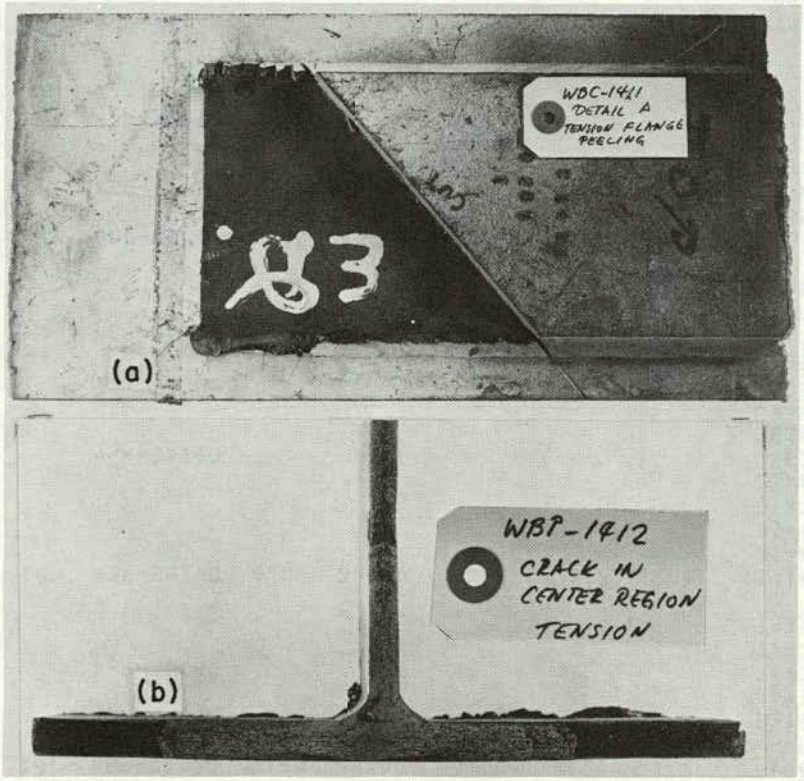

Figure E-2. Typical crack types. (a) peeling cover-plate crack, designation type P; (b) intersecting flange-web crack, designation type I.

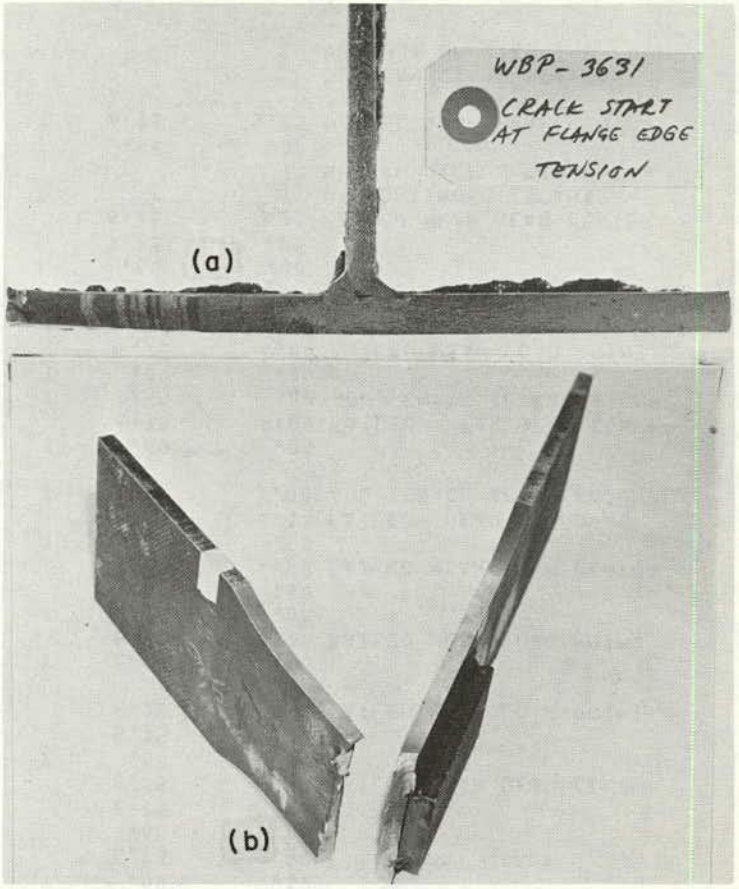

Figure E-3. Typical crack types: (a) edge crack, designation type E; (b) cover-plate crack, designation type C.

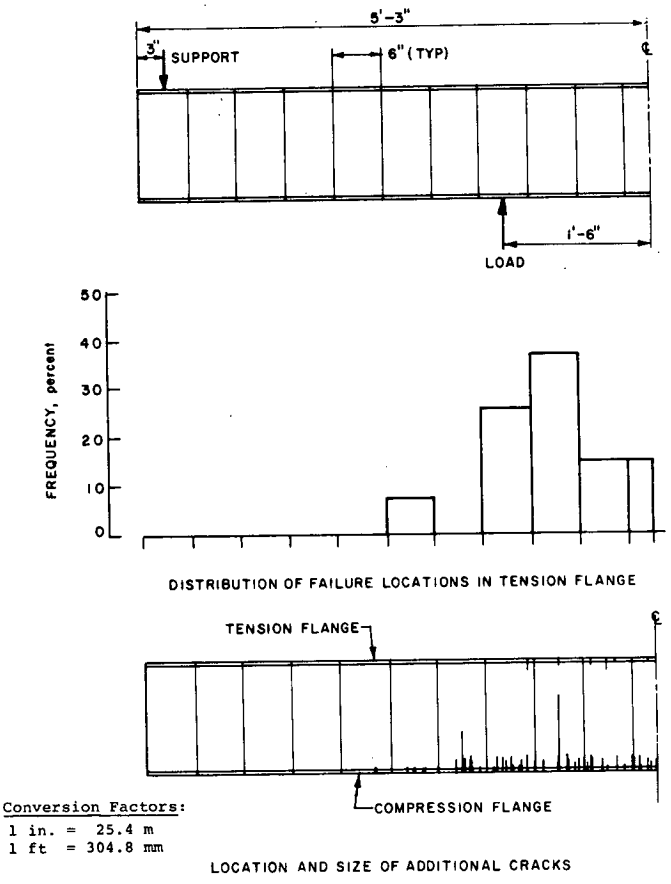

Figure E-4. Distribution of cracks in welded A514 steel beams.

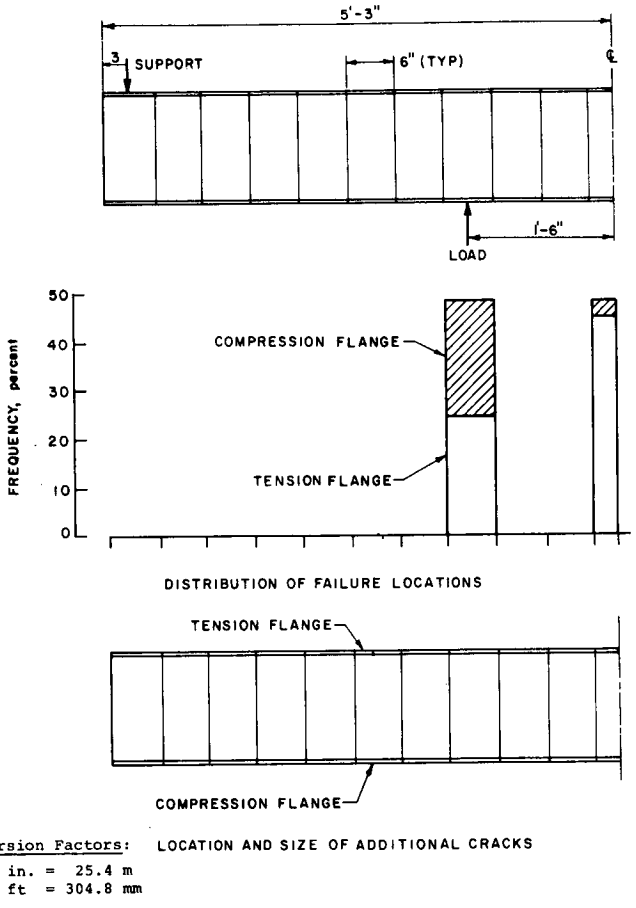

Figure E-5. Distribution of cracks in welded A36 steel beams.

(3) Minimum static stress, ksi.
(4) Modal stress range, ksi.
(5) Dispersion ratio, measure of dispersion for stress spectrum.
(6) Stress range in terms of RMS, ksi.
(7) Log-average count for set.
(8) Number of cycles associated with the recorded information on the same line.
(9) Crack distance from the support, in.
(10) Crack type:

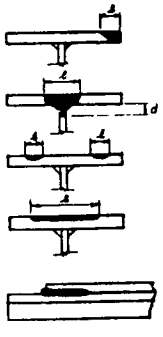

E for crack located at the Edge of a flange

I for crack at the Intersection of web and flange

C for Cresent-type crack

L for Long crack

P for Peeling flange plate

(11) Crack location: T for top flange (tension); B for bottom flange (compression).
(12) Crack length for crack in flange, L, in.
(13) Crack length for a second crack at the same distance from the support as for the crack recorded under (10); applicable to cresent-type cracks only, in.
(14) Crack depth for crack in web, d, in.
(15) Description of beam condition or crack location.

FRETTING FAILURES

The first of a set of three welded beams that were tested failed prematurely ($N = 1{,}093{,}625$) at the edge of a load-point bearing plate as a result of fretting fatigue. These beams were of A36 steel and were tested at $S_{rm} = 20$ ksi (138 MPa), $S_{\min} = -10$ ksi (−69 MPa), and $S_{rd}/S_{rm} = 0$. In an attempt to eliminate this problem, the test on the second beam was continued after a brass shim was placed between the bearing plates and the beam flanges, and the test on the third beam was temporarily discontinued. The second beam also failed by fretting at a bearing-plate edge ($N = 2{,}199{,}950$), and the brass shims showed evidence of much wear.

Before the test on the third beam was continued, the surface of the beam flange under the four load-point bearing plates (two on the top flange and two on the bottom flange) was ground to remove mill scale and flange material that might have contained microcracks as a result of fretting during prior cycles. Four different materials were placed between the bearing plates and flanges: (1) a ⅛-in.

rubber pad, (2) a 0.1-in. paper pad, (3) a ¼-in. plywood pad with lubricant, and (4) a ¼-in. plywood pad without lubricant. The edges of the bearing plates were ground to a gentle contour. The test was then continued and a fretting failure occurred at 2,996,680 cycles. An examination of the pads, however, suggested that the plywood or paper pads would prevent fretting failures in a virgin beam.

Since all of the beams in the first set failed by fretting, a duplicate set (set 121) was tested under the same stress spectrum; extra beams of this type and material were available. One beam was tested before testing of the other two beams was started. Plywood without lubrication was placed between the bearing plates and flanges at two locations, and paper pads were placed at the other two locations. The flanges were not ground. After about 120,000 cycles, the pads were examined and it was concluded that the paper pad was most effective. Consequently, ¼-in. paper pads were placed between the bearing plate and flange at all load-point locations and the test was continued. The location and appearance of the failure for this beam indicated that fretting was not involved. Paper pads were used in all subsequent tests, and no more problems with fretting were observed. Only the results for the duplicate set of beams are included in Table E-5.

APPENDIX F

DETAILED DISCUSSION OF FATIGUE-TEST RESULTS

RELATIONSHIPS BETWEEN MODAL STRESS RANGE AND LIFE

Extensive studies conducted over the past 100 years have shown that finite-life fatigue data can be satisfactorily represented by a linear SN curve in which the log of the number of cycles to failure, N, is plotted against either the stress parameter, S, or the log of the stress parameter. Constant-amplitude fatigue tests of simulated bridge beams (*2*) showed that stress range (the sum of the maximum stress and the minimum stress, tension and compression being taken as positive) is the most important stress parameter and that a log-SN curve provides a slightly better fit of data than a semilog-SN curve. Consequently, log-SN curves have been fitted to each compatible set of data in the present program.

Specifically, the equation

$$\log N = \log A - B \log S_{rm} \qquad \text{(F-1)}$$

was used to represent the data. In this equation, B is the reciprocal of the slope of the log SN curve, and log A is the x intercept of the curve, as shown in Figure F-1. (Since Figure F-1 is intended only to illustrate the mathematical form of the finite-life SN curve, a horizontal line representing the fatigue limit is not shown.) Eq. F-1 can also be written in the form

$$N = \frac{A}{S^B_{rm}} \qquad \text{(F-2)}$$

An available U.S. Steel curve-fitting computer program, REGRESS, which utilizes standard methods of regression analysis, was used to determine values of A and B that minimize the sum of the squares of the differences of individual data points from the curve in the N direction. The computer program also provides the sum of the squares of the differences and the root mean square of the differences, which is often called the standard error of the estimate. Parallel lines drawn a distance of 1.96 standard errors of the estimate from the best-fit line approximate the 95-percent confidence limits for a single future test and the 95-percent tolerance limits for the sample. The concept of confidence and tolerance limits is explained in Appendix D. The difference between the exact confidence limits and the straight-line approximate confidence limits for typical sets of data is also described in Appendix D.

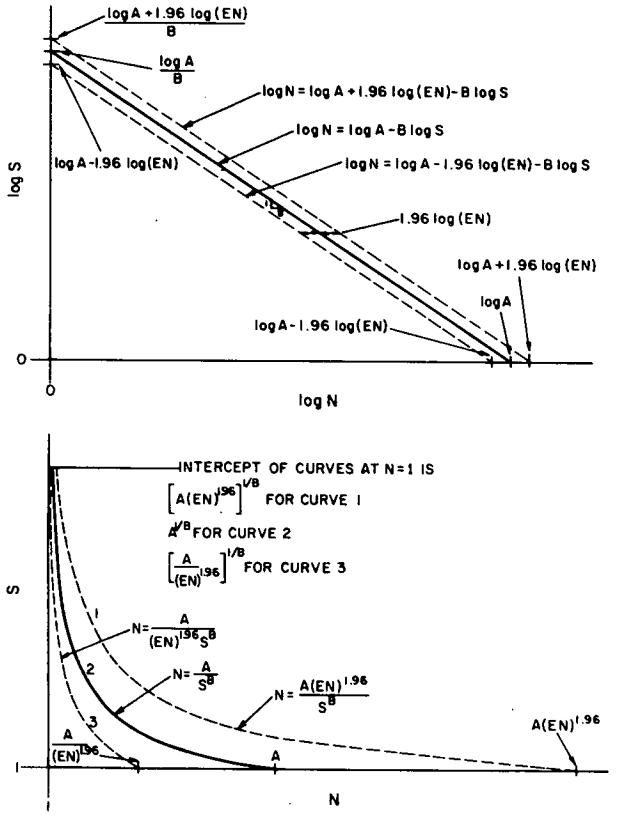

NOTES: DASHED LINES ARE APPROXIMATE CONFIDENCE LIMITS; log (EN) IS THE STANDARD ERROR OF ESTIMATE OF log N

Figure F-1. SN relationships.

A few sets of replicate data for the cover-plate specimens and cover-plate A beams included one or more tests that were discontinued without a failure after these specimens or beams had sustained a much greater number of cycles than the other specimens or beams within the set that had failed or than the extension of the SN scatter band from tests conducted at higher stress ranges. These discontinued tests suggest that a sharp break occurs in the SN curve for that type of specimen or beam and, consequently, that these sets of replicate tests should not be included in fitting a curve to the results of tests conducted at a higher stress range. Therefore, all sets of replicate tests that included discontinued tests were omitted when fitting a curve, but were included in plots that showed data points. Except for these few results and for the results of the long-life tests, there was no evidence that a fatigue limit or break in the SN curve occurred for any detail. Consequently, all subsequent correlations were made on the basis of straight SN curves without a fatigue limit.

Main Variables

In the present test program, two parameters were used to define the variable-amplitude stress-range spectrums (*33*): (1) the modal stress range, S_{rm}, which corresponds to the peak of the probability-density curve of stress ranges, and (2) the parameter S_{rd}, which is a measure of the width of the curve or the dispersion of the data. Consequently, S_{rm} was used as the stress parameter in the SN curves, and a separate curve was established for each different value of S_{rd}/S_{rm} used in the program. Separate curves were determined for each of the three types of specimens or beams (cover-plate specimens, cover-plate beams, and welded beams), because these different types were expected to have significantly different fatigue lives. Similarly, separate curves were established for cover-plate A and C beams, because preliminary studies indicated that the results were different. (Originally, only one type of cover-plate beam detail was planned. However, it was determined during the study that the fabrication technique used for this detail (welding the cover plate to the flange plate before it was welded to the web) yielded unconservative results that differed from those of past studies (*2*). Consequently, the remaining cover-plate beams were modified to obtain conservative results comparable with past constant-amplitude results.)

Different values of two variables that were shown to have a secondary effect in past work (*1*) initially were grouped together: (1) minimum stress, S_{min}, which was constant during each test, and (2) type of steel. However, the limited data for $S_{min} = 40$ ksi (276 MPa) were not included. The limited data for detail B of the cover-plate beams were initially included with the data for detail C, because past work (*2*) suggested that the results would not be significantly different. An investigation of the effect of these secondary variables, which is discussed later, confirmed that the original grouping of data was reasonable.

TABLE F-1

MODAL STRESS RANGE VS. LIFE CURVES

Detail	Dispersion Ratios	No. of Tests	Regression Coefficients* Log A**	A*** x 10^{-6}	B Best Fit	B Std Error	Std Error of Estimate of Log N**	Std Error of Estimate of N	Correlation Coefficient, R
Cover Plate B&C	0	27	9.135	1370	2.982	0.119	0.140	1.38	0.981
	0.25	6	8.594	393	2.677	0.116	0.043	1.10	0.996
	0.50	21	8.381	240	2.468	0.158	0.176	1.50	0.963
	1.00	12	8.567	369	2.732	0.370	0.167	1.42	0.919
Welded Beam D	0.0	24	10.81	64600	3.296	0.238	0.162	1.45	0.947
	0.25	9	10.91	81300	3.441	0.590	0.147	1.40	0.911
	0.50	15	9.346	2220	2.437	0.247	0.118	1.31	0.939
	1.00	9	9.698	4990	2.894	0.249	0.147	1.40	0.975
Cover Plate S	0	12	9.333	2150	2.681	0.068	0.066	1.16	0.997
	0.50	12	9.320	2090	2.746	0.115	0.095	1.25	0.991
	1.00	12	8.937	865	2.589	0.066	0.055	1.13	0.997
Cover Plate A	0	18	8.986	968	2.615	0.321	0.217	1.65	0.898
	0.25	6	9.703	5050	3.452	0.118	0.044	1.11	0.998
	0.50	18	8.235	172	2.088	0.179	0.150	1.41	0.946
	1.00	12	8.845	700	2.721	0.386	0.201	1.59	0.913
Cover Plate A+ (S_{min} = 40 ksi)	0	18	9.088	1225	2.719	0.348	0.252	1.79	0.890
	0.5	21	8.592	391	2.419	0.240	0.217	1.65	0.918

* Based on log N = log A - B log S_{rm}

** Log values are to the base 10.

*** Values of A x 10^{-6} are listed; thus, the first value of A is 1,370,000,000.

\+ A514 beams only; includes beams tested at S_{min} = 40 ksi in addition to those tested at S_{min} = 0 and 10 ksi.

Conversion Factor

1 ksi = 6.895 MPa

The best-fit values of A and B, and the parameters indicating the closeness of fit, are given in Table F-1. The values of A varied with the severity of the detail. The values of B ranged from 2.088 to 3.452; these values are consistent with past work (*2, 4*) that shows that B is roughly 3 for most structural details. The standard error of the coefficient B is a measure of the variation in B that can be expected as the result of sampling error. As explained in Appendix D, there is a 95-percent probability that the true B for the population is within an interval that results from adding and subtracting of 1.96 times the standard error from the best-fit value.

The standard errors of the estimate of log N, which is a measure of the amount of scatter of the data about the best-fit line, ranged from 0.043 to 0.217, as evident in Table F-1. The corresponding standard errors of the estimate of N ranged from 1.10 to 1.65. These values indicate a reasonable amount of scatter for fatigue data. The relationship of the standard error of log N to the 95-percent confidence limits for log N is shown in Figure F-1. Specifically, the approximate 95-percent confidence limits for the log SN curve are drawn a distance 1.96 times the standard error of the log N from the best-fit line as shown in Figure F-1. The relationship of the standard error of N to the confidence limits for N is also shown in Figure F-1. The standard error of N is raised to the 1.96 power to get a factor by which N is either multiplied or divided to get the confidence limits on N. For example, if the standard error of N for a set of data is 1.3, the factor would be 1.3 to the 1.96 power or 1.67. The 95-percent confidence limits for $N = 100{,}000$ would then be 100,000 divided by 1.67, or 60,000, and 100,000 times 1.67, or 167,000. The confidence limits for other values of N could be calculated in the same way, using the same factor.

The correlation coefficient also gives a measure of the closeness of fit of the best-fit line, or the amount of scatter about the line. A perfect fit (all data points on the line) gives a value of 1.00, and a completely random scatter of data gives a value of 0. The correlation coefficients in Table F-1 ranged from 0.897 to 0.998 and indicate an excellent fit.

Best-fit SN curves for different values of the dispersion ratio, S_{rd}/S_{rm}, are shown in Figures 11 and 12 for cover-plate C and B beams and for welded beam D, respectively; and in Figures F-2 and F-3 for cover-plate A beams and cover-plate specimens, respectively. In general, the scatter bands for the different values of the ratio overlapped; therefore, to avoid clutter, individual data points and confidence limits for various curves were omitted. Furthermore, curves are shown within the range of test data only. The SN curves are roughly parallel and show that the life corresponding to a given S_{rm} decreases as S_{rd}/S_{rm} (which is a measure of spectrum width) increases.

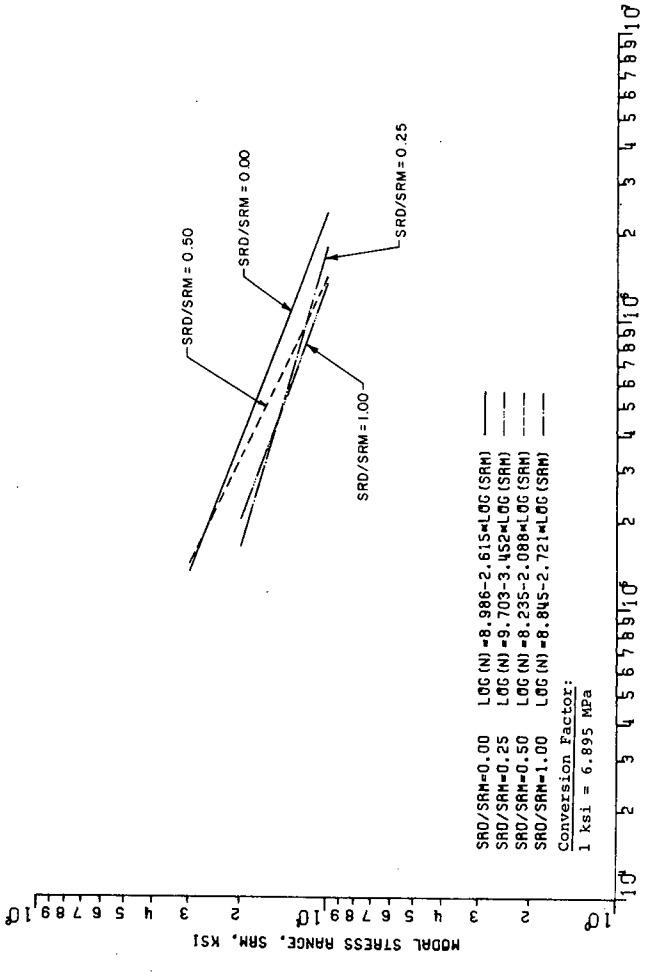

Figure F-2. Modal stress range vs. fatigue life for cover-plate B beams.

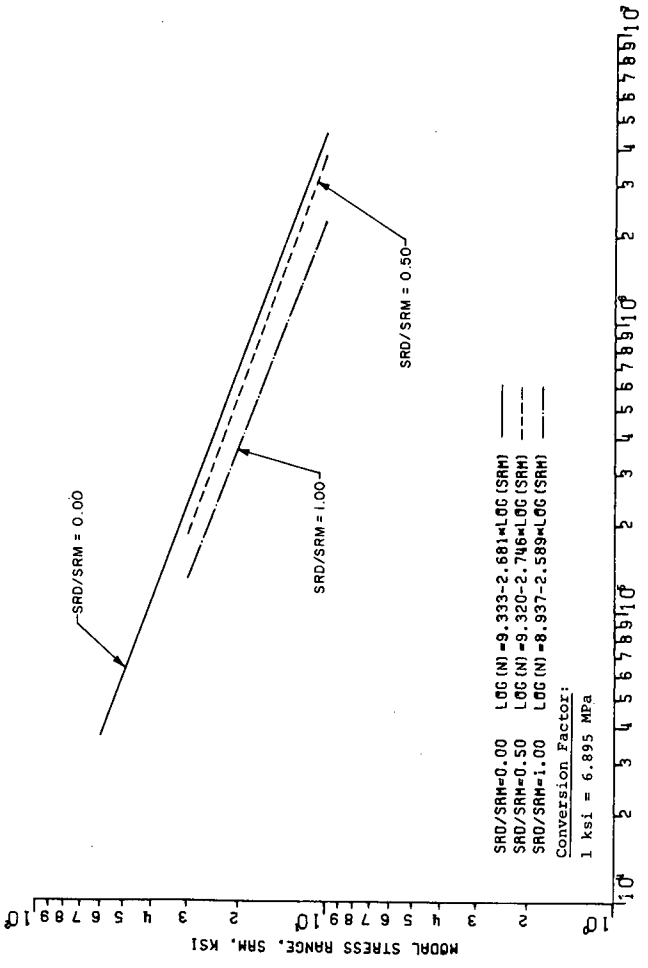

Figure F-3. Modal stress range vs. fatigue life for cover-plate specimens.

Secondary Variables

To determine how much improvement in the closeness of fit (standard error of the estimate) of the SN curves could be obtained by including the secondary variables, terms involving these variables were added to Eq. F-1, and new curves were fit to the sets of data from Table F-1. Specifically, the equation was modified as follows:

$$\log N = \log A - B \log S_{rm} + DS_{\min} + ES_t + F\beta \qquad \text{(F-3)}$$

in which $S_{\min}$ is the minimum stress in the test, S_t is the tensile strength of the material, and β is a detail identification index that is used only in comparing cover-plate C and B details. β is taken as 0 for detail C and as 1.0 for detail B.

Best-fit values for the coefficients A, B, D, E, and F, and the standard error of the estimate, were calculated by the computer program and are given in Table F-2. Since the standard error of the estimate is a measure of the scatter of data about the best-fit line, it is usually reduced by adding terms to the equation defining the line. Consequently, the standard error of the estimates is smaller in Table F-2 than in Table F-1; the differences between the two, however, were generally too small to be of practical importance except for the cover-plate A beams. Specifically, the differences in the standard errors of N ranged from 0 to 13 percent and averaged 7.5 percent. Furthermore, limited statistical calculations suggested that the difference in closeness of fit between Eqs. F-1 and F-2 is not statistically significant. Therefore, it is concluded that the test results can be adequately represented by Eq. F-1 without including secondary variables.

Even though the results showed that the standard error of the estimate cannot be greatly improved by including the secondary variables, the regression analyses suggested that some of these variables have a statistically significant effect that is interrelated with that of S_{rm}. (As indicated in Appendix D, a statistically significant difference is a difference that is not likely to have occurred by chance; the difference need not be large to be statistically significant.) Specifically, the analysis suggests that the type of steel has a statistically significant effect that is interrelated with S_{rm}. Other studies (*4, 27*) have shown significant differences between the fatigue lives of structural details of different steels within certain ranges of data, especially at short lives.

For cover-plate A beams, the closeness of fit was considerably improved by adding terms involving both $S_{\min}$ and S_t. As mentioned earlier, additional tests were performed on these beams at $S_{\min} = 40$ ksi (276 MPa) to determine whether a very high value of $S_{\min}$ would affect the fatigue life. Consequently, these data were combined with the data for $S_{\min} = 0$ and 10 ksi (69 MPa), and a best-fit line was calculated both with and without a term involving $S_{\min}$ to isolate the effect of $S_{\min}$. Only data for A514 steel were included. The results show that inclusion of the $S_{\min}$ term considerably improves the closeness of fit and means that $S_{\min}$ has a considerable effect on the fatigue life for this type of detail, especially if the $S_{\min}$ becomes quite large.

Semilog-SN Curves

To confirm that log-SN curves give a better fit of the present data than semilog-SN curves, semilog-SN curves were fit to all sets of data in Table F-1. Specifically, the following equation was used:

$$\log N = A - B S_{rm} \qquad \text{(F-4)}$$

in which A and B are the regression coefficients.

Best-fit values for these coefficients and the standard error of the estimate were determined by the computer program and are given in Table F-3. The values of A and B in Table F-3 are not directly comparable to the values of A and B in Table F-1 because the corresponding equations are different. In both tables, however, the deviations from the best-fit line are measured in terms of log N. Consequently, the standard error of the estimate of log N, or N, from the two tables may be compared to show the relative closeness of fit of the two types of curves. The results given in Table F-3 indicate that the standard errors for the semilog curves are generally slightly larger than those for the log curves. Thus, the log-SN curves provide a slightly better fit than the semilog-SN curves within the range of the test data. Actually, the log and semilog curves for a given set of data are not greatly different if the range of lives covered by the data is relatively small, say from 100,000 cycles to 2,000,000 cycles. As the range of lives becomes larger, however, the two types of curves become considerably different.

Comparisons With Results From Project 12-7

Two details used in the present study are comparable with details used in NCHRP Project 12-7(*2*) on constant-amplitude fatigue behavior: cover-plate C and welded-beam D. Consequently, the present constant-amplitude data for these two details were compared with the comparable Project 12-7 data to test whether the two sets of data come from the same population or, in other words, whether there is a statistically significant difference between the two. (The cover-plate B beams were also comparable to details in Project 12-7, but were not included in the analytical comparison because only six such beams were tested in the present study. However, the results for these six beams appear to agree with the results from Project 12-7.) The general procedure used in making this significance test is described in Appendix D. An available U.S. Steel computer program was utilized for this purpose. Briefly, F tests were made to determine the probability that differences in A and B that occurred by chance would be less than the observed differences. This probability is referred to as the confidence level and indicates the confidence that there is a real difference between the two sets of data. Usually, the differences between two sets are not considered to be statistically significant unless the confidence level is above 95 percent. Thus, as may be seen in Table F-4, the data from Projects 12-7 and 12-12 are not statistically different. This means that it has not been conclusively shown that a real difference exists between the two sets of data. Furthermore, the observed differences between the A and B values for the sets of data are so small that they would not be of practical significance even if they were shown to be statistically significant.

RELATIONSHIP BETWEEN CONSTANT- AND VARIABLE-AMPLITUDE RESULTS

There are many ways of relating variable-amplitude fa-

TABLE F-2

SN CURVES INCLUDING SECONDARY VARIABLES

Detail	Dispersion Ratio	No. of Tests	Log A**	A*** x 10^{-6}	Regression Coefficients* B Coeff	D Coeff x 10^3	E Coeff*** x 10^3	F Coeff*** x 10^3	Std Error of Estimate of Log N**	Std Error of Estimate of N	Diff From Table F1,+ percent: Std Error of Log N	Diff From Table F1,+ percent: Std Error of N
Cover Plate C&B	0.00	27	8.785	610	2.904	- 1.486	2.508	66.50	0.121	1.32	14	5
	0.25	6	8.594	393	2.677	-	-	-	0.043	1.10	0	0
	0.50	21	8.163	146	2.780	-12.95	6.707	-	0.179	1.31	2	13
	1.00	12	8.054	113	2.188	-19.48	-	101.6	0.134	1.36	20	4
Welded Beam D	0.00	24	10.95	89100	3.208	9.750	-2.458	-	0.159	1.44	2	1
	0.25	9	11.02	105000	3.535	-3.306	-	-	0.158	1.44	-7	0
	0.50	15	9.175	1500	2.085	5.789	-2.931	-	0.110	1.29	7	2
	1.00	9	9.698	4990	2.894	-	-	-	0.147	1.40	0	0
Cover Plate S	0.00	12	9.351	2240	2.684	-1.879	-	-	0.068	1.17	-4	-1
	0.50	12	9.330	2140	2.746	-2.004	-	-	0.100	1.26	-5	-1
	1.00	12	8.964	920	2.589	-5.282	-	-	0.049	1.12	11	1
Cover Plate A	0.00	18	9.680	4790	3.692	-15.93	7.554	-	0.101	1.26	53	24
	0.25	6	9.703	5050	3.452	-	-	-	0.044	1.11	0	0
	0.50	18	9.582	3820	2.596	-23.68	3.801	-	0.080	1.20	47	15
	1.00	12	8.940	871	2.721	-18.97	-	-	0.181	1.58	10	0
Cover Plate A++ (S_{min} = 40 ksi)	0.00	18	10.042	10960	3.262	-13.55	-	-	0.120	1.32	52	26
	0.50	21	9.067	1167	2.641	-11.96	-	-	0.100	1.26	54	24

* Based on $\log N = \log A - B \log S_{rm} + D S_{min} + E S_t + F_\beta$.

** Log values to the base 10.

*** Values of A x 10^{-6} are listed; thus, the first value of A is 610,000,000. Similarly, values of the coefficient x 10^3 are listed.

\+ Value from $\frac{\text{(Table F1 - Table F2) x 100}}{\text{Table F1}}$

++ A514 beams only; includes beams tested at S_{min} = 40 ksi in addition to those tested at S_{min} = 0 and 10 ksi.

Conversion Factor

1 ksi = 6.895 MPa

TABLE F-3

SEMILOG SN CURVES

Detail	Dispersion Ratio	No. of Tests	Regression Coefficients* A Best Fit	B Best Fit	Std Error x 10^3	Std Error of Estimate of Log N**	Std Error of Estimate of N	Diff From Table F1,*** percent Std Error of Log N	Std Error of N
Cover Plate C&B	0.0	27	6.751	64.95	2.88	0.154	1.43	-10	-4
	0.25	6	6.723	80.59	3.50	0.043	1.10	0	0
	0.50	21	6.682	69.57	7.90	0.290	1.95	-65	-30
	1.00	12	6.657	82.23	11.15	0.167	1.47	0	-4
Welded Beam D	0.0	24	7.364	44.91	3.76	0.184	1.53	-14	-6
	0.25	9	7.648	60.60	10.39	0.147	1.40	0	0
	0.50	15	6.913	37.31	4.01	0.124	1.33	-6	-2
	1.00	9	7.397	67.20	9.36	0.229	1.70	-56	-21
Cover Plate S	0.00	12	6.796	40.17	3.86	0.239	1.73	263	-49
	0.50	12	7.229	65.51	2.75	0.095	1.43	0	-14
	1.00	12	6.966	61.76	1.58	0.055	1.13	0	0
Cover Plate A	0.0	18	6.890	61.30	7.07	0.206	1.61	5	2
	0.25	6	7.290	103.9	3.56	0.044	1.11	0	0
	0.50	18	6.612	50.31	4.37	0.151	1.42	-1	-1
	1.00	12	6.944	81.90	11.61	0.201	1.59	0	0

* Based on log N = log A - Blog S_{rm}

** Log values to the base 10

*** Values from $\frac{\text{(Table F1 - Table F3) x 100}}{\text{Table F1}}$

TABLE F-4

CONSTANT-AMPLITUDE RESULTS FOR PROJECT 12-12 AND 12-7 STUDIES

Detail	Project	No. of Tests	Regression Coefficients* Log A**	B	Std Error of Estimate of Log N**	Confidence Level,*** percent Log A**	B
Cover Plate C	12-7	61	9.038	2.883	0.106	<50	80
	12-12	24	9.050	2.924	0.139		
Welded Beams D	12-7	56	10.835	3.345	0.146	<50	79
	12-12	24	10.811	3.296	0.162		

* Based on log N = log A - Blog S_r.

** Log values to the base 10.

*** Probability that a real difference exists between the two sets of data; for a further explanation see Appendix D.

tigue data to constant-amplitude data. Probably, the most convenient for bridge applications is the effective stress range concept. With this concept, the four lines in Figures 11, 12, and F-2 and the three lines in Figure F-3 are approximated by a single line relating the effective stress range, S_{re}, to the life, N. The effective stress range for a variable-amplitude spectrum is defined as the constant-amplitude stress range that would result in the same fatigue life as the variable-amplitude spectrum. Different methods of calculating S_{re} are discussed in the following.

Effective Stress Range From Rayleigh Distribution

In the first method of calculating S_{re}, which is based directly on the Rayleigh distribution discussed earlier, the effective stress range is given by

$$S_{re} = S_{rm} + C\,S_{r\hat{d}} = S_{rm}\,(1 + C\,S_{r\hat{d}}/S_{rm}) \qquad \text{(F-5)}$$

in which the best-fit value of the correlation factor, C, is determined from available data. Thus C defines a single stress range that has the same effect on fatigue behavior as the complete spectrum. *If* $C = 0.378$, S_{re} is the root mean square (RMS) of all stress ranges in the spectrum; if $C = 0.230$, S_{re} is the mean of the stress ranges.

The variation of S_{re}/S_{rm} with the dispersion ratio, $S_{r\hat{d}}/S_{rm}$, for these two values of C is shown in Figure 13. At a dispersion ratio of 0, which corresponds to constant-amplitude loading, $S_{re} = S_{rm}$ for both definitions of S_{re}. As the dispersion ratio increases, or in other words as the width of the spectrum becomes greater, S_{re} becomes increasingly larger than S_{rm}. At $S_{r\hat{d}}/S_{rm} = 1.0$, the S_{re} corresponding to the RMS value is about 11 percent greater than the value corresponding to the mean.

Values of C were determined for various groups of test data by calculating the value of C that results in the best-fit SN curve for each group. Each SN curve was defined by

$$\log N = \log A - B \log S_{re} \qquad \text{(F-6)}$$

and S_{re} was defined by Eq. F-5. The NLWOOD curve-fitting program (a nonlinear least-squares curve-fitting computer program) was used to determine values of A, B, and

C that result in the minimum sum of the squares of the deviations for each group. Each group included all compatible constant-amplitude data plus all compatible variable-amplitude data for the S_{rd}/S_{rm} values used. Thus, each value of C represents the value that would best interrelate the constant- and variable-amplitude data in that group.

The calculated values of C are given in Table F-5. Most of the values of C are between 0.230 and 0.378, which correspond to the mean and RMS, respectively, and tend to be closer to the latter. There is no consistent correlation between C and the type of steel, type of detail, or minimum stress. Furthermore, the fact that the best-fit curves from Table F-1 are roughly parallel suggests that C does not vary significantly with S_{rm}. The data show a trend toward larger C values for larger values of S_{rd}/S_{rm}. Consequently, a factor based on this trend could be incorporated into the expression for the effective stress range. However, Figure 13 suggests that the effect on S_{re} would be too small to justify the added complexity. Therefore, it is concluded that a single value of C should be used in Eq. F-5 for all types of steels, types of details, and minimum stresses. A value of 0.378, corresponding to the RMS, provides a reasonable and generally conservative approximation of C for practical purposes.

Effective Stress Range by RMS

The RMS can be calculated for a spectrum defined by a stress-range histogram (frequency-of-occurrence bar graph) by fitting a Rayleigh curve to the histogram to determine S_{rm} and S_{rd}, and calculating S_{re} from Eq. F-5 with $C = 0.378$. Alternatively, $S_{re\mathrm{RMS}}$ can be calculated directly from the stress-range histogram by using the formula

$$S_{re\mathrm{RMS}} = (\Sigma \alpha_i S^2_{ri})^{\frac{1}{2}} \qquad \text{(F-7)}$$

in which S_{ri} is the ith stress range in the spectrum and α_i is the fraction of stress ranges of that magnitude.

Figures 14, 15, F-4, and F-5 show the best-fit SN curves and approximate 95-percent confidence limits for a single future test for the constant-amplitude data; data points are shown for both the constant- and variable-amplitude data. Specifically, log $S_{re\mathrm{RMS}}$ is plotted against log N, and all variable-amplitude data points are transformed according to Eq. F-7. The best-fit line and the confidence limits are shown as solid and dashed lines, respectively, within the range of constant-amplitude data, and are extended as dash-dot lines beyond this range. The variable-amplitude data points, which generally fall within the scatter band and 95-percent confidence limits for the constant-amplitude data, show that the $S_{re\mathrm{RMS}}$ satisfactorily relates constant- and variable-amplitude data.

To determine whether there is a significant difference between the constant-amplitude data and the variable-amplitude data transformed by the RMS method, the best-fit curves were developed from Eq. F-6 for the variable-amplitude data for each detail. In Table F-6, these curves are compared with the best-fit constant-amplitude curves from Table F-1. The U.S. Steel computer program and

TABLE F-5

CALCULATION OF CORRELATION FACTOR *

Group	Detail**	Steel	S_{min}, ksi	Number of CA Tests+	Correlation Factor, C			
					$S_{rd}/S_{rm} = 0.25$	$S_{rd}/S_{rm} = 0.50$	$S_{rd}/S_{rm} = 1.0$	Combined
1	Cover plate C	A514	10	9	-	0.140 (18)	0.419 (15)	0.364 (24)
2	Cover plate C	A36	0	9	0.508 (15)	0.470 (18)	-	0.452 (24)
3	Cover plate B	A36	10	3	-	- (6)	-	0.542 (6)
4	Welded beam D	A514	0	9	-	0.347 (18)	0.466 (18)	0.446 (27)
5	Welded beam D	A36	-10	9	0.198 (15)	- (12)	-	0.397 (18)
6	Welded beam D	A36	0	6	- (9)	- (9)	-	0.553 (12)
7	Welded beam D	A36	-10,0	15	0.362 (24)	0.506 (21)	-	0.481 (30)
8	Cover plate S	A514	0	3	-	0.217 (9)	0.250 (9)	0.275 (15)
9	Cover plate S	A514	10	9	-	0.180 (15)	0.296 (15)	0.285 (21)
10	Cover plate S	A514	0,10	12	-	0.177 (24)	0.270 (24)	0.270 (36)
11	Cover plate A	A514	0	6	-	0.070 (12)	0.453 (12)	0.378 (18)
12	Cover plate A	A514	10	6	-	0.271 (15)	0.356 (12)	0.360 (21)
13	Cover plate A	A514	0,10	12	-	0.228 (27)	0.414 (24)	0.355 (39)
14	Cover plate A	A514	40	6	-	0.205 (12)	-	0.205 (12)
15	Cover plate A	A514	0,10,40	18	-	0.189 (39)	0.230 (30)	0.210 (51)
16	Cover plate A	A36	10	6	0.211 (12)	0.439 (9)	-	0.395 (15)

* Factor based on log N = log A - B log S_{re}, with $S_{re} = S_{rm} + CS_{rd}$; combined test data were used for $S_{rd}/S_{rm} = 0.0$ (constant amplitude) and for the value of S_{rd}/S_{rm} shown. The number in parenthesis is the total number of constant- and variable-amplitude tests included in that group.

** A = beams with cover-plate ends not cross-welded and web-flange welds placed last; B = cover-plate ends not cross-welded, cover-plate welds made last; C = beams with cover-plate ends cross-welded last; S = cover-plate specimens with cover-plate ends not cross-welded; D = welded beams without cover plates.

+ Number of constant-amplitude tests.

Conversion Factor

1 ksi = 6.895 MPa

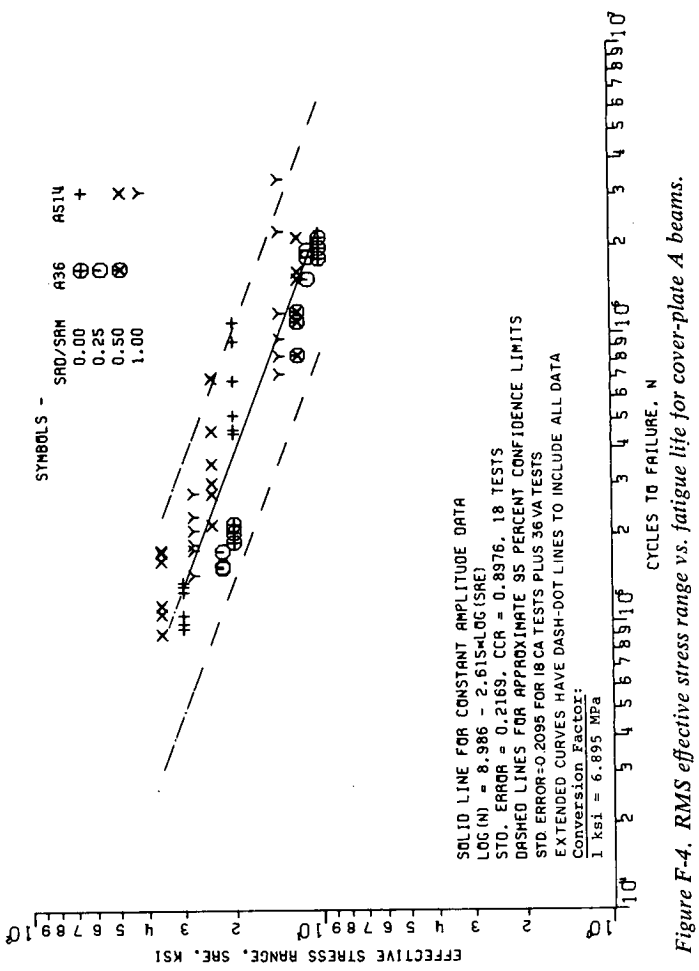

Figure F-4. RMS effective stress range vs. fatigue life for cover-plate A beams.

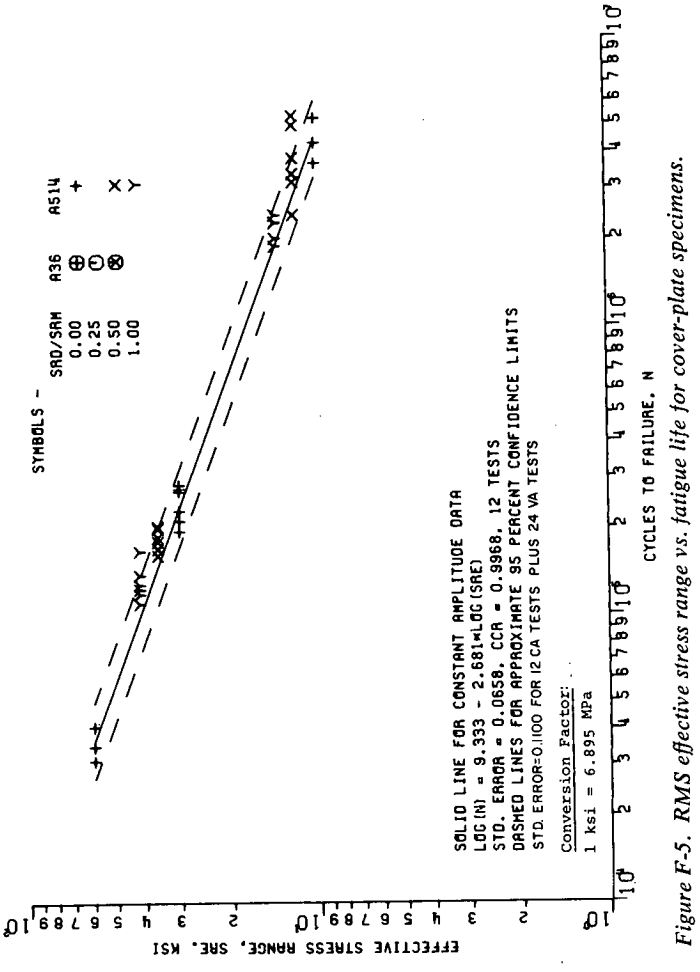

Figure F-5. RMS effective stress range vs. fatigue life for cover-plate specimens.

methods discussed earlier were used to determine whether the differences between the log A and B values for the constant- and variable-amplitude data are statistically significant. The calculated confidence levels are given in Table F-6. In most cases, the difference would not be considered statistically significant because the confidence level is below 95 percent. Furthermore, in most cases, the difference is also small from a practical standpoint. These results support the conclusion that $S_{re\text{RMS}}$ satisfactorily relates constant- and variable-amplitude data.

Effective Stress Range by Miner's Law

Miner's Law has been widely used for many years to show the cumulative effect on fatigue life of stress cycles of different magnitudes, and can be used as described in this section to calculate an effective stress range. Miner's Law states that

$$\sum \frac{\alpha_i N}{N_i} = 1.0 \qquad \text{(F-8)}$$

in which N is the fatigue life for a variable-amplitude spectrum, N_i is the fatigue life for a constant-amplitude loading corresponding to the ith stress range in the spectrum, and α_i is the fraction of stress ranges of that magnitude. By definition, the life, N, for a variable-amplitude spectrum is the same as the life, N, for a constant-amplitude loading of S_{re} and is given by

$$N = \frac{A}{S^B{}_{re}} \qquad \text{(F-9)}$$

The value of N_i is given by a similar equation in which S_{re} is replaced by S_{ri}. Hence,

$$\sum \alpha_i \left(\frac{A}{S^B{}_{re}}\right)\left(\frac{S^B{}_{ri}}{A}\right) = 1.0 \qquad \text{(F-10)}$$

and

$$S_{re} = (\Sigma \alpha_i S^B{}_{ri})^{1/B} \qquad \text{(F-11)}$$

B is the reciprocal of the slope of the log-SN curve, as shown in Figure F-1, and is about 3 for most structural details. Thus, Eq. F-11 is similar to Eq. F-7, which defines $S_{re\text{RMS}}$, but the S_{ri} term is cubed rather than squared.

The variation of S_{re}/S_{rm} with S_{rd}/S_{rm} for a spectrum defined by a Rayleigh curve and for $B = 3$ is shown in Figure 13. This curve is always slightly higher than the curves for other methods of calculating the effective stress range. Thus, $S_{re\text{MINER}}$ is somewhat more conservative than $S_{re\text{RMS}}$, but the maximum difference between the two is only about 11 percent.

The $S_{re\text{MINER}}$ for the variable-amplitude data was compared with the constant-amplitude data in the same way as $S_{re\text{RMS}}$ was compared with the constant-amplitude data. In calculating S_{re} for the variable-amplitude data, the value of B from the constant-amplitude data for that detail was used in Eq. F-11. The results are shown in Figures 16, 17, F-6,

TABLE F-6

STATISTICAL SIGNIFICANCE OF DIFFERENCES BETWEEN CA AND VA DATA *

Detail	Stress Spectrum*	Definition of Sre	No. of Tests	Coefficients** Log A	B	Std Error of Estimate of Log N**	Confidence Level,*** percent Log A**	B
Cover Plate B&C	CA	-	27	9.135	2.982	0.140		
	VA	RMS	39	8.615	2.509	0.166	99	73
	VA	MINER	39	8.588	2.460	0.183	>99	92
Welded Beam D	CA	-	24	10.81	3.296	0.162		
	VA	RMS	33	10.03	2.781	0.149	91	50
	VA	MINER	33	10.14	2.822	0.134	90	<50
Cover Plate S	CA	-	12	9.333	2.681	0.066		
	VA	RMS	24	9.421	2.672	0.077	<50	>99
	VA	MINER	24	9.418	2.645	0.082	<50	>99
Cover Plate A	CA	-	18	8.986	2.615	0.217		
	VA	RMS	36	8.633	2.293	0.192	62	75
	VA	MINER	36	8.608	2.263	0.200	64	80

* CA means constant amplitude; VA means variable amplitude.

** Based on log N = log A - B log S_{re}.

*** Probability that a real difference exists between the constant-amplitude curves and the variable-amplitude curves; for a further explanation see Appendix D.

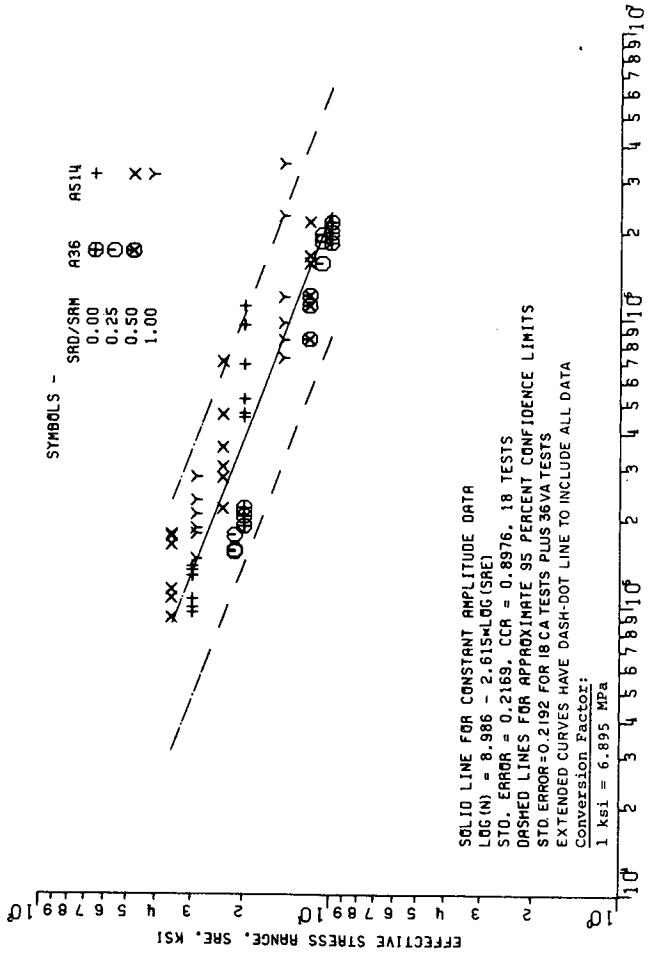

Figure F-6. Miner effective stress range vs. fatigue life for cover-plate A beams.

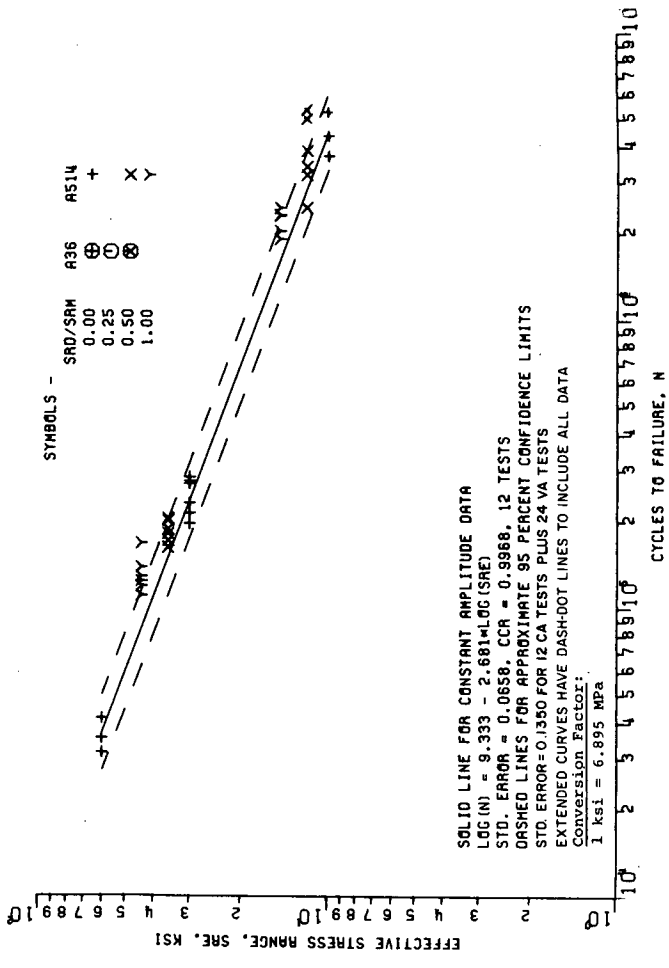

Figure F-7. Miner effective stress range vs. fatigue life for cover-plate specimens.

and F-7 and Table F-6. The curves in the figures show that the variable-amplitude data points generally fall within the scatter band defined by the 95-percent confidence limits for the constant-amplitude data. Furthermore, the differences in log A and B between the variable- and constant-amplitude data were generally not statistically or practically significant. Therefore, it is concluded that $S_{re\text{MINER}}$ satisfactorily relates variable- and constant-amplitude data.

Comparison of RMS and Miner Methods

To determine which method of calculating S_{re} provides the closest fit of the variable-amplitude data to the constant-amplitude regression line, the standard errors of the estimate were calculated for various details. For each detail, the constant-amplitude data were combined with the variable-amplitude data transformed by either the RMS or Miner method. The standard error of the estimate based on deviations of these data from the best-fit line for the constant-amplitude data was calculated as explained in Appendix D. The results are given in Table F-7 together with the standard errors of the estimate for the constant-amplitude data alone. Smaller values of the standard error indicate a closer fit. For all details except the welded beams, the RMS method provides a closer fit. In some of the details, the standard error is smaller for the combined data than for the constant-amplitude data. This means that there is less scatter in the transformed variable-amplitude data than in the constant-amplitude data.

TABLE F-7

COMPARISON OF RMS AND MINER METHODS OF RELATING CA AND VA DATA *

Detail	Stress Spectrum*	Definition of Sre	No. of Tests	Std Error of Estimate of Log N**
Cover Plate B&C	CA	-	27	0.140
	CA+VA	RMS	66	0.174
	CA+VA	Miner	66	0.195
Welded Beam D	CA	-	24	0.162
	CA+VA	RMS	57	0.135
	CA+VA	Miner	57	0.128
Cover Plate S	CA	-	12	0.066
	CA+VA	RMS	36	0.110
	CA+VA	Miner	36	0.135
Cover Plate A	CA	-	18	0.217
	CA+VA	RMS	54	0.210
	CA+VA	Miner	54	0.219

* CA means constant amplitude; VA means variable amplitude.

** Based on the deviations of the data points from the best-fit line for the constant-amplitude data.

COMPARISONS WITH AASHTO ALLOWABLE STRESSES

The results for all cover-plate beams from the present study are compared with AASHTO allowable fatigue provisions (*1*) in Figure 18. Specifically, the cover-plate-beam results, including details A, B, and C, are compared with the specified fatigue strength for AASHTO Category E (cover-plate ends) on the basis of $S_{re\text{RMS}}$. The allowable fatigue strength line was obtained by fitting a straight line defined by Eq. F-6 to the allowable stress ranges for three categories of design life: 100,000, 500,000, and 2,000,000 cycles. This line closely approximates the lower limits (95-percent tolerance limit) of previous constant-amplitude test results on cover-plate end details (*2*).

The scatter in Figure 18 is reasonable, considering that the data for several different steels, minimum stresses, and details are included in a single plot. Almost all of the data points lie above the line; thus, the AASHTO allowable stress line provides an approximate lower limit for the variable- and constant-amplitude test results that are plotted on the basis of the RMS effective stress range.

Figure 19 gives a similar comparison of the welded-beam results with the AASHTO allowable fatigue stress for Category B, longitudinal flange-web fillet welds. Again, the scatter is reasonable for this type of specimen, and almost all of the data points lie above the allowable stress line. Thus, the AASHTO allowable stress line provides an approximate lower limit for the variable-amplitude test results that are plotted on the basis of the RMS effective stress range.

SECONDARY TESTS

In addition to the main testing program, a few tests were performed on cover-plate specimens (detail S) to evaluate the effects of other test parameters. The results of these tests are discussed in the following paragraphs.

Effect of Number of Individual Loads

A 500-cycle control tape was used to program the variable-amplitude loading in the main fatigue-testing program. This tape defined 500 individual loads that satisfy the desired Rayleigh distribution; the loads were arranged in a random sequence. The 500-cycle tape was continuously cycled throughout a test so that the same 500-cycle random sequence was repeated many times. Two parameters in this procedure could affect the fatigue results: (1) the number of individual loads and (2) the sequence length. A given number of individual (usually different) loads can be arranged in a sequence of any length equal to an integer times the number of individual loads. For example, 500 individual loads could be arranged in a sequence 1,000 cycles long in which each individual load appears twice.

The smaller the number of individual loads, the poorer the fit of the desired Rayleigh distribution, which is a continuous curve. Similarly, a larger number of individual loads would provide a better fit. The improvement in the fit that can be obtained by using a given number of additional loads, however, decreases as the number of loads increases, and, above a certain number, very little improvement in fit can be obtained. Consequently, increasing the number of individual loads above this level would not affect fatigue results.

To determine whether a value of 500 loads is above this level, six specimens were tested with 100 individual loads in a 500-cycle sequence, and the results were compared with those for six similar specimens tested with 500 individual loads in a 500-cycle sequence. Thus, the sequence length was the same for both. The loads on both tapes followed the Rayleigh distribution curve for $S_{rm} = 30$ ksi (207 MPa) and $S_{rd}/S_{rm} = 1.0$. The minimum stress was 0.

The results are given in the first two lines of Table F-8. Since the fatigue data in this study fit a log-SN curve, the comparison between the two sets of data can best be made in terms of the log means. (The log mean is the antilog of the mean of the logs of the individual lives.) The log means for the 100-load and 500-load tests were 102.8 and 103.3 kilocycles, respectively. This shows that the fatigue results are not significantly affected by changing from a tape with 100 individual loads to one with 500 individual loads. Changing from 500 individual loads to a greater number of individual loads would have even less effect. Conse-

TABLE F-8

EFFECT OF NUMBER OF INDIVIDUAL LOADS AND SEQUENCE LENGTH *

Test Variable	Number of Individual Loads	Sequence Length	Log Means Life,** kilocycles
Load Levels	100***	500	102.8
	500	500	103.3
Sequence Length	100	100	102.8
	100***	500	102.8
	100	5000	99.9

* Tests performed on cover-plate specimens at a S_{rm} = 30 ksi, S_{rd}/S_{rm} = 1.0, and S_{min} = 0.

** The antilog of the mean of the logs of the lives for six tests.

*** These two listings are for the same set of data.

quently, the 500 individual loads used in the present study are more than sufficient, and even 100 individual loads would have been adequate.

Effect of Sequence Length

To test the effect of sequence length, a 500-cycle random sequence of 500 individual loads was repeated throughout each test in the program. The sequence was random within the 500-cycle block, but was not random over the entire length of the tests. As the sequence (or block) length increases, the corresponding fatigue behavior will approach that for a truly random loading, and further increases in sequence length will have no effect.

To determine whether a 500-cycle sequence is sufficient to approach the truly random behavior, six specimens were tested at each of three sequence lengths: 100, 500, and 5,000 cycles. In each sequence, 100 individual loads were used that satisfied a Rayleigh distribution for $S_{rm} = 30$ ksi (207 MPa) and $S_{rd}/S_{rm} = 1.0$. The minimum stress was 0. In the 100-cycle sequence, each of the 100 individual loads occurred only once. In the 5,000-cycle sequence, each of the 100 individual loads was repeated 50 times. The sequence in each 100-cycle block in the 5,000-cycle sequence, of course, was different.

The results are given in the last three lines of Table F-8. The log means for the sequence lengths are very close and show that the 500-cycle sequence used in the present study is more than sufficient to represent truly random conditions; even a 100-cycle sequence appears to be adequate.

Effect of Vibration Stresses

Field measurements of stresses in bridges show that vibration stresses are superimposed on the major stress cycle caused by the passage of a vehicle. For most types of bridges, these vibration stress cycles have a much smaller amplitude but a higher frequency, f, than the major stress cycles. If the ratio of the frequency of the vibration cycles to that of the major cycles is an odd integer and the two types of cycles are in phase, the vibration cycles reinforce the positive and negative peaks of the major stress cycles. Thus, the over-all stress range, S_r, is the sum of the stress ranges for the two types of cycles, as illustrated in Figure F-8. For convenience, the vibration cycles are shown as triangular waves, although the actual vibration cycles approximate sine waves. Both the amplitude ratio, S_{rm}/S_r, and the frequency ratio, f_v/f, vary considerably with the type of bridge and vehicle; however, 7 appears to be a fairly representative value for the frequency ratio, and the amplitude ratio is generally less than 0.2.

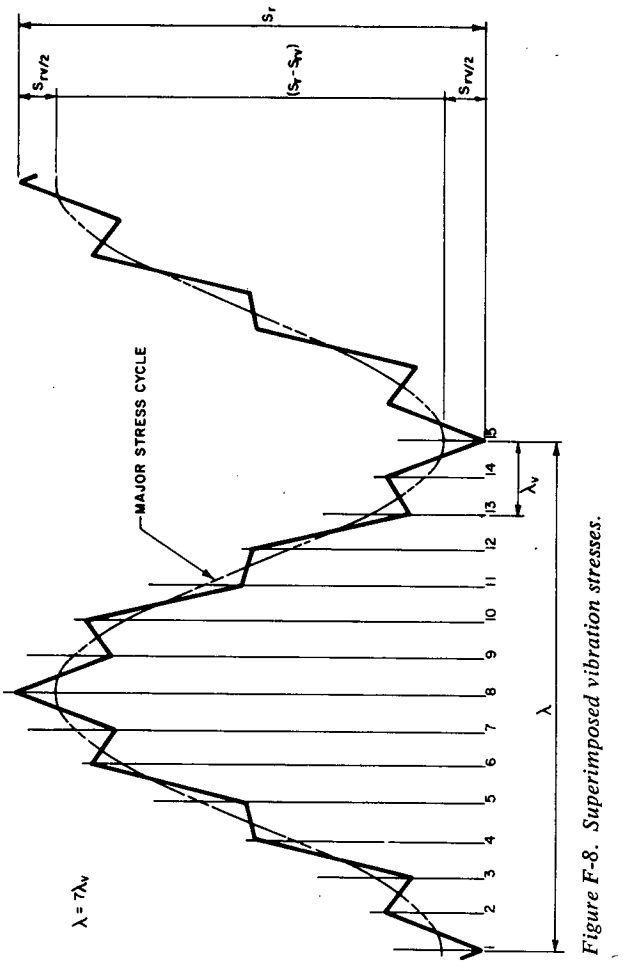

Figure F-8. Superimposed vibration stresses.

The effect of these vibrations on fatigue life can be estimated by Miner's Law. To do this, it is assumed that the over-all stress range cycles, S_r, and the vibration cycles, S_{rv}, have the same effect as if they had been applied at different times rather than simultaneously. This appears to be a reasonable concept, except when the amplitude ratio approaches 1 and the two types of cycles tend to lose their separate identities.

Specifically, a formula will be developed to show the ratio of fatigue lives, in terms of major stress cycles, for two members subjected to the same constant-amplitude over-all stress range, S_r, but one with a vibration stress and one without. The following definitions apply:

N = life for a stress range of S_r;
N_v = life for a stress range of S_{rv};
α = frequency ratio f_v/f;
N' = number of major stress cycles to failure when vibration cycles are present; and

$\alpha N'$ = total number of vibration cycles that occur while N' major stress cycles are being applied.

From Miner's Law,

$$\frac{N'}{N}+\frac{\alpha N'}{N_v}=1 \qquad \text{(F-12)}$$

which can be expressed as

$$\frac{N}{N'}=1+\frac{\alpha N}{N_v} \qquad \text{(F-13)}$$

From Eq. F-7,

$$N=\frac{A}{S_r^B} \qquad \text{(F-14)}$$

and

$$N_v=\frac{A}{S^B{}_{rv}} \qquad \text{(F-15)}$$

Therefore,

$$\frac{N}{N'}=1+\alpha\left(\frac{A}{S_r^B}\right)\left(\frac{S^B{}_{rv}}{A}\right)=1+\alpha\left(\frac{S_{rv}}{S_r}\right)^B \qquad \text{(F-16)}$$

TABLE F-9

STRESS AMPLITUDES FOR VIBRATION TESTS *

Amplitude Ratio**	Point	Major Stress Amplitude,*** percent	Vibration Stress Amplitude, S_{rv}, percent	Total Amplitude, S_r, percent
0.1	1	4.995	-4.995	00.0
0.1	2	9.447	+4.995	14.4
0.1	3	21.921	-4.995	16.9
0.1	4	39.947	+4.995	44.9
0.1	5	59.953	-4.995	55.0
0.1	6	77.979	+4.995	83.0
0.1	7	90.453	-4.995	85.5
0.1	8	94.91	+4.995	99.9
0.2	1	9.99	-9.99	00.0
0.2	2	13.95	+9.99	23.9
0.2	3	25.04	-9.99	15.0
0.2	4	41.06	+9.99	51.0
0.2	5	58.84	-9.99	48.9
0.2	6	74.86	+9.99	84.9
0.2	7	85.95	-9.99	76.0
0.2	8	89.91	+9.99	99.9

* See Figure G-8 for explanation of amplitudes.

** S_{rv}/S_r

*** Based on a sine wave.

Although this equation applies specifically to constant-amplitude major and vibration stresses, the same approach could be used to calculate a similar effect for variable-amplitude major cycles.

When α and S_{rv}/S_r are both 1, the vibration cycles are the same as the over-all cycles, and Eq. F-16 should result in $N/N'=1$. Instead, because the over-all cycles and vibration cycles are being treated as separate cycles according to the original assumptions, Eq. F-16 results in 2, which is not reasonable when S_{rv}/S_r approaches 1. Therefore, Eq. F-16 should not be used when S_{rv}/S_r approaches 1.

The ratio of fatigue lives with and without vibration stresses was calculated from Eq. F-16 for a B of 3, a frequency ratio of 7, and amplitude ratios of 0.1 and 0.2. The calculated reduction in life for amplitude ratios of 0.1 and 0.2 were 1.0 and 10.2 percent, respectively.

Three cover-plate specimens (detail S) were tested at each of the two aforementioned amplitude ratios (sets 23 and 24). In both cases, the over-all stress range S_r was 30 ksi (207 MPa), the minimum stress was 0, and the frequency ratio was 7. Total amplitudes corresponding to the peaks and valleys of the vibration stresses were calculated for each case by adding (or subtracting) a value of 0.1 or 0.2 times S_r to (or from) the corresponding amplitude for a sinusoidal major stress cycle. The maximum amplitudes for the major stress cycles were equal to 0.91 and 0.83 for the two cases.

The resulting amplitudes expressed as a percent of S_r are given in Table F-9 for the two different amplitude ratios. Eight amplitudes corresponding to the peaks and valleys shown in Figure F-8 are also given. For $S_{rv}/S_r=0.1$, the vibration stresses were so small that the successive amplitudes continually increased. For $S_{rv}/S_r=0.2$, the vibration stresses were large enough so that successive amplitudes alternately increased and decreased.

The results of the fatigue tests and the results of the theoretical analysis with $B=2.68$, the slope of the SN curve for cover-plate specimens, are given in Table F-10. The log means of N for the three sets of data were in reverse order from that predicted by the theoretical study, but the differences among the sets were small. A test of the statistical significance of the difference between the log means for the set of data for $S_{rv}=0$ and the set for either $S_{rv}/S_r=0.1$ or $S_{rv}/S_r=0.2$ indicated that the differences are not statistically significant because the sample size is so small. Larger sets of data would have to be tested to show effects as small as those suggested by the theoretical study.

TABLE F-10

EFFECT OF SUPERIMPOSED VIBRATION STRESSES

Amplitude Ratio*	Frequency Ratio*	Log Mean Life From Tests, kilocycles	Ratio of Lives** Test	Ratio of Lives** Analysis***
0.0	-	257	1	1
0.1	7	266	1.03	0.99
0.2	7	335	1.30	0.91

* Amplitude ratio equals S_{rv}/S_r; frequency ratio equals f_v/f.

** Life with superimposed vibration stresses, N, divided by life without superimposed vibration stresses, N'.

*** $\frac{N}{N'}=1+\frac{f_v}{f}\left(\frac{S_{rv}}{S_r}\right)^{2.68}$.

APPENDIX G

DETAILED DISCUSSION OF CRACK INITIATION AND PROPAGATION

CRACK-GROWTH TESTS

The relationship between crack depth and number of cycles for the tests of the A514 steel wedge-opening-loading (WOL) specimens are plotted in Figures G-1 and G-2 for the constant- and variable-amplitude loadings, respectively. These results can best be interpreted in terms of the stress

intensity, K, at the crack tip and the crack-growth rate, da/dN, in which a is the crack depth and N is the number of cycles (*25*). The growth rate was determined for each increment of crack growth by dividing the change in crack depth by the change in cycles for the increment. For the variable-amplitude tests, the crack-growth rate is an average rate for the 500-cycle blocks defining the spectrum.

The stress intensity is a function of the applied load, P, and the distance from the load point to the crack tip and was determined from an available stress analysis for WOL specimens (*23*). During each test, the load range, P_r, and minimum load, P_{min}, were held constant, but the stress-intensity range, K_r, and minimum stress intensity, K_{min}, increased as the crack depth increased. The variation of the K values for each test is given in Table 3.

The log of da/dN is plotted as a function of the log of the K_r in Figure G-3 for the constant-amplitude tests. Data for different combinations of P_{min} and P_r fall within a relatively small scatter band. K_{min} varies considerably for these data as a result of the differences in P_{min} and the variation of K_{min} with crack depth that was discussed earlier. Consequently, it is concluded that K_{min} has little effect on the crack-growth rate.

Parallel lines are ploted to show the approximate scatter band for the data. These lines, and the best-fit line for the data, can be defined in a form similar to the SN curves discussed earlier. Specifically,

$$\log(da/dN) = \log A + B \log K_r \qquad \text{(G-1)}$$

and

$$da/dN = AK_r^B \qquad \text{(G-2)}$$

The constants A and B depend on the material properties and have the same meaning (Figure F-1) as the A and B values for SN curves.

The crack-growth rate is shown in Figure 21 as a function of the modal stress intensity range, K_{rm}, for three values of K_{rd}/K_{rm}, including two variable-amplitude spectrums. These results are for a random sequence of loads. The lines representing the three values of K_{rd}/K_{rm} are approximately parallel and show that the crack-growth rate for a given K_{rm} increases as the spectrum width measured by K_{rd}/K_{rm} increases. This is consistent with the results of the fatigue tests.

The curves for the three spectrum widths can be shifted together by plotting K_{rRMS} instead of K_{rm}, as the stress-intensity parameter (see Fig. 22). As indicated in the figure, the line through these data is defined by Eq. G-1 or Eq. G-2, with $\log A = -9.11$ (or $A = 7.68 \times 10^{-10}$) and $B = 2.60$. Thus, the RMS method for relating variable- and constant-amplitude data applies to the crack-growth rate as well as to the total fatigue life.

Crack-growth data for several different variable-amplitude loading sequences, including a random sequence, are plotted in Figure G-4. The data fall within a narrow scatter band and show that the loading sequence as represented by the chosen load spectrum has little effect on the crack-growth rate.

Crack-growth tests on A36 steel were not performed because previous work showed that the constant-amplitude crack-growth rates are roughly the same for all structural steels. The variable-amplitude crack-growth rates are also expected to be approximately the same for these steels.

CRACK DATA FROM COVER-PLATE BEAM TESTS

The lengths of cracks visible on the surface of the tension flange of the cover-plate beams at various lives are given in Appendix E. To determine whether these data could be correlated with basic crack-growth data, curves of crack length vs. life were plotted for many cover-plate A and B beams. These plots were erratic, probably as a result of the difficulty of determining exactly where the surface crack terminated. Therefore, it was concluded that the beam crack growth data are not consistent enough to permit meaningful correlations with the basic WOL crack-growth data.

The crack-length data for the cover-plate beams, however, provide valuable information on the initiation and propagation phases of fatigue life for such beams. The initiation and propagation lives for A514-steel cover-plate C beams were determined from these data and are plotted in Figure 25. The initiation life was taken as the log-mean life for the last observation without a crack and the first observation with a crack. Only beams, for which the life difference between these two observations was small, were included in the figure. The propagation life was obtained by subtracting initiation life from the total fatigue life. The initiation-life curve shown in Figure 25 was fit to the data by observation. The results in Figure 25 show that the initiation life is an important part of the total fatigue life for this type of detail.

In the cover-plate A and B beams, semielliptical cracks developed at the ends of longitudinal fillet welds joining the cover plate to the flange plate. The ratio of the crack length, l, to the crack depth, a, is an important parameter in vari-

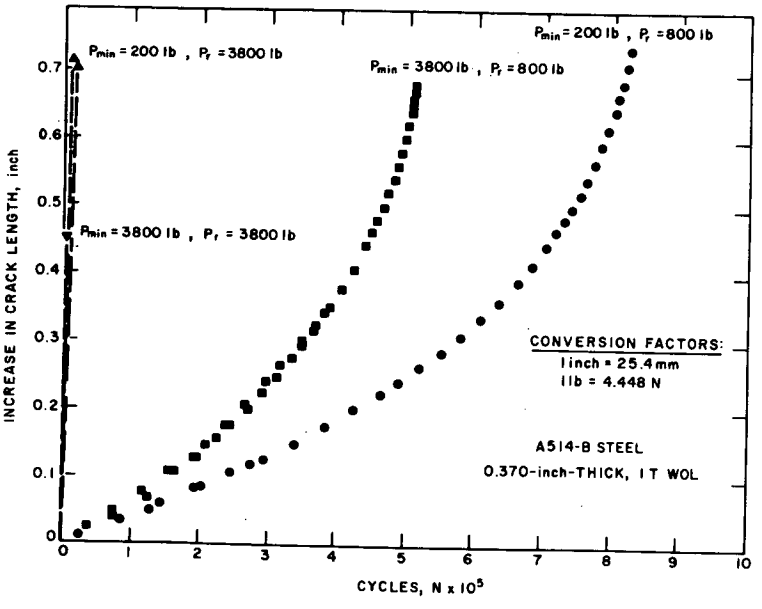

Figure G-1. Crack growth for constant-amplitude loadings.

ous crack-growth correlations. Consequently, to provide information useful to other investigators, the ratio l/a was determined from the cracked surface of several tested beams and are plotted in Figure G-5. The shape of the crack at certain stages was often apparent from the surface texture. All beams that furnished clear evidence of the crack shape were included on the plot. Several beams, which had cracks at the low-stress end of the cover plate after failure had occurred at the high-stress end, were opened to determine the crack shape and were also included on the plot. The plot shows that l/a was approximately 4 over the observed range of depths from 0.1 to 0.37 in. (2.5 to 9.4 mm).

PREDICTION OF BEAM FATIGUE LIVES FROM BASIC DATA

The fatigue life of a structural detail can be divided into two phases: (1) initiation and (2) propagation (*26*). Comprehensive basic data are available on the propagation phase (*25*), and a smaller amount are available on the initiation phase (*26*). These basic data, together with information on stress conditions, were used to predict the total fatigue lives of four beam conditions. To illustrate the uncertainties involved, several different approaches were used in making these predictions. Specifically, predictions were made for constant-amplitude loading of A36- and A514-steel beams at stress ranges of 10 and 30 ksi (69 and 207 MPa).

The basic data on the propagation phase are available from several sources (*25, 26, 38*). There is considerable scatter among the data for different structural steels and from different sources—although a single, lower bound crack-growth curve is frequently used for all structural steels (*25*). The limited amount of available data (*26, 38*) for weld metal and heat-affected zone suggests that the crack-growth rate is less in weld metal and heat-affected zone than in base metal. Part of the crack propagation in the beams occurred in the heat-affected zone and part in the base metal. Consequently, there is considerable uncertainty about what crack-growth data should be used in the predictions. It was decided to use the individual mean curves from published crack-growth data on A36 and A514 steels (*25*) except as noted later. These curves are defined by Eq. G-2 with values of $A = 2.4 \times 10^{-10}$ and $B = 3.0$ for A36 steel and $A = 4.4 \times 10^{-9}$ and $B = 2.25$ for A514 steel. The previously published data for A514 steel rather than the data obtained in the present program were used in the predictions because the published data are more comprehensive and because the present crack-growth data were not obtained from the heat of steel used for the beam flanges. If the crack-growth data for weld metal had been used instead of the data for the base metal, the calculated lives would have been longer.

The data on the initiation phase were available from tests conducted at the U.S. Steel Research Laboratory on A36 and A517 steels. These data are plotted in Figure G-6 and were used in the present calculations. The specified longitudinal mechanical properties of A517 are the same as those of A514 steel. The curves shown in Figure G-6 were obtained from tests on specimens containing a machined

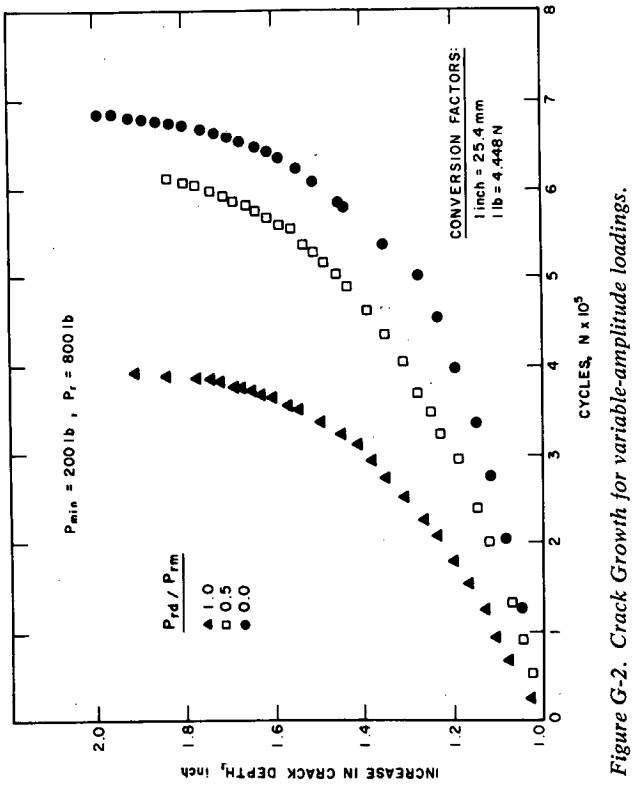

Figure G-2. Crack Growth for variable-amplitude loadings.

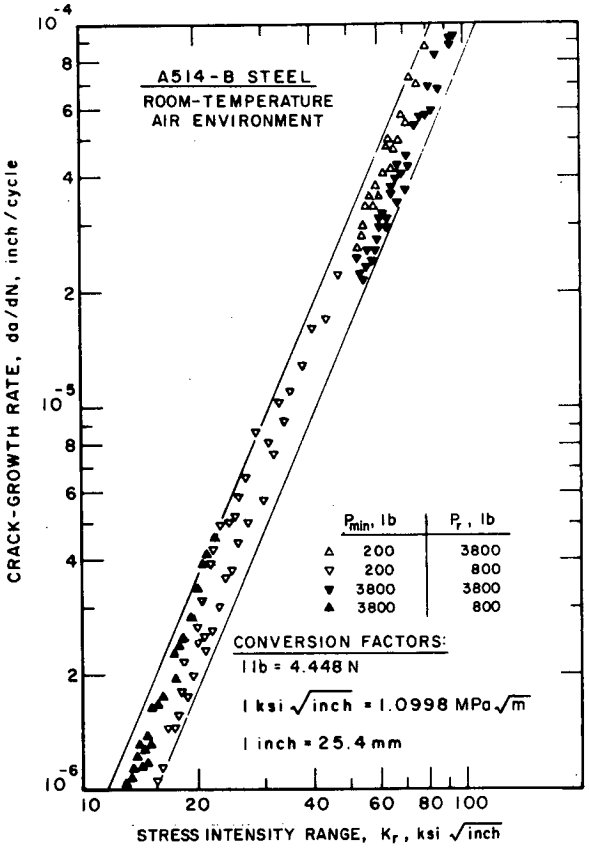

Figure G-3. Crack-growth rate as a function of stress-intensity range for constant-amplitude tests.

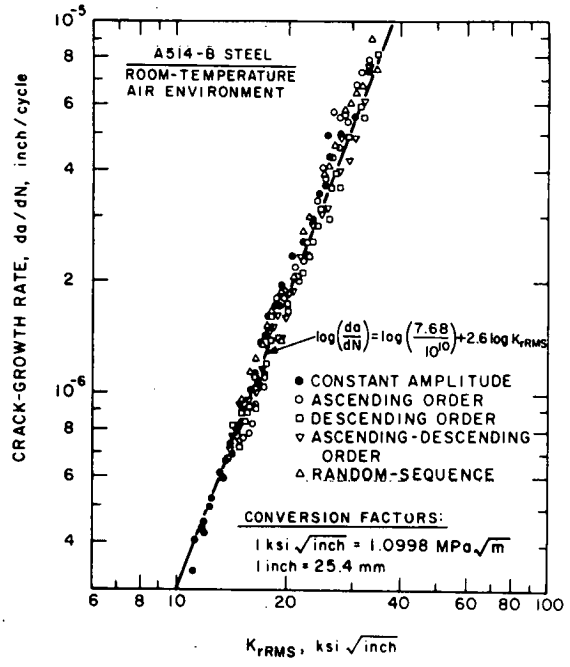

Figure G-4. Crack-growth rates for various loading sequences.

notch with a stress concentration factor of 2.5 and tested under several different nominal stress ranges. The theoretical magnified stress range was determined by multiplying the theoretical elastic stress-concentration factor times the nominal stress range even when the resulting stress exceeded the yield strength of the material. The curves do not include any effects of the amount of area affected by the stress concentration. A small circular hole in a plate illustrates this effect. Such a hole has a stress concentration factor of 3, regardless of its diameter; a larger diameter, however, affects a larger area and may have a greater effect on fatigue behavior.

In these basic tests, crack initiation was detected by magnified visual observations of the specimen surface in the region of the machined notch. When the surface crack was first observed, it had a finite length ranging between 0.01 to 0.03 in. (0.25 to 0.76 mm). The average crack depth corresponding to this range of lengths was estimated to be about 0.005 in. (0.13 mm), and this value was used as the end point for the initiation phase when predicting the total life of the beams. The observed range of initial crack size indicates that there was considerable variation in the end point for the initiation phase. This variable did not cause excessive scatter in the initiation data; however, it adds considerably to the uncertainty in predicting the total life of the beams because the end point of the initiation phase is used as the starting point for the propagation phase. A relatively small difference in the assumed starting point for the propagation phase has a relatively larger effect on the calculated total life of the beams because most of the propagation life occurs while the crack is small.

Crack initiation data for the base metal was used in predicting the fatigue lives of the beams, even though initiation apparently occurred in the heat-affected zone (or in weld metal) because no initiation data are available for weld metal or heat-affect zone.

In addition to the uncertainties regarding the basic crack initiation and propagation data, there are considerable uncertainties regarding the exact stress distribution in the region of the cross weld at the cover-plate end before and after cracking. The magnitude and effect of the residual stresses at the cross weld at the end of the cover plate are not precisely known. Similarly, the exact peak value and variation of the stress concentration factor, F (actual stress at point divided by nominal stress at that point), are not precisely known; they probably vary along the cross weld of each beam and among the cross welds of different beams. Furthermore, it is not known precisely how these local stresses should be incorporated into the calculation of the stress intensity range, K_{rm}, used in estimating the propagation life and even what basic equation should be used to calculate K_{rm}.

To predict the total life of a fabricated member, such as a cover-plate C beam, from basic crack data, an assumption must be made regarding each of these uncertainties. By choosing the right combination of assumptions, it is often possible to make predictions that approximate the observed fatigue lives of fabricated members that have already been tested. It is much more difficult to accurately predict the fatigue lives of fabricated members before they are tested. The calculations presented herein are intended to illustrate several different approaches of varying complexity that could be used in predicting fatigue life from basic data and to show how they compare with the test results. Several of these methods were suggested by crack-growth experts.

In Table G-1, the total fatigue life predicted by each approach is compared with the corresponding actual life. The listed actual lives were calculated from the experimental regression Eq. F-3 and the appropriate regression coefficients given in Table F-2 for $S_{rd}/S_{rm} = 0$. The values $S_{\min}$ and β were taken as 0.

In all approaches, the propagation life was determined by (1) calculating the stress intensity as a function of the crack depth, a, and nominal modal stress range, S_{rm}; (2) obtaining the crack-growth rate, da/dN, corresponding to a given crack depth from basic crack growth data; (3) dividing a desired increment of depth, Δa, by da/dN to obtain a corresponding increment of life, ΔN; and (4) summing these life increments to obtain the total propagation life. The final crack size was always taken as 0.3 in. (8 mm). Since K_r is very high for this crack depth, very little life remains thereafter. An example of the incremental calculations of propagation life is given in Table G-2.

The stress intensity range was related to a and S_{rm} by

$$K_{rm} = C\,F\,S_{rm}\sqrt{a\pi} \qquad \text{(G-3)}$$

in which S_{rm} is the nominal stress range, C is a factor that applies to a crack in a uniform-thickness flange (effect of cover-plate end not included), and F is the stress concentration factor at the cover-plate end.

Equations of curves defining C as a function of the ratio of crack depth to plate thickness, a/t, are available for several different shapes of cracks and nominal stress distributions (*39*). Since the cross weld in the cover plate causes

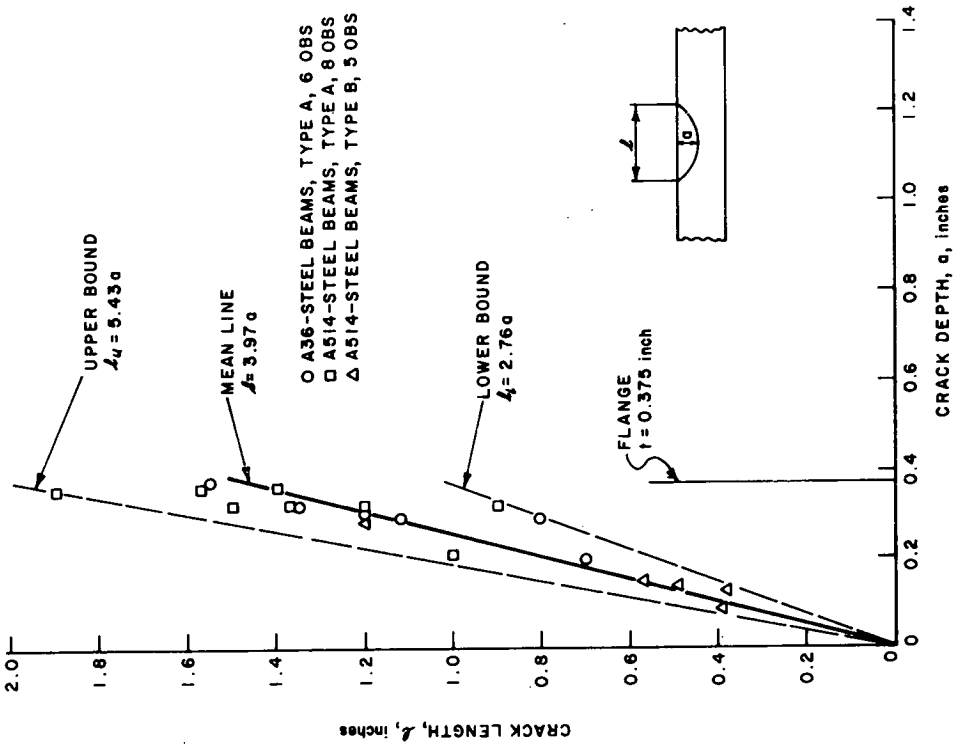

Figure G-5. Length-to-depth ratio for semielliptical cracks in cover-plate A and B beams.

a crack to develop across most of the flange, the curve for a full-width surface crack in an I-beam flange was used to define C in the first four approaches. A curve for this case is shown in Figure 6 of Reference (*40*); the following empirical equation approximates this curve:

$$C = 1.08 + 0.5a/t + 1.6(a/t)^2 + 0.7(a/t)^3 \qquad \text{(G-4)}$$

Previous investigators (*3*) hypothesized that the cracks initiate at many points along a cross weld before growing together to form a single long crack and, consequently, that C should be defined for a semielliptical surface crack in axially loaded plates. Therefore, the following equation based on this hypothesis (*3*) was used in the final three approaches:

$$C = 1 + 0.12\,\frac{(1 - a/b)}{\phi_0}\sqrt{\sec\frac{\pi a}{2t}} \qquad \text{(G-5)}$$

in which b is the long semiaxis of the crack (half length of the crack at the surface), and ϕ_0 is the elliptical integral and is defined by

$$\phi_0 = \int_0^{\pi/2} \sqrt{1 - [1 - (a/b)^2]\sin^2\chi}\, d\chi \qquad \text{(G-6)}$$

The value of b used in conjunction with Eq. G-5 was taken as $2a$; however, in the final approach, b was taken as $1.088a^{0.946}$, as suggested by previous investigators (*3*), even though the experimental data from the present program indicated that a/b is about twice this value. As illustrated in Figure G-7a, Eq. G-5 gives a considerably smaller value of C than Eq. G-4, since the crack for the former case covers a much smaller fraction of the total cross sectional area of the flange. Several different methods of varying complexity were assumed in defining F, as discussed later.

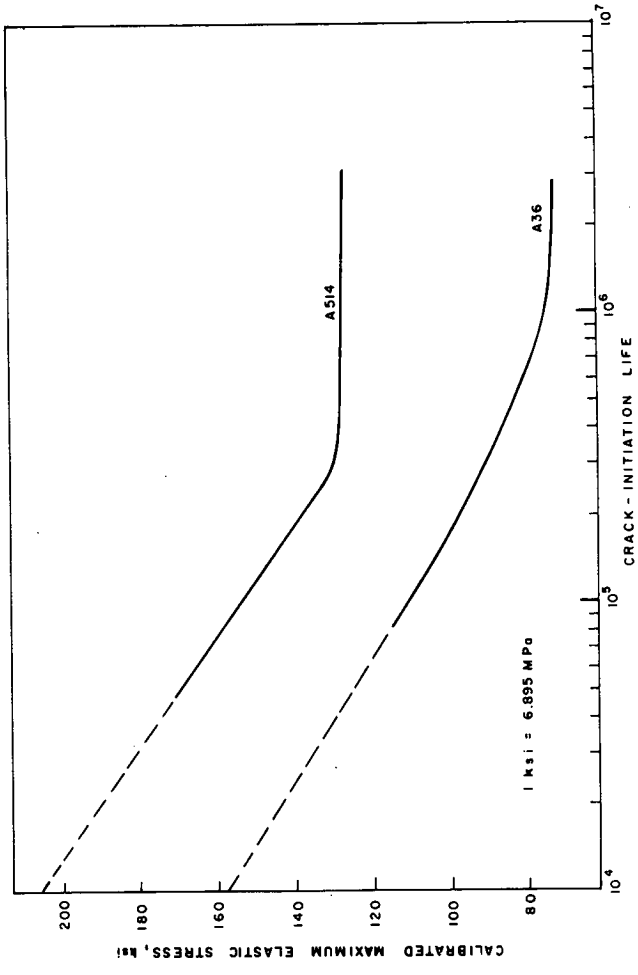

Figure G-6. Crack-initiation behavior of various steels.

TABLE G-1

PREDICTION OF FATIGUE LIVES OF COVER-PLATE C BEAMS FROM CRACK INITIATION AND PROPAGATION DATA*

Calculation Method	S_{rm}, ksi	Steel	Stress-Concentration Factor*			Range of a, in.	Range of K_r, ksi $\sqrt{in.}$	Predicted Life, kilocycles			Actual Life***, kilocycles		
			Initiation	Peak	Variation**			Initiation	Propagation	Total	Mean	Lower Limit	Upper Limit
1	10	A36	-	1.0	C	0.0127-0.300	2.2 - 27.4	-	6129.0	6129.0	1142.4	661.9	1971.6
	10	A514	-	1.0	C	0.0045-0.300	1.3 - 27.4	-	1475.3	1475.3	1594.1	923.7	2751.2
	30	A36	-	1.0	C	0.0085-0.300	4.8 - 82.2	-	308.3	308.3	47.0	27.2	81.1
	30	A514	-	1.0	C	0.0019-0.300	2.5 - 82.2	-	180.7	180.7	65.6	38.0	113.2
2	10	A36	-	1.0	C	0.005-0.300	1.36-27.4	-	11791.2	11791.2	1142.4	661.9	1971.6
	10	A514	-	1.0	C	0.005-0.300	1.36-27.4	-	1415.2	1415.2	1594.1	923.7	2751.2
	30	A36	-	1.0	C	0.005-0.300	4.10-82.2	-	436.7	436.7	47.0	27.2	81.1
	30	A514	-	1.0	C	0.005-0.300	4.10-82.2	-	119.5	119.5	65.6	38.0	113.2
3	10	A36	-	2.0	L	0.005-0.300	2.70-28.7	-	1711.1	1711.1	1142.4	661.9	1971.6
	10	A514	12.8	2.0	L	0.005-0.300	2.70-28.7	1236.2	357.9	1594.1	1594.1	923.7	2751.2
	30	A36	-	2.0	L	0.005-0.300	8.11-86.1	-	63.4	63.4	47.0	27.2	81.1
	30	A514	5.9	2.0	L	0.005-0.300	8.11-86.1	35.4	30.2	65.6	65.6	38.0	113.2
4	10	A36	7.4	7.4	D	0.005-0.300	10.11-28.7	978.4	164.0	1142.4	1142.4	661.9	1971.6
	10	A514	12.7	12.7	D	0.005-0.300	17.35-28.7	1536.0	58.1	1594.1	1594.1	923.7	2751.2
	30	A36	4.4	4.4	D	0.005-0.300	17.87-86.1	34.5	12.5	47.0	47.0	27.2	81.1
	30	A514	10.5	10.5	D	0.005-0.300	41.8-86.1	0.2	65.4	65.6	65.6	38.0	113.2
5+	10	A36	-	4.85	P	0.0010-0.300	2.2 - 15.0	-	1255.8	1255.8	1142.4	661.9	1971.6
	10	A514	12.8	4.85	P	0.0003-0.300	1.3 - 15.0	1212.8	381.3	1594.1	1594.1	923.7	2751.2
	30	A36	-	4.85	P	0.00045-0.300	4.8 - 44.9	-	57.2	57.2	47.0	27.2	81.1
	30	A514	6.0	4.85	P	0.00013-0.300	2.5 - 44.9	30.7	34.9	65.6	65.6	38.0	113.1
6	10	A36	8.7	4.85	P	0.005-0.300	5.15-15.0	238.2	904.2	1142.4	1142.4	661.9	1971.6
	10	A514	12.7	4.85	P	0.005-0.300	5.15-15.0	1302.3	291.8	1594.1	1594.1	923.7	2751.2
	30	A36	4.1	4.85	P	0.005-0.300	15.4-44.9	13.5	33.5	47.0	47.0	27.2	81.1
	30	A514	6.2	4.85	P	0.005-0.300	15.4-44.9	41.0	24.6	65.6	65.6	38.0	113.2
7++	10	A36	-	4.85	P	0.003-0.300	3.62-11.9	-	2111.3	2111.3	1142.4	661.9	1971.6
	10	A514	-	4.85	P	0.003-0.300	3.62-11.9	-	2111.3	2111.3	1594.1	923.7	2751.2
	30	A36	-	4.85	P	0.003-0.300	10.9-35.7	-	78.2	78.2	47.0	27.2	81.1
	30	A514	-	4.85	P	0.003-0.300	10.9-35.7	-	78.2	78.2	65.6	38.0	113.2

* The symbols used in the table are defined as follows: S_{rm} = modal stress range, a = crack depth, K_r = stress-intensity range. For all sets, the minimum stress, S_{min}, equals 0 or 10 ksi and the dispersion ratio, S_{rd}/S_{rm}, equals 0. The stress-intensity factor ranges from 1.09 through 2.83.

** C = constant, L = linear variation, D = dual linear variation, P = parabolic variation. A complete explanation of these variations is given in the text For A36: $\frac{da}{dN} = 2.4 \times 10^{-10} (K_r)^{3.0}$ For A514: $\frac{da}{dN} = 4.4 \times 10^{-9} (K_r)^{2.25}$

*** Actual life determined from best-fit regression line for cover-plate B and C beams with S_{rd}/S_{rm} and S_{min} equal to zero.

Note

Prediction of propagation life for A514-steel cover-plate C beams taken from Figure 25 for stress ranges of 10 and 30 ksi is 695.0 and 36.8 kilocycles, respectively.

Conversion Factors: 1 ksi = 6.89 MN/m^2, 1 in. = 25.4 mm, 1 ksi $\sqrt{in.}$ = 1.0998 MPa $\sqrt{m}$

TABLE G-2

TYPICAL INCREMENTAL CALCULATION OF CRACK PROPAGATION *

a	C	F	K_r	ΔN	∑N
.0075	1.09	4.796	8.029	40248	40248
.0125	1.10	4.660	10.144	19959	60208
.0175	1.11	4.524	11.741	12870	73078
.0225	1.12	4.388	13.019	9442	82520
.0275	1.13	4.252	14.067	7484	90005
.0325	1.14	4.116	14.938	6249	96255
.0375	1.15	3.980	15.665	5419	101675
.0425	1.16	3.844	16.269	4838	106513
.0475	1.17	3.708	16.765	4421	110934
.0525	1.18	3.572	17.165	4119	115053
.0575	1.20	3.436	17.478	3902	118955
.0625	1.21	3.300	17.708	3751	122707
.0675	1.23	3.164	17.862	3655	126363
.0725	1.24	3.028	17.941	3607	129970
.0775	1.26	2.892	17.950	3602	133573
.0825	1.27	2.756	17.888	3639	137213
.0875	1.29	2.620	17.757	3720	140934
.0925	1.31	2.484	17.558	3849	144783
.0975	1.33	2.348	17.289	4031	148814
.1025	1.35	2.212	16.952	4276	153091
.1075	1.37	2.076	16.544	4600	157691
.1125	1.39	1.940	16.065	5025	162716
.1175	1.42	1.804	15.512	5581	168298
.1225	1.44	1.668	14.885	6317	174615
.1275	1.46	1.592	14.735	6511	181127
.1325	1.49	1.576	15.123	6023	187150
.1375	1.51	1.560	15.512	5581	192731
.1425	1.54	1.544	15.904	5179	197911
.1475	1.57	1.528	16.297	4813	202724
.1525	1.60	1.512	16.693	4478	207203
.1575	1.62	1.496	17.091	4173	211376
.1625	1.65	1.480	17.491	3893	215269
.1675	1.68	1.464	17.894	3636	218905
.1725	1.72	1.448	18.299	3399	222305
.1775	1.75	1.432	18.707	3182	225488
.1825	1.78	1.416	19.117	2982	228470
.1875	1.82	1.400	19.529	2797	231267
.1925	1.85	1.384	19.943	2626	233894
.1975	1.89	1.368	20.360	2468	236362
.2025	1.93	1.352	20.778	2322	238685
.2075	1.97	1.336	21.198	2187	240872
.2125	2.00	1.320	21.619	2061	242934
.2175	2.04	1.304	22.041	1945	244879
.2225	2.09	1.288	22.465	1837	246717
.2275	2.13	1.272	22.889	1737	248454
.2325	2.17	1.256	23.314	1644	250099
.2375	2.22	1.240	23.738	1557	251656
.2425	2.26	1.224	24.163	1476	253133
.2475	2.31	1.208	24.587	1401	254534
.2525	2.36	1.192	25.010	1331	255866
.2575	2.40	1.176	25.432	1266	257133
.2625	2.45	1.160	25.852	1205	258339
.2675	2.50	1.144	26.270	1149	259488
.2725	2.56	1.128	26.685	1096	260584
.2775	2.61	1.112	27.097	1047	261631
.2825	2.66	1.096	27.506	1001	262632
.2875	2.72	1.080	27.910	958	263591
.2925	2.78	1.064	28.310	918	264509
.2975	2.83	1.048	28.705	880	265390

*Symbols are defined in the text, calculations are for S_{rm} = 10 ksi

$$K_r = CFS_{rm}\sqrt{\pi a}, \quad \Delta N = \frac{\Delta a}{K_r^3(2.4\times10^{-10})}$$

Plotted in Fig. G8 for F max = 5.0

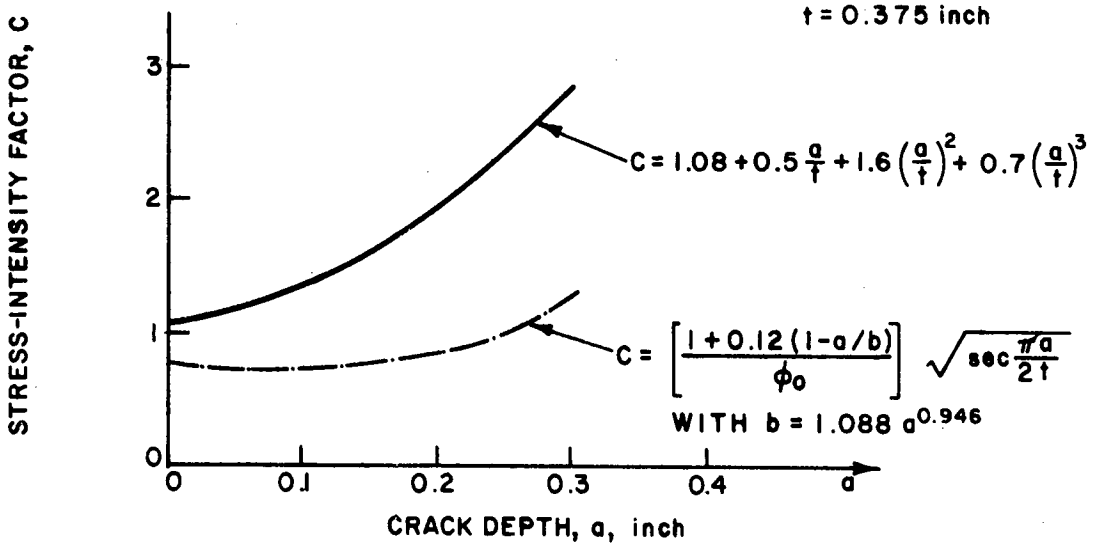

a. STRESS-INTENSITY FACTOR AS A FUNCTION OF CRACK DEPTH

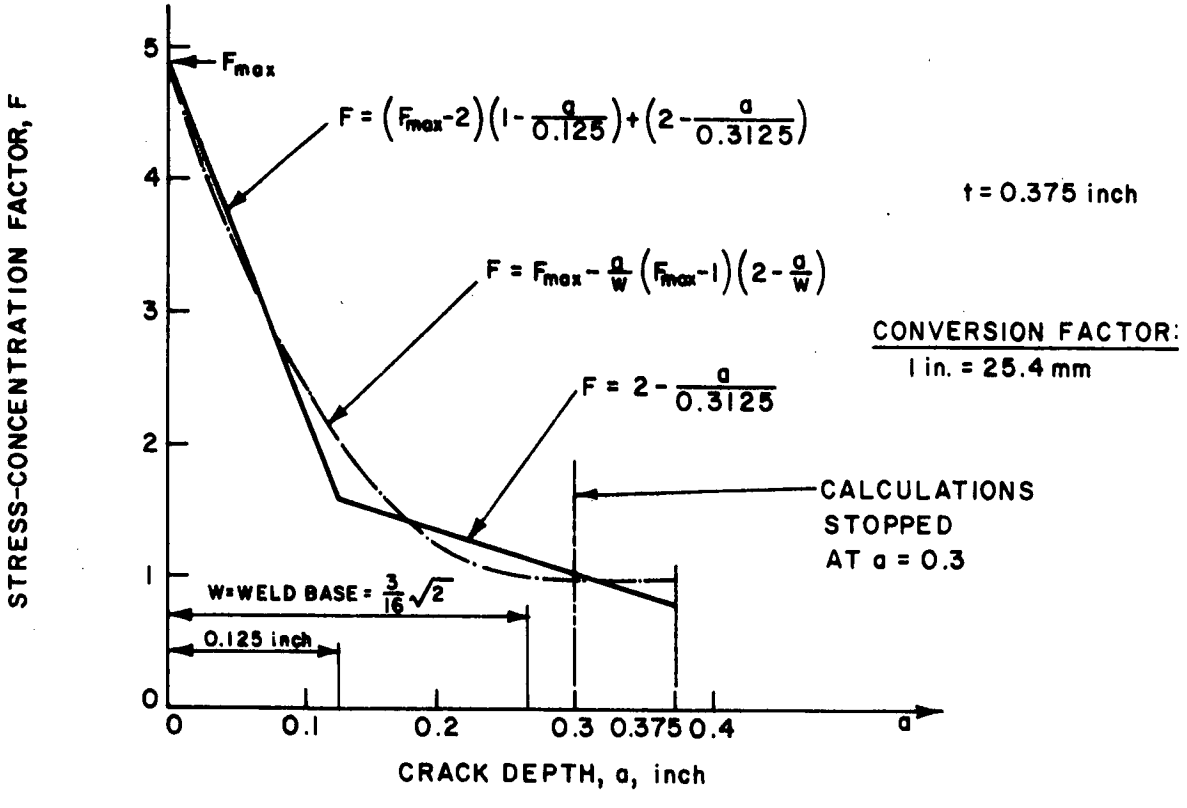

b. STRESS-CONCENTRATION FACTOR AS A FUNCTION OF CRACK DEPTH

Figure G-7. Factors used in calculating stress intensity as a function of crack depth.

The propagation life provides a lower bound for the total fatigue life and is often used (*38*) to make an approximate prediction of the total fatigue life. Therefore, in the first two approaches, the propagation life is calculated and compared with the total observed fatigue life.

In the first approach, the propagation life was calculated by starting with a crack depth that corresponded to the crack-growth threshold (*26*) (that is, the value of K_r below which a fatigue crack will not propagate). This approach gives the maximum propagation life that could pos-

sibly occur. The threshold decreases as the stress ratio (minimum stress divided by maximum stress) increases (*26*). Although the nominal stress ratio is zero for the beams, it was hypothesized that residual tensile stresses equal to the actual yield strength of the steel, S_y, existed at cover-plate end, so that the internal stresses varied during cyclic loading from $S_y - S_{rm}$ to S_y. The resulting stress ratios are 0.76 and 0.27 for the A36-steel beams with $S_{rm} = 10$ and 30 ksi (69 and 207 MPa), respectively, and 0.91 and 0.74 for the A514-steel beams with $S_{rm} = 10$ and 30 ksi, respectively. The corresponding K_{rm} values are given in Table G-1. The stress concentration factor, F, was taken as 1.0 in calculating these K_{rm} values, since it was hypothesized in this approach that the stress concentration affected only initiation and not propagation. The calculated propagation lives were well above the actual total fatigue lives except for the A514-steel beam with $S_{rm} = 10$ ksi.

In the second approach, the propagation life was again calculated on the basis of a stress concentration factor of 1.0, but the initial crack depth for the propagation phase was taken as 0.005 in. (0.13 mm)—the depth of crack corresponding to the end point of the initiation phase in the crack-initiation tests. For one of the four cases listed (A36 steel, $S_{rm} = 10$ ksi), the K_{rm} value corresponding to this initial crack depth was well below the crack-growth threshold; in another case (A36 steel, $S_{rm} = 30$ ksi), it was slightly below the threshold. This means that no crack growth should occur according to the basic data. Nevertheless, the K_{rm} values below the threshold were calculated by using the same da/dN vs. K_{rm} curve that was used above the threshold. Again, all calculated propagation lives were well above the actual total lives, except the calculated propagation life for the A514-steel beam with $S_{rm} = 10$ ksi. The propagation life, of course, could be changed considerably by using a slightly different initial a.

In the third approach, the initial crack depth for the propagation phase was taken as 0.005 in. (0.13 mm) and the stress concentration factor was assumed to linearly decrease from 2.0 on the top face to 0.8 on the opposite face of the flange. The value of 2 approximates the peak factor of 2.06 calculated in a finite element analysis (*24*). This calculated factor is sensitive to the element size used in the analysis and is probably smaller than the true peak factor. The area affected by a stress raiser usually decreases as its severity increases. Consequently, stresses more than twice the nominal stress probably extend only to a small depth and may not greatly affect crack propagation. The K values corresponding to the initial crack depth of 0.005 in. are all above the crack-growth threshold previously discussed. The propagation lives calculated in this way are above the actual total lives for the A36-steel beams, but below the actual total lives for the A514-steel beams.

With the aid of Figure G-8, an initiation stress concentration factor that would make the total predicted life equal the actual life was also determined for each A514-steel beam and is listed in Table G-1. These factors are both well above 2 and are considerably different.

In the fourth approach, a single peak stress concentration that makes the total predicted life equal to the actual life was determined by plotting initiation, propagation, and total

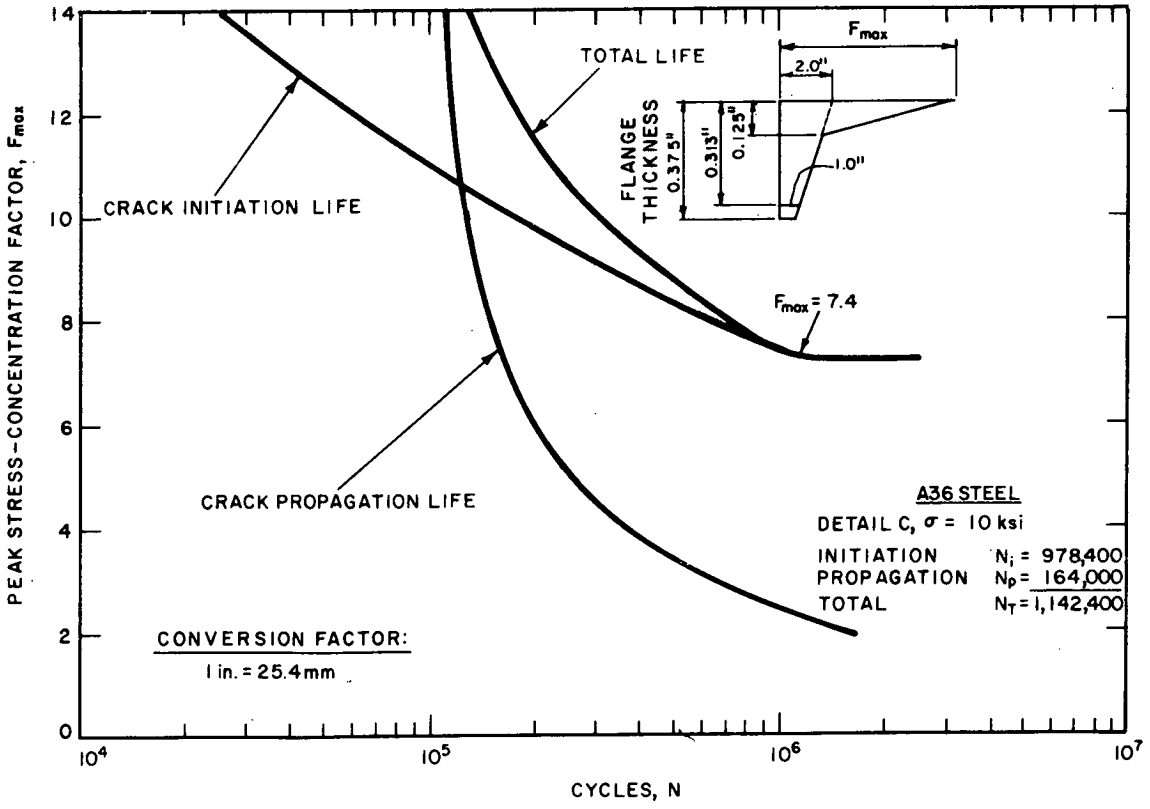

Figure G-8. Crack initiation and propagation lives as a function of peak stress concentration factor.

lives as a funcion of the peak stress concentration factor, as shown in Figure G-8. The stress concentration factor was assumed to vary with depth as illustrated in the figure. At a crack depth of ⅛ in. (3 mm) and greater, this factor is the same as in the third approach, but at a depth less than ⅛ in. it increases linearly to the peak value at the top surface. This peak value was used in calculating the initiation life. The calculated peak factors were larger than 2 and varied considerably for the four cases. The propagation life was always a very small portion of the total life. This was true because a relatively high stress concentration factor was required to reach the high initiation threshold (fatigue limit) shown in Figure G-6. The actual propagation lives, as shown in Figure 25 for cover-plate C beams, were considerably greater than the calculated propagation lives.

In the fifth, sixth, and seventh approaches, C was defined by Eq. G-5 and F was assumed to vary parabolically from a peak value of 4.85 at the flange surface to 1.00 at a distance from the surface equal to the base of the weld. This parabolic variation is defined by Ref. (*41*) as:

$$F = F_{max} - (F_{max} - 1)(a/w)(2 - a/w) \qquad \text{(G-7)}$$

in which w is the base of the cross weld and F_{max} is the peak stress concentration factor at the surface. F_{max} was taken as 4.85, as suggested by a current study at Lehigh University, and w was taken as $3/16\sqrt{2}$ in. (6.7 mm). In Figure G-7b, the variation of F defined by Eq. G-7 is compared with the dual linear variation used in the fourth approach; a value of $F_{max} = 4.85$ was used for both curves in this comparison. The curves for the two methods are not greatly different.

In the fifth approach, the maximum possible propagation life was calculated by assuming that the initial crack depth for the propagation phase corresponded to the crack-growth threshold described in the first approach. For both A36-steel beams, the calculated propagation life exceeded the actual total life but was within the experimental scatter band. For both A514-steel beams, the calculated propagation life was well below the actual total life, and the initiation stress concentration factor that makes the total predicted life equal to the actual life was calculated. These calculated initiation stress concentration factors were well above the peak factor of 4.85 used in the propagation calculations.

In the sixth approach, the initial crack depth for the propagation phase was taken as 0.005 in. (0.13 mm). The calculated propagation life was below the actual life for all beams, and the initiation stress concentration factor that makes the total predicted life equal to the actual life was again calculated. These calculated initiation stress concentration factors were generally well above 4.85.

In the seventh approach, the total life was assumed to consist of propagation from an initial crack with a depth of 0.003 in. (0.08 mm) as suggested by previous investigators (*3, 41*). In the previous investigations, this assumed initial crack depth made the propagation life calculated from Eqs. G-3, G-6, and G-7 (with $F_{max} \cong 2.4$) approximately equal to the actual total life of beams with a stiffener cross welded to the tension flange. A crack-growth curve for plain welded beams was used in this approach (instead of the individual mean curves for two different steels) to be consistent with the approach used in the previous investigations (*3, 41*). The values of A and B for this mean curve are 2×10^{-10} and 3.0, respectively. The calculated propagation lives for this approach are well above the mean value of the actual total lives, but roughly approximate the upper limits of these total lives.

All seven approaches require many critical assumptions to predict the fatigue life of a fabricated member from basic crack initiation and propagation data. The results obtained from these approaches illustrate the large effects of these critical assumptions on the predicted fatigue life. To consistently obtain accurate predictions of the fatigue life of fabricated members from basic data, considerably more information is needed on the uncertainties discussed earlier. Furthermore basic crack initiation and propagation data should be obtained for a single continuous test rather than two separate tests on different types of small specimens, as is usually done. This approach would eliminate inconsistencies in combining the two types of basic data to obtain a total fatigue life for a structural member.

COMPRESSION-FLANGE CRACKING

A significant number of cracks occurred in the compression flange of the welded beams and cover-plate C beams. Specifically, 7 out of 18, A36-steel welded beams tested at $S_{min} = -10$ ksi (−69 MPa) failed as a result of cracks in the bottom (compression) flange subjected to stresses varying from 10 ksi in tension to 10 ksi or greater in compression. The stresses in the top flange varied from 10 ksi in compression to 10 ksi or greater in tension. In all of the beams that failed by compression-flange cracking, the failure location was near a load point. In almost all of the beams that failed by tension-flange cracking, the failure location was in the central pure-moment region. Similar results occurred in Project 12-7 study where 3 out of 6, A36-steel welded beams tested at $S_{min} = -10$ ksi failed in the nominal compression flange near the load points. This suggests that compression-flange cracking was influenced by the local stresses in the region of the load point. The compression-flange cracking in Project 12-12 was not influenced by fretting at the load points because of the experimental procedures discussed earlier.

Two out of 15, A36-steel welded beams tested at $S_{min} = 0$ failed as a result of cracks in the bottom (compression) flange subjected to compressive stresses varying from 0 to a value of 20 ksi (138 MPa) or greater. The failure region was near the load point for one of these and in the central pure-moment region for the other. A36-steel welded beams were not tested at $S_{min} = 0$ in Project 12-7, but none of the 6 beams tested at $S_{min} = 2$ ksi (13.8 MPa) failed by compression-flange cracking.

None of the A514-steel welded beams, all of which were tested at $S_{min} = 0$, failed by compression-flange cracking, but considerable cracking did occur in the compression flange. Seven out of 8 compression-flange cracks that exceeded 3.5 in. (89 mm) in length occurred in the shear span near the load point. Although no tests were conducted in Project 12-7 on A514-steel welded beams at $S_{min} = 0$,

the beams tested at $S_{min} = 2$ ksi exhibited significant compression-flange cracking.

Four out of 66 cover-plate C beams failed as a result of compression-flange cracking; and five additional cover-plate C beams had significant compression-flange cracks that did not cause failure. All four beams that failed by compression-flange cracking were A36-steel beams; three were tested at $S_{min} = 0$ and $S_{rm} = 10$ ksi, and one was tested at $S_{min} = 0$ and $S_{rm} = 5$ ksi. The compression-flange cracks, like the tension-flange cracks, occurred at the high-stress end of the cover plate. Similar compression-flange cracks occurred at the ends of cover plates in Project 12-7.

The reason that some beams tested at $S_{min} = 0$ failed in the compression flange rather than in the tension flange has not been convincingly explained. The applied stresses in the compression flange vary from 0 to a maximum in compression. High tensile residual stresses on portions of the cross section near the welds could make the actual stress range in the compression flange about the same as that in the tension flange. It is even conceivable that the stress range on that portion of the cross section may sometimes be worse for the compression flange than for the tension flange as a result of the sequence in welding the flanges to the web or other fabrication procedures. However, cracks that initiated in such regions of tensile stress would not be expected to propagate through adjacent regions of compressive residual stress.

The fatigue lives for the welded or cover-plate beams that failed as a result of compression-flange cracks did not appear to be consistently different from the fatigue lives for similar beams that failed in the tension flange when subjected to the same loading conditions. This result is consistent with the Project 12-7 study that showed that the observed compression-flange failures were within the scatter band for the tension-flange failures of similar specimens.

THE TRANSPORTATION RESEARCH BOARD is an agency of the National Research Council, which serves the National Academy of Sciences and the National Academy of Engineering. The Board's purpose is to stimulate research concerning the nature and performance of transportation systems, to disseminate information that the research produces, and to encourage the application of appropriate research findings. The Board's program is carried out by more than 150 committees and task forces composed of more than 1,800 administrators, engineers, social scientists, and educators who serve without compensation. The program is supported by state transportation and highway departments, the U.S. Department of Transportation, and other organizations interested in the development of transportation.

The Transportation Research Board operates within the Commission on Sociotechnical Systems of the National Research Council. The Council was organized in 1916 at the request of President Woodrow Wilson as an agency of the National Academy of Sciences to enable the broad community of scientists and engineers to associate their efforts with those of the Academy membership. Members of the Council are appointed by the president of the Academy and are drawn from academic, industrial, and governmental organizations throughout the United States.

The National Academy of Sciences was established by a congressional act of incorporation signed by President Abraham Lincoln on March 3, 1863, to further science and its use for the general welfare by bringing together the most qualified individuals to deal with scientific and technological problems of broad significance. It is a private, honorary organization of more than 1,000 scientists elected on the basis of outstanding contributions to knowledge and is supported by private and public funds. Under the terms of its congressional charter, the Academy is called upon to act as an official—yet independent—advisor to the federal government in any matter of science and technology, although it is not a government agency and its activities are not limited to those on behalf of the government.

To share in the tasks of furthering science and engineering and of advising the federal government, the National Academy of Engineering was established on December 5, 1964, under the authority of the act of incorporation of the National Academy of Sciences. Its advisory activities are closely coordinated with those of the National Academy of Sciences, but it is independent and autonomous in its organization and election of members.

TRANSPORTATION RESEARCH BOARD
National Research Council
2101 Constitution Avenue, N.W.
Washington, D.C. 20418

ADDRESS CORRECTION REQUESTED

NON-PROFIT ORG.
U.S. POSTAGE
PAID
WASHINGTON, D.C.
PERMIT NO. 42970

000015M001
JAMES W HILL

IDAHO TRANS DEPT DIV OF HWYS
P O BOX 7129
BOISE ID 83707